



Universiteit  
Leiden  
The Netherlands

## **mRNA and drug delivery with lipid-based nanoparticles**

Zeng, Y.

### **Citation**

Zeng, Y. (2022, December 6). *mRNA and drug delivery with lipid-based nanoparticles*. Retrieved from <https://hdl.handle.net/1887/3492640>

Version: Publisher's Version

License: [Licence agreement concerning inclusion of doctoral thesis in the Institutional Repository of the University of Leiden](#)

Downloaded from: <https://hdl.handle.net/1887/3492640>

**Note:** To cite this publication please use the final published version (if applicable).

# **mRNA and Drug Delivery with Lipid-based Nanoparticles**

Proefschrift

ter verkrijging van  
de graad van doctor aan de Universiteit Leiden,  
op gezag van rector magnificus prof.dr.ir. H. Bijl,  
volgens besluit van het college voor promoties  
te verdedigen op dinsdag 6 December 2022  
klokke 12.30 uur

door

**Zeng Ye**

geboren te Hunan, China

in 1990

## **Promotiecommissie:**

### **Promotor:**

Prof. dr. A. Kros

Leiden University

### **Copromotor:**

Dr. A. L. Boyle

Leiden University

### Overige commissieleden:

Prof. dr. M. Ubbink (voorzitter)

Leiden University

Prof. dr. R.T. Dame (secretaris)

Leiden University

Prof. dr. Pascal. Jonkheijm

Twente University

Dr. R.E. Kieltyka

Leiden University

Dr. P. Vader

Utrecht University Medical Center

## **Table of Contents**

<b>Chapter 1</b>	<b>5</b>
Introduction	
<b>Chapter 2</b>	<b>29</b>
Efficient mRNA Delivery Using Fusogenic Coiled-coil Peptides	
<b>Chapter 3</b>	<b>63</b>
Coiled-coil Peptide Dimers Enhance Liposomal Drug Delivery	
<b>Chapter 4</b>	<b>91</b>
Efficient mRNA Delivery to Cardiomyocytes <i>in vitro</i> Using Fusogenic LNPs	
<b>Chapter 5</b>	<b>115</b>
Lipid Nanoparticle-based mRNA Candidates Elicit Potent T cell Immune Responses	
<b>Chapter 6</b>	<b>141</b>
Summary and Outlook	



# **Chapter 1**

## **Introduction**

## 1.1 Nanomedicine and its history

Many drug candidates show potent biological activity but also exhibit poor water solubility, chemical instability, short half-lives in circulation, or inefficient cell uptake, and will therefore likely face significant delivery challenges.<sup>1</sup> Fortunately, a recent advance in nanotechnology for healthcare applications, named nanomedicine, could address those shortcomings and limitations, enhance the therapeutic efficacy of traditional drugs, and revolutionize the pharmaceutical industry landscape.<sup>2</sup> Nanoscale delivery vehicles are designed to aid the transport of diagnostic or therapeutic agents through biological barriers and to improve the physical, chemical, and biological properties (*e.g.* solubility, circulating half-life, less off-target side effects) of drug candidates.<sup>3, 4</sup> Within the field of nanomedicine a wide range of applications, such as drug delivery, vaccine development, antibacterials, diagnostics, imaging tools, wearable devices, implants, high-throughput screening platforms, and other healthcare-related areas are studied.<sup>5</sup>

The progress of nanomedicine has undergone different stages during the last 60 years (**Fig. 1**).<sup>6-15</sup> In 1964, researchers discovered the structure of liposomes and proposed them as carriers for drugs.<sup>6</sup> Thereafter a variety of other nanoscale biomaterials including dendrimers,<sup>16</sup> polymers,<sup>7</sup> targeted liposomes,<sup>15</sup> and PLGA nanoparticles<sup>14</sup> were explored for their potential to deliver drugs. With the FDA approval in 1995 of doxorubicin-loaded liposomes, marketed as Doxil<sup>®</sup>,<sup>10</sup> the field of nanomedicines entered a new era, and many other lipid-based pharmaceuticals entered the clinic to treat cancer, fungal infections, pain management, and to function as anti-viral therapies (**Table 1**).<sup>17-30</sup> To date, a variety of organic and inorganic nanomaterials have been applied as drug delivery vehicles.<sup>9-13, 31, 32</sup> In 2018 the first siRNA lipid nanoparticle (Onpattro) was approved and the successful authorization for two mRNA Covid-19 vaccines in 2020 kickstarted the era of gene therapy taking center stage in the field of nanomedicine.<sup>33, 34</sup>

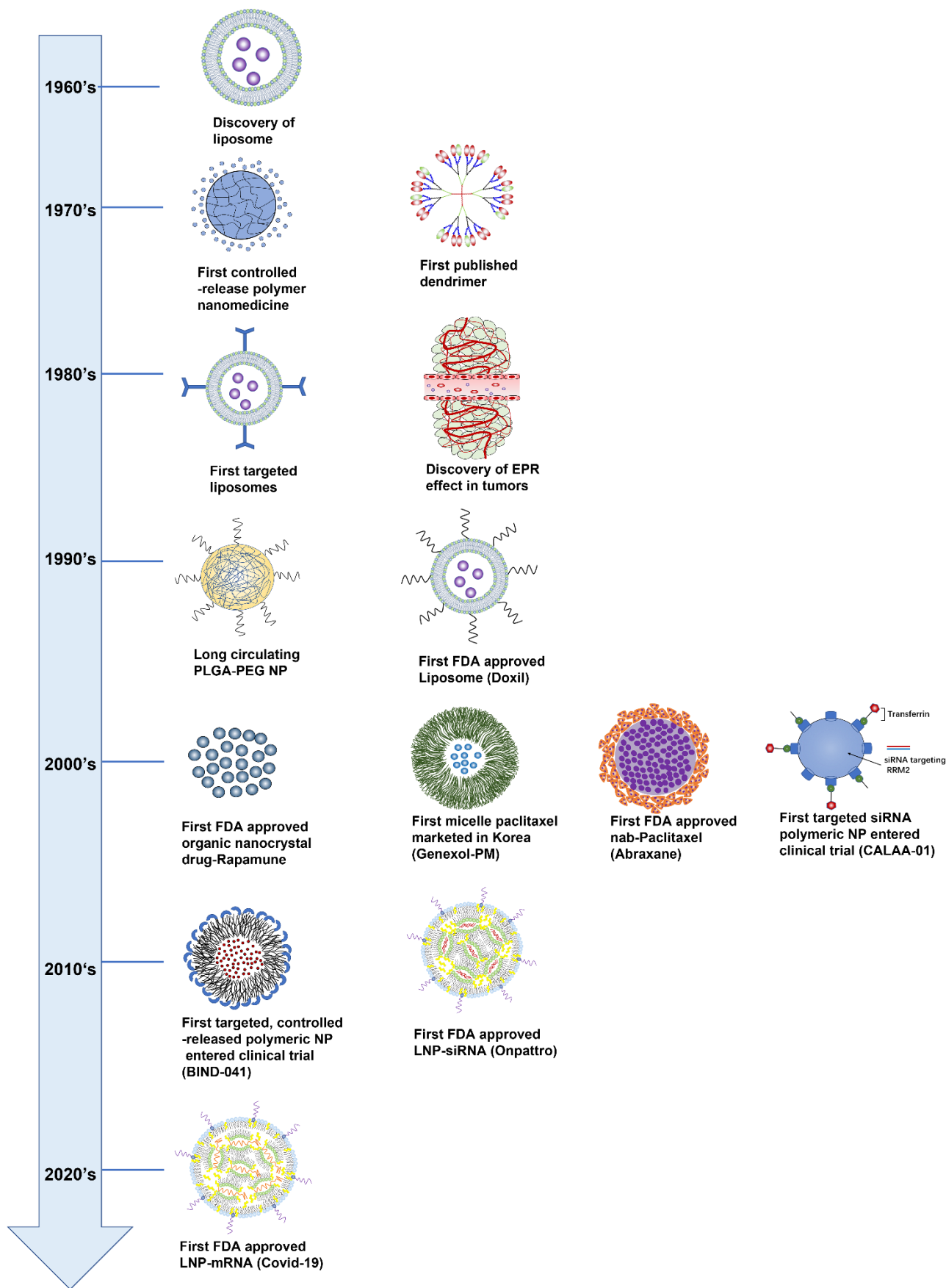


**Figure 1.** Important milestones in the field of nanomedicine.

The clinically approved liposome and albumin nanoparticles are defined as so-called first-generation nanomedicines, which overcome physicochemical barriers such as poor solubility or passive diffusion of drug molecules.<sup>3,35</sup> Compared to conventional pharmaceuticals, nanomedicines generally have a large specific surface area and flexibility of surface functionalization enabling different drug loading, retention, and controlled release. As a result, these nanocarriers improve the solubility of poorly-soluble hydrophobic drugs, improve bioavailability, therapeutic effects, and/or release drugs in a sustained, controlled, or stimuli-triggered manner.<sup>36</sup> With these properties, systemic side effects and administration dosage and frequency could be substantially reduced.

More recently, nanomedicines have developed into more advanced nanosystems, so-called second-generation drug delivery systems. These formulations have increased circulation half-life and reduced immunogenicity, while targeting moieties have been introduced to promote cell-specific targeting. Typically these targeting moieties are designed to specifically bind to overexpressed receptors on the surface of cells to target high selectivity for a variety of applications.<sup>37</sup> As targeting moieties, a variety of molecules are being used including small peptides, natural proteins, monoclonal antibodies, aptamers, polymers, carbohydrates, and small targeting molecules (**Fig. 2**).

**Table 1.** Clinically approved liposome-based products

Clinical products (Approval year)	Administration	Active agent	Lipids/Drug ratio (molar ratio)	Indication	Company
Doxil® (1995)	i.v.	Doxorubicin	HSPC:Cholesterol:PEG200-DSPE (56:39.5:5)	Ovarian, breast cancer, Kaposi's sarcoma	Sequus Pharmaceuticals
Abelcet® (1995)	i.v.	Amphotericin B	DMPC:DMPG (70:30)	Invasive severe fungal infections	Sigma-Tau Pharmaceuticals
Amphotec® (1996)	i.v.	Amphotericin B	Cholesteryl sulphate: Amphotericin B (1:1)	Severe fungal infections	Ben Venue Laboratories Inc.
DaunoXome® (1996)	i.v.	Daunorubicin	DSPC:Cholesterol (2:1)	AIDS-related Kaposi's sarcoma	NeXstar Pharmaceuticals
Ambisome® (1997)	i.v.	Amphotericin B	HSPC:DSPG:Cholesterol:Amphotericin B (2:0.8:1:0.4)	Presumed fungal infections	Astellas Pharma
Inflexal®V (1997)	i.m.	Inactivated hemagglutinine of Influenza virus strains A and B	DOPC:DOPE (75:25)	Influenza	Crucell, Berna Biotech
Depocyt® (1999)	Spinal	Cytarabine/Ara-C	DOPC, DPPG, Cholesterol and Triolein	Neoplastic meningitis	SkyPharma Inc.
Epaxal® (1999)	i.m.	Inactivated hepatitis A virus(strain RGSB)	DOPC:DOPE (75:25)	Hepatitis A	Crucell, Berna Biotech
Myocet® (2000)	i.v.	Doxorubicin	EPC:Cholesterol (55:45)	Combination therapy with cyclophosphamide in metastatic breast cancer	Elan Pharmaceuticals
Visudyne® (2000)	i.v.	Verteporphin	Verteporphin,DMPC,EPG	Choroidal neovascularisation	Novartis
Mepact® (2001)	i.v.	Mifamurtide	DOPS:POPC (30:70)	High-grade, resectable, non-metastatic osteosarcoma	Takeda Pharmaceutical Limited
DepoDur™® (2004)	Epidural	Morphine sulfate	DOPC,DPPG,Cholesterol, and Triolein	Pain management	SkyPharma Inc.
Exparel® (2011)	i.v.	Bupivacaine	DEPC,DPPG,Cholesterol, and Tricaprylin	Pain management	Pacira Pharmaceuticals, Inc.
Marqibo® (2012)	i.v.	Vincristine	SM:Cholesterol (60:40)	Acute lymphoblastic leukaemia	Talon Pharmaceutics, Inc.
Onivyde™® (2015)	i.v.	Irinotecan	DSPC:MPEG-2000:DSPE (3:2:0.015)	Combination therapy with fluorouracil and leucovorin in metastatic adenocarcinoma of the pancreas	Merrimack Pharmaceutics, Inc.

i.v. (intravenous); i.m. (intramuscular); HSPC (hydrogenated soy phosphatidylcholine); PEG (polyethylene glycol); DSPE (distearoyl-sn-glycero-phosphoethanolamine); DSPC (distearoylphosphatidylcholine); DOPC (dioleoylphosphatidylcholine); DPPG (dipalmitoylphosphatidylglycerol); EPC (egg phosphatidylcholine); DOPS (dioleoylphosphatidylserine); POPC (palmitoyloleoylphosphatidylcholine); SM (sphingomyelin); MPEG (methoxy polyethylene glycol); DMPC (dimyristoyl phosphatidylcholine); DMPG (dimyristoyl phosphatidylglycerol); DSPG (distearoylphosphatidylglycerol); DEPC (dierucoylphosphatidylcholine); DOPE (dioleoyl-sn-glycero-phosphoethanolamine)

## 1.2 Lipid-based nanomedicines

Lipid-based nanoparticles are still the most widely employed nanocarrier in drug delivery and diagnostic applications.<sup>30, 38, 39</sup> Liposomes have been successful in delivering anti-cancer, anti-fungal, antibiotic, anesthetic, anti-inflammatory, and gene-based drugs. By careful design, long-circulating (e.g. by PEGylation), triggered release, and ligand-targeted delivery is obtained *in vivo*.<sup>38</sup>

As a drug delivery system, lipid-based nanomedicines such as liposomes possess multiple advantages: (i) liposomes can deliver both hydrophobic and hydrophilic molecules due to their amphiphilic lipid molecules that self-assemble into a hydrophilic core and a hydrophobic lipid layer; (ii) lipids are non-toxic and biodegradable; the large pool of lipid varieties enable us to manipulate the liposome structures and properties to achieve different goals by changing the lipid types and ratios; (iii) liposomes exhibit higher tissue accumulation through the enhanced permeability and retention (EPR) effect and better pharmacokinetics, which leads to enhanced therapeutic efficacy and reduced toxicity; (iv) liposomes protect the encapsulated drug, improving drug stability and prolonging its circulation half-life; (v) the large surface of liposomes could be further decorated with different functional moieties (polymers, ligands, and antibodies) to construct targeting and controlled-release drug delivery systems.<sup>38-40</sup> In summary, lipid-based nanomedicines have a proven track record in the successful delivery of a wide range of therapeutics for various diseases.

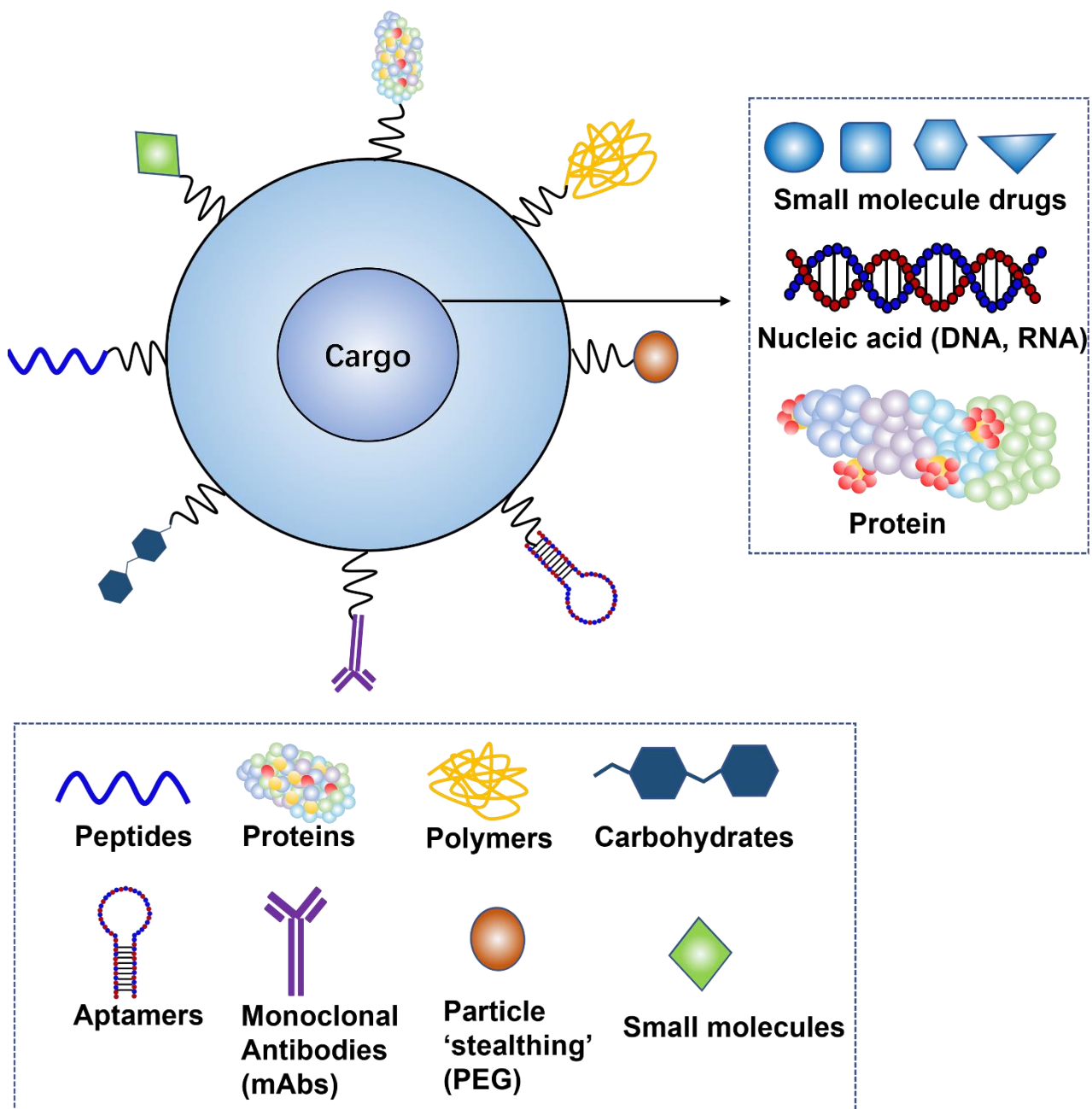


**Figure 2.** The schematic representation of engineered nanomedicines. The various surface modifications that are commonly pre-engineered could specifically target cells, and the types of encapsulated cargos are highlighted.

### 1.3 RNA therapy

Gene therapy has attracted attention over the last decades, as it possesses the potential to treat a genetic disorder from its origins by counteracting or replacing a malfunctioning gene within the cells adversely affected by the condition.<sup>41</sup> Genetic cargo containing DNA, mRNA, small interfering RNA (siRNA), and microRNA (miRNA) mimics, can either express specific genes, knockdown gene expression, or upregulate target genes via several mechanisms.<sup>42</sup> For DNA therapy, once the DNA cargo is internalized into target cells and released into the cytoplasm, it still needs to undergo nuclear trafficking and transcription into RNA, and its functionality depends on the nuclear envelope breakdown during cell division; this represents a major hurdle to DNA delivery efficacy.<sup>43, 44</sup> In contrast, RNA delivery is relatively simple as it only needs to reach the cytoplasm of cells to be functional and typically (m)RNA is less immunogenic compared to DNA.

Messenger RNA (mRNA) has recently come into focus as a potential new drug class to deliver genetic information, which provides tremendous flexibility and a broad therapeutic utility.<sup>45</sup> Potential applications include protein replacement therapies, vaccines, and gene editing (**Fig. 3**).

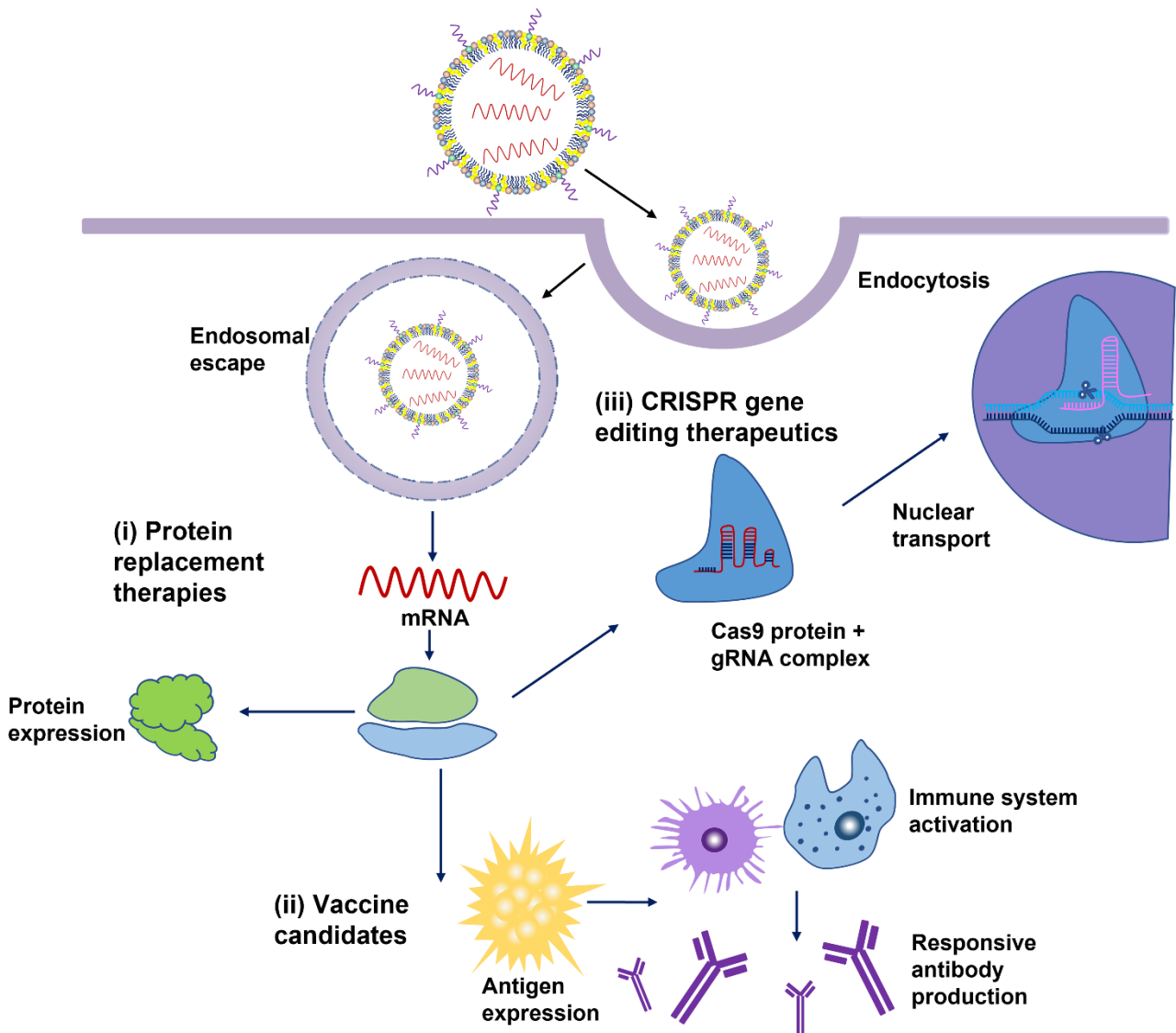


**Figure 3.** Therapeutic applications of mRNA-nanomedicines include: (i) protein replacement therapies, (ii) vaccine candidates, and (iii) CRISPR gene editing therapeutics.

The development of *in vitro*-transcribed (IVT)-mRNA-based therapeutics has the following advantages: (i) mRNA has no potential risk of insertional mutagenesis since it does not integrate into the genome; (ii) mRNA degradation can be achieved by physiological metabolic pathways; (iii) industrial production of IVT mRNA is relatively simple and inexpensive.<sup>46</sup> The IVT-mRNA produced from a plasmid DNA backbone contains a 5' cap, a 5' untranslated sequence (UTR), an open reading frame coding for the protein of interest, a 3' UTR, and a poly(A) tail (**Fig. 4**), all of these fragments can influence mRNA stability and translation.<sup>46, 47</sup>

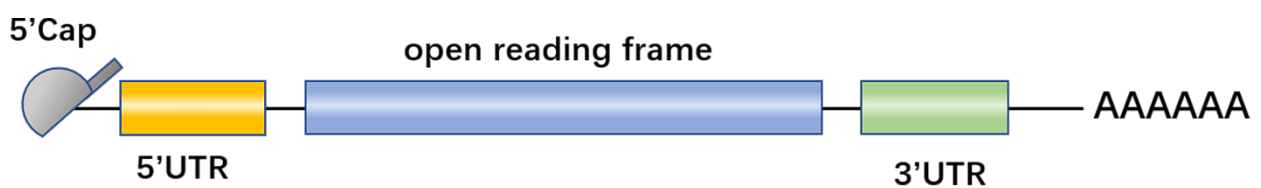


**Figure 4.** The key structural elements of *in vitro*-transcribed (IVT) mRNA.

### 1.3.1 mRNA as a protein replacement therapy

Genetic disorders originate from inherited or acquired gene mutations, resulting in abnormal protein expression.<sup>48</sup> Using IVT mRNA as a therapeutic drug to express a desired protein is the most straightforward application. The therapeutic proteins translated by mRNA are generally engineered to display low immunogenicity, prolonged stability, and efficient expression.<sup>44</sup> mRNA exerts its effect at the cytoplasm and expresses protein transiently and degrades via extracellular ribonucleases easily, which avoids the adverse effect of permanent expression. Therapeutic mRNA can be applied to restore the malfunction of a single defined protein caused by rare monogenic diseases, and it can be translated to modulate cellular behavior by expressing transcription of growth factors like vascular endothelial growth factor (VEGF) and cystic fibrosis transmembrane conductance regulator (CFTR).<sup>49</sup>

mRNA as a therapeutic has been studied to treat a range of hereditary or acquired metabolic diseases and regenerative medicine.<sup>50</sup> For example, in a mouse model of a lethal congenital lung disease caused by surfactant protein B (SP-B) deficiency, local delivery of modified SP-B mRNA to the lung greatly restored wild-type SP-B expression, and treated mice survived.<sup>51</sup> In another study intramyocardial injection of modified mRNA encoding human vascular endothelial growth factor A (VEGF-A) improved heart regeneration in the myocardial infarction mice model.<sup>52</sup> Finally, sustained mRNA delivery expressing therapeutic human  $\alpha$ -galactosidase protein resulted in clinically relevant biomarker reduction in a mouse Fabry disease model.<sup>53</sup>

### 1.3.2 mRNA vaccines

Vaccines play a critical role in maintaining global health by preventing infection and transmission of multiple diseases worldwide. Vaccines work by exposing a patient to a part or whole pathogen, thus activating the immune system of the subject.<sup>54</sup> Traditional vaccines include live-attenuated, inactivated, and replication-defective pathogens as well as subunit and conjugate vaccines.<sup>55</sup> Traditional vaccine technologies have been used across a wide range of bacterial and viral pathogens, and the widespread utilization of clinically approved live-attenuated vaccines completely eradicated the smallpox virus and greatly reduced the incidences of polio, measles-mumps-rubella (MMR), yellow fever, and other childhood diseases.<sup>56</sup> However, they have not been successful in some diseases such as persistent infections, rapidly evolving pathogens with high sequence variability, complex viral antigens, and emerging pathogens.<sup>54</sup> The newly emerging infectious virus outbreaks require rapid vaccine technology development and large-scale production, and non-infectious disease like cancer also demand novel vaccine technology since conventional approaches are not applicable. Thus, novel vaccine platforms are highly needed.

Recently, novel *in vitro*-transcribed (IVT) mRNA vaccine technology offers the potential to revolutionize vaccine development as they are well-suited to address the limitations of existing conventional vaccine technology, especially as vaccine platforms against infectious diseases and several types of cancer.<sup>46</sup> mRNA-based vaccines possess multiple advantages over conventional vaccines. First, multiple proteins can be translated: mRNA can be engineered to translate into different

types of proteins to act as antigens to stimulate immune responses.<sup>57, 58</sup> Second, safety: mRNA translation is achieved by the ribosomes in the cytoplasm, requiring no need to enter the nucleus, thus efficacy can be greatly enhanced compared to DNA-based vaccines, which also rule out the potential risk to integrate into genomes.<sup>57, 58</sup> Third, efficacy: diversified modification and delivery vectors can enhance the stability and translation efficiency of mRNA.<sup>57, 58</sup> The functional carriers enable the rapid uptake and efficient expression of mRNA in the cytoplasm and can be administered repeatedly. Finally, production: mRNA vaccines are capable of rapid and large-scale manufacturing with the *in vitro* transcription technology advances greatly boosting the process of vaccine development.<sup>57, 58</sup> Researchers have successfully adopted mRNA vaccines to elicit protective immunity against many infectious diseases (*e.g.* Zika virus, powassan virus, HIV-1 virus, influenza virus) in animal models with the technology of LNP-mRNA delivery tools.<sup>59-62</sup>

**Table 2.** Representative clinical trials of lipid nanoparticle-mRNA therapeutics against infections, cancer, and genetic disorders

Name	Disease	Encoded protein	Administration route	ClinicalTrials.gov identifier	Phase
<b>Infections</b>					
CVnCoV	SARS-CoV-2	Spike	i.m.	NCT04652102	III
LNP-nCoVsaRNA	SARS-CoV-2	Spike	i.m.	ISRCTN17072692	I
ARCT-021	SARS-CoV-2	Spike	i.m.	NCT04728347	II
ARCoV	SARS-CoV-2	Receptors-binding domain	i.m.	ChiCTR2000034112	I
mRNA-1440	Influenza H10N8	Haemagglutinin	i.m.	NCT03076385	I
mRNA-1851	Influenza H7N9	Haemagglutinin	i.m.	NCT03345043	I
mRNA-1893	Zika virus	Pre-membrane and envelope glycoproteins	i.m.	NCT040649-5	I
mRNA-1345	Respiratory syncytial virus	F glycoproteins	i.m.	NCT04528719	I
mRNA-1653	Metapneumovirus and parainfluenza virus type 3 (MPV/PIV3)	MPV and PIV3 F glycoproteins	i.m.	NCT03392389	I
mRNA-1647	Cytomegalovirus	Pentameric complex and B glycoproteins	i.m.	NCT04232280	II
mRNA-1388	Chikungunya virus	Chikungunya virus antigens	i.m.	NCT03325075	I
CV7202	Rabies virus	G glycoproteins	i.m.	NCT03713086	I
mRNA-1944	Chikungunya virus	Antibody against chikungunya virus	i.v.	NCT03829348	I
<b>Cancer</b>					
mRNA-5671/V941	Non-small-cell lung cancer, colorectal cancer, pancreatic adenocarcinoma	KRAS antigens	i.m.	NCT03948763	I
mRNA-4157	Melanoma	Personalized neoantigens	i.m.	NCT03897881	II
mRNA-4650	Gastrointestinal cancer	Personalized neoantigens	i.m.	NCT03480152	I/II
FixVac	Melanoma	NY-ESO-1, tyrosinase, MAGE-A3, TPTE	i.v.	NCT02410733	I
TNBC-MERIT	Triple-negative breast cancer	Personalized neoantigens	i.v.	NCT02316457	I
HARE-40	HPV-positive cancers	HPV oncoproteins E6 and E7	i.d.	NCT03418480	I/II
RO7198457	Melanoma	Personalized neoantigens	i.v.	NCT03815058	II
W_ova1	Ovarian cancer	Ovarian cancer antigens	i.v.	NCT04163094	I
<b>Genetic disorders</b>					
mRNA-3704	Methylmalonic acidaemia	Methylmalonyl-CoA mutase	i.v.	NCT03810690	I/II
mRNA-3927	Propionic acidaemia	Propionyl-CoA carboxylase	i.v.	NCT04159103	I/II
MRT5201	Ornithine transcarbamylase deficiency	Ornithine transcarbamylase	i.v.	NCT03767270	I/II
MRT5005	Cystic fibrosis	Cystic fibrosis transmembrane conductance regulator	Inhalation	NCT03375047	I/II
NTLA-2001	Transthyretin amyloidosis with polyneuropathy	CRIPR-Cas9 gene editing system	i.v.	NCT04601051	I

HPV, human papillomavirus; i.m., intramuscular; i.v., intravenous; KRAS, Kirsten rat sarcoma 2 viral oncogene homologue; MAGE-A3, melanoma antigen family A; NY-ESO-1, New York esophageal squamous cell carcinoma; SARS-CoV-2, severe acute syndrome coronavirus 2; TPTE, putative tyrosine-protein phosphatase; CoA, coenzyme A; CRISPR-Cas9, clustered regularly interspaced short palindromic repeats (CRISPR)-CRISPR associated protein 9.

## 1.4 mRNA delivery with lipid nanoparticles

mRNA is very large (300–5,000 kDa, ~1–15 kb), hydrophilic, and membrane impermeable due to its negative charges. Furthermore, mRNA is inherently unstable and susceptible to endonuclease degradation with an intracellular half-life < 7 hours.<sup>63</sup> RNA delivery needs to overcome multiple barriers, such as enzymatic degradation, uptake by the reticuloendothelial system, lack of selective tissue accumulation, kidney filtration, and limited intracellular entry and endosomal escape.<sup>64</sup> An ideal mRNA delivery vector must therefore protect against serum endonucleases, evade immune detection, prevent nonspecific interactions, avoid renal clearance, and promote cell entry.<sup>42</sup>

Developing safe and effective gene vectors has been the main focus. Gene vectors can be categorized into two major classes: viral and nonviral vectors. In fact, ~70% of gene therapy clinical trials carried out so far have used modified viruses such as retroviruses, lentiviruses, adenoviruses, and adeno-associated viruses (AAVs).<sup>42</sup> Viral vectors can efficiently transduce mammalian cells, however, the potential carcinogenesis,<sup>65</sup> immunogenicities,<sup>66</sup> broad tropisms,<sup>67</sup> limited packaging capacity, and difficult industrial manufacturing limited their wide applications.<sup>68</sup> Non-viral vectors could overcome those limitations with different biomaterial designs and modifications, including lipids, lipid-like materials, polymers, and inorganic nanoparticles.<sup>45</sup>

Lipid-based nanocarriers are the oldest and most commonly used vector for nucleic acid delivery.<sup>42, 69-71</sup> Initially, permanent cationic lipids were used to encapsulate and transfect RNA to target cells. The positively charged (cationic) amine head groups form an electrostatic complex with the negatively charged RNA, permitting compaction of the RNA in the core of the lipid-based nanoparticles.<sup>72</sup> However, these cationic liposomes often suffered from poor pharmacokinetics, cellular toxicity, aggregation with erythrocytes, recruitment of the immune response (interaction with Toll-like receptor or other intracellular proteins), and rapid plasma clearance.<sup>71, 73, 74</sup> Thus, lipid nanoparticles composing ionizable lipids with less toxicity were designed to encapsulate RNA. These lipids are charged at mildly acidic pH and form a complex with RNA to assemble into stable lipid-nanoparticles (LNPs) that are neutral under physiological pH conditions.<sup>71</sup> These LNPs consist of both amorphous and lamellar core structures, whereas the core structure contains a mixture of amorphous, unilamellar, and polymorphic structures.<sup>75, 76</sup> They possess no extra charges, therefore they are exempt from maintaining the balance of the charges and transfection efficacy. They have been considered the most advanced methods for RNA-based therapeutics, as evidenced by the clinical approvals of three LNP formulations, Alnylam's Patisiran (ONPATRO™), Pfizer's BNT162b2 and Moderna's mRNA-1273.<sup>77</sup> Many other lipid nanoparticle-mRNA formulations have been developed and are under clinical evaluation for the prevention and treatment of virus infections, cancer, and genetic diseases (**Table 2**).<sup>42, 47, 48, 50, 54, 78-84</sup>

LNPs are composed of (i) an ionizable lipid or cationic lipid or polymeric biomaterials bearing tertiary or quaternary amines that can efficiently condense mRNA; (ii) a zwitterionic lipid that serves as a helper lipid to enhance stability and fusogenicity, such as DSPC, DOPE; (iii) cholesterol or cholesterol analogs to stabilize the formulation by modulating membrane integrity and rigidity; (iv) a polyethylene glycol (PEG)-lipid to enhance the stability by decreasing particle aggregation, and to prolong blood circulation time.<sup>80, 85</sup>

After administration, there are multiple extracellular and intracellular barriers awaiting LNP-mRNA formulations to overcome in order to function *in vivo* (**Fig. 5**).<sup>45, 50, 80</sup> First, mRNA needs to be protected from extracellular ribonucleases abundantly present in blood and skin after systemic or local delivery.<sup>45, 50, 80</sup> Second, LNPs should avoid clearance by renal glomerular filtration and the mononuclear phagocyte system (MPS).<sup>45, 50, 80</sup> Third, LNPs need to reach the target tissue and organs, cross the cell membrane, and be internalized by the target cells.<sup>45, 50, 80</sup> Finally, the mRNA must escape from endo/lysosomes, and be transported into the cytoplasm.<sup>45, 50, 80</sup>

Lipid nanoparticle-mRNA formulations are usually manufactured by rapid microfluidic mixing where mRNA is encapsulated in the interior core through electrostatic interactions with the ionizable lipids.<sup>47, 86</sup> This stable nanostructure protects mRNA molecules from nuclease degradation in physiological fluids.<sup>47, 86</sup> The PEG-lipids reduce recognition by the MPS and clearance by renal filtration, improving the stability and circulation lifetime of LNPs.<sup>47, 87, 88</sup> The targeted delivery of LNP-mRNA can be improved by modifying and optimizing the nanoparticles, for example, selective organ targeting (lung, spleen, and liver, respectively) can be achieved by the addition of supplemental molecules.<sup>89</sup> Moreover, surface modification of nanoparticles with targeting moieties (*e.g.* antibodies) can also be engineered to deliver mRNA into inflammatory leukocytes for treating inflammatory bowel disease,<sup>90</sup> and targeting epidermal growth factor receptor (EGFR)-positive tumor cells for cancer treatments.<sup>91</sup> Once LNP-mRNA reaches target cells, they are usually internalized by cells through multiple endocytosis mechanisms depending on nanoparticles' properties and cell types, including macropinocytosis and clathrin-mediated and caveolae-mediated endocytosis.<sup>47, 92-94</sup> After cellular internalization, LNP-mRNA needs to escape from the endosome into the cytoplasm, which is crucial for effective mRNA delivery and translation into the corresponding protein.<sup>95-97</sup>

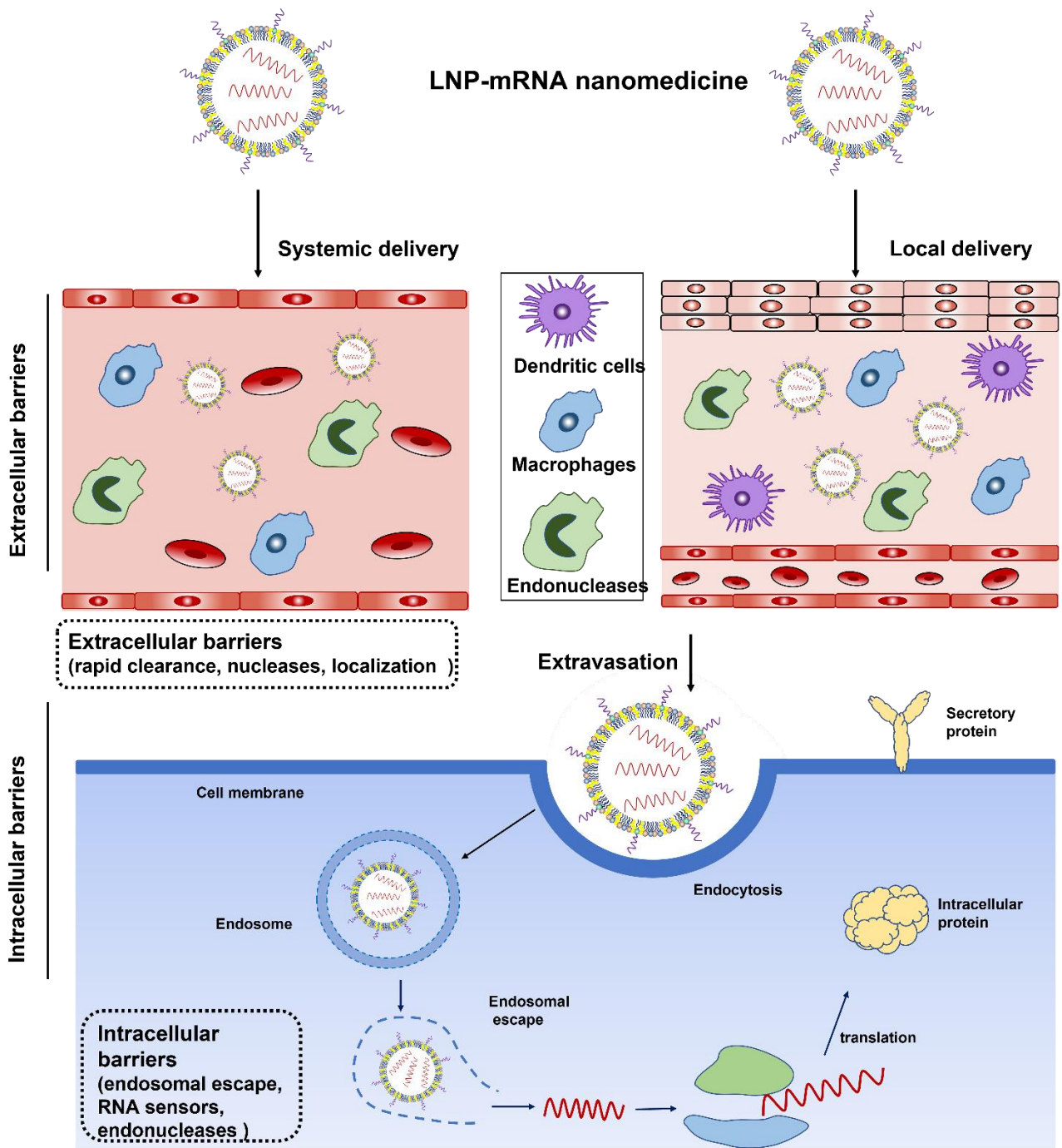


**Figure 5.** Physiological barriers (extracellular and intracellular) for lipid nanoparticle–mRNA (LNP–mRNA) nanomedicine after systemic and local delivery.

## 1.5 Endosomal escape

LNPs gain entry into the cells by exploiting membrane-derived endocytic pathways, the genetic cargo accumulates in the early endosome, which acts as a sorting and recycling organelle from which genetic cargo should rapidly escape into the cytosol to avoid progressive and fatal degradation.<sup>98</sup> Their transfection performance depends on this endo/lysosomal escape efficiency. Studies showed that only <2% of siRNA delivered by LNPs was able to escape endosomal compartments into the

cytoplasm.<sup>95</sup> For mRNA it was found that less than 5% delivered by LNPs was able to reach the cytoplasm.<sup>99</sup> In general, LNP enter cells via the formation of early endosomes (EE), where the pH gradually lowers from 6.5 to 5.5. Maturation into late endosomes further lowers the pH 5.5-5.0. Finally, LNPs fuse with lysosomes with pH down to 4.5-5.5, where multiple enzymes (lipases, nucleases, glycosidase, proteases, phosphatases, sulfatases) dismantle the LNP assembly.<sup>100</sup>

The delivery vectors are considered able to escape from endosomes through the proton sponge effect, the buffering capacity attenuates the decline of acidic endosomal pH, thus driving the osmotic pressure increase and ultimate endosomal rupture.<sup>64, 101, 102</sup> Current research is focused on amplifying endosomal escape and minimizing the toxicity of delivery vectors, therefore achieving satisfactory transfection performances. To accomplish these challenging goals, new materials have been designed, which are responsive to external stimuli, such as light, redox state, enzymes, and pH.<sup>103</sup> For LNPs, optimizing the pKa of ionizable lipids, using branched tails and biodegradable lipids, modulating the type (*e.g.* cholesterol, helper lipids [DSPC, DOPE]) and the ratio of lipids have been reported to increase the endosomal escape.<sup>76, 93, 104-113</sup>

## 1.6 Membrane fusion

Membrane fusion, one of the most fundamental processes in life, mediates housekeeping functions—endocytosis, constitutive secretion, and recycling of membrane components.<sup>114</sup> It underlies many cellular activities, such as viral infection, fertilization, and neurotransmitter release, and usually occurs when two separate lipid membranes merge into a single continuous bilayer.<sup>115</sup> The most typical membrane fusion is exocytosis, whereby an incoming vesicle docks to the membrane, opposing membranes are connected forming a hemifusion stalk, then fusion pores expand to release their contents (*e.g.* hormones or neurotransmitters) into the extracellular milieu, or to deposit receptors, transporters, channels or adhesion molecules into the limiting membrane.<sup>116, 117</sup>

Unlike typical endocytosis which needs to undergo endosome/lysosome degradation after internalization, membrane fusion has been recognized as able to overcome endosomal entrapment by driving direct fusion with the plasma membrane and subsequent delivery into the cytosol (**Fig. 6**).<sup>118</sup> With membrane fusion, the delivery efficiency of nanomedicine could be greatly improved. Among membrane fusion machinery components, SNARE (soluble N-ethylmaleimide-sensitive factor attachment protein receptor) proteins have been well-characterized and identified as critical components for multiple processes.<sup>119</sup> Inspired by SNARE proteins, our lab has innovated artificial coiled-coil peptides that could mediate efficient liposomal delivery with enhanced therapeutic effect.<sup>120-122</sup>

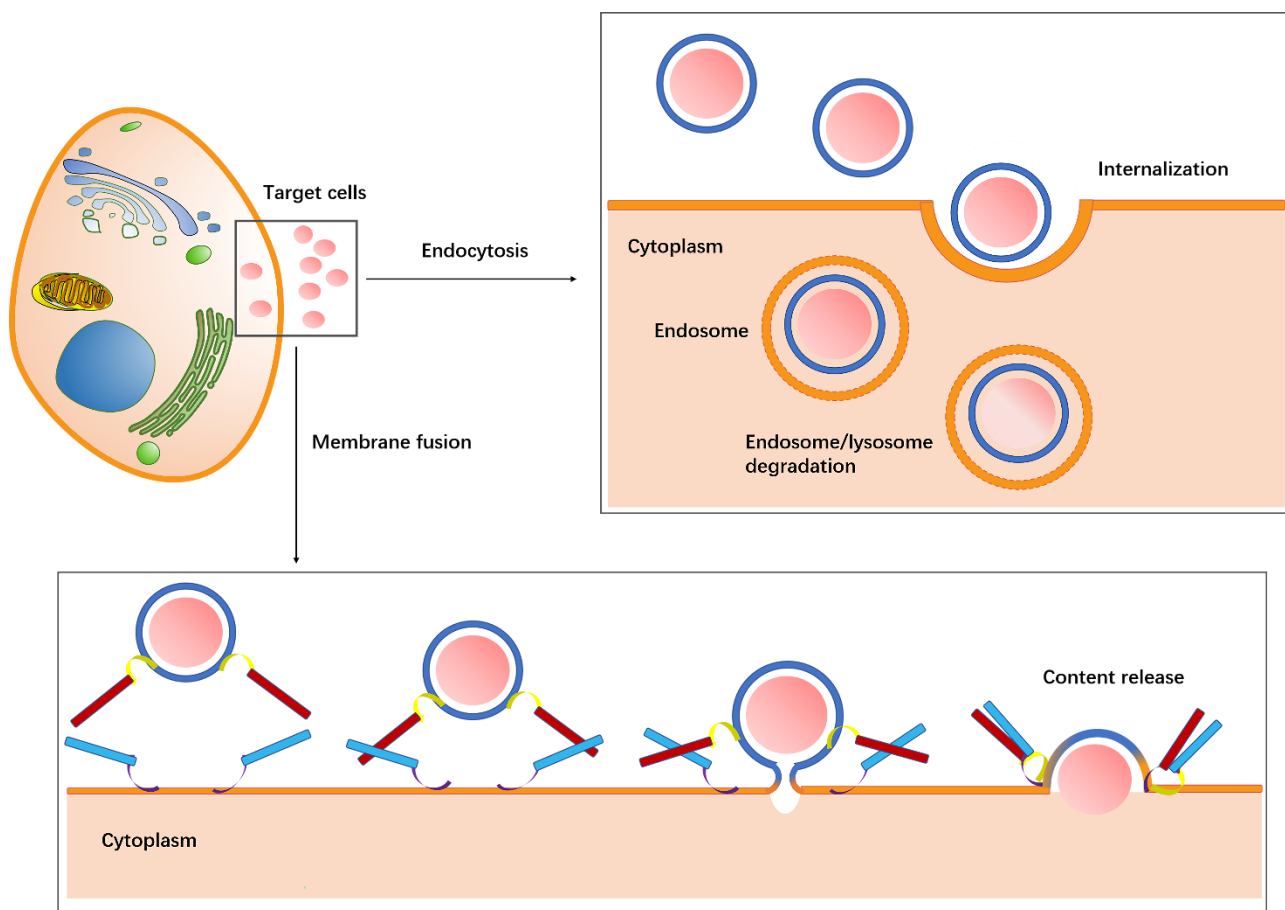


**Figure 6.** Cellular uptake differences between endocytosis and membrane fusion.

## 1.7 Aim and outline of this thesis

This thesis focuses on the application of lipid-based nanomedicine in drug delivery, including small molecular antitumor drugs and biomacromolecules including mRNA, and evaluates their biological performance. We have modified liposomes and LNPs with fusogenic coiled-coil peptides to enhance the drug/mRNA delivery efficiency (**Chapter 2-4**), and also investigated how the lipid composition of LNPs influences the immune response (**Chapter 5**).

In **Chapter 2** fusogenic coiled-coil peptides are used to facilitate mRNA delivery *in vitro*. By modifying LNPs with coiled-coil peptides, we show that enhanced transfection efficiency can be achieved independent of cell type. This study shows that the fusogenic coiled-coil LNP system enhances mRNA transfection and holds great promise for future mRNA-based therapies.

In **Chapter 3** we will demonstrate that a coiled-coil peptide dimer facilitates drug delivery within cells and is mainly driven by membrane fusion. By careful peptide dimer design, we investigated their structural differences, membrane binding affinity, cellular uptake efficiency, and pharmacological effects after encapsulating antitumor drugs. It was shown that the parallel PK4 dimer induces the highest cellular uptake, and superior antitumor efficacy compared to the other designs. This study offers important mechanistic insights into the design of coiled-coil driven membrane

fusion systems and also provided novel strategies to develop peptide-based biomaterials to induce improved drug delivery efficiency.

In **Chapter 4**, we further applied the coiled-coil peptide modified LNP to transfect the human-induced pluripotent stem cell-derived cardiomyocytes (iPSC-CMs). Different incubation methods of coiled-coil peptide modified LNPs are compared and a novel 1-step incubation protocol is developed resulting in a high mRNA transfection efficiency. Furthermore, the enhanced mRNA transfection was independent of LNP lipid composition when following the 1-step incubation protocol. This study forms the basis of future *in vivo* research towards the development of efficient cardiomyocyte transfection and stimulation of cardiac repair and ultimately regeneration to rescue the ischemic myocardium.

In **Chapter 5**, we evaluated the influence of lipid compositions of LNPs on immune responses by studying a panel of LNP formulations. This was done by keeping the ionizable lipids constant, replacing cholesterol with  $\beta$ -sitosterol, and changing the fusogenic helper lipid DOPE content. We studied the ability of this LNP library to induce antigen presentation and T cell proliferation, and identified four leading LNP formulations (C12-200-cho-10%DOPE, C12-200-sito-10%DOPE, cKK-E12-cho-10%DOPE and cKK-E12-sito-30%DOPE) that induced robust T cell proliferation and enhanced IFN- $\gamma$ , TNF- $\alpha$ , IL-2 expression. This study proved that T cell proliferation is strongly dependent on LNP composition.

**Chapter 6** summarizes the main finding of this thesis and discusses the future perspectives about the coiled-coil peptides modified nanomedicines and their use in mRNA-based therapies.

## 1.8 References

1. Ulldemolins, A.; Seras-Franzoso, J.; Andrade, F.; Rafael, D.; Abasolo, I.; Gener, P.; Schwartz, S., Jr., Perspectives of nano-carrier drug delivery systems to overcome cancer drug resistance in the clinics. (2578-532X (Electronic)).
2. Shi, J.; Votruba, A. R.; Farokhzad, O. C.; Langer, R., Nanotechnology in Drug Delivery and Tissue Engineering: From Discovery to Applications. *Nano Letters* **2010**, *10* (9), 3223-3230.
3. Riehemann, K.; Schneider, S. W.; Luger, T. A.; Godin, B.; Ferrari, M.; Fuchs, H., Nanomedicine—Challenge and Perspectives. *Angewandte Chemie International Edition* **2009**, *48* (5), 872-897.
4. Kim, B. Y. S.; Rutka, J. T.; Chan, W. C. W., Nanomedicine. *New England Journal of Medicine* **2010**, *363* (25), 2434-2443.
5. Pelaz, B.; Alexiou, C.; Alvarez-Puebla, R. A.; Alves, F.; Andrews, A. M.; Ashraf, S.; Balogh, L. P.; Ballerini, L.; Bestetti, A.; Brendel, C.; Bosi, S.; Carril, M.; Chan, W. C. W.; Chen, C.; Chen, X.; Chen, X.; Cheng, Z.; Cui, D.; Du, J.; Dullin, C.; Escudero, A.; Feliu, N.; Gao, M.; George, M.; Gogotsi, Y.; Grünweller, A.; Gu, Z.; Halas, N. J.; Hampp, N.; Hartmann, R. K.; Hersam, M. C.; Hunziker, P.; Jian, J.; Jiang, X.; Jungebluth, P.; Kadhiresan, P.; Kataoka, K.; Khademhosseini, A.; Kopeček, J.; Kotov, N. A.; Krug, H. F.; Lee, D. S.; Lehr, C.-M.; Leong, K. W.; Liang, X.-J.; Ling Lim, M.; Liz-Marzán, L. M.; Ma, X.; Macchiarini, P.; Meng, H.; Möhwald, H.; Mulvaney, P.; Nel, A. E.; Nie, S.; Nordlander, P.; Okano, T.; Oliveira, J.; Park, T. H.; Penner, R. M.; Prato, M.; Puntès, V.; Rotello, V. M.; Samarakoon, A.; Schaak, R. E.; Shen, Y.; Sjöqvist, S.; Skirtach, A. G.; Soliman, M. G.;

- Stevens, M. M.; Sung, H.-W.; Tang, B. Z.; Tietze, R.; Udugama, B. N.; VanEpps, J. S.; Weil, T.; Weiss, P. S.; Willner, I.; Wu, Y.; Yang, L.; Yue, Z.; Zhang, Q.; Zhang, Q.; Zhang, X.-E.; Zhao, Y.; Zhou, X.; Parak, W. J., Diverse Applications of Nanomedicine. *ACS Nano* **2017**, *11* (3), 2313-2381.
6. Bangham, A. D.; Horne, R. W., Negative staining of phospholipids and their structural modification by surface-active agents as observed in the electron microscope. *Journal of Molecular Biology* **1964**, *8* (5), 660-IN10.
  7. Langer, R.; Folkman, J., Polymers for the sustained release of proteins and other macromolecules. *Nature* **1976**, *263* (5580), 797-800.
  8. Matsumura, Y.; Maeda, H., A New Concept for Macromolecular Therapeutics in Cancer Chemotherapy: Mechanism of Tumor-tropic Accumulation of Proteins and the Antitumor Agent Smancs1. *Cancer Research* **1986**, *46* (12\_Part\_1), 6387-6392.
  9. Davis, M. E., The First Targeted Delivery of siRNA in Humans via a Self-Assembling, Cyclodextrin Polymer-Based Nanoparticle: From Concept to Clinic. *Molecular Pharmaceutics* **2009**, *6* (3), 659-668.
  10. Barenholz, Y., Doxil® — The first FDA-approved nano-drug: Lessons learned. *Journal of Controlled Release* **2012**, *160* (2), 117-134.
  11. Weissig, V.; Pettinger, T. K.; Murdock, N., Nanopharmaceuticals (part 1): products on the market. (1178-2013 (Electronic)).
  12. Weissig, V.; Guzman-Villanueva, D., Nanopharmaceuticals (part 2): products in the pipeline. (1178-2013 (Electronic)).
  13. Bernabeu, E.; Cagel, M.; Lagomarsino, E.; Moretton, M.; Chiappetta, D. A., Paclitaxel: What has been done and the challenges remain ahead. *International Journal of Pharmaceutics* **2017**, *526* (1), 474-495.
  14. Gref, R.; Minamitake, Y.; Peracchia, M. T.; Trubetsky, V.; Torchilin, V.; Langer, R., Biodegradable Long-Circulating Polymeric Nanospheres. *Science* **1994**, *263* (5153), 1600-1603.
  15. Leserman, L. D.; Barbet, J.; Kourilsky, F.; Weinstein, J. N., Targeting to cells of fluorescent liposomes covalently coupled with monoclonal antibody or protein A. *Nature* **1980**, *288* (5791), 602-604.
  16. Menjoge, A. R.; Kannan, R. M.; Tomalia, D. A., Dendrimer-based drug and imaging conjugates: design considerations for nanomedical applications. *Drug Discovery Today* **2010**, *15* (5), 171-185.
  17. Forssen, E. A., The design and development of DaunoXome® for solid tumor targeting in vivo. *Advanced Drug Delivery Reviews* **1997**, *24* (2), 133-150.
  18. Murry, D. J.; Blaney, S. M., Clinical Pharmacology of Encapsulated Sustained-Release Cytarabine. *Annals of Pharmacotherapy* **2000**, *34* (10), 1173-1178.
  19. Leonard, R. C. F.; Williams, S.; Tulpule, A.; Levine, A. M.; Oliveros, S., Improving the therapeutic index of anthracycline chemotherapy: Focus on liposomal doxorubicin (Myocet™). *The Breast* **2009**, *18* (4), 218-224.
  20. Alphandéry, E.; Grand-Dewyse, P.; Lefèvre, R.; Mandawala, C.; Durand-Dubief, M., Cancer therapy using nanoformulated substances: scientific, regulatory and financial aspects. *Expert Review of Anticancer Therapy* **2015**, *15* (10), 1233-1255.
  21. Webb, M. S.; Harasym, T. O.; Masin, D.; Bally, M. B.; Mayer, L. D., Sphingomyelin-cholesterol liposomes significantly enhance the pharmacokinetic and therapeutic properties of vincristine in murine and human tumour models. *British Journal of Cancer* **1995**, *72* (4), 896-904.
  22. Drummond, D. C.; Noble, C. O.; Guo, Z.; Hong, K.; Park, J. W.; Kirpotin, D. B., Development of a Highly Active Nanoliposomal Irinotecan Using a Novel Intraliposomal Stabilization Strategy. *Cancer Research* **2006**, *66* (6), 3271-3277.
  23. Lister, J., Amphotericin B Lipid Complex (Abelcet®) in the treatment of invasive mycoses: the North American experience. *European Journal of Haematology* **1996**, *56* (S57), 18-23.
  24. Stone, N. R. H.; Bicanic, T.; Salim, R.; Hope, W., Liposomal Amphotericin B (AmBisome®): A Review of the Pharmacokinetics, Pharmacodynamics, Clinical Experience and Future Directions. *Drugs* **2016**, *76* (4), 485-500.

25. Guo, L. S. S.; Fielding, R. M.; Lasic, D. D.; Hamilton, R. L.; Mufson, D., Novel antifungal drug delivery: stable amphotericin B-cholesteryl sulfate discs. *International Journal of Pharmaceutics* **1991**, *75* (1), 45-54.
26. Alam, M.; Hartrick, C. T., Extended-Release Epidural Morphine (DepoDur™): An Old Drug with a New Profile. *Pain Practice* **2005**, *5* (4), 349-353.
27. Angst, M. S.; Drover, D. R., Pharmacology of Drugs Formulated with DepoFoam™. *Clinical Pharmacokinetics* **2006**, *45* (12), 1153-1176.
28. Clarke, P. D.; Adams, P.; Ibáñez, R.; Herzog, C., Rate, intensity, and duration of local reactions to a virosome-adjuvanted vs. an aluminium-adsorbed hepatitis A vaccine in UK travellers. *Travel Medicine and Infectious Disease* **2006**, *4* (6), 313-318.
29. Glück, R.; Metcalfe, I. C., New technology platforms in the development of vaccines for the future. *Vaccine* **2002**, *20*, B10-B16.
30. Bulbake, U.; Doppalapudi, S.; Kommineni, N.; Khan, W., Liposomal Formulations in Clinical Use: An Updated Review. *Pharmaceutics* **2017**, *9* (2).
31. Ventola, C. L., Progress in Nanomedicine: Approved and Investigational Nanodrugs. (1052-1372 (Print)).
32. Shi, J.; Kantoff, P. W.; Wooster, R.; Farokhzad, O. C., Cancer nanomedicine: progress, challenges and opportunities. *Nature Reviews Cancer* **2017**, *17* (1), 20-37.
33. Verbeke, R.; Lentacker, I.; De Smedt, S. C.; Dewitte, H., The dawn of mRNA vaccines: The COVID-19 case. *Journal of Controlled Release* **2021**, *333*, 511-520.
34. Akinc, A.; Maier, M. A.; Manoharan, M.; Fitzgerald, K.; Jayaraman, M.; Barros, S.; Ansell, S.; Du, X.; Hope, M. J.; Madden, T. D.; Mui, B. L.; Semple, S. C.; Tam, Y. K.; Ciufolini, M.; Witzigmann, D.; Kulkarni, J. A.; van der Meel, R.; Cullis, P. R., The Onpatro story and the clinical translation of nanomedicines containing nucleic acid-based drugs. *Nature Nanotechnology* **2019**, *14* (12), 1084-1087.
35. Ferrari, M., Frontiers in cancer nanomedicine: directing mass transport through biological barriers. *Trends in Biotechnology* **2010**, *28* (4), 181-188.
36. Zhang, C.; Yan, L.; Wang, X.; Zhu, S.; Chen, C.; Gu, Z.; Zhao, Y., Progress, challenges, and future of nanomedicine. *Nano Today* **2020**, *35*, 101008.
37. Petros, R. A.; DeSimone, J. M., Strategies in the design of nanoparticles for therapeutic applications. *Nature Reviews Drug Discovery* **2010**, *9* (8), 615-627.
38. Allen, T. M.; Cullis, P. R., Liposomal drug delivery systems: From concept to clinical applications. *Advanced Drug Delivery Reviews* **2013**, *65* (1), 36-48.
39. Grimaldi, N.; Andrade, F.; Segovia, N.; Ferrer-Tasies, L.; Sala, S.; Veciana, J.; Ventosa, N., Lipid-based nanovesicles for nanomedicine. *Chemical Society Reviews* **2016**, *45* (23), 6520-6545.
40. Filipczak, N.; Pan, J.; Yalamarty, S. S. K.; Torchilin, V. P., Recent advancements in liposome technology. *Adv Drug Deliv Rev* **2020**, *156*, 4-22.
41. Naldini, L., Gene therapy returns to centre stage. *Nature* **2015**, *526* (7573), 351-360.
42. Yin, H.; Kanasty, R. L.; Eltoukhy, A. A.; Vegas, A. J.; Dorkin, J. R.; Anderson, D. G., Non-viral vectors for gene-based therapy. *Nature Reviews Genetics* **2014**, *15* (8), 541-555.
43. Buck, J.; Grossen, P.; Cullis, P. R.; Huwyler, J.; Witzigmann, D., Lipid-Based DNA Therapeutics: Hallmarks of Non-Viral Gene Delivery. *ACS Nano* **2019**, *13* (4), 3754-3782.
44. Sahin, U.; Karikó, K.; Türeci, Ö., mRNA-based therapeutics — developing a new class of drugs. *Nature Reviews Drug Discovery* **2014**, *13* (10), 759-780.
45. Hajj, K. A.; Whitehead, K. A., Tools for translation: non-viral materials for therapeutic mRNA delivery. *Nature Reviews Materials* **2017**, *2* (10), 17056.
46. Pardi, N.; Hogan, M. J.; Porter, F. W.; Weissman, D., mRNA vaccines — a new era in vaccinology. *Nature Reviews Drug Discovery* **2018**, *17* (4), 261-279.

47. Kim, J.; Eygeris, Y.; Gupta, M.; Sahay, G., Self-assembled mRNA vaccines. *Advanced Drug Delivery Reviews* **2021**, *170*, 83-112.
48. Zhao, W.; Hou, X.; Vick, O. G.; Dong, Y., RNA delivery biomaterials for the treatment of genetic and rare diseases. *Biomaterials* **2019**, *217*, 119291.
49. Trepotec, Z.; Lichtenegger, E.; Plank, C.; Aneja, M. K.; Rudolph, C., Delivery of mRNA Therapeutics for the Treatment of Hepatic Diseases. *Molecular Therapy* **2019**, *27* (4), 794-802.
50. Hou, X.; Zaks, T.; Langer, R.; Dong, Y., Lipid nanoparticles for mRNA delivery. *Nature Reviews Materials* **2021**, *6* (12), 1078-1094.
51. Kormann, M. S. D.; Hasenpusch, G.; Aneja, M. K.; Nica, G.; Flemmer, A. W.; Herber-Jonat, S.; Huppmann, M.; Mays, L. E.; Illenyi, M.; Schams, A.; Griese, M.; Bittmann, I.; Handgretinger, R.; Hartl, D.; Rosenecker, J.; Rudolph, C., Expression of therapeutic proteins after delivery of chemically modified mRNA in mice. *Nature Biotechnology* **2011**, *29* (2), 154-157.
52. Zangi, L.; Lui, K. O.; von Gise, A.; Ma, Q.; Ebina, W.; Ptaszek, L. M.; Später, D.; Xu, H.; Tabebordbar, M.; Gorbатов, R.; Sena, B.; Nahrendorf, M.; Briscoe, D. M.; Li, R. A.; Wagers, A. J.; Rossi, D. J.; Pu, W. T.; Chien, K. R., Modified mRNA directs the fate of heart progenitor cells and induces vascular regeneration after myocardial infarction. *Nature Biotechnology* **2013**, *31* (10), 898-907.
53. DeRosa, F.; Smith, L.; Shen, Y.; Huang, Y.; Pan, J.; Xie, H.; Yahalom, B.; Heartlein, M. W., Improved Efficacy in a Fabry Disease Model Using a Systemic mRNA Liver Depot System as Compared to Enzyme Replacement Therapy. *Molecular Therapy* **2019**, *27* (4), 878-889.
54. Gebre, M. S.; Brito, L. A.; Tostanoski, L. H.; Edwards, D. K.; Carfi, A.; Barouch, D. H., Novel approaches for vaccine development. *Cell* **2021**, *184* (6), 1589-1603.
55. Plotkin Stanley, A., Vaccines: the Fourth Century. *Clinical and Vaccine Immunology* **2009**, *16* (12), 1709-1719.
56. Younger, D. S.; Younger, A. P. J.; Guttmacher, S., Childhood Vaccination: Implications for Global and Domestic Public Health. *Neurologic Clinics* **2016**, *34* (4), 1035-1047.
57. Karikó, K.; Muramatsu, H.; Welsh, F. A.; Ludwig, J.; Kato, H.; Akira, S.; Weissman, D., Incorporation of Pseudouridine Into mRNA Yields Superior Nonimmunogenic Vector With Increased Translational Capacity and Biological Stability. *Molecular Therapy* **2008**, *16* (11), 1833-1840.
58. Karikó, K.; Muramatsu, H.; Ludwig, J.; Weissman, D., Generating the optimal mRNA for therapy: HPLC purification eliminates immune activation and improves translation of nucleoside-modified, protein-encoding mRNA. *Nucleic Acids Research* **2011**, *39* (21), e142-e142.
59. Richner, J. M.; Himansu, S.; Dowd, K. A.; Butler, S. L.; Salazar, V.; Fox, J. M.; Julander, J. G.; Tang, W. W.; Shresta, S.; Pierson, T. C.; Ciaramella, G.; Diamond, M. S., Modified mRNA Vaccines Protect against Zika Virus Infection. *Cell* **2017**, *168* (6), 1114-1125.e10.
60. VanBlargan, L. A.; Himansu, S.; Foreman, B. M.; Ebel, G. D.; Pierson, T. C.; Diamond, M. S., An mRNA Vaccine Protects Mice against Multiple Tick-Transmitted Flavivirus Infections. *Cell Reports* **2018**, *25* (12), 3382-3392.e3.
61. Pardi, N.; LaBranche, C. C.; Ferrari, G.; Cain, D. W.; Tombácz, I.; Parks, R. J.; Muramatsu, H.; Mui, B. L.; Tam, Y. K.; Karikó, K.; Polacino, P.; Barbosa, C. J.; Madden, T. D.; Hope, M. J.; Haynes, B. F.; Montefiori, D. C.; Hu, S.-L.; Weissman, D., Characterization of HIV-1 Nucleoside-Modified mRNA Vaccines in Rabbits and Rhesus Macaques. *Molecular Therapy - Nucleic Acids* **2019**, *15*, 36-47.
62. Pardi, N.; Parkhouse, K.; Kirkpatrick, E.; McMahon, M.; Zost, S. J.; Mui, B. L.; Tam, Y. K.; Karikó, K.; Barbosa, C. J.; Madden, T. D.; Hope, M. J.; Krammer, F.; Hensley, S. E.; Weissman, D., Nucleoside-modified mRNA immunization elicits influenza virus hemagglutinin stalk-specific antibodies. *Nature Communications* **2018**, *9* (1), 3361.
63. Houseley, J.; Tollervey, D., The Many Pathways of RNA Degradation. *Cell* **2009**, *136* (4), 763-776.

64. Kim, B.; Park, J.-H.; Sailor, M. J., Rekindling RNAi Therapy: Materials Design Requirements for In Vivo siRNA Delivery. *Advanced Materials* **2019**, *31* (49), 1903637.
65. Du, Z.; Podsypanina, K.; Huang, S.; McGrath, A.; Toneff, M. J.; Bogoslovskaja, E.; Zhang, X.; Moraes, R. C.; Fluck, M.; Allred, D. C.; Lewis, M. T.; Varmus, H. E.; Li, Y., Introduction of oncogenes into mammary glands in vivo with an avian retroviral vector initiates and promotes carcinogenesis in mouse models. *Proceedings of the National Academy of Sciences* **2006**, *103* (46), 17396-17401.
66. Verdera, H. C.; Kuranda, K.; Mingozzi, F., AAV Vector Immunogenicity in Humans: A Long Journey to Successful Gene Transfer. *Molecular Therapy* **2020**, *28* (3), 723-746.
67. Bulcha, J. T.; Wang, Y.; Ma, H.; Tai, P. W. L.; Gao, G., Viral vector platforms within the gene therapy landscape. *Signal Transduction and Targeted Therapy* **2021**, *6* (1), 53.
68. Thomas, C. E.; Ehrhardt, A.; Kay, M. A., Progress and problems with the use of viral vectors for gene therapy. *Nature Reviews Genetics* **2003**, *4* (5), 346-358.
69. Woodle, M. C.; Scaria, P., Cationic liposomes and nucleic acids. *Current Opinion in Colloid & Interface Science* **2001**, *6* (1), 78-84.
70. Meka, R. R.; Godeshala, S.; Marepally, S.; Thorat, K.; Reddy Rachamalla, H. K.; Dhayani, A.; Hiwale, A.; Banerjee, R.; Chaudhuri, A.; Vemula, P. K., Asymmetric cationic lipid based non-viral vectors for an efficient nucleic acid delivery. *RSC Advances* **2016**, *6* (81), 77841-77848.
71. Rietwyk, S.; Peer, D., Next-Generation Lipids in RNA Interference Therapeutics. *ACS Nano* **2017**, *11* (8), 7572-7586.
72. Aldosari, B. N.; Alfaqih, I. M.; Almurshedi, A. S., Lipid Nanoparticles as Delivery Systems for RNA-Based Vaccines. *Pharmaceutics* **2021**, *13* (2).
73. Landesman-Milo, D.; Peer, D., Toxicity profiling of several common RNAi-based nanomedicines: a comparative study. *Drug Delivery and Translational Research* **2014**, *4* (1), 96-103.
74. Peer, D., Immunotoxicity derived from manipulating leukocytes with lipid-based nanoparticles. *Advanced Drug Delivery Reviews* **2012**, *64* (15), 1738-1748.
75. Eygeris, Y.; Patel, S.; Jozic, A.; Sahay, G., Deconvoluting Lipid Nanoparticle Structure for Messenger RNA Delivery. *Nano Letters* **2020**, *20* (6), 4543-4549.
76. Patel, S.; Ashwanikumar, N.; Robinson, E.; Xia, Y.; Mihai, C.; Griffith, J. P.; Hou, S.; Esposito, A. A.; Ketova, T.; Welsher, K.; Joyal, J. L.; Almarsson, Ö.; Sahay, G., Naturally-occurring cholesterol analogues in lipid nanoparticles induce polymorphic shape and enhance intracellular delivery of mRNA. *Nature Communications* **2020**, *11* (1), 983.
77. Zhang, Y.; Sun, C.; Wang, C.; Jankovic, K. E.; Dong, Y., Lipids and Lipid Derivatives for RNA Delivery. *Chemical Reviews* **2021**, *121* (20), 12181-12277.
78. Xiong, Q.; Lee, G. Y.; Ding, J.; Li, W.; Shi, J., Biomedical applications of mRNA nanomedicine. *Nano Research* **2018**, *11* (10), 5281-5309.
79. Guan, S.; Rosenecker, J., Nanotechnologies in delivery of mRNA therapeutics using nonviral vector-based delivery systems. *Gene Therapy* **2017**, *24* (3), 133-143.
80. Kowalski, P. S.; Rudra, A.; Miao, L.; Anderson, D. G., Delivering the Messenger: Advances in Technologies for Therapeutic mRNA Delivery. *Molecular Therapy* **2019**, *27* (4), 710-728.
81. Uchida, S.; Perche, F.; Pichon, C.; Cabral, H., Nanomedicine-Based Approaches for mRNA Delivery. *Molecular Pharmaceutics* **2020**, *17* (10), 3654-3684.
82. Meng, C.; Chen, Z.; Li, G.; Welte, T.; Shen, H., Nanoplatforms for mRNA Therapeutics. *Advanced Therapeutics* **2021**, *4* (1), 2000099.
83. Weng, Y.; Li, C.; Yang, T.; Hu, B.; Zhang, M.; Guo, S.; Xiao, H.; Liang, X.-J.; Huang, Y., The challenge and prospect of mRNA therapeutics landscape. *Biotechnology Advances* **2020**, *40*, 107534.

84. Gillmore, J. D.; Gane, E.; Taubel, J.; Kao, J.; Fontana, M.; Maitland, M. L.; Seitzer, J.; O'Connell, D.; Walsh, K. R.; Wood, K.; Phillips, J.; Xu, Y.; Amaral, A.; Boyd, A. P.; Cehelsky, J. E.; McKee, M. D.; Schiermeier, A.; Harari, O.; Murphy, A.; Kyratsous, C. A.; Zambrowicz, B.; Soltys, R.; Gutstein, D. E.; Leonard, J.; Sepp-Lorenzino, L.; Lebowitz, D., CRISPR-Cas9 In Vivo Gene Editing for Transthyretin Amyloidosis. *New England Journal of Medicine* **2021**, *385* (6), 493-502.
85. Eygeris, Y.; Gupta, M.; Kim, J.; Sahay, G., Chemistry of Lipid Nanoparticles for RNA Delivery. *Accounts of Chemical Research* **2022**, *55* (1), 2-12.
86. Leung, A. K. K.; Tam, Y. Y. C.; Chen, S.; Hafez, I. M.; Cullis, P. R., Microfluidic Mixing: A General Method for Encapsulating Macromolecules in Lipid Nanoparticle Systems. *The Journal of Physical Chemistry B* **2015**, *119* (28), 8698-8706.
87. Jokerst, J. V.; Lobovkina, T.; Zare, R. N.; Gambhir, S. S., Nanoparticle PEGylation for imaging and therapy. *Nanomedicine* **2011**, *6* (4), 715-728.
88. Knop, K.; Hoogenboom, R.; Fischer, D.; Schubert, U. S., Poly(ethylene glycol) in Drug Delivery: Pros and Cons as Well as Potential Alternatives. *Angewandte Chemie International Edition* **2010**, *49* (36), 6288-6308.
89. Cheng, Q.; Wei, T.; Farbiak, L.; Johnson, L. T.; Dilliard, S. A.; Siegwart, D. J., Selective organ targeting (SORT) nanoparticles for tissue-specific mRNA delivery and CRISPR-Cas gene editing. *Nature Nanotechnology* **2020**, *15* (4), 313-320.
90. Veiga, N.; Goldsmith, M.; Granot, Y.; Rosenblum, D.; Dammes, N.; Kedmi, R.; Ramishetti, S.; Peer, D., Cell specific delivery of modified mRNA expressing therapeutic proteins to leukocytes. *Nature Communications* **2018**, *9* (1), 4493.
91. Rosenblum, D.; Gutkin, A.; Kedmi, R.; Ramishetti, S.; Veiga, N.; Jacobi, A. M.; Schubert, M. S.; Friedmann-Morvinski, D.; Cohen, Z. R.; Behlke, M. A.; Lieberman, J.; Peer, D., CRISPR-Cas9 genome editing using targeted lipid nanoparticles for cancer therapy. *Science Advances* *6* (47), eabc9450.
92. Li, B.; Zhang, X.; Dong, Y., Nanoscale platforms for messenger RNA delivery. *WIREs Nanomedicine and Nanobiotechnology* **2019**, *11* (2), e1530.
93. Miao, L.; Lin, J.; Huang, Y.; Li, L.; Delcassian, D.; Ge, Y.; Shi, Y.; Anderson, D. G., Synergistic lipid compositions for albumin receptor mediated delivery of mRNA to the liver. *Nature Communications* **2020**, *11* (1), 2424.
94. Zhang, X.; Zhao, W.; Nguyen, G. N.; Zhang, C.; Zeng, C.; Yan, J.; Du, S.; Hou, X.; Li, W.; Jiang, J.; Deng, B.; McComb, D. W.; Dorkin, R.; Shah, A.; Barrera, L.; Gregoire, F.; Singh, M.; Chen, D.; Sabatino, D. E.; Dong, Y., Functionalized lipid-like nanoparticles for in vivo mRNA delivery and base editing. *Science Advances* *6* (34), eabc2315.
95. Gilleron, J.; Querbes, W.; Zeigerer, A.; Borodovsky, A.; Marsico, G.; Schubert, U.; Manygoats, K.; Seifert, S.; Andree, C.; Stöter, M.; Epstein-Barash, H.; Zhang, L.; Koteliansky, V.; Fitzgerald, K.; Fava, E.; Bickle, M.; Kalaidzidis, Y.; Akinc, A.; Maier, M.; Zerial, M., Image-based analysis of lipid nanoparticle-mediated siRNA delivery, intracellular trafficking and endosomal escape. *Nature Biotechnology* **2013**, *31* (7), 638-646.
96. Sahay, G.; Querbes, W.; Alabi, C.; Eltoukhy, A.; Sarkar, S.; Zurenko, C.; Karagiannis, E.; Love, K.; Chen, D.; Zoncu, R.; Buggan, Y.; Schroeder, A.; Langer, R.; Anderson, D. G., Efficiency of siRNA delivery by lipid nanoparticles is limited by endocytic recycling. *Nature Biotechnology* **2013**, *31* (7), 653-658.
97. Wittrup, A.; Ai, A.; Liu, X.; Hamar, P.; Trifonova, R.; Charisse, K.; Manoharan, M.; Kirchhausen, T.; Lieberman, J., Visualizing lipid-formulated siRNA release from endosomes and target gene knockdown. *Nature Biotechnology* **2015**, *33* (8), 870-876.
98. Patel, S.; Ashwanikumar, N.; Robinson, E.; DuRoss, A.; Sun, C.; Murphy-Benvenuto, K. E.; Mihai, C.; Almarsson, Ö.; Sahay, G., Boosting Intracellular Delivery of Lipid Nanoparticle-Encapsulated mRNA. *Nano*

*Letters* **2017**, *17* (9), 5711-5718.

99. Paramasivam, P.; Franke, C.; Stöter, M.; Höijer, A.; Bartesaghi, S.; Sabirsh, A.; Lindfors, L.; Arteta, M. Y.; Dahlén, A.; Bak, A.; Andersson, S.; Kalaidzidis, Y.; Bickle, M.; Zerial, M., Endosomal escape of delivered mRNA from endosomal recycling tubules visualized at the nanoscale. *Journal of Cell Biology* **2021**, *221* (2), e202110137.

100. Schlich, M.; Palomba, R.; Costabile, G.; Mizrahy, S.; Pannuzzo, M.; Peer, D.; Decuzzi, P., Cytosolic delivery of nucleic acids: The case of ionizable lipid nanoparticles. *Bioengineering & Translational Medicine* **2021**, *6* (2), e10213.

101. Liu, Z.; Wang, S.; Tapeinos, C.; Torrieri, G.; Känkänen, V.; El-Sayed, N.; Python, A.; Hirvonen, J. T.; Santos, H. A., Non-viral nanoparticles for RNA interference: Principles of design and practical guidelines. *Advanced Drug Delivery Reviews* **2021**, *174*, 576-612.

102. Karimi, M.; Ghasemi, A.; Sahandi Zangabad, P.; Rahighi, R.; Moosavi Basri, S. M.; Mirshekari, H.; Amiri, M.; Shafaei Pishabad, Z.; Aslani, A.; Bozorgomid, M.; Ghosh, D.; Beyzavi, A.; Vaseghi, A.; Aref, A. R.; Haghani, L.; Bahrami, S.; Hamblin, M. R., Smart micro/nanoparticles in stimulus-responsive drug/gene delivery systems. *Chemical Society Reviews* **2016**, *45* (5), 1457-1501.

103. Degors, I. M. S.; Wang, C.; Rehman, Z. U.; Zuhorn, I. S., Carriers Break Barriers in Drug Delivery: Endocytosis and Endosomal Escape of Gene Delivery Vectors. *Accounts of Chemical Research* **2019**, *52* (7), 1750-1760.

104. Jayaraman, M.; Ansell, S. M.; Mui, B. L.; Tam, Y. K.; Chen, J.; Du, X.; Butler, D.; Eltepu, L.; Matsuda, S.; Narayanannair, J. K.; Rajeev, K. G.; Hafez, I. M.; Akinc, A.; Maier, M. A.; Tracy, M. A.; Cullis, P. R.; Madden, T. D.; Manoharan, M.; Hope, M. J., Maximizing the Potency of siRNA Lipid Nanoparticles for Hepatic Gene Silencing In Vivo\*\*. *Angewandte Chemie International Edition* **2012**, *51* (34), 8529-8533.

105. Hajj, K. A.; Ball, R. L.; Deluty, S. B.; Singh, S. R.; Strelkova, D.; Knapp, C. M.; Whitehead, K. A., Branched-Tail Lipid Nanoparticles Potently Deliver mRNA In Vivo due to Enhanced Ionization at Endosomal pH. *Small* **2019**, *15* (6), 1805097.

106. Maier, M. A.; Jayaraman, M.; Matsuda, S.; Liu, J.; Barros, S.; Querbes, W.; Tam, Y. K.; Ansell, S. M.; Kumar, V.; Qin, J.; Zhang, X.; Wang, Q.; Panesar, S.; Hutabarat, R.; Carioto, M.; Hettinger, J.; Kandasamy, P.; Butler, D.; Rajeev, K. G.; Pang, B.; Charisse, K.; Fitzgerald, K.; Mui, B. L.; Du, X.; Cullis, P.; Madden, T. D.; Hope, M. J.; Manoharan, M.; Akinc, A., Biodegradable Lipids Enabling Rapidly Eliminated Lipid Nanoparticles for Systemic Delivery of RNAi Therapeutics. *Molecular Therapy* **2013**, *21* (8), 1570-1578.

107. Sabnis, S.; Kumarasinghe, E. S.; Salerno, T.; Mihai, C.; Ketova, T.; Senn, J. J.; Lynn, A.; Bulychev, A.; McFadyen, I.; Chan, J.; Almarsson, Ö.; Stanton, M. G.; Benenato, K. E., A Novel Amino Lipid Series for mRNA Delivery: Improved Endosomal Escape and Sustained Pharmacology and Safety in Non-human Primates. *Molecular Therapy* **2018**, *26* (6), 1509-1519.

108. Hassett, K. J.; Benenato, K. E.; Jacquinet, E.; Lee, A.; Woods, A.; Yuzhakov, O.; Himansu, S.; Deterling, J.; Geilich, B. M.; Ketova, T.; Mihai, C.; Lynn, A.; McFadyen, I.; Moore, M. J.; Senn, J. J.; Stanton, M. G.; Almarsson, Ö.; Ciaramella, G.; Brito, L. A., Optimization of Lipid Nanoparticles for Intramuscular Administration of mRNA Vaccines. *Molecular Therapy - Nucleic Acids* **2019**, *15*, 1-11.

109. Whitehead, K. A.; Dorkin, J. R.; Vegas, A. J.; Chang, P. H.; Veiseh, O.; Matthews, J.; Fenton, O. S.; Zhang, Y.; Olejnik, K. T.; Yesilyurt, V.; Chen, D.; Barros, S.; Klebanov, B.; Novobrantseva, T.; Langer, R.; Anderson, D. G., Degradable lipid nanoparticles with predictable in vivo siRNA delivery activity. *Nature Communications* **2014**, *5* (1), 4277.

110. Alabi, C. A.; Love, K. T.; Sahay, G.; Yin, H.; Luly, K. M.; Langer, R.; Anderson, D. G.,

- Multiparametric approach for the evaluation of lipid nanoparticles for siRNA delivery. *Proceedings of the National Academy of Sciences* **2013**, *110* (32), 12881-12886.
111. Kauffman, K. J.; Dorkin, J. R.; Yang, J. H.; Heartlein, M. W.; DeRosa, F.; Mir, F. F.; Fenton, O. S.; Anderson, D. G., Optimization of Lipid Nanoparticle Formulations for mRNA Delivery in Vivo with Fractional Factorial and Definitive Screening Designs. *Nano Letters* **2015**, *15* (11), 7300-7306.
112. Li, B.; Luo, X.; Deng, B.; Wang, J.; McComb, D. W.; Shi, Y.; Gaensler, K. M. L.; Tan, X.; Dunn, A. L.; Kerlin, B. A.; Dong, Y., An Orthogonal Array Optimization of Lipid-like Nanoparticles for mRNA Delivery in Vivo. *Nano Letters* **2015**, *15* (12), 8099-8107.
113. Cheng, Q.; Wei, T.; Jia, Y.; Farbiak, L.; Zhou, K.; Zhang, S.; Wei, Y.; Zhu, H.; Siegwart, D. J., Dendrimer-Based Lipid Nanoparticles Deliver Therapeutic FAH mRNA to Normalize Liver Function and Extend Survival in a Mouse Model of Hepatorenal Tyrosinemia Type I. *Advanced Materials* **2018**, *30* (52), 1805308.
114. White Judith, M., Membrane Fusion. *Science* **1992**, *258* (5084), 917-924.
115. Jahn, R.; Lang, T.; Südhof, T. C., Membrane Fusion. *Cell* **2003**, *112* (4), 519-533.
116. Martens, S.; McMahon, H. T., Mechanisms of membrane fusion: disparate players and common principles. *Nature Reviews Molecular Cell Biology* **2008**, *9* (7), 543-556.
117. Diao, J.; Su, Z.; Ishitsuka, Y.; Lu, B.; Lee, K. S.; Lai, Y.; Shin, Y.-K.; Ha, T., A single-vesicle content mixing assay for SNARE-mediated membrane fusion. *Nature Communications* **2010**, *1* (1), 54.
118. Marsden, H. R.; Tomatsu, I.; Kros, A., Model systems for membrane fusion. *Chemical Society Reviews* **2011**, *40* (3), 1572-1585.
119. Jahn, R.; Scheller, R. H., SNAREs — engines for membrane fusion. *Nature Reviews Molecular Cell Biology* **2006**, *7* (9), 631-643.
120. Yang, J.; Bahreman, A.; Daudey, G.; Bussmann, J.; Olsthoorn, R. C. L.; Kros, A., Drug Delivery via Cell Membrane Fusion Using Lipopeptide Modified Liposomes. *ACS Central Science* **2016**, *2* (9), 621-630.
121. Yang, J.; Shimada, Y.; Olsthoorn, R. C. L.; Snaar-Jagalska, B. E.; Spaink, H. P.; Kros, A., Application of Coiled Coil Peptides in Liposomal Anticancer Drug Delivery Using a Zebrafish Xenograft Model. *ACS Nano* **2016**, *10* (8), 7428-7435.
122. Kong, L.; Askes, S. H. C.; Bonnet, S.; Kros, A.; Campbell, F., Temporal Control of Membrane Fusion through Photolabile PEGylation of Liposome Membranes. *Angewandte Chemie International Edition* **2016**, *55* (4), 1396-1400.

## **Chapter 2**

### **Efficient mRNA Delivery Using Fusogenic Coiled-coil Peptides**

## **Abstract**

Gene delivery has great potential in modulating protein expression in specific cells to treat diseases. Such therapeutic gene delivery demands sufficient cellular internalization and endosomal escape. Of the various nonviral nucleic acid delivery systems, lipid nanoparticles (LNPs) are the most advanced. Unfortunately most nonviral delivery systems like LNPs, are very inefficient in delivering nucleic acids to cells as the large majority is unable to escape endosomes/lysosomes. Here, we develop a highly efficient gene delivery system using fusogenic coiled-coil peptides. We modified LNPs, carrying EGFP-mRNA, and cells with complementary coiled-coil lipopeptides. Coiled-coil formation between these lipopeptides induced fast nucleic acid uptake and enhanced GFP expression. The cellular uptake of coiled-coil modified LNPs is likely driven by membrane fusion thereby omitting typical endocytosis pathways. This direct cytosolic delivery circumvents the problems commonly observed with the limited endosomal escape of mRNA. Therefore fusogenic coiled-coil peptide modification of existing LNP formulations to enhance nucleic acid delivery efficiency could be beneficial for several gene therapy applications.

## Introduction

An understanding of both the human genome and disease mechanisms has expanded our knowledge of gene-dysregulation related diseases, paving the way for novel gene therapies.<sup>1-3</sup> Gene therapy potentially enables the treatment of disease at the genetic level by correcting or replacing malfunctioning genes.<sup>4</sup> This repair or replacement could be achieved by delivering exogenous nucleic acids such as DNA, mRNA, small interfering RNA (siRNA), microRNA (miRNA), or antisense oligonucleotides (ASO) to the tissue or organ of interest.<sup>2</sup> However, the complexity of cell membranes and cellular barriers impedes the efficient transfer of the genetic cargo into the organs, tissue, and cells of interest, resulting in a poor therapeutic effect.<sup>4,5</sup>

Since nucleic acid-based drugs are unable to enter cells and are inherently unstable *in vivo*, a drug delivery system is required. An ideal gene vector should transfect the desired tissue or organ efficiently, while the vector should be non-toxic, non-immunogenic, and ideally easy to formulate. State-of-the-art gene vectors are divided into two major classes: viral and nonviral. As viral vectors typically possess high cellular transduction efficiency, many gene therapy clinical trials are using modified viral vectors such as lentiviruses, retroviruses, adenoviruses, and adenovirus-associated viruses.<sup>4,6-8</sup> However, widespread use of viral vectors is hampered because of side-effects including potential carcinogenesis, immunogenicity, broad tropism, limited DNA packaging capacity, and difficulty of vector production.<sup>2,9,10</sup> In contrast, nonviral vectors could potentially circumvent these limitations, especially in terms of safety and the size of encapsulated genetic cargo.<sup>11</sup> Nonviral gene vectors in (pre)clinical applications are commonly composed of lipids,<sup>12</sup> lipoids,<sup>13</sup> or are polymer-based.<sup>2</sup>

Currently, the most advanced nonviral nucleic acid delivery system is lipid nanoparticles (LNPs).<sup>14,15</sup> LNPs are composed of an ionizable lipid to condense the genetic cargo and release it after entering the cells; a cholesterol moiety to stabilize the LNP structure; a helper lipid; and a PEGylated lipid to improve colloidal stability and reduce protein absorption.<sup>16</sup> The first siRNA drug, named Onpattro (Patisiran), was approved in 2018 by the FDA and was designed to treat polyneuropathies induced by hereditary transthyretin-mediated amyloidosis (hATTR) in adults. This therapy has been a milestone for nonviral nucleic acid-based therapies.<sup>1</sup> Onpattro is a lipid nanoparticle (LNP) formulation that upon intravenous administration binds serum apolipoprotein E (ApoE), which acts as an endogenous targeting ligand to the low-density lipoprotein receptor present in hepatocytes.<sup>17</sup>

LNPs cell entry relies on endocytosis, and the efficacy is dependent on the delivery of encapsulated siRNA to the cytoplasm.<sup>15</sup> However, LNPs (and other nanoparticles) transport the encapsulated macromolecules to different subcellular destinations, the majority of which accumulates in lysosomes for degradation.<sup>18</sup> Studies showed only <2% of the siRNA in LNPs was able to escape endosomal compartments, resulting in release into the cytoplasm;<sup>19</sup> and <5% of cytoplasmic mRNA of LNPs was distributed outside of endosomes, corresponding to endosome escaped events.<sup>20</sup> Therefore, there is an urgent need to overcome this major limitation of inefficient nucleic acid delivery into cells. Many attempts have been reported to facilitate endosomal escape by using polyplex-mediated endosomal swelling nanomaterials,<sup>21,22</sup> cell-penetrating peptides (CPPs),<sup>23,24</sup> or exogenous stimuli-responsive biomaterials responding to specific biochemical conditions, such as a change in pH or redox state but to date, there is still a lack of modified systems resulting in efficient endosomal

escape.<sup>21,25</sup>

One way that cells transfer components is via membrane fusion. Therefore, membrane fusion is critical for many biological processes, including organelle inheritance in cell growth and division, chemical synaptic transmission in the nervous system, and the modulation of synaptic strength in memory and learning.<sup>26</sup> The docking of transport vesicles to the target plasma membrane in neuronal exocytosis is triggered by coiled-coil formation between complementary SNARE protein subunits.<sup>27</sup> Inspired by the SNARE protein complex, our group has developed a synthetic membrane fusion system based on a heterodimeric coiled-coil peptide pair and we have demonstrated direct drug delivery into the cytosol of living cells *in vitro* and *in vivo*.<sup>28-30</sup>

In this study, we applied our fusogenic coiled-coil peptides to efficiently deliver LNPs into cells to enhance genetic cargo transfection efficacy via membrane fusion. We developed coiled-coil peptide modified LNPs encapsulating EGFP-mRNA to induce efficient cellular delivery and concomitant GFP expression (**Scheme 1**). The Onpattro LNP formulation was modified with lipopeptide CPE4 (CPE4-LNP) while cells were pretreated with the complementary lipopeptide CPK4. The addition of CPE4-LNP to the cells resulted in efficient LNP uptake and protein expression, which was observed and studied by confocal microscopy and flow cytometry. By applying different endocytosis inhibitors and a lysosome tracker, the internalization pathway was investigated. This study demonstrates that, by utilizing coiled-coil peptides, significant amounts of genetic cargo can be delivered to cells by evading endocytosis pathways.

## Results

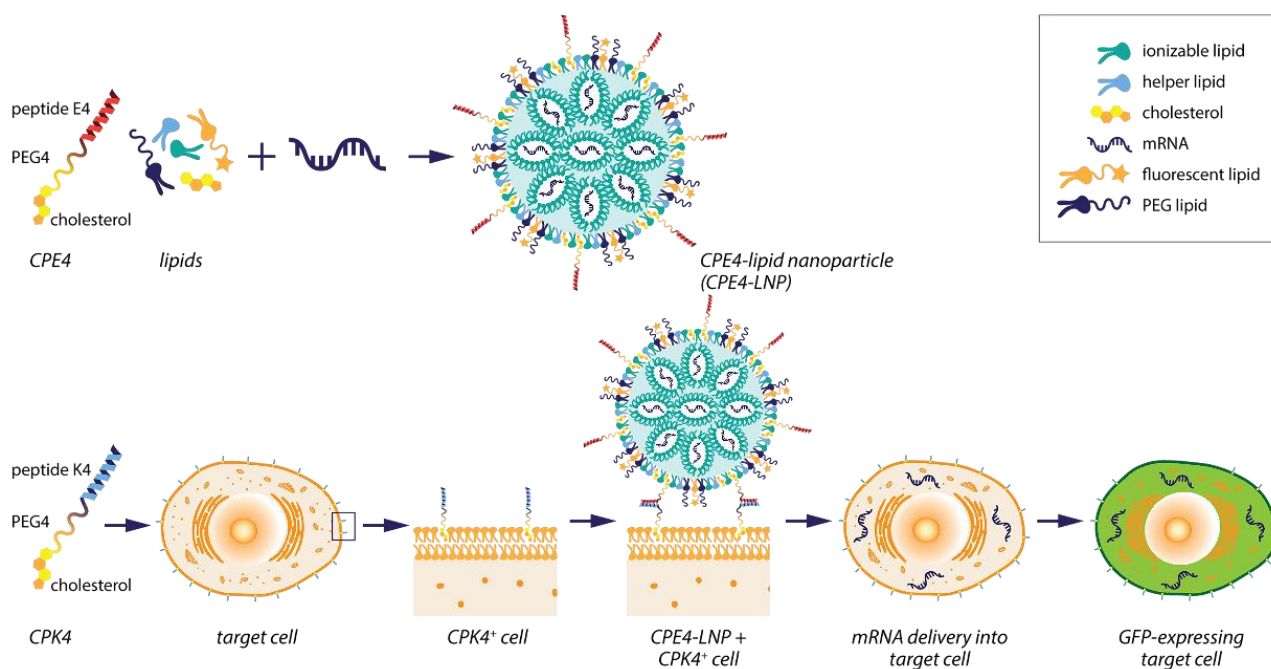
### Comparison of K3/E3 and K4/E4 coiled-coil interactions

Our previous studies showed that both the K3/E3 and K4/E4 coiled-coil pairs (where 3 and 4 correspond to the number of heptad repeats within the peptides), induced efficient and targeted membrane fusion between liposomes, and liposomes with cells, both *in vitro* and *in vivo*.<sup>28-30</sup> In order to determine which pair was most suitable for this study we evaluated their coiled-coil forming and cargo delivery properties. Circular dichroism (CD) spectroscopy (**SI Fig. 1a**), confirmed both K3/E3 and K4/E4 pairs formed coiled coils efficiently. The K4/E4 pair is composed of one additional heptad repeat compared to K3/E3, and as expected the former peptide pair yielded a more-folded complex. Cellular internalization of En-modified fluorescent liposomes in Kn-modified HeLa cells was subsequently quantified by flow cytometry (**SI Fig. 1b**), demonstrating that both K3/E3 and K4/E4 induced cellular uptake, however K4/E4 exhibited significantly higher cell uptake. When comparing the mean fluorescence intensity (MFI) of fluorescent cells (**SI Fig. 1c-1d**), we observed that the K4/E4 pair is the most fusogenic as the cells showed the highest levels of fluorescence. We also observed that CPK4 modified liposomes were able to enter cells efficiently, even in the absence of E4 on the cell surface, presumably due to interactions between the positively charged CPK4 lipopeptides and the negatively charged cell membranes.

Next, we studied whether these findings were also valid for the delivery of LNPs to cells. We formulated LNPs encapsulating Alexa488-labeled nucleic acid and modified these with 1 mol% of either CPE3 or CPE4 yielding CPE3-LNP and CPE4-LNP. HeLa cells were pretreated with the complementary CPKn and internalization of the LNPs was quantified by fluorescence measurements.

Again, the CPK4/CPE4 pair exhibited enhanced cellular internalization as compared to the CPK3/CPE3 pair (SI Fig. 1e-1f).

Therefore, we utilized the K4/E4 peptide pair with CPK4 at the cell membrane and CPE4 in the LNPs in the following experiments to achieve optimal coiled-coil formation and to exclude undesirable electrostatic interactions between positive CPK4 decorated LNPs and negatively charged cell membrane.

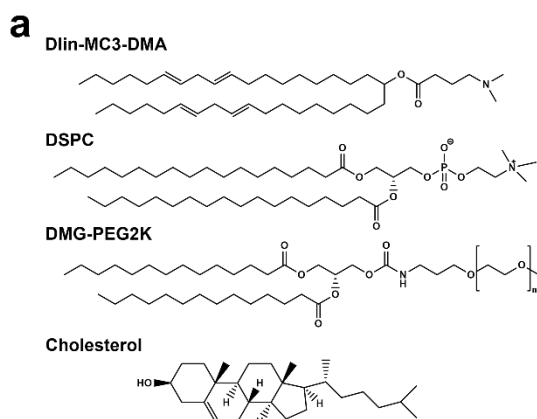


**Scheme 1.** Schematic representation of the nonviral lipid nanoparticles (LNPs) that induce efficient mRNA delivery within cells when modified with fusogenic coiled-coil peptides.

### Lipid nanoparticle characterization

The lipid composition of the clinically approved LNP formulation Onpattro (Dlin-MC3-DMA:cholesterol:DSPC:DMG-PEG2K=50:38.5:10:1.5) has been optimized for potent silencing of protein expression in cells by delivery of siRNA.<sup>1</sup> To investigate the efficacy of coiled-coil mediated mRNA delivery into cells, we opted to formulate CPE4-LNPs with the same lipid composition as Onpattro and added 1 mol% of CPE4 (Fig. 1a-b). Dynamic light scattering (DLS) was used to determine the hydrodynamic diameters of both plain and CPE4-modified LNPs after encapsulating EGFP-mRNA. These diameters were found to be 80 and 95 nm respectively with low polydispersities (PDI) (Fig. 1c). Both formulations had a near-neutral zeta-potential, thus the presence of 1 mol% CPE4 did not influence the surface charge significantly. mRNA encapsulation efficiency was slightly lower for CPE4-LNP, which might be due to electrostatic repulsion between the negatively charged peptide E and the mRNA (Fig. 1c). Nonetheless, the encapsulation efficiency exceeded 85%. Cryogenic transmission electron microscopy (cryo-EM) imaging revealed a spherical morphology for CPE4-LNP, similar to plain LNP, and the majority of both LNPs (>80%) had a diameter of 30-70 nm (Fig. 1d-e). The long-term colloidal stability of both LNPs was determined for 10 days and no discernable deviations were observed in either diameter or PDI, indicating that both LNP formulations

were stable over this timeframe (**Fig. 1f**). Upon replacing EGFP-mRNA with Alexa488 labeled nucleic acid, the size distribution and morphology were identical to the EGFP-mRNA encapsulated LNPs (**SI Fig. 2a-2c**). In summary, the addition of 1 mol% of coiled-coil peptide CPE4 to Onpattro LNPs did not change the physicochemical properties of LNPs, thus differences in cell uptake and protein expression can be related to the presence of coiled-coils (*vide infra*).



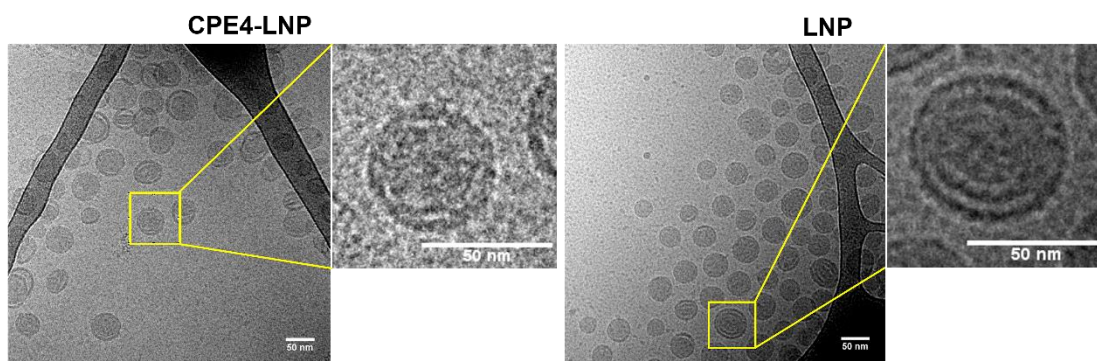
**b**

Lipid compositions of LNPs (mol%).		
	CPE4-LNP	LNP
Dlin-MC3-DMA	50	50
Cholesterol	37.5	38.5
DSPC	10	10
DMG-PEG2K	1.5	1.5
CPE4	1	

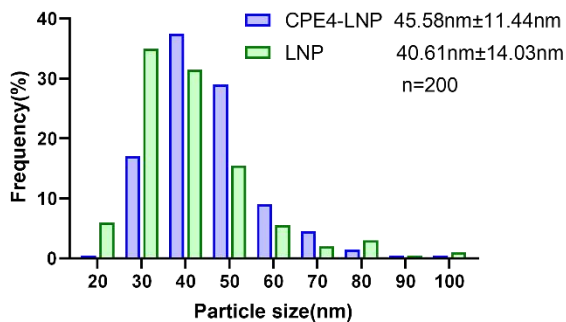
**c**

Characterization of LNP formulations.				
LNPs	Hydrodynamic diameter (nm)	PDI	Zeta potential (mV)	EE (%)
CPE4-LNP	94.1±2.3	0.167±0.04	-4.37±0.65	85.30±5.14
LNP	80.6±1.8	0.132±0.06	-2.27±0.30	95.13±1.62

**d**



**e**



**f**

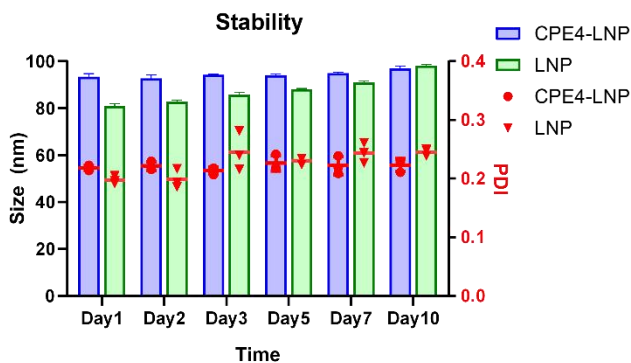


**Figure 1. Design and characterization of LNPs carrying EGFP-mRNA.** (a) Structures of lipids used for the preparation of LNPs. (b) Lipid composition of LNPs (mol %). (c) Characterization of LNPs. (d) Cryo-EM images of LNPs. Scale bar is 50 nm. (e) Size distribution of EGFP-mRNA encapsulated LNPs as determined by cryo-EM. The values were calculated from the size distribution frequency. (f) Long-term stability of LNPs. LNPs were stored at 4 °C in PBS buffer. The nanoparticle diameter and PDI were monitored by DLS (mean  $\pm$  s.d., n = 3).

### Cell uptake of LNPs

The uptake of LNPs containing Alexa-488 nucleic acid in HeLa cells and the influence of the E4/K4 coiled-coil pair was studied using confocal microscopy and flow cytometry measurements for qualitative and quantitative analysis (**SI Fig. 3a**). The Onpattro LNP formulation served as a control, and 1 mol % of red-fluorescent PE-LR was added to follow the uptake and location of the lipids. Confocal microscopy imaging revealed that CPK4 decorated HeLa cells induced abundant Alexa488-labeled nucleic acid internalization after only 15 minutes of incubation with CPE4-LNP (**Fig. 2a**). If LNPs enter cells via a process of membrane fusion, it is expected that the lipid dye LR-PE remains mainly bound to the plasma membrane while the content (*i.e.* nucleic acid) enters the cytoplasm.<sup>31,32</sup> Interestingly, colocalization of Alexa488 nucleic acid and LR-PE decreased, indicating that membrane fusion and content nucleic acid release indeed had occurred when using the coiled coils peptides CPE4/CPK4. In contrast, in plain LNP or control experiments in which only one of the coiled-coil peptides was present, only limited nucleic acid and lipid uptake could be detected.

Flow cytometry was used to quantify the cellular uptake of the LNPs. The most efficient uptake was observed when HeLa cells were pretreated with CPK4 and incubated with CPE4-LNP, in accordance with the confocal microscopy study. Within 15 minutes of incubation 99.9% of the cells had nucleic acid internalized, while plain LNP or the control experiments revealed negligible delivery (**Fig. 2b**). In addition, the mean fluorescence intensity (MFI) analysis of the Alexa488-nucleic acid internalized by cells was significantly higher when coiled-coil peptides were used over all other LNPs (**Fig. 2c-2d**). These results confirmed that the fusogenic coiled-coil system induced rapid and efficient nucleic acid internalization.

To study whether the E4/K4 pair is able to enhance nucleic acid delivery in other cell types, Chinese hamster ovary (CHO), mouse fibroblast NIH/3T3, and human T cell lymphocyte Jurkat cells were transfected with LNPs. Again, CPK4-pretreated cells incubated with CPE4-LNP for 15 minutes resulted in the highest uptake of nucleic acid, regardless of cell type (**Fig. 3a, SI Fig. 3b-3c**). In line with previous experiments in HeLa cells, negligible nucleic acid delivery was observed for plain LNP and all control groups with CHO and NIH/3T3 cells, consistent with flow cytometry data (**Fig. 3b-4c**). Jurkat cells are regarded as a hard-to-transfect cell line.<sup>33,34-36</sup> By applying our fusogenic coiled-coil peptides, CPK4-pretreated Jurkat cells incubated with CPE4-LNPs produced superior nucleic acid internalization (**Fig. 3a-3c, SI Fig. 3d**), as compared to all other groups, which showed only limited nucleic acid uptake.

Altogether, this cell uptake study confirmed that fusogenic coiled-coil modified LNP can efficiently deliver nucleic acid in high yields to various cell lines as compared to the clinically approved Onpattro LNP formulation.

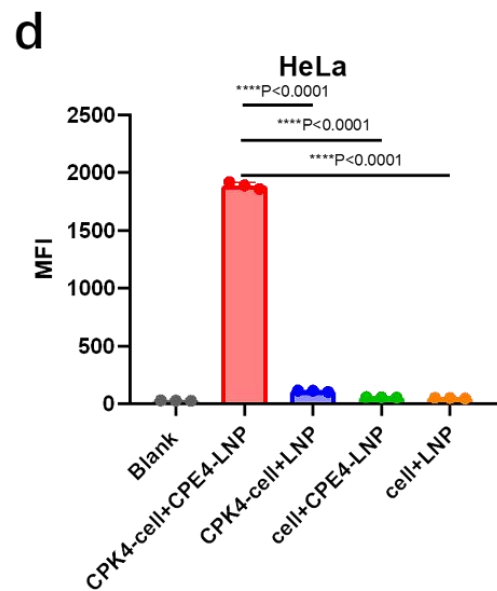
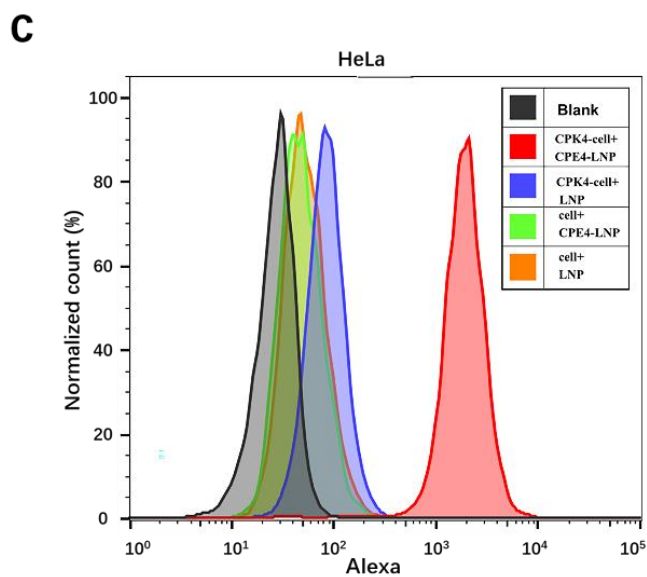
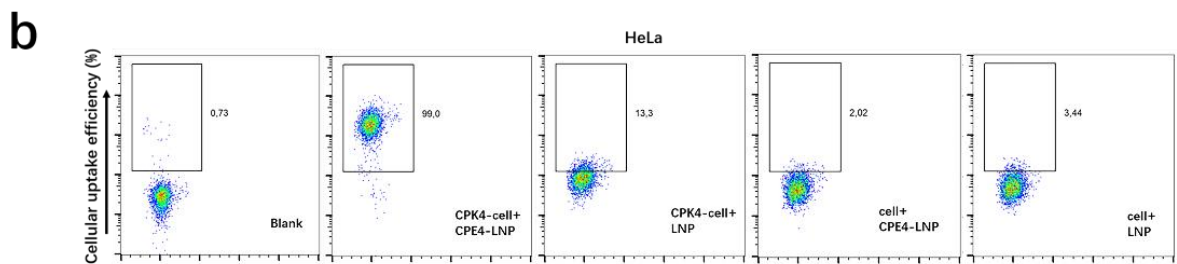
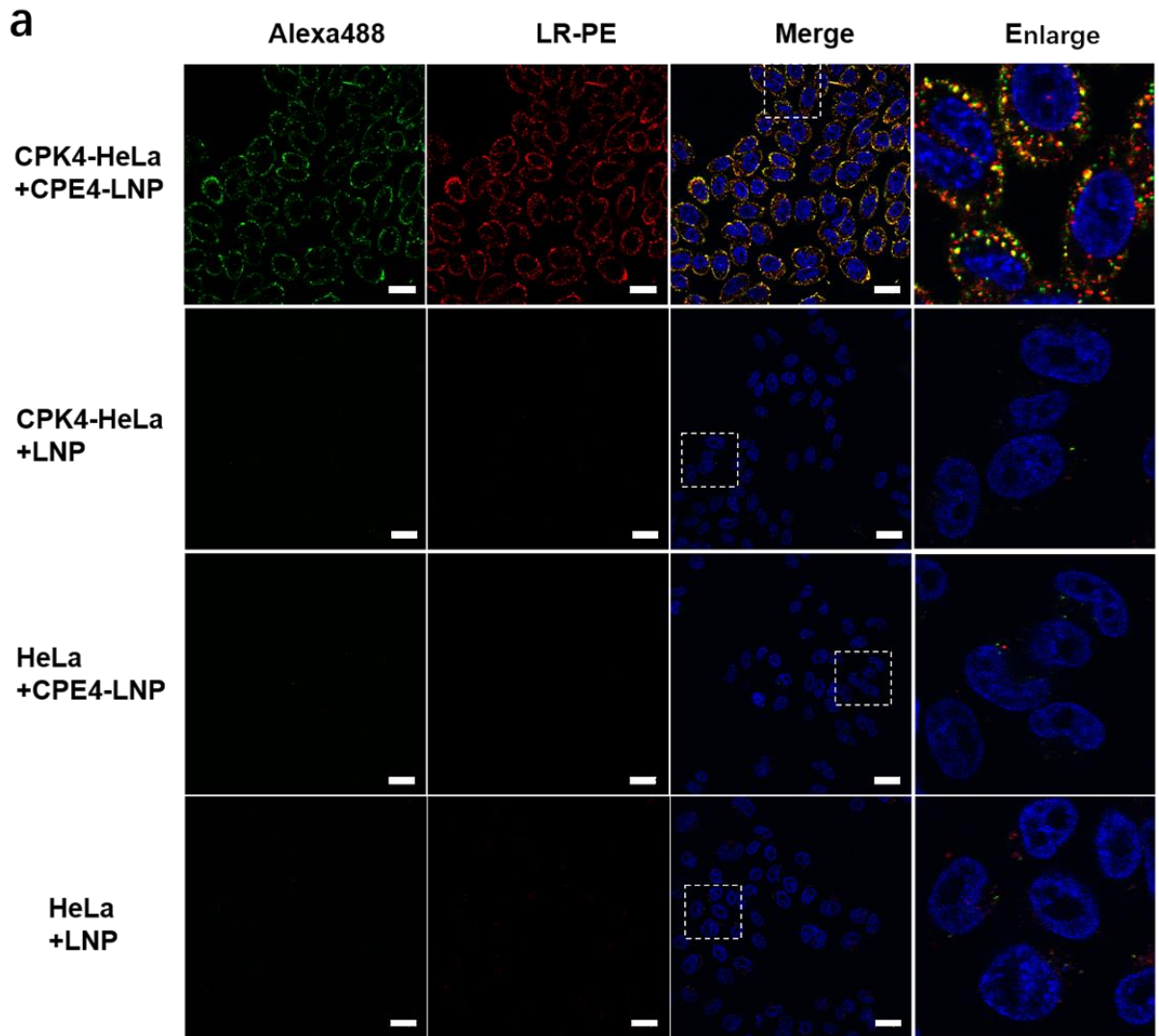


**Figure 2. Nucleic acid delivery to HeLa cells using fusogenic coiled-coil LNPs.** (a) Confocal microscopy images of cellular internalization of LNPs with HeLa cells. HeLa cells were pretreated with micellar CPK4 (10  $\mu$ M, 200  $\mu$ L) for 2 hours. After removal of the supernatant, cells were incubated with CPE4-LNP containing Alexa488-nucleic acid (200  $\mu$ M, 200  $\mu$ L) for 15 minutes, washed, and imaged. Blue: Hoechst 33342; green: Alexa488-nucleic acid; red: LR-PE; BF: bright field. Scale bar is 20  $\mu$ m. (b) Cellular internalization efficiency of LNPs with HeLa cells quantified by flow cytometry. (c-d) Fluorescence intensity of cells treated with LNPs carrying Alexa488-nucleic acid. An unpaired student t-test was used to determine the significance of the comparisons of data indicated in d (\*P < 0.05; \*\*P < 0.01; \*\*\*P < 0.001; \*\*\*\*P < 0.0001). In all panels, error bars represent the mean  $\pm$  s.d. (n=3).

### Evaluation of lysosome colocalization

Effective nucleic acid internalization and subsequent transfection require efficient escape of the genetic cargo from endosomes/lysosomes into the cytosol.<sup>37,38</sup> However, this is typically an inefficient process, as most of the cargo is not released thus the therapeutic effect is lowered. Therefore novel approaches that facilitate direct cytosolic delivery, and bypass endosomal entrapment, resulting in enhanced transfection efficiency are needed.

Coiled-coil mediated uptake of LNPs was studied as a function of time. For this, CPK4-pretreated cells were incubated with CPE4-LNPs encapsulating fluorescent nucleic acids for 15 minutes and cell uptake was studied. Confocal imaging revealed negligible nucleic acid colocalization with lysosomes during the following 0-8 h, with the majority being dispersed in the cytosol (**Fig. 4a,b**). In contrast, Gilleron *et al* quantified siRNA delivered to cells using LNPs and found that up to 70% was colocalized with lysosomes.<sup>19</sup>

Our data strongly suggests that fusogenic coiled-coil peptides enhance the cellular uptake of LNPs and increase the delivery of genetic cargo to the cytosol of cells, bypassing accumulation in endosomes and lysosomes. Therefore this approach holds promise for efficient transfection of cells with functional mRNA.

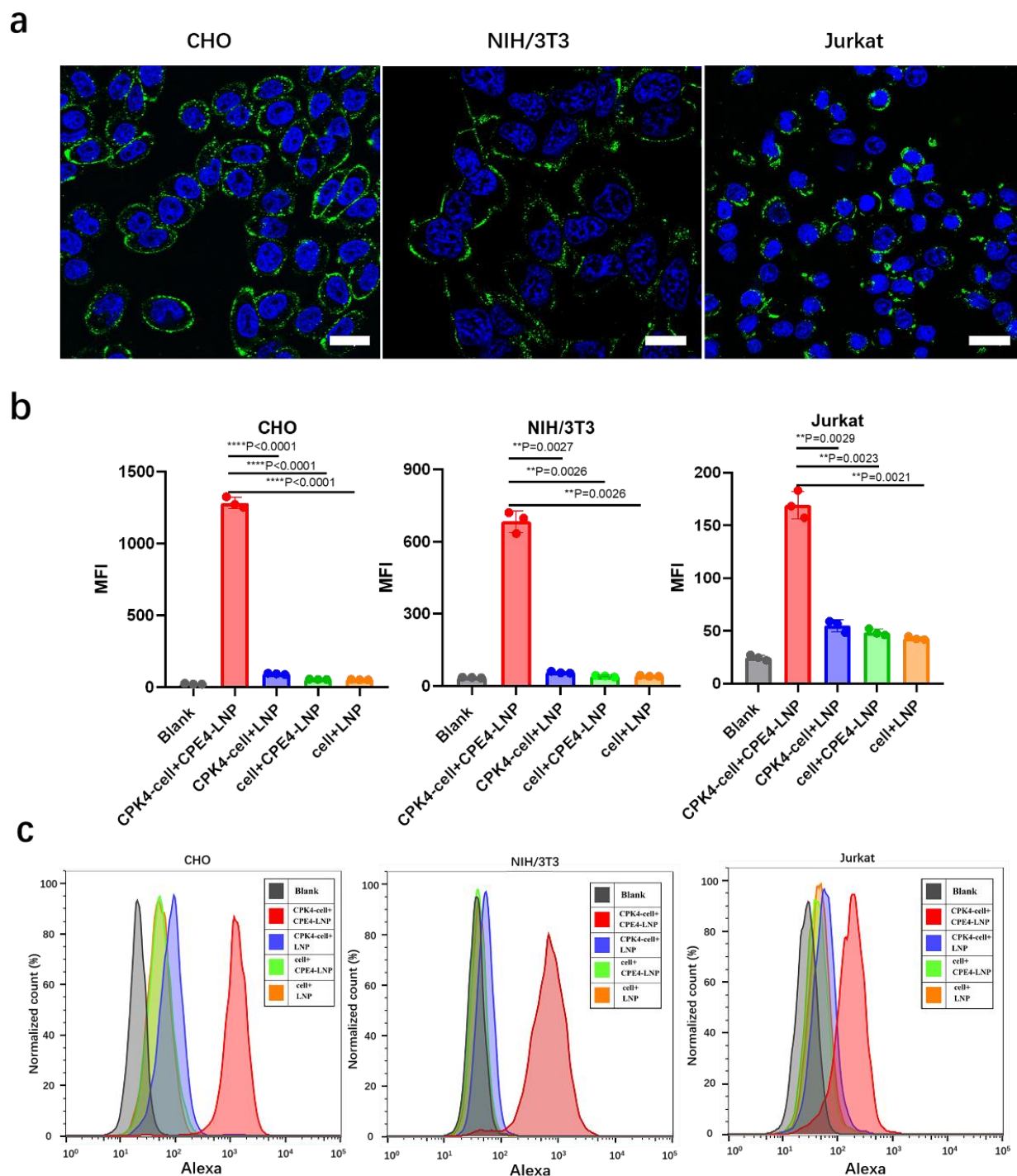


**Figure 3. Evaluation of cellular nucleic acid delivery by coiled-coil functionalized LNPs with other cell lines.** (a) Confocal images of LNPs with CHO, NIH/3T3, and Jurkat cells. Blue: Hoechst 33342; green: Alexa488-nucleic acid. Scale bar is 20  $\mu\text{m}$ . (b-c) The fluorescence intensity of internalized LNPs in CHO, NIH/3T3, and Jurkat cells. Alexa488-nucleic acid served as the fluorescent dye. Cells were pretreated with a micellar CPK4 solution (10  $\mu\text{M}$ , 200  $\mu\text{L}$ , 2 h), and after removal of the medium LNPs containing Alexa488-nucleic acid were added (200  $\mu\text{M}$ , 200  $\mu\text{L}$ , 15 min), and the cells were washed again before confocal and flow cytometry measurements. Unpaired student t-test was used to determine the significance of the comparisons of data indicated in b (\* $P < 0.05$ ; \*\* $P < 0.01$ ; \*\*\* $P < 0.001$ ; \*\*\*\* $P < 0.0001$ ). In all panels, error bars represent mean  $\pm$  s.d. (n=3).

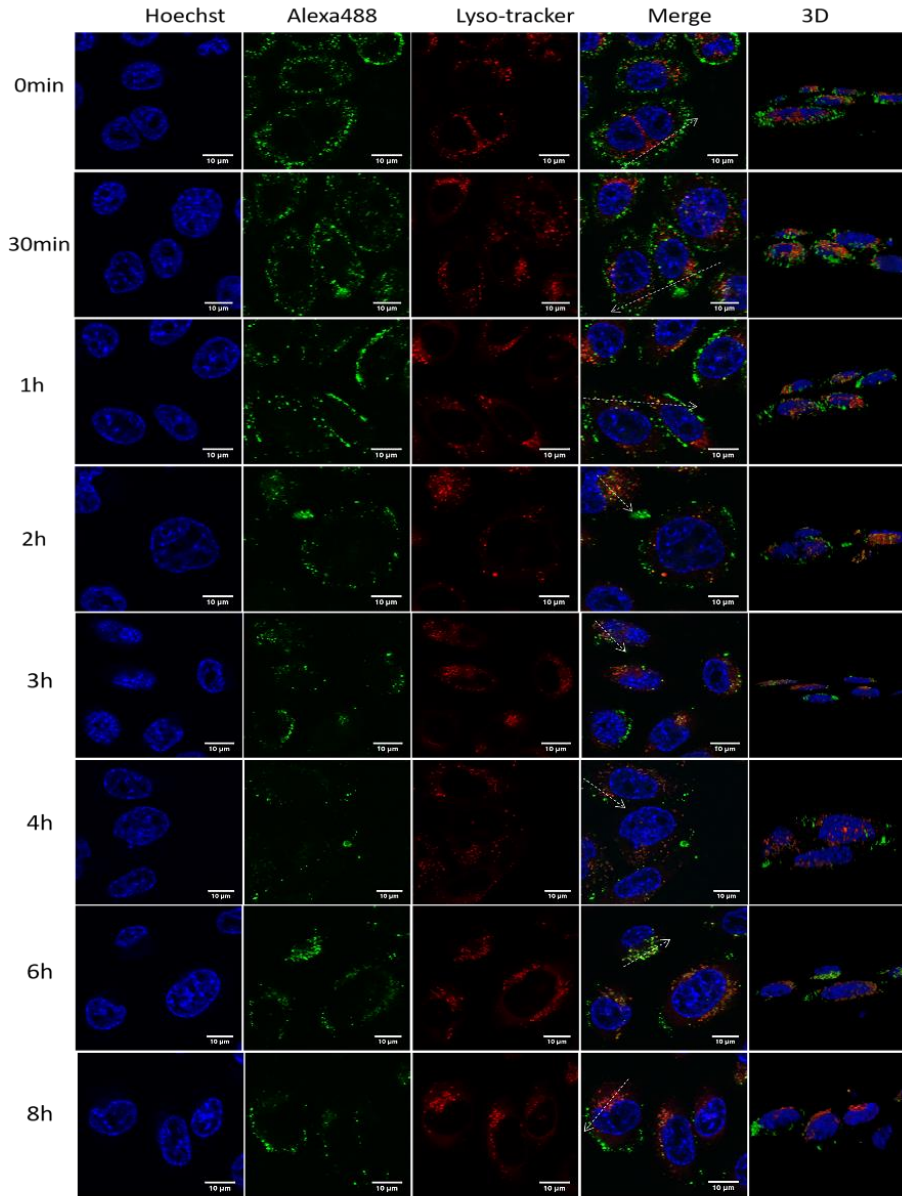
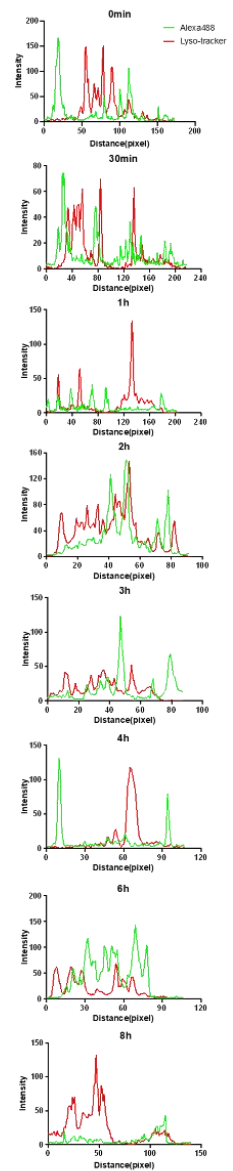
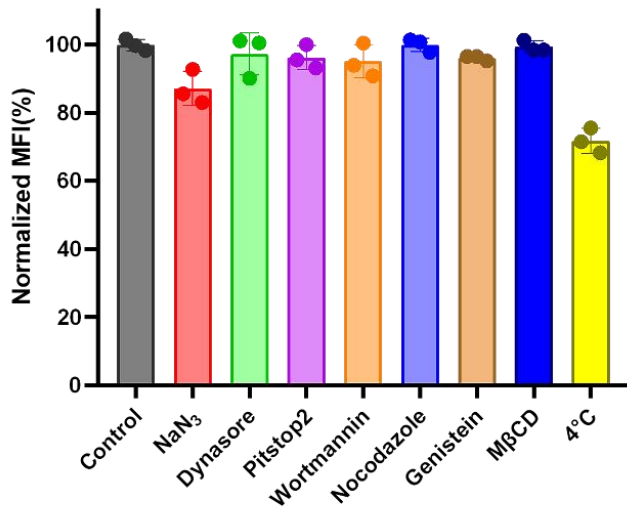
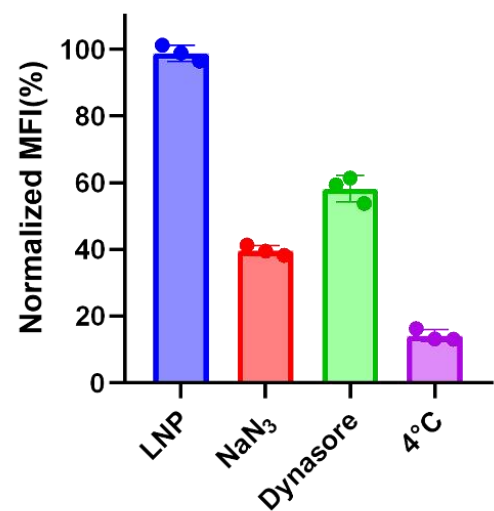
### Cellular internalization of LNPs

As our fusogenic coiled-coil system appears to facilitate membrane fusion, we wanted to discover whether the internalization mechanism of coiled-coil peptide modified LNPs was different from plain LNPs. Therefore coiled-coil mediated cell uptake of LNPs was studied in the presence of different cellular endocytosis inhibitors (*i.e.* Wortmannin,<sup>39,40</sup> Nocodazole,<sup>41</sup> Pitstop 2,<sup>42</sup> Dynasore,<sup>43,44</sup> Genistein,<sup>45,46</sup> Methyl- $\beta$ -cyclodextrin (M $\beta$ CD),<sup>45,47</sup> and Sodium azide<sup>48</sup>).

Cellular internalization of nucleic acid in the presence of endocytosis inhibitors was analyzed by flow cytometry (**Fig. 4c**), and the fluorescence intensity was normalized against the non-inhibitor treated group (control: CPK4-HeLa+CPE4-LNP). None of the endocytosis inhibitors appeared to influence nucleic acid internalization, although incubation at 4°C seemed to decrease the internalization efficiency slightly. Confocal imaging also demonstrated that there was no apparent adverse effects on nucleic acid delivery as the overall distribution in the presence of all tested inhibitors was still comparable to the control group (**SI Fig. 4a**). These results support the hypothesis that the dominant pathway for coiled-coil mediated nucleic acid delivery is independent of endocytosis and is mainly membrane fusion mediated. This pathway avoids endosomal entrapment of genetic cargo and results in enhanced transfection.

For unmodified LNP, cell entry is dependent on endocytic pathways.<sup>38,49</sup> Jerome *et al.* showed that dynasore reduced LNP uptake by around ~75%.<sup>19</sup> Hence, unmodified LNP were evaluated as a contrast to the fusogenic coiled-coil LNP system. As expected, after 4 hours of incubation, flow cytometry and confocal imaging of the cellular uptake of plain LNP showed nucleic acid internalization was remarkably reduced by NaN<sub>3</sub>, dynasore, and incubation at 4 °C (**Fig. 4d**, **SI Fig. 4b**). These results confirm that internalization of unmodified LNP is mainly mediated by clathrin-dependent endocytosis.

In summary, while unmodified LNP uptake is mediated by the clathrin-dependent endocytic pathway, our fusogenic coiled-coil LNP system successfully delivered nucleic acid into cells through membrane fusion, avoiding endosomal entrapment of nucleic acid and resulting in enhanced nucleic acid delivery.

**a****b****c****d**

**Figure 4. Investigation of cellular delivery pathways of LNPs by fusogenic coiled-coil peptides. (a)** Confocal images of coiled-coil mediated uptake of LNPs as a function of incubation time in HeLa cells after 15 min uptake; lysosome colocalization is studied by staining lysosomes with lyso-tracker deep red. HeLa cells were pretreated with CPK4 (10  $\mu$ M, 200  $\mu$ L) for 2 hours and incubated with CPE4-LNP carrying Alexa488-nucleic acid (200  $\mu$ M, 200  $\mu$ L) for 15 min, washed, and replaced by medium. Imaging was performed as a function of time. Blue: Hoechst 33342; green: Alexa488-nucleic acid; red: lyso-tracker deep red. Scale bar is 10  $\mu$ m. **(b)** Quantitative colocalization analysis of Alexa488-nucleic acid (green curve) and lysosomes (red curve) in the dashed arrow area of the merge channel as a function of time. **(c)** Quantification of Alexa488-nucleic acid delivery to CPK4-pretreated HeLa cells using CPE4-LNP (200  $\mu$ M, 200  $\mu$ L) after incubation for 15 min in the presence of various endocytosis inhibitors. Fluorescence intensity was normalized to Alexa-488-nucleic acid delivery in the absence of inhibitors. **(d)** Quantification of cellular internalization efficiency of unmodified LNP (200  $\mu$ M, 200  $\mu$ L) after a 4 h incubation period in the presence of various endocytosis inhibitors. Error bars represent mean  $\pm$  s.d. (n=3).

### mRNA Transfection

Gene therapy requires a high transfection efficiency to fulfill successful gene modulating effects. We have shown that fusogenic coiled-coil peptides can improve the delivery of nucleic acids to the cytosol of cells. We then evaluated the transfection performance of the modified LNPs. For this, EGFP-mRNA was encapsulated in LNPs and after transfection, the expression of green fluorescent protein (GFP) was quantified as an easily detectible indicator for functional mRNA delivery. The mRNA concentrations of LNPs were determined by the RiboGreen RNA assay.

Four cell lines were used to study the gene transfection efficiency: HeLa, CHO, NIH/3T3, and Jurkat. Confocal imaging of transfected HeLa cells showed that CPK4-pretreated HeLa cells incubated with CPE4-LNP carrying EGFP-mRNA for 2 hours achieved the highest level of GFP expression, as almost every cell produced strong and uniform GFP expression (**Fig. 5a**). In contrast, the commonly used commercial transfection reagent lipofectamine 3K only transfected a few cells. Onpattro LNP and the control groups that lack one of the peptides achieved only minor GFP expression. Quantitative analysis by flow cytometry confirmed the confocal imaging study (**Fig. 5b**). The fusogenic coiled-coil mediated LNP delivery achieved almost quantitative GFP expression in all cells (99.9%), while lipofectamine 3K mediated transfection resulted in 54.7% GFP positive cells. In addition, all other groups lacking either one or both peptides failed to induce relevant levels of GFP expression. Analysis of the GFP mean fluorescence intensity also illustrated that coiled-coil mediated delivery induced a 50-fold increase in GFP expression as compared to Onpattro LNP and all other groups (**Fig. 5c-5d**). Interestingly, non-CPK4 pretreated HeLa cells incubated with CPE4-LNP induced a reasonable level of GFP-positive cells. However, the MFI in these GFP-positive cells was significantly lower as compared to the fusogenic coiled-coil group. The prolonged incubation time of the cells with CPE4-LNP in this experiment (2 hours) might be the cause for this observation.

Next, transfection of cells with EGFP-mRNA was investigated in other cell lines. CHO and NIH/3T3 cells also showed a robust GFP expression using the fusogenic coiled-coil peptides (**SI Fig. 5a-5d**). Again, the peptide-mediated delivery of mRNA was superior compared to plain LNP or the control groups lacking one of the peptides. Transfection enhancement by the fusogenic coiled-coil LNP system compared to plain LNP was >50-fold in HeLa cells, 63-fold in CHO cells, and 29-fold in NIH/3T3 cells (**SI Fig. 7a-7c**).

Finally, mRNA transfection in T lymphocyte Jurkat cells was studied. Confocal imaging and flow cytometry data revealed that most Jurkat cells became GFP positive and GFP expression intensity (MFI) was highest when the fusogenic coiled-coil peptides were used (SI Fig. 6a-6d). Again, transfection was significantly higher when compared to plain LNP or control groups missing one of the peptides. Interestingly, lipofectamine 3K transfection of Jurkat cells was very inefficient. Overall, GFP expression levels in Jurkat were lower compared to HeLa cells, but still, the fusogenic coiled-coil LNP system induced a significant level of transfection enhancement, which was >3-fold higher compared to Onpattro LNP (SI Fig. 7d).

In summary, LNP-mediated mRNA delivery using fusogenic coiled-coil peptides is an effective approach to obtaining high levels of protein expression in various cell lines and could act as a potent nonviral vector able to achieve efficient mRNA transfection of cells.

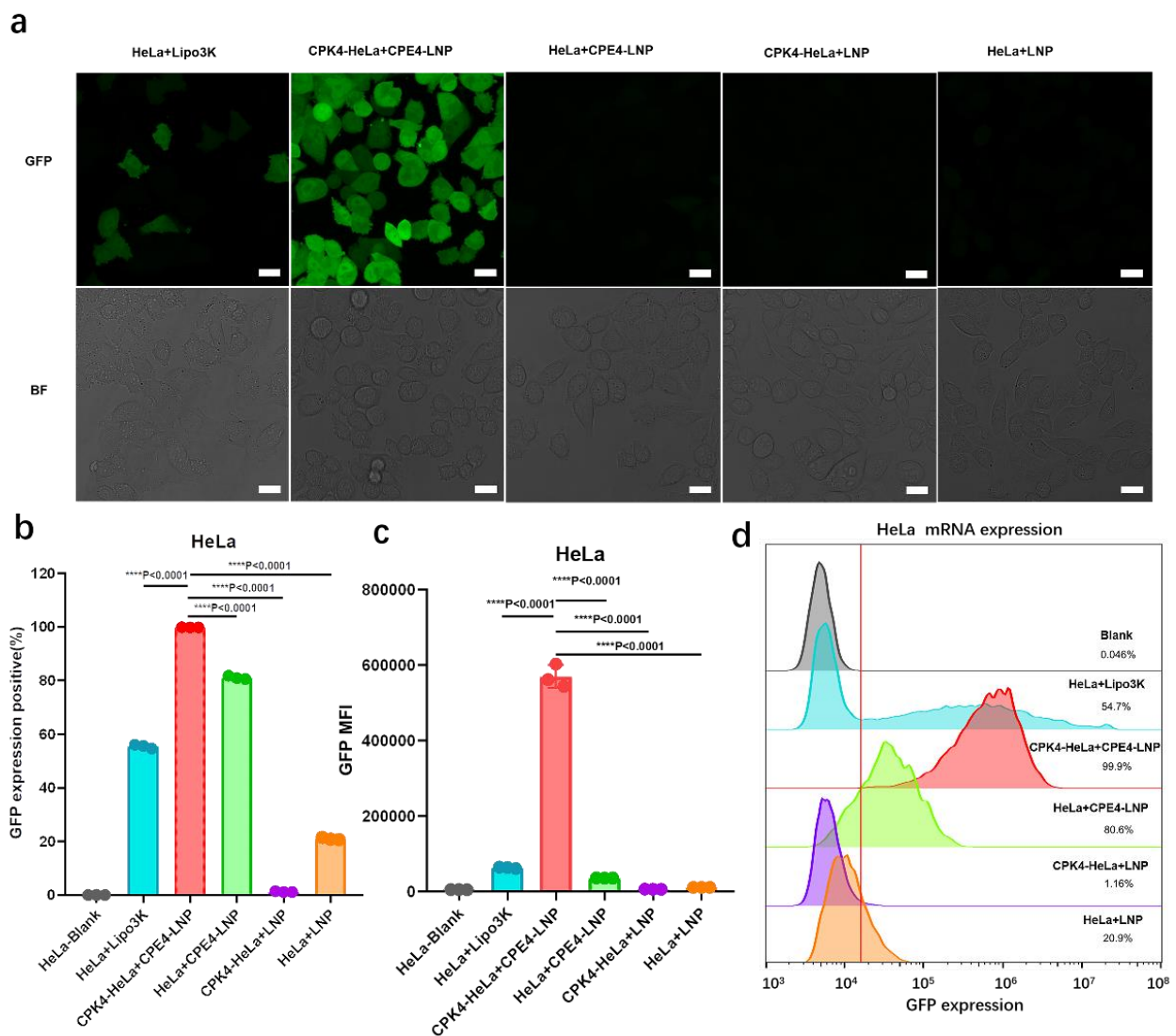


**Figure 5. Transfection efficiency of the coiled-coil system with HeLa cells. (a)** Confocal images of the EGFP-mRNA transfection of LNPs. Lipo3K: lipofectamine 3K; GFP: green fluorescent protein; BF: bright field. Scale bar is 20  $\mu$ m. **(b)** The quantification of EGFP-mRNA transfection efficiency of LNPs. **(c-d)** The GFP expression

fluorescence intensity (GFP MFI) of LNPs. HeLa cells were first incubated with CPK4 (10  $\mu$ M, 200  $\mu$ L, 2 h), followed by incubation with EGFP-mRNA encapsulated LNPs (1  $\mu$ g/mL, 2 h). Cells were then washed 3 times and cultured for another 18-24 h before confocal and flow cytometry measurements. Unpaired student t-test was used to determine the significance of the comparisons of data indicated in **b**, and **c**, (\*P < 0.05; \*\*P < 0.01; \*\*\*P < 0.001; \*\*\*\*P < 0.0001). In all panels, error bars represent mean  $\pm$  s.d. (n=3).

### Cytotoxicity assay of LNPs

For successful nucleic acid-based therapies it is important to keep a balance between transfection efficiency and cytotoxicity of the gene vector. Thus, the expression of GFP was studied as a function of the dose of LNPs carrying EGFP-mRNA, and the cell viability was determined in parallel. Near quantitative GFP expressing cells were obtained at a dose of 1  $\mu$ g/mL EGFP-mRNA (**SI Fig. 8a**). Next, cell viability after transfection was determined using the cell proliferation reagent WST-1. No significant toxicity was observed at all tested doses of EGFP-mRNA, and cell viability differences between plain LNP and coiled-coil modified LNP were not statistically significant. Interestingly, at higher doses the commercial reagent Lipofectamine 3K was shown to be more toxic (**SI Fig. 8b**). Altogether, these results demonstrate that our coiled-coil gene delivery system achieves potent transfection efficiency without altering the cytotoxicity profile of LNPs.

## Discussion and conclusion

Nonviral vectors can be used to encapsulate a wide variety of nucleic acid-based cargoes with a large range of molecular weights, including RNA (e.g. siRNA, mRNA, microRNA, ASO), DNA (e.g. plasmids), and genome editing tools (e.g. CRISPR/Cas, base editing, prime editing). The delivery of these cargoes using these vectors greatly facilitates precise and permanent correction of diseased genes.<sup>2,50,51</sup> Furthermore, multiple variants can be encapsulated and delivered using the same vector. To date, the design of novel nonviral vectors mainly focuses on establishing effective formulations capable of silencing, correcting, or introducing specific genes with minimal adverse effects.<sup>2,52</sup>

In this study, we showed that fusogenic coiled-coil peptides can induce efficient cellular internalization and potent transfection of nucleic acids *in vitro*. The introduction of 1 mol% of lipopeptide CPE4 to the Onpattro LNP formulation did not alter physicochemical parameters such as size, zeta-potential, and mRNA encapsulation efficiency. However, CPE4 exerted a significantly enhanced internalization and transfection effect when target cells were pretreated with the complementary lipopeptide CPK4. Qualitative evaluation of transfection with confocal microscopy and quantitative analysis with flow cytometry revealed efficient nucleic acid uptake within 15 minutes of incubation when the fusogenic coiled-coil peptides were used. In contrast, plain LNP and all control groups were unable to deliver measurable amounts of nucleic acid within this time frame. Coiled-coil mediated LNP transfection to cells is fast (within 2 hours of incubation) when compared to other cationic and lipid nanoparticles; these typically require longer incubation times (up to 24-72 h) to obtain significant transfection.<sup>53,54</sup> Furthermore we confirmed that the coiled-coil system is functional on various cell lines including CHO and the hard to transfect Jurkat cells.

Gene delivery into cells using non-viral vectors often suffers from a poor ability to escape from the endosomal and/or lysosomal compartments. For siRNA, the endosomal escape was determined to be around 1-2%, making delivery very inefficient and thus lowering the potential therapeutic effect.<sup>19</sup>

This is because endosomal escape is often spatio-temporally limited and only occurs in the brief stage of endo-lysosomal maturation.<sup>19,38</sup> Various approaches have been investigated to enhance endosomal escape efficiency, examples are the introduction of cell-penetrating peptides,<sup>23,24</sup> endosome disrupting peptides,<sup>24,55</sup> and photochemical internalization.<sup>56,57</sup> However, these approaches typically lack cell selectivity<sup>58</sup> and cause membrane destruction<sup>57</sup> resulting in cytotoxicity.<sup>59,60</sup> Using fusogenic coiled-coil peptides we managed to circumvent endosomal entrapment, resulting in direct cytosolic delivery of nucleic acid. This direct delivery was proven by performing uptake studies in the presence of common endocytosis inhibitors and quantifying the fraction of nucleic acid inside CPE4-LNP localized in lysosomes. Transfection of cells with EGFP-mRNA using fusogenic coiled-coil peptides resulted in an enhanced transfection performance as shown by the near-quantitative number of GFP positive cells and the high expression level of GFP in these cells as compared to plain LNP (up to a 63-fold increase in GFP expression). Furthermore, the control studies revealed that both coiled-coil peptides are required for efficient transfection, highlighting the importance of the coiled-coil interaction for the delivery of mRNA and concomitant protein expression. Our approach also outperformed the commercial reagent lipofectamine 3K in all studies. Thus using fusogenic coiled-coil peptides lowers the amount of mRNA required to reach a desired expression level, which is also beneficial for cell viability. In this study, EGFP-mRNA was used, but any other nucleic acid could be delivered in a similar fashion.

The current approach requires pretreatment of cells with CPK4, rendering it impractical for *in vivo* applications via systemic administration. Nevertheless, *in vitro/ex vivo* delivery and other *in vivo* delivery approaches other than *i.v.* injections, such as local/subcutaneous injections may be feasible. A potential application could be adoptive cell therapy.<sup>61,62,63</sup> Except for viral transduction, other attempts of lymphocyte transfection often apply electroporation and nucleofection to deliver exogenous genes into T cells,<sup>64,65</sup> but it requires specialized equipment, disrupts membrane, produces cytokine, causes cytoplasmic content loss and cytotoxicity, and unable to penetrate membrane across cells consistently.<sup>66,67</sup> Coiled-coil mediated LNP delivery might also be applicable to the gene-editing field, such as CRISPR/Cas9 editing<sup>68,69</sup> and prime gene editing.<sup>70</sup> The highly efficient, transient, non-integrating Cas9 expression could greatly reduce the off-target effects, immune responses, and integration into the genome, which could be accomplished by our nonviral fusogenic coiled-coil delivery system.

In conclusion, fusogenic coiled-coil peptides can significantly enhance the delivery of nucleic acid to cells using LNPs. By circumventing the endosomal pathway, the genetic cargo is delivered to the cytosol of cells. For EGFP-mRNA this resulted in an up to a 63-fold increase in protein expression as compared to unmodified LNP, opening new avenues for nucleic acids based therapies. Furthermore, we showed efficient transfection in various cell lines with substantial improvement as compared to the commercial transfection reagent lipofectamine 3K. Thus modification of LNPs with fusogenic coiled-coil peptides could serve as a promising strategy to enhance LNP efficacy to deliver nucleic acid based therapies *in vitro*, *ex vivo*, and potentially *in vivo*.

## Methods

### Chemicals.

All Fmoc-protected amino acids were purchased from Novabiochem. Piperidine, trifluoroacetic acid, acetonitrile, dimethylformamide (DMF) were purchased from Biosolve; dichloromethane (DCM), and ethanol were purchased from Sigma-Aldrich. 1,2-distearoyl-*sn*-glycero-3-phosphocholine (DSPC), 1,2-dimyristoyl-*rac*-glycero-3-methoxypolyethylene glycol-2000 (DMG-PEG2K), 1,2-dioleoyl-*sn*-glycero-3-phosphocholine (DOPC), 1,2-dioleoyl-*sn*-glycero-3-phosphoethanolamine (DOPE), 1,2-dioleoyl-*sn*-glycero-3-phosphoethanolamine-N-(7-nitro-2-1,3-benzoxadiazol-4-yl) (PE-NBD), 1,2-dioleoyl-*sn*-glycero-3-phosphoethanolamine-N-(lissamine rhodamine B sulfonyl) (PE-LR), were purchased from Avanti Polar Lipids, DLin-MC3-DMA was purchased from Biorbyt (Cambridge, England), and dynasore, wortmannin, nocodazole, pitstop2, genistein, methyl- $\beta$ -cyclodextrin (M $\beta$ CD), sodium azide (NaN<sub>3</sub>), cholesterol was purchased from Sigma-Aldrich. Lyso-tracker deep red was purchased from Thermofisher. Triton™ X-100 was purchased from Acros Organics. QuantiT™ RiboGreen® RNA reagent and rRNA standards were purchased from Life Technologies. WST-1 reagent was purchased from Sigma-Aldrich. Nucleic acid: Alexa488-nucleic acid (Alexa488-5'-AACCATACACCTACTACCTCA-3') was purchased from Integrated DNA technology; cleancap EGFP-mRNA was purchased from Trilink biotechnology.

### Lipopeptide synthesis and purification.

Peptide E3 (EIAALEK)<sub>3</sub>, K3 (KIAALKE)<sub>3</sub>, E4 (EIAALEK)<sub>4</sub> and K4 (KIAALKE)<sub>4</sub> were synthesized using Fmoc chemistry and standard solid-phase peptide synthesis protocols on a 0.1 mmol scale as described previously.<sup>28</sup> Fmoc deprotection was performed using 20% piperidine in DMF at 90 °C for 60 s. Amide coupling was achieved using 5 eq. of protected amino acid, 5 eq. DIC as activator and 5 eq. Oxyma as activator base, heated at 95 °C for 240 seconds. Lipidated peptides (CPK3, CPE3, CPK4, CPE4) were made on resin via the coupling of 2.5 equivalents of N<sub>3</sub>-PEG<sub>4</sub>-COOH, with 2.5 eq of HBTU and 5 eq. of DIPEA in DMF overnight at room temperature. After washing the resin with DMF, the azide was reduced using 10 eq. of PME3 (1 M in toluene), with 4:1 dioxane:water as solvent for 2.5 hours. The resin was then washed thoroughly with 4:1 dioxane:water, MeOH and DMF. Lipidation was achieved using 2 eq. cholesteryl hemisuccinate, 2 eq. HBTU and 4 eq. DIPEA in 1:1 DMF:DCM. After the final coupling the resin was washed with DMF, MeOH, and DCM, dried under vacuum, and the peptide was cleaved using a mixture of TFA:TIPS:EDDT:water (92.5:2.5:2.5:2.5) for 1 hour, after which the peptide was precipitated in cold diethyl ether, collected via centrifugation and lyophilized. All peptides were purified by HPLC on a Shimadzu system consisting of two KC-20AR pumps and an SPD-20A or SPD-M20A detector equipped with a Kinetix Evo C18 column. Eluents consisted of 0.1% TFA in water (A) and 0.1% TFA in MeCN (B), with all peptides eluted using a gradient of 20-90% B over 35 minutes, with a flow rate of 12 mL/min. Collected fractions were checked for purity via LC-MS, with the pure fractions being pooled and lyophilized. LC-MS spectra were recorded using a Thermo Scientific TSQ quantum access MAX mass detector connected to an Ultimate 3000 liquid chromatography system fitted with a 50x4.6 mm Phenomenex Gemini 3  $\mu$ m C18 column.

### Lipid nanoparticles formulation.

Lipids and lipopeptides were combined at the desired molar ratios and concentrations from stock solutions dissolved in chloroform:methanol (1:1). Solvents were evaporated under a nitrogen flow

and residual solvent was removed *in vacuo* for at least 30 minutes. The lipid film was dissolved in absolute ethanol and used for assembly (total [lipid] was 1  $\mu\text{mol}$ ). A solution of mRNA was made by diluting nucleic acid (Alexa488-nucleic acid or EGFP-mRNA) in 50 mM citrate buffer (pH = 4, RNase free  $\text{H}_2\text{O}$ ). The solutions were loaded into two separate syringes and connected to a T-junction microfluidic mixer. The solutions were mixed in a 3:1 flow ratio of nucleic acid:lipids (1.5 mL/min for the nucleic acid solution, 0.5 mL/min for the lipids solution, N/P ratio was 16:1). After mixing, the solution was directly loaded in a 20 k MWCO dialysis cassette (Slide-A-Lyzer™, Thermo Scientific) and dialyzed against 1 x PBS overnight. After overnight dialysis, mRNA encapsulation efficiency was determined by Quant-iT™ RiboGreen™ RNA Assay Kit as described below. For confocal cellular uptake experiments, 1 mol% of PE-LR was added with the other lipids.

### **Biophysical characterization.**

The size and zeta potential of LNPs were measured using a Malvern zetasizer Nano ZS. Long term stability of LNPs was assessed by measuring the hydrodynamic radius using DLS for 10 days.

The morphology of LNPs was analyzed by cryogenic transmission electron microscopy (cryo-EM). Vitrification of concentrated LNPs (lipids  $\sim 10$  mM) was performed using a Leica EM GP operating at 21 °C and 95 % room humidity (RH). Sample suspensions were placed on glow discharged 100  $\mu\text{m}$  lacey carbon film supported on 200 mesh copper grids (Electron Microscopy Sciences). Optimal results were achieved using a 60-second pre-blot and a 1-second blot time. After vitrification, sample grids were maintained below -170 °C, and imaging was performed on a Tecnai T12 (Thermo Fisher) with a biotwin lens and LaB6 filament operating at 120 keV equipped with an Eagle 4 K $\times$ 4 K CCD camera (Thermo Fisher). Images were acquired at a nominal underfocus of -2 to -3  $\mu\text{m}$  (49,000 $\times$  magnification) with an electron dose of  $\sim 2000$  e/nm<sup>2</sup>. The size distribution of LNPs was based on 100 particles (Fiji ImageJ) from cryo images normalized by percentage distribution.

Circular dichroism measurements: CD spectra were recorded on a JASCO J-815 CD spectrometer fitted with a Peltier temperature controller. Unless otherwise specified, samples were measured at 20 °C in a quartz cuvette with a 2 mm path length. Spectra were recorded from 200 to 250 nm at 1 nm intervals, with a bandwidth of 1 nm, with the final spectrum consisting of the average of 5 sequentially recorded spectra. The mean residue molar ellipticity ( $\theta$ , deg cm<sup>2</sup> dmol<sup>-1</sup>) was calculated according to equation ( $[\theta] = (100 * [\theta]_{obs}) / (c * n * l)$ ),  $[\theta]_{obs}$  representing the observed ellipticity in mdeg, c the peptide concentration in mM, n the number of peptide bonds and l the path length of the cuvette in cm.

### **mRNA encapsulation efficiency.**

The encapsulation efficiency (EE%) of EGFP-mRNA was measured using a Quant-iT™ RiboGreen™ RNA Assay Kit (Invitrogen). For the determination of non-encapsulated EGFP-mRNA, LNPs after dialysis were diluted with 1 x TE buffer (RNase free) and treated with the RiboGreen™ reagent. For the determination of the total amount of EGFP-mRNA, LNPs after dialysis were treated with 1% Triton X-100 in TE buffer (RNase free) and incubated for 5 minutes followed by dilution with TE buffer and treatment with the RiboGreen™ reagent. The supplied RNA standards were used to generate a standard curve and changes in fluorescence was measured in 96-well plates using a TECAN Infinite M1000 Pro microplate reader. The percentage of mRNA encapsulation (EE%) was determined using the fraction of  $(F_{\text{total RNA}} - F_{\text{free RNA}}) / F_{\text{total RNA}} * 100\%$ .

### **Cell culture, and cell uptake study.**

Cell culture: HeLa, CHO, NIH/3T3, and Jurkat cell lines purchased from ATCC were cultured according to ATCC guidelines. The DMEM and RPMI-1640 growth media (Sigma Aldrich) containing sodium bicarbonate, without sodium pyruvate and HEPES, were supplemented with 10% fetal bovine serum (Sigma), 1% L-glutamine (Thermo Fisher Scientific), and 1% penicillin/streptomycin (Thermo Fisher Scientific). HeLa, CHO, and NIH/3T3 were cultured with DMEM medium, and Jurkat was cultured with RPMI-1640 medium, at 37 °C in the presence of 5% CO<sub>2</sub>.

Cell uptake (flow cytometry measurements): Flow cytometry analysis (FACs) of cellular uptake efficiency was performed to compare internalization efficiency differences. All lipids with a certain ratio (molar ratio DOPC:DOPE:cholesterol=2:1:1, 1 mol% of NBD-PE) were dried under N<sub>2</sub> flow, hydrated with PBS and sonicated at 55°C for 3 min. The CPE and CPK modified liposomes (CPE3-lipo, CPE4-lipo, CPK3-lipo, and CPK4-lipo) were made the same way while adding 1 mol% of CPE3, CPE4, CPK3, and CPK4 into the lipid mixture. CPK3, CPK4, CPE3, CPE4 lipid films were made, hydrated with complete DMEM, and sonicated for 10 min at room temperature. For cellular uptake efficiency tests, HeLa cells were pretreated with CPK3, CPK4, CPE3, CPE4 in DMEM for 2 h, then NBD labeled liposomes CPE3-lipo, CPE4-lipo, CPK3-lipo, and CPK4-lipo were added to the cells (15 min). After 15 min incubation, the medium was removed and cells were washed with PBS, digested with trypsin, washed, and resuspended in PBS, followed by flow cytometry measurements. For the cellular internalization efficiency of CPE3-LNP and CPE4-LNP, both LNPs were prepared as previously described by encapsulating Alexa488 nucleic acid, 1 mol% of CPE3 and CPE4 lipopeptides were added to the other lipids, and then proceeded to form LNPs, as described above, was followed.

Cell uptake (confocal imaging): Cells were seeded in an 8-well confocal slide at a density of  $5 \times 10^4$  cells/well and incubated at 37 °C in 5% CO<sub>2</sub>, and after 18 h, the medium was removed and medium containing CPK4 (10 μM, 200 μL) and Hoechst 33342 (5 μM, 200 μL) was added and incubated for 2 h at 37 °C in 5% CO<sub>2</sub>. Next, cells were washed with PBS (3X), and incubated with CPE4-LNP (200 μM, 200 μL) containing Alexa488 labeled nucleic acid for 15 min. The supernatant was removed and cells were washed with PBS, and DMEM free of phenol red indicator was added for confocal microscopy measurements using a Leica TCS SP8 confocal laser scanning microscope. For flow cytometry measurements, cells were seeded in 24-well plates at a density of  $2.5 \times 10^5$  cells/well, the rest of the procedure was the same as for the confocal measurements.

Endocytosis inhibitor assay (confocal imaging): HeLa cells were pretreated with nocodazole (40 μM), wortmannin (0.25 μM), dynasore (80 μM), pitstop2 (20 μM), genistein (200 μM), methyl-β-cyclodextrin (MβCD, 10 mM) or sodium azide (0.1% w/v) in DMEM medium for 1 h, after which the medium was replaced with medium containing lyso-tracker deep red (75 nM), CPK4 (10 μM), and fresh inhibitors and incubated for 2 h, then Alexa488 nucleic acid encapsulated CPE4-LNP (200 μM) were incubated in the presence of the inhibitors. After 15 min, the cells were washed three times, and phenol red indicator free DMEM was added for confocal microscopy imaging. When performing cellular uptake assays at 4 °C, cells were first incubated with lyso-tracker deep red (75 nM) and CPK4 (10 μM) for 2 h at 37 °C, then 1 h at 4 °C. The medium was removed and cells were washed and incubated for 15 min at 4 °C in the presence of CPE4-LNP (200 μM), followed by confocal imaging.

Endocytosis inhibitor assay (flow cytometry measurements): Cells were seeded on 24-well plates at a density of  $2.5 \times 10^5$  cells/well. After 18 h, the medium was removed and cells were incubated with inhibitors and CPK4 in medium (10  $\mu$ M) for 2 h. Then Alexa488 nucleic acid encapsulated CPE4-LNP (200  $\mu$ M, 15 min) was added in the presence of fresh inhibitors. The cells were washed, digested, and flow cytometry measurements using a Guava easyCyte machine (Luminex Corporation) were performed.

For the endocytosis pathway assay of unmodified LNPs, the cells were preincubated with endocytosis inhibitors for 2 h, then LNPs were added to the cells in the presence of fresh inhibitors and incubated for 4 h, and washed before the confocal imaging and flow cytometry measurements.

#### **Lysosome colocalization study.**

HeLa cells were seeded on 8-well confocal plates at a density of  $5 \times 10^4$  cells/well. After overnight growth the cells were treated with lyso-tracker deep red (75 nM) and CPK4 (10  $\mu$ M) for 2 h. The supernatant was removed, and Alexa488 nucleic acid encapsulated CPE4-LNP (200  $\mu$ M) was added and incubated for 15 min. The medium was removed, and lyso-tracker deep red (75 nM) in DMEM was added and incubated at different times before confocal imaging.

#### **Transfection assay.**

CPE4-LNPs and LNPs encapsulating EGFP-mRNA were prepared as described previously. HeLa, CHO, NIH/3T3, and Jurkat were cultured in 8-well confocal plates at the density of  $2 \times 10^4$  cells/well overnight before cells were pretreated with CPK4-medium (10  $\mu$ M) for 2 h, washed three times with PBS, then LNPs (1  $\mu$ g/mL) were added to the cells and incubated for 2 h, then the medium was removed and washed three times, refreshed with fresh medium for continuous 18-24 h culturing before confocal imaging and flow cytometry measurements. The concentration of LNPs was determined by Quant-iT Ribogreen RNA assay. The commercial transfection agent lipofectamine 3K/EGFP-mRNA was prepared according to the manufacturers protocol using the same amount of EGFP-mRNA, and cells were transfected for 2 h and refreshed with medium before 18-24 h culturing.

#### **Cell viability measurements.**

HeLa cells were seeded on 96-well plates at a density of  $1 \times 10^4$  cells per well overnight, then the same procedure as previously described was followed but different concentrations of LNPs (0.25  $\mu$ g/mL, 0.5  $\mu$ g/mL, 1  $\mu$ g/mL, 1.5  $\mu$ g/mL, 2  $\mu$ g/mL) were added. After 24 h incubation, cell proliferation reagent WST-1 solution (20  $\mu$ L, Sigma-Aldrich) was added to the medium (200  $\mu$ L) and cells were incubated for another 4 h at 37 °C. The absorbance at 450 nm was measured at room temperature using a Tecan infinite M1000. The cell viability was normalized with a control (blank HeLa cells), which was set at 100% cell survival.

#### **Statistical analysis.**

All experiments were performed in triplicate (n=3) unless specified otherwise, and the significance was determined using an unpaired student t-test (Graphpad Prism) for all comparisons. \* $p \leq 0.05$ , \*\* $p \leq 0.01$ , \*\*\* $p \leq 0.001$ , \*\*\*\* $p < 0.0001$ .

## References

1. Akinc, A.; Maier, M. A.; Manoharan, M.; Fitzgerald, K.; Jayaraman, M.; Barros, S.; Ansell, S.; Du, X.; Hope, M. J.; Madden, T. D.; Mui, B. L.; Semple, S. C.; Tam, Y. K.; Ciufolini, M.; Witzigmann, D.; Kulkarni, J. A.; van der Meel, R.; Cullis, P. R., The Onpattro story and the clinical translation of nanomedicines containing nucleic acid-based drugs. *Nature Nanotechnology* **2019**, *14* (12), 1084-1087.
2. Yin, H.; Kanasty, R. L.; Eltoukhy, A. A.; Vegas, A. J.; Dorkin, J. R.; Anderson, D. G., Non-viral vectors for gene-based therapy. *Nature Reviews Genetics* **2014**, *15* (8), 541-555.
3. Guan, S.; Rosenecker, J., Nanotechnologies in delivery of mRNA therapeutics using nonviral vector-based delivery systems. *Gene Therapy* **2017**, *24* (3), 133-143.
4. Naldini, L., Gene therapy returns to centre stage. *Nature* **2015**, *526* (7573), 351-360.
5. Somia, N.; Verma, I. M., Gene therapy: trials and tribulations. *Nature Reviews Genetics* **2000**, *1* (2), 91-99.
6. Li, C.; Samulski, R. J., Engineering adeno-associated virus vectors for gene therapy. *Nature Reviews Genetics* **2020**, *21* (4), 255-272.
7. Kuzmin, D. A.; Shutova, M. V.; Johnston, N. R.; Smith, O. P.; Fedorin, V. V.; Kukushkin, Y. S.; van der Loo, J. C., The clinical landscape for AAV gene therapies. *Nature Reviews Drug Discovery* **2021**, *20* (3), 173-175.
8. Dunbar, C. E.; High, K. A.; Joung, J. K.; Kohn, D. B.; Ozawa, K.; Sadelain, M., Gene therapy comes of age. *Science* **2018**, *359* (6372), eaan4672.
9. Thomas, C. E.; Ehrhardt, A.; Kay, M. A., Progress and problems with the use of viral vectors for gene therapy. *Nature Reviews Genetics* **2003**, *4* (5), 346-358.
10. Bessis, N.; GarciaCozar, F. J.; Boissier, M. C., Immune responses to gene therapy vectors: influence on vector function and effector mechanisms. *Gene Therapy* **2004**, *11* (1), S10-S17.
11. Sabnis, S.; Kumarasinghe, E. S.; Salerno, T.; Mihai, C.; Ketova, T.; Senn, J. J.; Lynn, A.; Bulychev, A.; McFadyen, I.; Chan, J.; Almarsson, Ö.; Stanton, M. G.; Benenato, K. E., A Novel Amino Lipid Series for mRNA Delivery: Improved Endosomal Escape and Sustained Pharmacology and Safety in Non-human Primates. *Molecular Therapy* **2018**, *26* (6), 1509-1519.
12. Witzigmann, D.; Kulkarni, J. A.; Leung, J.; Chen, S.; Cullis, P. R.; van der Meel, R., Lipid nanoparticle technology for therapeutic gene regulation in the liver. *Advanced Drug Delivery Reviews* **2020**, *159*, 344-363.
13. Zhao, Y.; Zheng, Z.; Cohen, C. J.; Gattinoni, L.; Palmer, D. C.; Restifo, N. P.; Rosenberg, S. A.; Morgan, R. A., High-Efficiency Transfection of Primary Human and Mouse T Lymphocytes Using RNA Electroporation. *Molecular Therapy* **2006**, *13* (1), 151-159.
14. Slivac, I.; Guay, D.; Mangion, M.; Champeil, J.; Gaillet, B., Non-viral nucleic acid delivery methods. *Expert Opinion on Biological Therapy* **2017**, *17* (1), 105-118.
15. Do, H. D.; Couillaud, B. M.; Doan, B.-T.; Corvis, Y.; Mignet, N., Advances on non-invasive physically triggered nucleic acid delivery from nanocarriers. *Advanced Drug Delivery Reviews* **2019**, *138*, 3-17.
16. Zhang, Y.; Sun, C.; Wang, C.; Jankovic, K. E.; Dong, Y., Lipids and Lipid Derivatives for RNA Delivery. *Chemical Reviews* **2021**, *121* (20), 12181-12277.
17. Yonezawa, S.; Koide, H.; Asai, T., Recent advances in siRNA delivery mediated by lipid-based nanoparticles. *Advanced Drug Delivery Reviews* **2020**, *154-155*, 64-78.
18. Kowalski, P. S.; Rudra, A.; Miao, L.; Anderson, D. G., Delivering the Messenger: Advances in Technologies for Therapeutic mRNA Delivery. *Molecular Therapy* **2019**, *27* (4), 710-728.
19. Akinc, A.; Querbes, W.; De, S.; Qin, J.; Frank-Kamenetsky, M.; Jayaprakash, K. N.; Jayaraman, M.; Rajeev, K. G.; Cantley, W. L.; Dorkin, J. R.; Butler, J. S.; Qin, L.; Racie, T.; Sprague, A.; Fava, E.; Zeigerer, A.; Hope, M. J.; Zerial, M.; Sah, D. W. Y.; Fitzgerald, K.; Tracy, M. A.; Manoharan, M.;

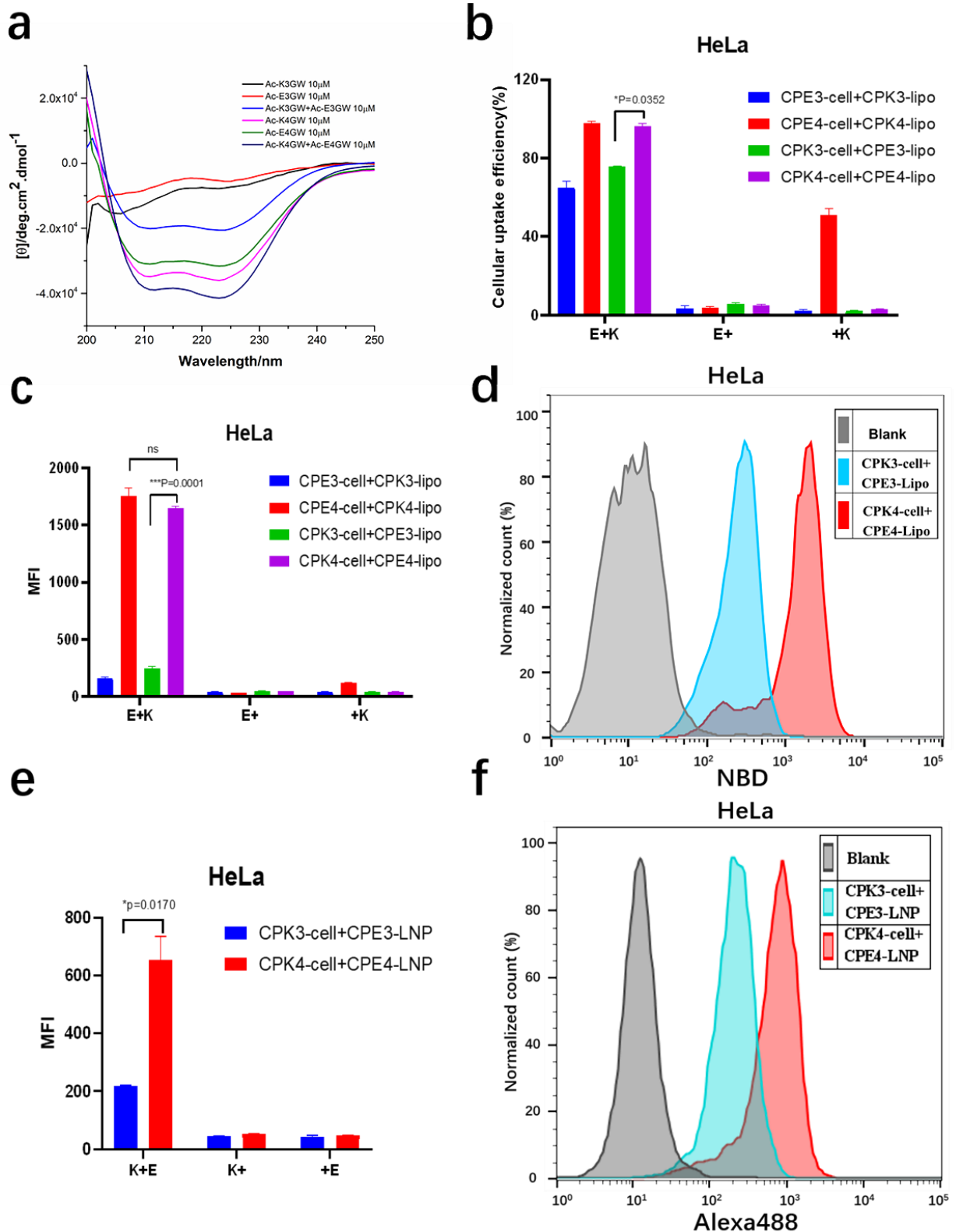
- Koteliansky, V.; Fougerolles, A. d.; Maier, M. A., Targeted Delivery of RNAi Therapeutics With Endogenous and Exogenous Ligand-Based Mechanisms. *Molecular Therapy* **2010**, *18* (7), 1357-1364.
20. Wittrup, A.; Ai, A.; Liu, X.; Hamar, P.; Trifonova, R.; Charisse, K.; Manoharan, M.; Kirchhausen, T.; Lieberman, J., Visualizing lipid-formulated siRNA release from endosomes and target gene knockdown. *Nature Biotechnology* **2015**, *33* (8), 870-876.
21. Gilleron, J.; Querbes, W.; Zeigerer, A.; Borodovsky, A.; Marsico, G.; Schubert, U.; Manygoats, K.; Seifert, S.; Andree, C.; Stöter, M.; Epstein-Barash, H.; Zhang, L.; Koteliansky, V.; Fitzgerald, K.; Fava, E.; Bickle, M.; Kalaidzidis, Y.; Akinc, A.; Maier, M.; Zerial, M., Image-based analysis of lipid nanoparticle-mediated siRNA delivery, intracellular trafficking and endosomal escape. *Nature Biotechnology* **2013**, *31* (7), 638-646.
22. Paramasivam, P.; Franke, C.; Stöter, M.; Höijer, A.; Bartesaghi, S.; Sabirsh, A.; Lindfors, L.; Arteta, M. Y.; Dahlén, A.; Bak, A.; Andersson, S.; Kalaidzidis, Y.; Bickle, M.; Zerial, M., Endosomal escape of delivered mRNA from endosomal recycling tubules visualized at the nanoscale. *Journal of Cell Biology* **2021**, *221* (2), e202110137.
23. Degors, I. M. S.; Wang, C.; Rehman, Z. U.; Zuhorn, I. S., Carriers Break Barriers in Drug Delivery: Endocytosis and Endosomal Escape of Gene Delivery Vectors. *Accounts of Chemical Research* **2019**, *52* (7), 1750-1760.
24. Zhu, J.; Qiao, M.; Wang, Q.; Ye, Y.; Ba, S.; Ma, J.; Hu, H.; Zhao, X.; Chen, D., Dual-responsive polyplexes with enhanced disassembly and endosomal escape for efficient delivery of siRNA. *Biomaterials* **2018**, *162*, 47-59.
25. Endoh, T.; Ohtsuki, T., Cellular siRNA delivery using cell-penetrating peptides modified for endosomal escape. *Advanced Drug Delivery Reviews* **2009**, *61* (9), 704-709.
26. Wang, Y.-H.; Hou, Y.-W.; Lee, H.-J., An intracellular delivery method for siRNA by an arginine-rich peptide. *Journal of Biochemical and Biophysical Methods* **2007**, *70* (4), 579-586.
27. Chen, Y. A.; Scheller, R. H., SNARE-mediated membrane fusion. *Nature Reviews Molecular Cell Biology* **2001**, *2* (2), 98-106.
28. Jahn, R.; Scheller, R. H., SNAREs — engines for membrane fusion. *Nature Reviews Molecular Cell Biology* **2006**, *7* (9), 631-643.
29. Yang, J.; Bahreman, A.; Daudey, G.; Bussmann, J.; Olsthoorn, R. C. L.; Kros, A., Drug Delivery via Cell Membrane Fusion Using Lipopeptide Modified Liposomes. *ACS Central Science* **2016**, *2* (9), 621-630.
30. Yang, J.; Shimada, Y.; Olsthoorn, R. C. L.; Snaar-Jagalska, B. E.; Spink, H. P.; Kros, A., Application of Coiled Coil Peptides in Liposomal Anticancer Drug Delivery Using a Zebrafish Xenograft Model. *ACS Nano* **2016**, *10* (8), 7428-7435.
31. Kong, L.; Askes, S. H. C.; Bonnet, S.; Kros, A.; Campbell, F., Temporal Control of Membrane Fusion through Photolabile PEGylation of Liposome Membranes. *Angewandte Chemie International Edition* **2016**, *55* (4), 1396-1400.
32. Kulkarni, J. A.; Witzigmann, D.; Leung, J.; van der Meel, R.; Zaifman, J.; Darjuan, M. M.; Grisch-Chan, H. M.; Thöny, B.; Tam, Y. Y. C.; Cullis, P. R., Fusion-dependent formation of lipid nanoparticles containing macromolecular payloads. *Nanoscale* **2019**, *11* (18), 9023-9031.
33. Tezgel, A. Ö.; Gonzalez-Perez, G.; Telfer, J. C.; Osborne, B. A.; Minter, L. M.; Tew, G. N., Novel Protein Transduction Domain Mimics as Nonviral Delivery Vectors for siRNA Targeting NOTCH1 in Primary Human T cells. *Molecular Therapy* **2013**, *21* (1), 201-209.
34. McKinlay, C. J.; Benner, N. L.; Haabeth, O. A.; Waymouth, R. M.; Wender, P. A., Enhanced mRNA delivery into lymphocytes enabled by lipid-varied libraries of charge-altering releasable transporters. *Proceedings of the National Academy of Sciences* **2018**, *115* (26), E5859-E5866.

35. Xie, Y.; Kim, N. H.; Nadithe, V.; Schalk, D.; Thakur, A.; Kılıç, A.; Lum, L. G.; Bassett, D. J. P.; Merkel, O. M., Targeted delivery of siRNA to activated T cells via transferrin-polyethylenimine (Tf-PEI) as a potential therapy of asthma. *Journal of Controlled Release* **2016**, *229*, 120-129.
36. Ding, Q.; Si, X.; Liu, D.; Peng, J.; Tang, H.; Sun, W.; Rui, M.; Chen, Q.; Wu, L.; Xu, Y., Targeting and liposomal drug delivery to CD40L expressing T cells for treatment of autoimmune diseases. *Journal of Controlled Release* **2015**, *207*, 86-92.
37. Patel, S.; Ashwanikumar, N.; Robinson, E.; DuRoss, A.; Sun, C.; Murphy-Benenato, K. E.; Mihai, C.; Almarsson, Ö.; Sahay, G., Boosting Intracellular Delivery of Lipid Nanoparticle-Encapsulated mRNA. *Nano Letters* **2017**, *17* (9), 5711-5718.
38. Arcaro, A.; Wymann, M. P., Wortmannin is a potent phosphatidylinositol 3-kinase inhibitor: the role of phosphatidylinositol 3,4,5-trisphosphate in neutrophil responses. *Biochemical Journal* **1993**, *296* (2), 297-301.
39. Tao, W.; Mao, X.; Davide, J. P.; Ng, B.; Cai, M.; Burke, P. A.; Sachs, A. B.; Sepp-Lorenzino, L., Mechanistically Probing Lipid-siRNA Nanoparticle-associated Toxicities Identifies Jak Inhibitors Effective in Mitigating Multifaceted Toxic Responses. *Molecular Therapy* **2011**, *19* (3), 567-575.
40. Vercauteren, D.; Piest, M.; van der Aa, L. J.; Al Soraj, M.; Jones, A. T.; Engbersen, J. F. J.; De Smedt, S. C.; Braeckmans, K., Flotillin-dependent endocytosis and a phagocytosis-like mechanism for cellular internalization of disulfide-based poly(amido amine)/DNA polyplexes. *Biomaterials* **2011**, *32* (11), 3072-3084.
41. von Kleist, L.; Stahlschmidt, W.; Bulut, H.; Gromova, K.; Puchkov, D.; Robertson, Mark J.; MacGregor, Kylie A.; Tomilin, N.; Pechstein, A.; Chau, N.; Chircop, M.; Sakoff, J.; von Kries, Jens P.; Saenger, W.; Kräusslich, H.-G.; Shupliakov, O.; Robinson, Phillip J.; McCluskey, A.; Haucke, V., Role of the Clathrin Terminal Domain in Regulating Coated Pit Dynamics Revealed by Small Molecule Inhibition. *Cell* **2011**, *146* (3), 471-484.
42. Macia, E.; Ehrlich, M.; Massol, R.; Boucrot, E.; Brunner, C.; Kirchhausen, T., Dynasore, a Cell-Permeable Inhibitor of Dynamin. *Developmental Cell* **2006**, *10* (6), 839-850.
43. Preta, G.; Cronin, J. G.; Sheldon, I. M., Dynasore - not just a dynamin inhibitor. *Cell Communication and Signaling* **2015**, *13* (1), 24.
44. Vercauteren, D.; Vandenbroucke, R. E.; Jones, A. T.; Rejman, J.; Demeester, J.; De Smedt, S. C.; Sanders, N. N.; Braeckmans, K., The Use of Inhibitors to Study Endocytic Pathways of Gene Carriers: Optimization and Pitfalls. *Molecular Therapy* **2010**, *18* (3), 561-569.
45. Rejman, J.; Bragonzi, A.; Conese, M., Role of clathrin- and caveolae-mediated endocytosis in gene transfer mediated by lipo- and polyplexes. *Molecular Therapy* **2005**, *12* (3), 468-474.
46. Rodal, S. K.; Skretting, G.; Garred, Ø.; Vilhardt, F.; van Deurs, B.; Sandvig, K., Extraction of Cholesterol with Methyl- $\beta$ -Cyclodextrin Perturbs Formation of Clathrin-coated Endocytic Vesicles. *Molecular Biology of the Cell* **1999**, *10* (4), 961-974.
47. Novakowski, S.; Jiang, K.; Prakash, G.; Kastrup, C., Delivery of mRNA to platelets using lipid nanoparticles. *Scientific Reports* **2019**, *9* (1), 552.
48. Sahay, G.; Querbes, W.; Alabi, C.; Eltoukhy, A.; Sarkar, S.; Zurenko, C.; Karagiannis, E.; Love, K.; Chen, D.; Zoncu, R.; Buganim, Y.; Schroeder, A.; Langer, R.; Anderson, D. G., Efficiency of siRNA delivery by lipid nanoparticles is limited by endocytic recycling. *Nature Biotechnology* **2013**, *31* (7), 653-658.
49. Hajj, K. A.; Whitehead, K. A., Tools for translation: non-viral materials for therapeutic mRNA delivery. *Nature Reviews Materials* **2017**, *2* (10), 17056.
50. Miller, J. B.; Zhang, S.; Kos, P.; Xiong, H.; Zhou, K.; Perelman, S. S.; Zhu, H.; Siegwart, D. J., Non-Viral CRISPR/Cas Gene Editing In Vitro and In Vivo Enabled by Synthetic Nanoparticle Co-Delivery of Cas9 mRNA and sgRNA. *Angewandte Chemie International Edition* **2017**, *56* (4), 1059-1063.
51. Krohn-Grimberghe, M.; Mitchell, M. J.; Schloss, M. J.; Khan, O. F.; Courties, G.; Guimaraes, P. P.

- G.; Rohde, D.; Cremer, S.; Kowalski, P. S.; Sun, Y.; Tan, M.; Webster, J.; Wang, K.; Iwamoto, Y.; Schmidt, S. P.; Wojtkiewicz, G. R.; Nayar, R.; Frodermann, V.; Hulsmans, M.; Chung, A.; Hoyer, F. F.; Swirski, F. K.; Langer, R.; Anderson, D. G.; Nahrendorf, M., Nanoparticle-encapsulated siRNAs for gene silencing in the haematopoietic stem-cell niche. *Nature Biomedical Engineering* **2020**, *4* (11), 1076-1089.
52. Dong, Y.; Love, K. T.; Dorkin, J. R.; Sirirungruang, S.; Zhang, Y.; Chen, D.; Bogorad, R. L.; Yin, H.; Chen, Y.; Vegas, A. J.; Alabi, C. A.; Sahay, G.; Olejnik, K. T.; Wang, W.; Schroeder, A.; Lytton-Jean, A. K. R.; Siegwart, D. J.; Akinc, A.; Barnes, C.; Barros, S. A.; Carioto, M.; Fitzgerald, K.; Hettinger, J.; Kumar, V.; Novobrantseva, T. I.; Qin, J.; Querbes, W.; Koteliensky, V.; Langer, R.; Anderson, D. G., Lipopeptide nanoparticles for potent and selective siRNA delivery in rodents and nonhuman primates. *Proceedings of the National Academy of Sciences* **2014**, *111* (11), 3955-3960.
53. Sago, C. D.; Lokugamage, M. P.; Paunovska, K.; Vanover, D. A.; Monaco, C. M.; Shah, N. N.; Gamboa Castro, M.; Anderson, S. E.; Rudoltz, T. G.; Lando, G. N.; Munnill Tiwari, P.; Kirschman, J. L.; Willett, N.; Jang, Y. C.; Santangelo, P. J.; Bryksin, A. V.; Dahlman, J. E., High-throughput in vivo screen of functional mRNA delivery identifies nanoparticles for endothelial cell gene editing. *Proceedings of the National Academy of Sciences* **2018**, *115* (42), E9944-E9952.
54. Ball, R. L.; Hajj, K. A.; Vizelman, J.; Bajaj, P.; Whitehead, K. A., Lipid Nanoparticle Formulations for Enhanced Co-delivery of siRNA and mRNA. *Nano Letters* **2018**, *18* (6), 3814-3822.
55. Van Rossenberg, S. M.; Sliedregt-Bol, K. M.; Meeuwenoord, N. J.; Van Berkel, T. J.; Van Boom, J. H.; Van Der Marel, G. A.; Biessen, E. A., Targeted lysosome disruptive elements for improvement of parenchymal liver cell-specific gene delivery. *Journal of Biological Chemistry* **2002**, *277* (48), 45803-45810.
56. de Bruin, K. G.; Fella, C.; Ogris, M.; Wagner, E.; Ruthardt, N.; Bräuchle, C., Dynamics of photoinduced endosomal release of polyplexes. *Journal of Controlled Release* **2008**, *130* (2), 175-182.
57. Selbo, P. K.; Weyergang, A.; Høgset, A.; Norum, O.-J.; Berstad, M. B.; Vikdal, M.; Berg, K., Photochemical internalization provides time- and space-controlled endolysosomal escape of therapeutic molecules. *Journal of Controlled Release* **2010**, *148* (1), 2-12.
58. Tai, W.; Gao, X., Functional peptides for siRNA delivery. *Advanced Drug Delivery Reviews* **2017**, *110-111*, 157-168.
59. Saar, K.; Lindgren, M.; Hansen, M.; Eiríksdóttir, E.; Jiang, Y.; Rosenthal-Aizman, K.; Sassian, M.; Langel, Ü., Cell-penetrating peptides: A comparative membrane toxicity study. *Analytical Biochemistry* **2005**, *345* (1), 55-65.
60. Martens, T. F.; Remaut, K.; Demeester, J.; De Smedt, S. C.; Braeckmans, K., Intracellular delivery of nanomaterials: How to catch endosomal escape in the act. *Nano Today* **2014**, *9* (3), 344-364.
61. Sahin, U.; Karikó, K.; Türeci, Ö., mRNA-based therapeutics — developing a new class of drugs. *Nature Reviews Drug Discovery* **2014**, *13* (10), 759-780.
62. Foster, J. B.; Barrett, D. M.; Karikó, K., The Emerging Role of In Vitro-Transcribed mRNA in Adoptive T Cell Immunotherapy. *Molecular Therapy* **2019**, *27* (4), 747-756.
63. Rosenberg, S. A.; Restifo, N. P., Adoptive cell transfer as personalized immunotherapy for human cancer. *Science* **2015**, *348* (6230), 62-68.
64. DiTommaso, T.; Cole, J. M.; Cassereau, L.; Buggé, J. A.; Hanson, J. L. S.; Bridgen, D. T.; Stokes, B. D.; Loughhead, S. M.; Beutel, B. A.; Gilbert, J. B.; Nussbaum, K.; Sorrentino, A.; Toggweiler, J.; Schmidt, T.; Gyulveszi, G.; Bernstein, H.; Sharei, A., Cell engineering with microfluidic squeezing preserves functionality of primary immune cells in vivo. *Proceedings of the National Academy of Sciences* **2018**, *115* (46), E10907-E10914.
65. Roth, T. L.; Puig-Saus, C.; Yu, R.; Shifrut, E.; Carnevale, J.; Li, P. J.; Hiatt, J.; Saco, J.; Krystofinski, P.; Li, H.; Tobin, V.; Nguyen, D. N.; Lee, M. R.; Putnam, A. L.; Ferris, A. L.; Chen, J.

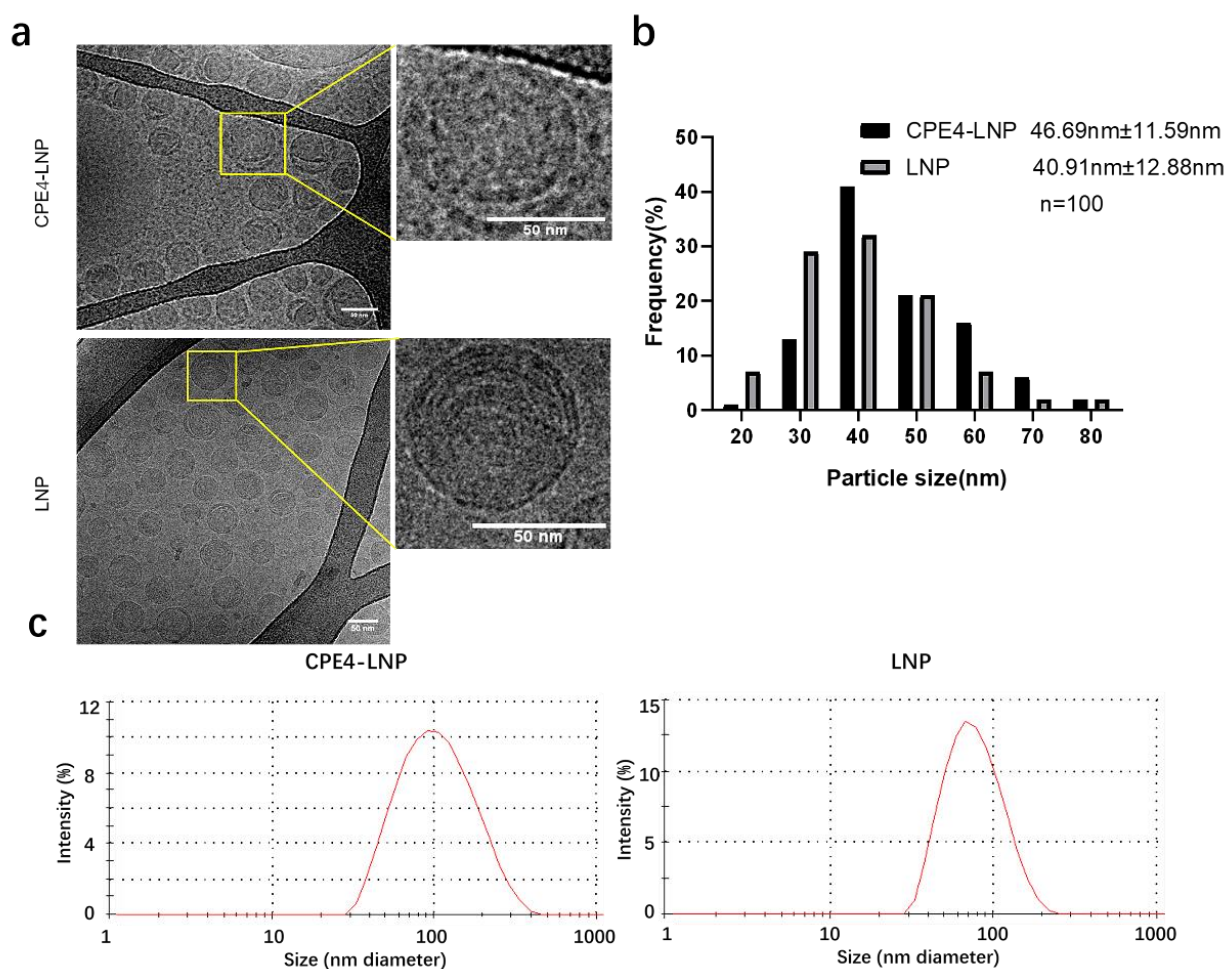
- W.; Schickel, J.-N.; Pellerin, L.; Carmody, D.; Alkorta-Aranburu, G.; del Gaudio, D.; Matsumoto, H.; Morell, M.; Mao, Y.; Cho, M.; Quadros, R. M.; Gurumurthy, C. B.; Smith, B.; Haugwitz, M.; Hughes, S. H.; Weissman, J. S.; Schumann, K.; Esensten, J. H.; May, A. P.; Ashworth, A.; Kupfer, G. M.; Greeley, S. A. W.; Bacchetta, R.; Meffre, E.; Roncarolo, M. G.; Romberg, N.; Herold, K. C.; Ribas, A.; Leonetti, M. D.; Marson, A., Reprogramming human T cell function and specificity with non-viral genome targeting. *Nature* **2018**, *559* (7714), 405-409.
66. Wang, X.; Rivière, I., Clinical manufacturing of CAR T cells: foundation of a promising therapy. *Molecular Therapy - Oncolytics* **2016**, *3*, 16015.
67. Pardi, N.; Hogan, M. J.; Porter, F. W.; Weissman, D., mRNA vaccines — a new era in vaccinology. *Nature Reviews Drug Discovery* **2018**, *17* (4), 261-279.
68. Finn, J. D.; Smith, A. R.; Patel, M. C.; Shaw, L.; Youniss, M. R.; van Heteren, J.; Dirstine, T.; Ciullo, C.; Lescarbeau, R.; Seitzer, J.; Shah, R. R.; Shah, A.; Ling, D.; Growe, J.; Pink, M.; Rohde, E.; Wood, K. M.; Salomon, W. E.; Harrington, W. F.; Dombrowski, C.; Strapps, W. R.; Chang, Y.; Morrissey, D. V., A Single Administration of CRISPR/Cas9 Lipid Nanoparticles Achieves Robust and Persistent In Vivo Genome Editing. *Cell Reports* **2018**, *22* (9), 2227-2235.
69. Liu, J.; Chang, J.; Jiang, Y.; Meng, X.; Sun, T.; Mao, L.; Xu, Q.; Wang, M., Fast and Efficient CRISPR/Cas9 Genome Editing In Vivo Enabled by Bioreducible Lipid and Messenger RNA Nanoparticles. *Advanced Materials* **2019**, *31* (33), 1902575.
70. Anzalone, A. V.; Randolph, P. B.; Davis, J. R.; Sousa, A. A.; Koblan, L. W.; Levy, J. M.; Chen, P. J.; Wilson, C.; Newby, G. A.; Raguram, A.; Liu, D. R., Search-and-replace genome editing without double-strand breaks or donor DNA. *Nature* **2019**, *576* (7785), 149-157.

# Supporting Information

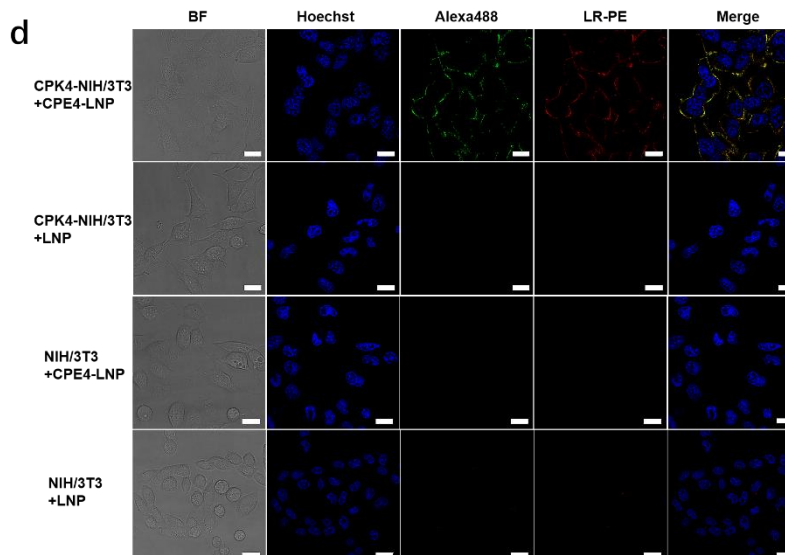
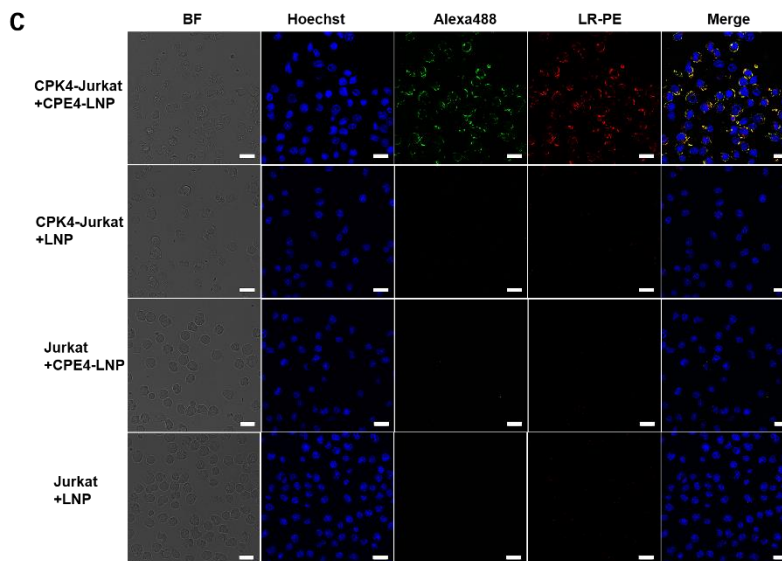
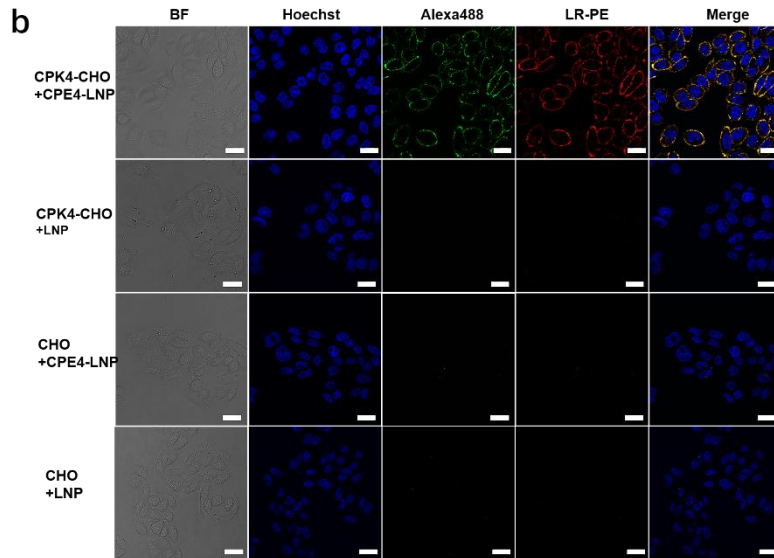
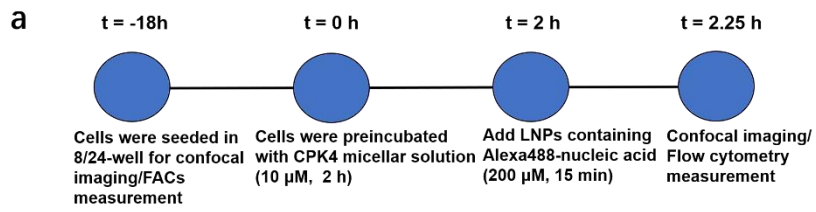


SI Figure 1. Evaluation of coiled-coil peptide pair mediated uptake in liposomes and LNPs. (a) CD spectra of K3/E3 and K4/E4 pairs. Peptides were dissolved at a total concentration of 10  $\mu$ M in PBS at pH 7.4, and spectra

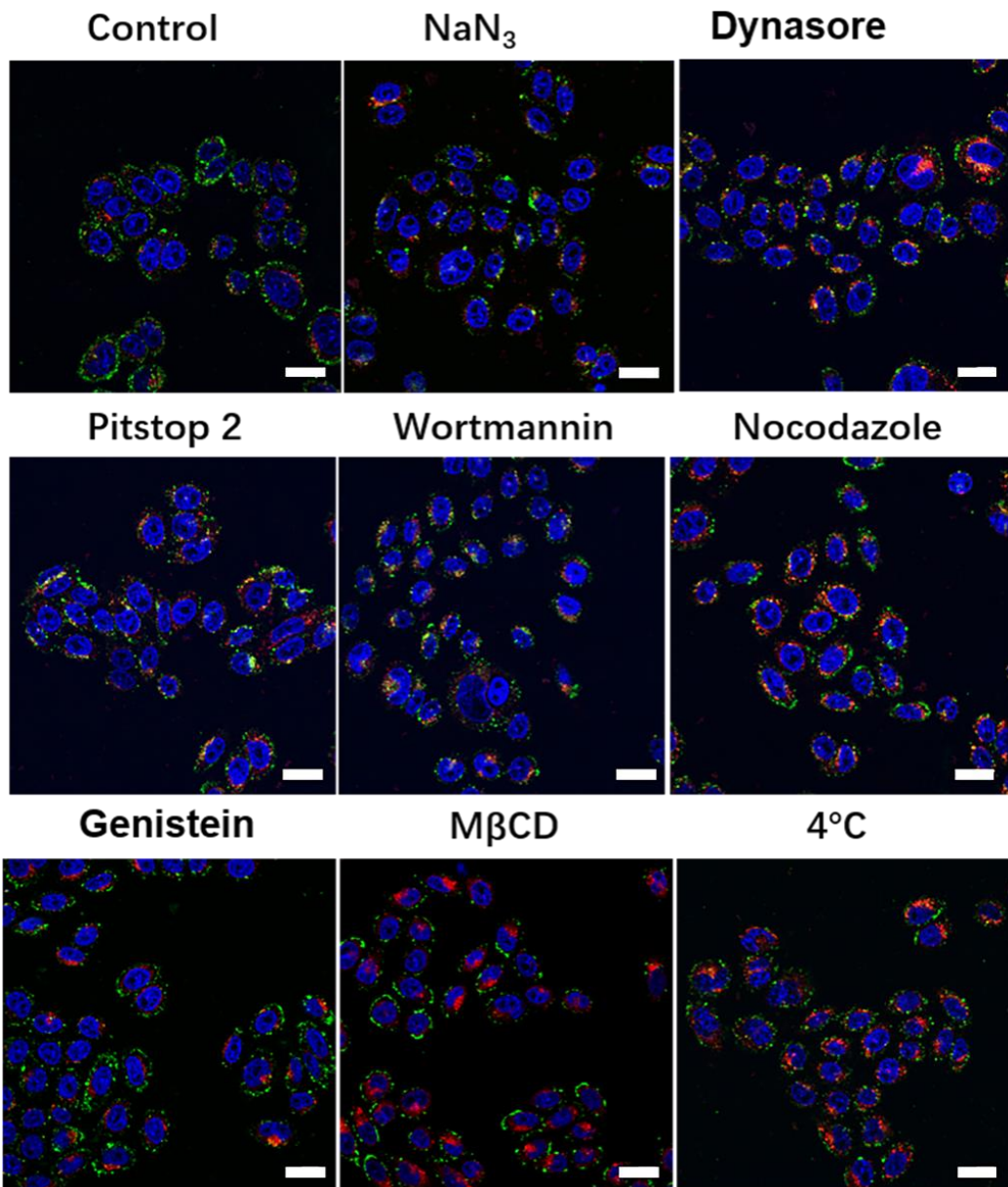
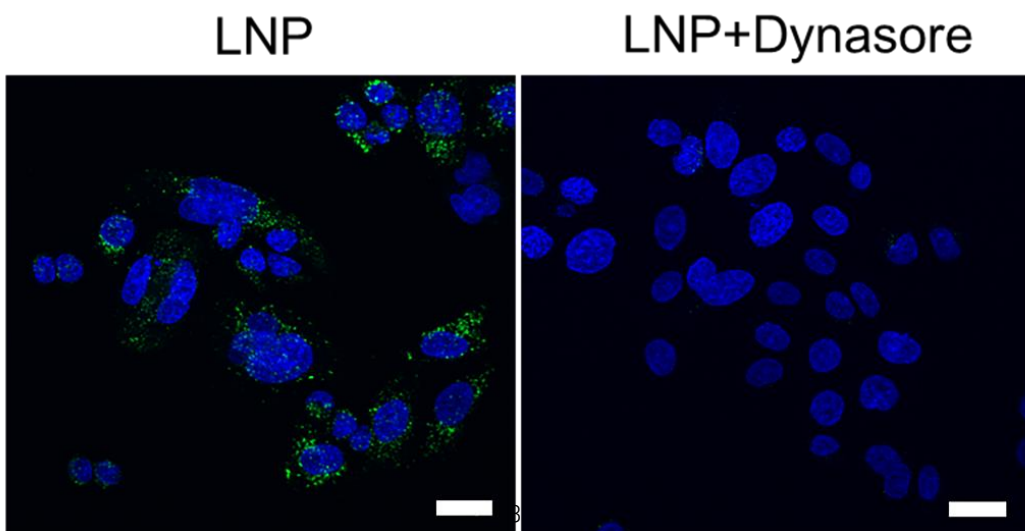
were measured at 20°C. **(b)** Cellular uptake of liposomes in HeLa cells. Uptake efficiency was calculated by quantifying the NBD-positive cells. **(c-d)** The fluorescence intensity (MFI) of cellular internalization of liposomes with HeLa cells. Lipid compositions of liposomes: DOPC/DOPE/cholesterol=2:1:1, 1 mol% of the NBD-PE served as the fluorescent dye, 1 mol% of the CPK (3 or 4) or CPE (3 or 4) were added for lipopeptide modified liposomes. E+K: both E and K peptide included; E+: only E peptide included; K+: only K peptide included. **(e-f)** The fluorescence intensity of cellular internalization of LNPs encapsulated nucleic acid by CPE3/4-LNP with HeLa cells pretreated with CPK3/4. Alexa488 labeled nucleic acid was encapsulated and served as the fluorescent dye. Unpaired t-test was used to determine the significance of the comparisons of data indicated in **b**, **c**, and **d** (\*P < 0.05; \*\*P < 0.01; \*\*\*P < 0.001; \*\*\*\*P < 0.0001). In all panels, error bars represent mean  $\pm$  s.d. (n=3).



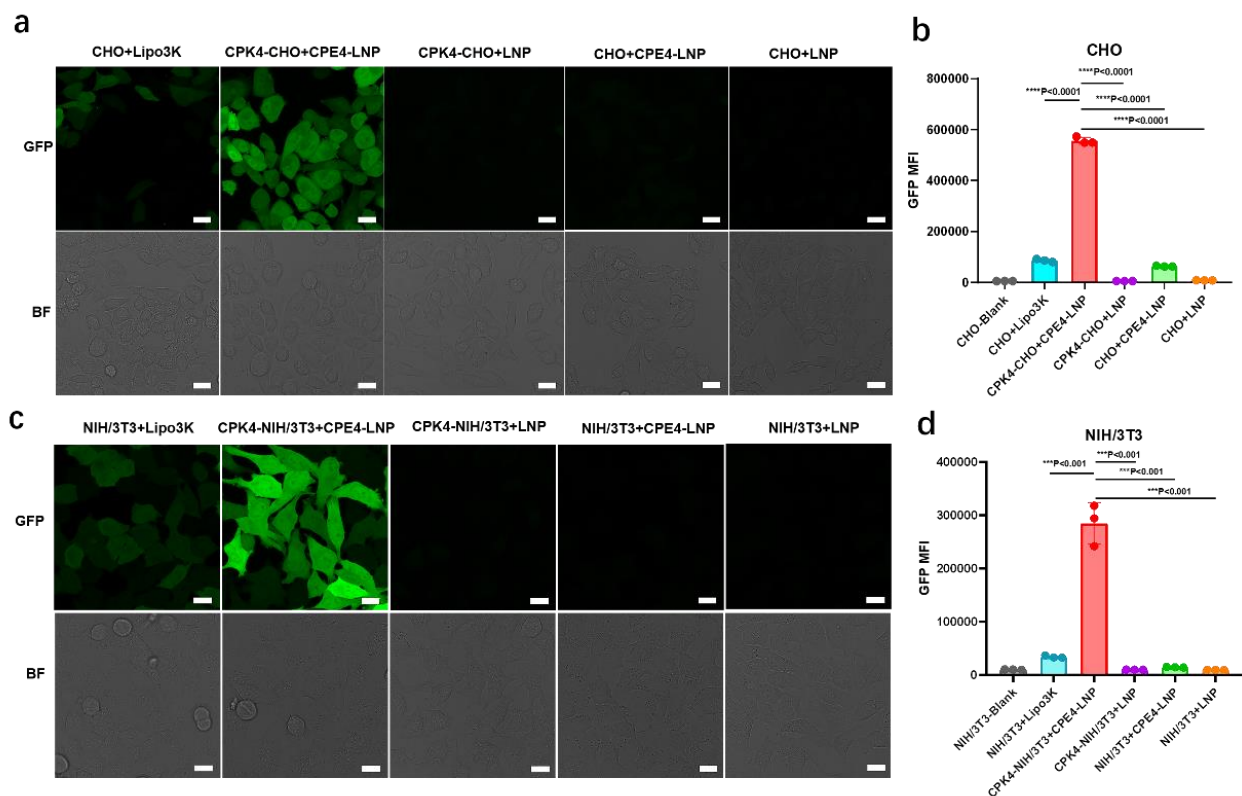
**SI Figure 2 (a)** Cryo-EM images of Alexa488-nucleic acid encapsulated CPE4-LNP and LNP. **(b)** Size distribution of Alexa488-nucleic acid encapsulated LNPs as determined by cryo-EM. The values derived from the frequency distribution graphs represent mean  $\pm$  s.d. (n=100). Scale bar is 50 nm. **(c)** Size distribution of Alexa488-nucleic acid encapsulated LNPs according to DLS.



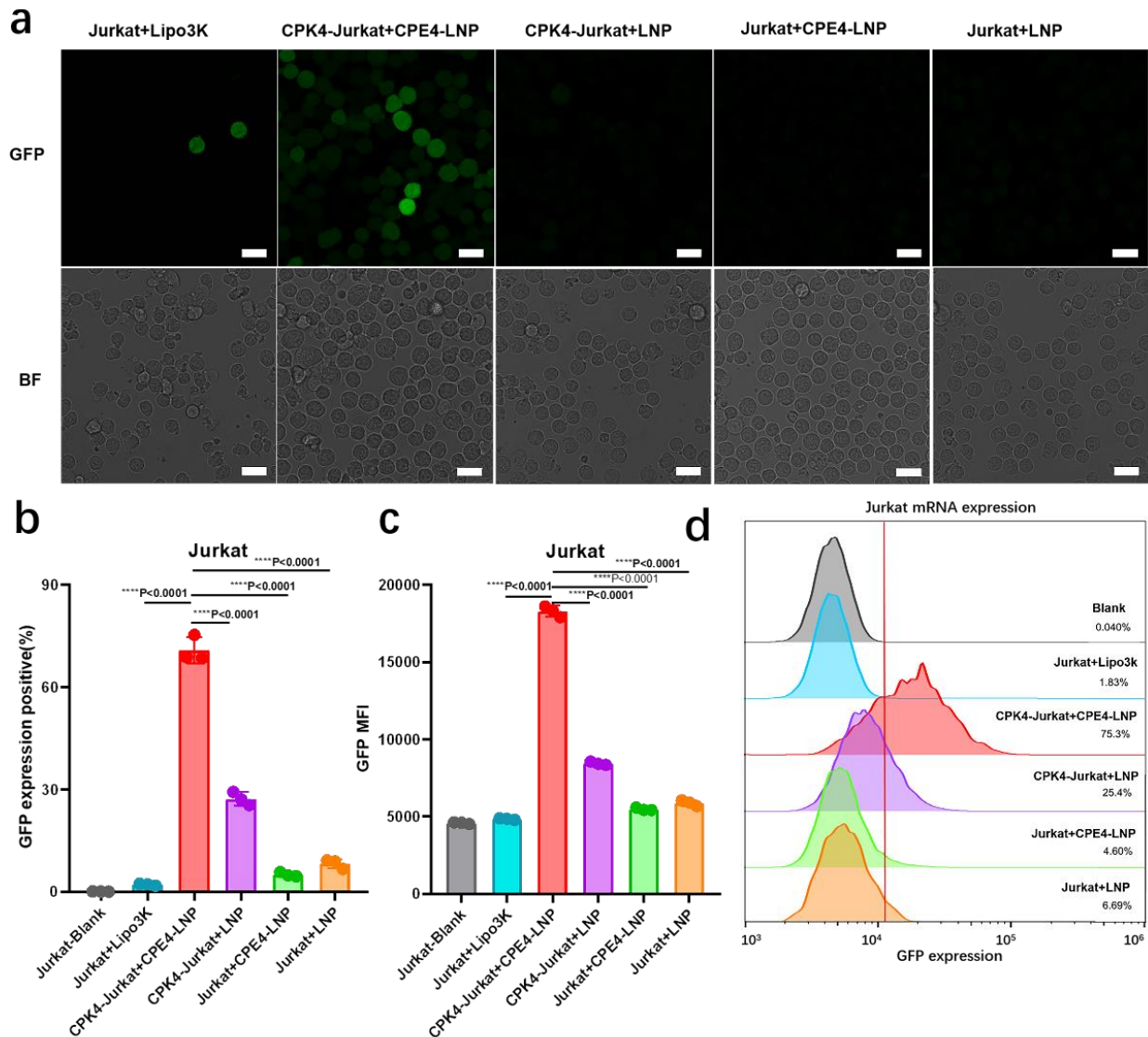
**SI Figure 3.** (a) Schematic representation of the LNPs uptake experiments with cells. (b) Confocal microscopic images of LNPs uptake with CHO cells. (c) with NIH/3T3 cells. (d) with Jurkat cells. Cells were preincubated with a micellar CPK4 solution (10  $\mu$ M, 200  $\mu$ L, 2 h). After removal of the medium, the LNPs containing Alexa488-nucleic acid were added (200  $\mu$ M, 200  $\mu$ L, 15 min), then cells were washed before imaging. Blue: Hoechst 33342; green: Alexa488-nucleic acid; red: LR-PE; BF: bright field. Scale bar is 20  $\mu$ m.

**a****b**

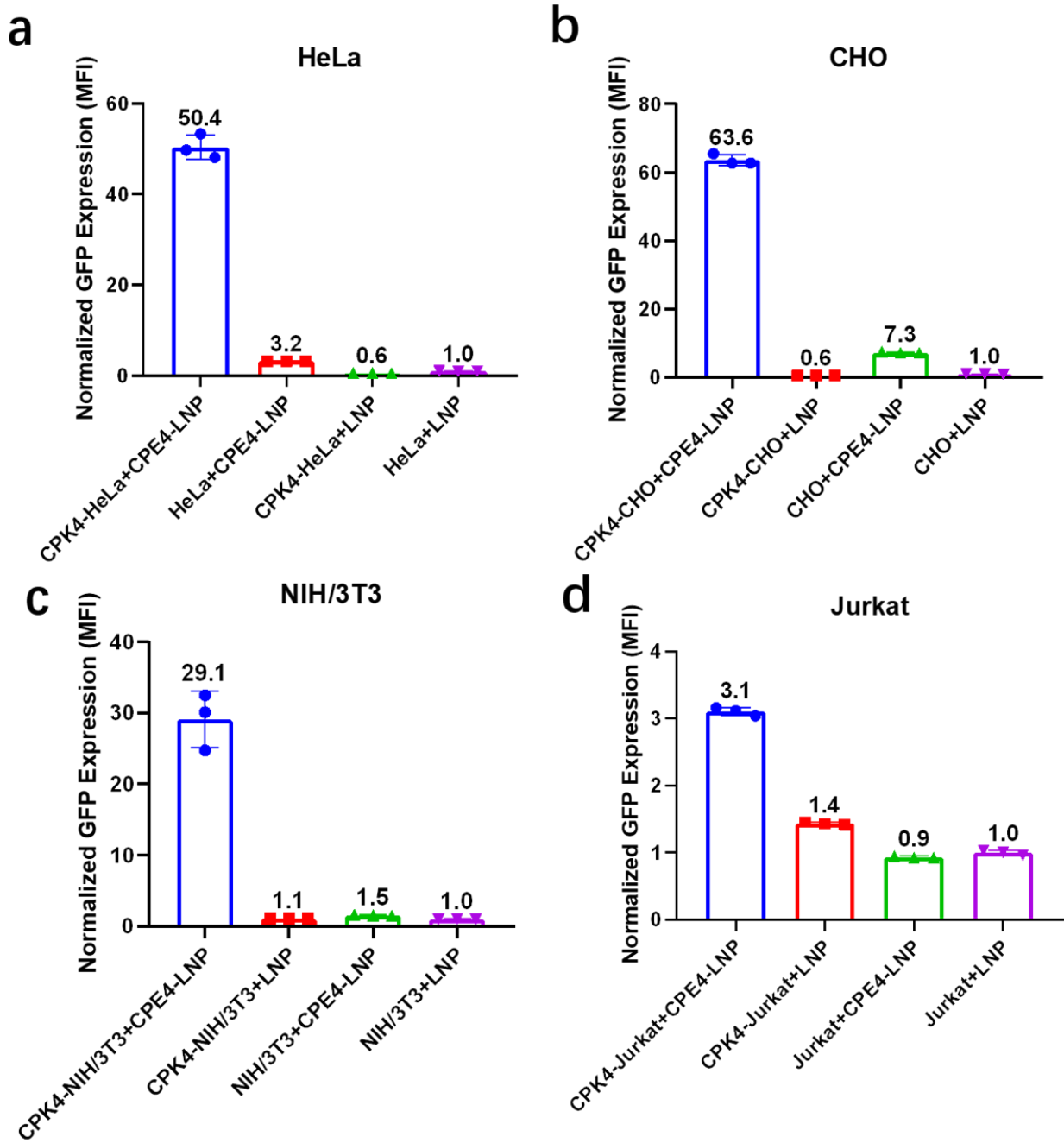
**SI Figure 4. (a)** Confocal microscopic images of cellular uptake of CPE4-LNP with CPK4-HeLa cells in the presence of endocytosis inhibitors. HeLa cells were first treated with different endocytosis inhibitors (1 h), followed by lyso-tracker deep red (75 nM, 200  $\mu$ L) and CPK4 (10  $\mu$ M, 200  $\mu$ L, 2 h, in the presence of fresh inhibitors) incubation, then CPE4-LNP (200  $\mu$ M, 200  $\mu$ L, 15 min) were added together with fresh inhibitors, then cells were washed and added with phenol red free DMEM before imaging. Blue: Hoechst 33342; green: Alexa488-nucleic acid; red: lyso-tracker deep red. **(b)** Confocal microscopic images of cellular internalization of LNP with HeLa cells with endocytosis inhibitor dynasore. HeLa cells were pretreated with dynasore (80  $\mu$ M, 200  $\mu$ L, 1 h), then LNP (200  $\mu$ M, 200  $\mu$ L, 4 h) were incubated with the presence of fresh dynasore, and cells were washed before imaging. Blue: Hoechst 33342; green: Alexa488-nucleic acid. Scale bar is 20  $\mu$ m.



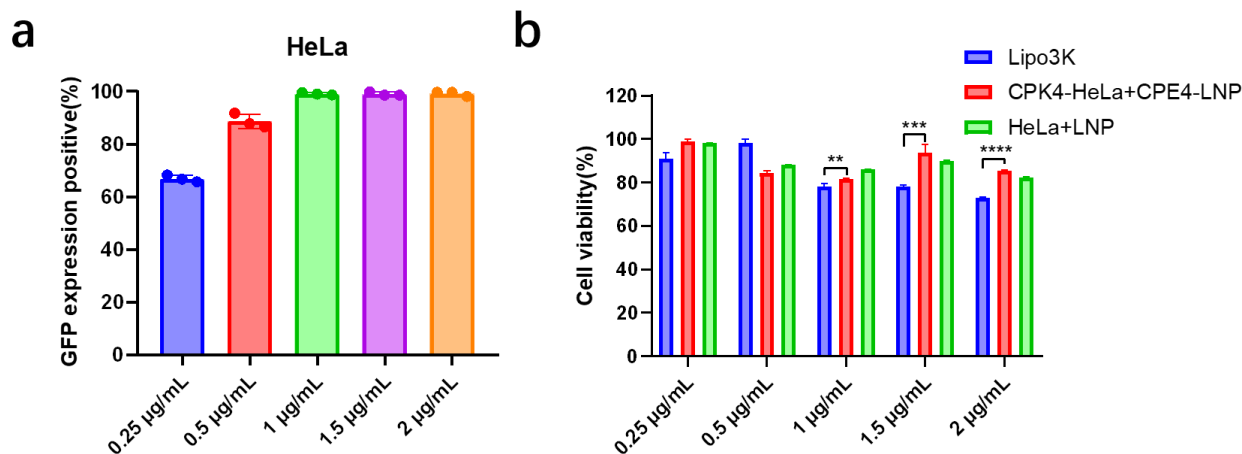
**SI Figure 5 (a)** Confocal microscopic images of the EGFP-mRNA transfection of LNPs with CHO cells. Scale bar is 20  $\mu$ m. **(b)** The GFP expression fluorescence intensity (GFP MFI) of LNPs with CHO cells. **(c)** Confocal microscopic images of the EGFP-mRNA transfection of LNPs with NIH/3T3 cells. Scale bar is 20  $\mu$ m. **(d)** The GFP expression fluorescence intensity (GFP MFI) of LNPs with NIH/3T3 cells. Cells were pretreated with CPK4 solution (10  $\mu$ M, 200  $\mu$ L, 2 h), after removal of the medium, EGFP-mRNA encapsulated LNPs were added (1  $\mu$ g/mL, 200  $\mu$ L, 2 h), and then cultured for another 18-24 h before imaging and flow cytometry measurements. Lipo3K: lipofectamine 3K; GFP: green fluorescent protein; BF: bright field. Unpaired student t-test was used to determine the significance of the comparisons of data indicated in **b**, and **d** (\*P < 0.05; \*\*P < 0.01; \*\*\*P < 0.001; \*\*\*\*P < 0.0001). In all panels, error bars represent mean  $\pm$  s.d. (n=3).



**SI Figure 6. Transfection efficiency of the fusogenic coiled-coil peptide system with Jurkat cells. (a)** Confocal microscopic images of the EGFP-mRNA transfection of LNPs. Lipo3K: lipofectamine 3K; GFP: green fluorescent protein; BF: bright field. Scale bar is 20  $\mu$ m. **(b)** The quantification of EGFP-mRNA transfection efficiency of LNPs. **(c-d)** The GFP expression fluorescence intensity (GFP MFI) of LNPs. Jurkat cells were first incubated with CPK4 (10  $\mu$ M, 200  $\mu$ L, 2 h), followed by EGFP-mRNA encapsulated LNPs were incubated (1  $\mu$ g/mL, 200  $\mu$ L, 2 h), after that, cells were washed 3 times and cultured for another 18-24h before imaging and flow cytometry measurements. Unpaired student t-test was used to determine the significance of the comparisons of data indicated in **b**, and **c** (\* $P < 0.05$ ; \*\* $P < 0.01$ ; \*\*\* $P < 0.001$ ; \*\*\*\* $P < 0.0001$ ). In all panels, error bars represent mean  $\pm$  s.d. (n=3).



**SI Figure 7. GFP fluorescence enhancement.** The protein expression fold number of GFP fluorescence intensity (GFP MFI) of groups normalized to plain LNP (a) with HeLa cells, (b) with CHO cells, (c) with NIH/3T3 cells, (d) with Jurkat cells. In all panels, error bars represent mean  $\pm$  s.d. (n=3).



**SI Figure 8 (a)** Transfection efficiency of different concentrations of EGFP-mRNA encapsulated CPE4-LNP with HeLa cells pretreated with CPK4. HeLa cells were first incubated with CPK4 (10  $\mu$ M, 200  $\mu$ L, 2 h), followed by different concentrations of EGFP-mRNA encapsulated CPE4-LNP incubation (2 h), then the medium was removed, cells were washed and cultured for another 18-24 h before flow cytometry measurements. **(b)** The cell viability evaluation of EGFP-mRNA encapsulated LNPs after transfection. HeLa cells were first incubated with CPK4 (10  $\mu$ M, 200  $\mu$ L, 2 h), followed by different concentrations of EGFP-mRNA encapsulated LNPs incubation (2 h), then the medium was removed, and cells were washed and cultured for another 24 h. After that, WST-1 solution (20  $\mu$ L) was added to the medium (200  $\mu$ L) and incubated for 4 h before measuring. Unpaired student t-test was used to determine the significance of the comparisons of data indicated in **b** (\* $P < 0.05$ ; \*\* $P < 0.01$ ; \*\*\* $P < 0.001$ ; \*\*\*\* $P < 0.0001$ ). In all panels, error bars represent mean  $\pm$  s.d. (n=3).

## **Chapter 3**

### **Coiled-coil Peptide Dimers Enhance Liposomal Drug Delivery**

## Abstract

An ideal nanomedicine design improves the therapeutic efficacy of a drug. However, most nanomedicines enter the cell via endosomal/lysosomal pathways and typically only a small fraction of cargo enters the cytosol inducing a therapeutic effect. To circumvent these inefficient drug delivery pathways, alternative approaches are desired. SNARE proteins, and related peptide mimics, mediate the fusion of membranes and can be used to trigger fast, productive drug delivery *in vitro* and *in vivo*. Previously we used the heterodimeric peptide pair E/K to induce membrane fusion. In this study, we synthesized dimeric coiled-coil peptide variants of peptide K to facilitate liposome fusion with peptide E modified liposomes and cells. Various dimer designs were compared and the parallel PK4 dimer induced the strongest coiled-coil interaction resulting in a higher cellular uptake of the liposome-encapsulated cargo, as compared to linear dimer designs. Using a wide spectrum of endocytosis inhibitors, it was shown that membrane fusion was the main cellular uptake pathway. Delivery of the antitumor drug doxorubicin (DOX) resulted in enhanced cellular delivery and concomitant antitumor efficacy *in vitro*. These findings not only offer important mechanistic insights into the design of coiled-coil driven membrane fusion systems but also provide novel strategies to develop peptide-based biomaterials.

## Introduction

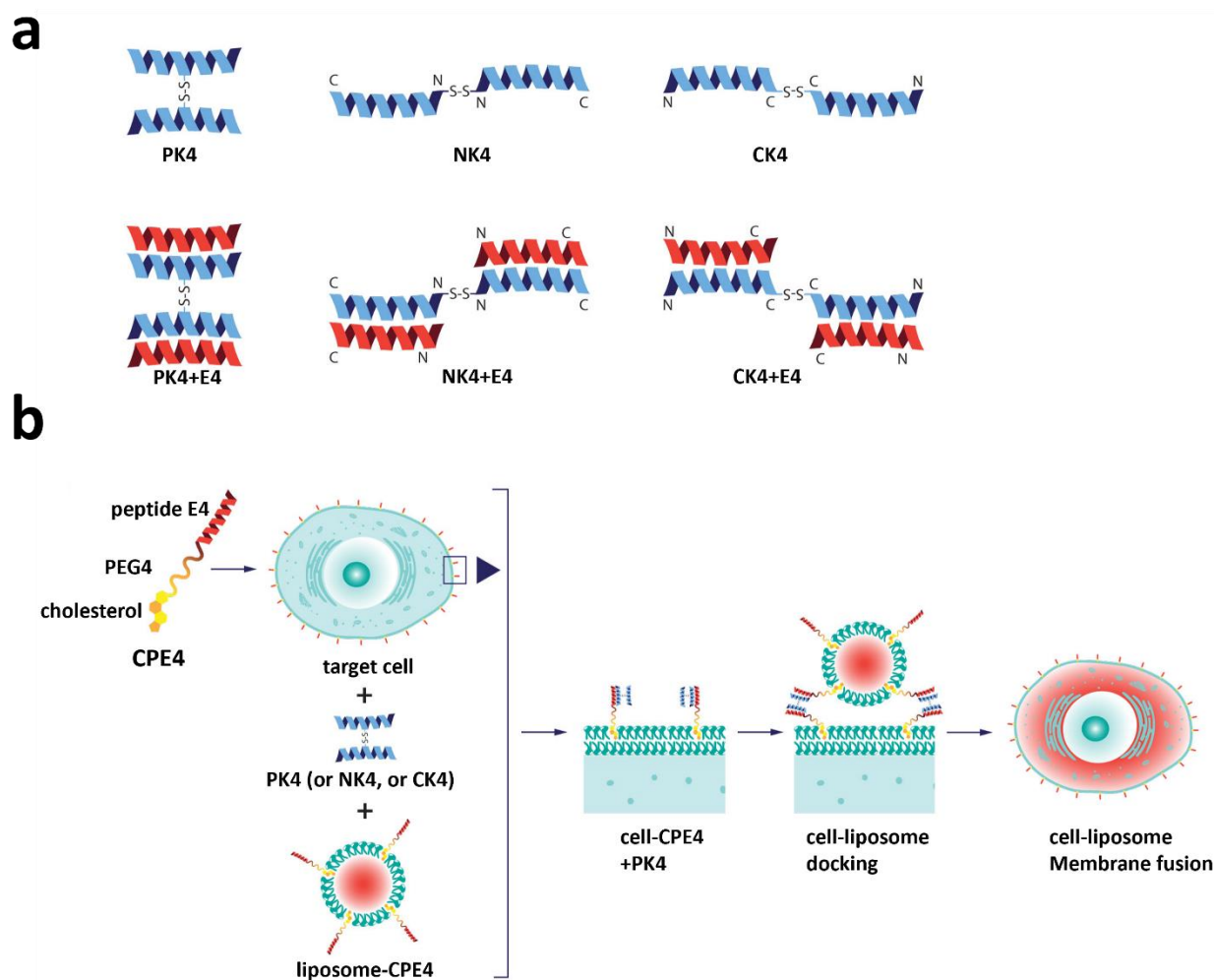
During the last decades, nanomedicines with improved drug delivery efficiency have been developed by amplifying drug bioavailability, improving pharmacokinetic/pharmacodynamic profiles, and/or minimizing undesired off-target or other side effects of encapsulated drugs.<sup>1-3</sup> Several nanomedicines based on liposomes, albumin NPs, and polymeric micelles have been approved for cancer treatment and several nanomedicine candidates for chemotherapy, hyperthermia, radiation therapy, gene therapy, and immunotherapy are in clinical trials.<sup>4-6</sup> Nanomedicines have been customized to enter cells through different endocytosis pathways, delivering their cargo to the cell.<sup>7, 8</sup> However, endocytosis often impedes drug delivery efficiency since the majority of the nanomedicine cargo faces endo/lysosome degradation, lowering the therapeutic efficacy. Therefore, novel drug delivery systems circumventing endo/lysosome pathways and/or entrapment would greatly enhance intracellular drug delivery efficiency.

Peptides have attracted great attention in the nanomedicine field due to their diversity and ease of modification and conjugation to drug delivery nanoparticles.<sup>9, 10</sup> For example, cell-penetrating peptides (CPP) have been widely investigated for their cell-penetrating abilities<sup>11, 12</sup> and chemically synthesized CPPs covalently or noncovalently conjugated to biomaterials greatly enhanced cell penetration and drug efficacy.<sup>13, 14</sup> Besides direct penetration, CPP-cargo conjugates mainly gain their entry to the cells through energy-dependent endocytosis, such as macropinocytosis or clathrin-mediated endocytosis.<sup>15-17</sup> Moreover, CPP dimerization significantly lowered the cell-penetrating concentration required by efficient Tat-TAR interaction inhibition of HIV-1,<sup>11</sup> and achieved potent antitumor effects.<sup>18, 19</sup> Based on the advances made in this field, various CPP-derived peptide therapeutics have been clinically evaluated.<sup>20-23</sup> Unfortunately, to date there are no CPP-based drug conjugates/nanomedicines approved by the FDA. This might be due to their lack of cell and tissue specificity, drug delivery inefficiency, slow drug release profile, poor stability, rapid renal clearance, and severe adverse effects like high toxicity.<sup>21, 24, 25</sup>

Thus there is still a pressing need to find alternatives to deliver drugs efficiently into cells. Membrane fusion is a vital process for the transport of (bio)chemicals across membranes in eukaryotic cells, from the exquisite compartmental organization of cells to the precise timing of chemical synaptic transmission of nervous system activities.<sup>26-28</sup> The docking of transport vesicles to the target plasma membrane in neuronal exocytosis is triggered by the coiled-coil formation of complementary SNARE protein subunits.<sup>27</sup> Inspired by the SNARE protein complex to trigger the membrane fusion process between liposomes and cells, we previously developed complementary pairs of coiled-coil peptides K/E conjugated to lipids able to trigger membrane fusion, inducing fast and efficient liposomal drug delivery *in vitro* and *in vivo*.<sup>29-31</sup> Peptide K is an amphipathic helical peptide and was specifically designed to interact with peptide E, but when confined to a membrane, it also interacts with lipid bilayers.<sup>32</sup>

Due to this dual affinity to both peptide E and lipid membranes, in this chapter, we investigate whether dimerization of peptide K could enhance liposomal drug delivery to cells. The influence of peptide dimerization on their solution properties was studied as well as the ability to induce fusion of liposomes with cells to control drug delivery (**Scheme 1**). By varying the position of peptide conjugation, three novel dimer designs were synthesized. Coiled-coil interactions and cell membrane

binding affinities were compared by circular dichroism spectroscopy and flow cytometry measurements. Next, the cellular uptake of liposomes was also evaluated by flow cytometry and confocal microscopy. The *in vitro* antitumor effect of the chemotherapeutic doxorubicin (DOX) encapsulated in liposomes was quantified as a function of dimer design. This study could aid the development of efficient delivery systems of drugs into cells using liposome-cell fusion.



**Scheme 1. Schematic illustration of the cell-liposome membrane fusion process triggered by K4-dimers and E4.** (a) schematic representation of K4-dimers and coiled-coil structure of K4-dimers with complementary E4. (b) Liposomal drug delivery to cells through membrane fusion induced by different coiled-coils.

## Results and discussion

### Peptide design

Peptide K was previously designed to form a parallel heterodimeric coiled-coil complex with peptide E,<sup>32</sup> but we discovered it also has a high affinity to fluid phospholipid membranes. Upon binding, peptide K induces positive membrane curvature and destabilization, facilitating membrane fusion.<sup>33-35</sup> Due to these competing interactions, we rationalized that a Peptide K-dimer might interact simultaneously with peptide E as well as with a membrane, resulting in enhanced fusion. How these

dual interactions will result in membrane fusion is most likely dependent on the exact structure of these dimers. In this study, we designed three K4-dimers by peptide K4 dimerization via a disulfide bond. For this, a cysteine was introduced at either the N- or C-terminus, or at the f-position in the 2<sup>nd</sup> heptad of peptide K. Upon oxidative dimerization the parallel dimer PK4 and the linear dimers NK4 (N-terminal conjugation) and CK4 (C-terminal conjugation) were obtained (**Scheme 1a**). Based on the structure, linear K4-dimers may form a ‘tetramer-like’ homodimer structure or a hairpin structure, stabilizing the  $\alpha$ -helix structure. Since the hydrophobic faces of both K peptides are oriented in opposite directions, it was expected that PK4 may not be able to dimerize, but rather interact with other dimers resulting in aggregation.

The secondary structure of the peptide dimers and their ability to interact with peptide E was studied using circular dichroism (CD) spectroscopy. In line with previous studies, peptide K4 folds into an  $\alpha$ -helix as evidenced by the two minima at 208 and 222 nm. Peptides NK4 and CK4 also adopt a highly helical conformation comparable to monomeric K4. In contrast, PK4 adopted a skewed non- $\alpha$ -helix spectrum, indicative of aggregation (**Fig. 1a, Table S3**). Peptide E4 adopts an  $\alpha$ -helical secondary structure and upon mixing with equimolar PK4 coiled-coil formation was observed (**Fig. 1b**). The helicity observed for the PK4+E4 mixture is much higher as compared to the calculated average, which assumes no interaction (**Table S3**). The linear dimer NK4 also adopts an  $\alpha$ -helical structure, and the helicity increased upon mixing with E4 (**Fig. 1c, Table S3**). In contrast, the CD-spectrum of a mixture of linear dimer CK4 and E4 did not indicate effective coiled-coil formation (**Fig. 1d, Table S3**). This suggests that the ‘tetramer-like’ homodimer or helical hairpin of CK4 is too stable, preventing interaction with E4, but the less stable homodimer of NK4 does form heteromeric coiled coils with E4, and the parallel PK4 forms highly enhanced coiled-coil interactions with E4.

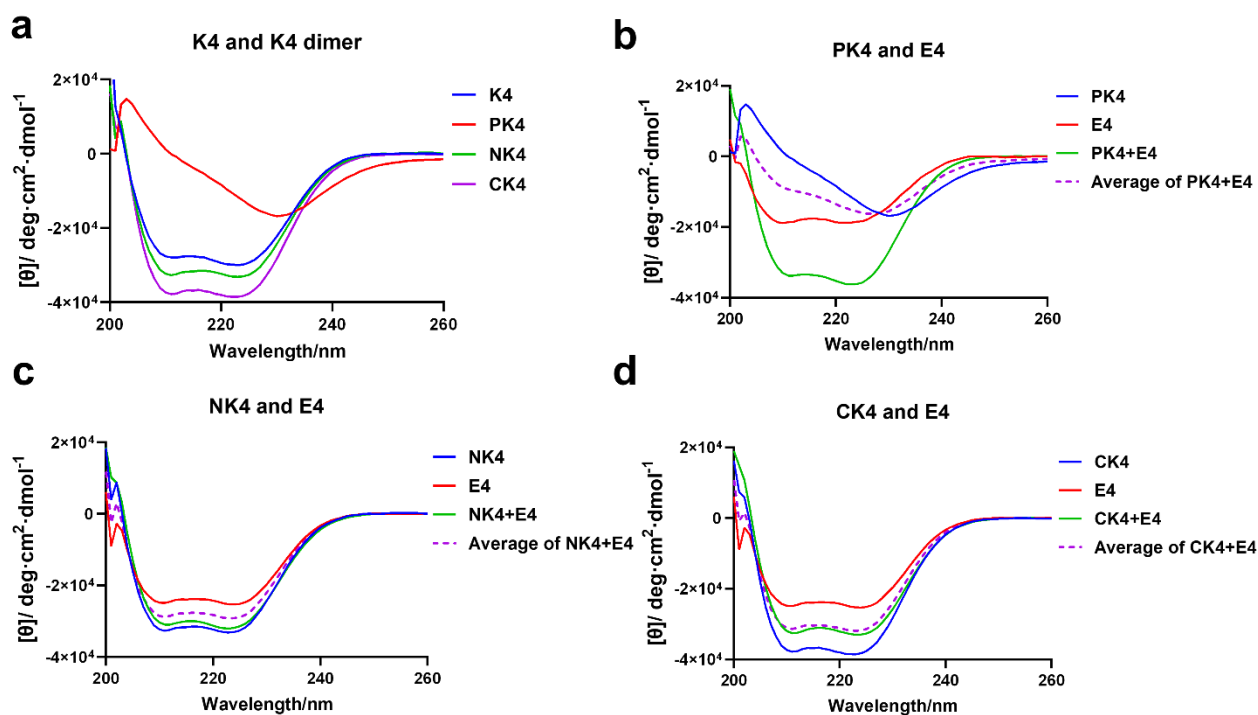


**Figure 1.** CD spectra of (a) K4 monomer and K4-dimers, (b) PK4 ± E4, (c) NK4 ± E4, and (d) CK4 ± E4. Solid

lines are measured spectra, dotted lines are calculated average spectra from the K4-dimers and peptide E4. Spectra were recorded in PBS (pH 7.2) at 20 °C. K4-dimer, 5  $\mu$ M; K4 monomer, 10  $\mu$ M; E4, 10  $\mu$ M.

### **Cell membrane labeling efficiency between dimers**

In previous studies, the addition of a fluorescently labeled E4 peptide, dubbed Fluo-E4, to CPK4-pretreated cells resulted in a uniformly fluorescent cell membrane due to the formation of coiled coils between CPK4 and Fluo-E4. To confirm whether coiled-coil formation between K4-dimers and E4 also occurs at the surface of cells, a cell membrane labeling assay was performed. HeLa cells were preincubated with CPE4 as described previously.<sup>31</sup> Next, the cells were treated with the various K4-dimers and finally carboxyfluorescein-labeled E4 (Fluo-E4) was added (**Fig. 2a**). Interestingly, cell membrane labeling efficiency varied between the various K4-dimers (**Fig. 2b**). PK4 displayed the highest fluorescence on the cell membrane, indicating efficient coiled-coil formation between PK4 and CPE4. In contrast, the linear K4-dimers NK4 and CK4 showed a lower degree of fluorescence. We also studied the importance of pretreating cells with CPE4. Plain cells incubated with PK4 also exhibited membrane binding albeit the observed fluorescence was not homogeneously distributed (**SI Fig. 1a**). Most likely, the positively charged PK4 peptides form aggregates in solution which bind to the negatively charged cell membrane via attractive electrostatic interactions. The addition of the linear dimers NK4 or CK4 to plain cells did not result in any detectable binding.

The differences in binding of the various K4-dimers was quantified by flow cytometry (**Fig. 2c**). CPE4 pretreated cells revealed a high binding affinity for K4 and K4-dimers. In contrast, in the absence of CPE4 hardly any peptide K(-dimer) binding was observed. These results were consistent with the CD and confocal imaging results. PK4-dimer associated effectively with the cell membrane by either forming coiled-coils with CPE4 or directly interacting with the cell membrane. In contrast, the linear dimers NK4 and CK4 showed a weaker ability to induce coiled-coil interactions, resulting in a low cell membrane affinity.

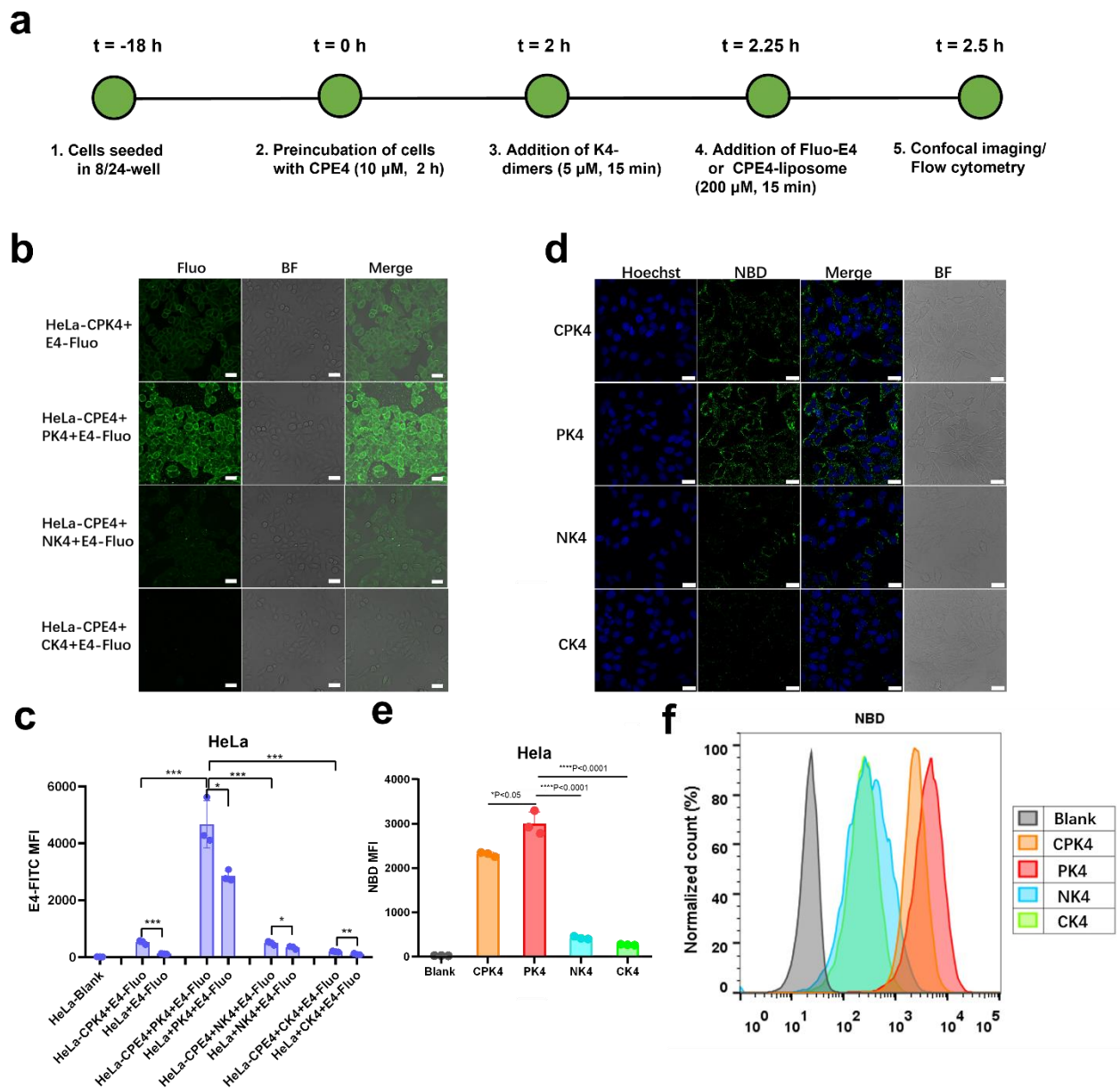


**Figure 2. Cell labeling and cell uptake studies.** (a) Schematic representation of the cell labeling and cell uptake experiments of K4 dimer with cells. (b) Confocal images of cell membrane labeling between K4 monomer and dimers with complementary Fluo-E4. Green: fluorescein-E4; BF: bright field; scale bar is 30  $\mu$ m. (c) Quantification of cell membrane labeling efficiency by flow cytometry measurements. (d) Confocal images of K4 monomer and dimers with fluorescent NBD-PE labeled CPE4-liposomes. (e-f) Quantification of NBD-liposome intensity between monomer and dimers. Green: NBD-PE; blue: Hoechst 33342. BF: bright field; scale bar is 30  $\mu$ m. Unpaired student t-test was used to determine the significance of data comparisons (\*\*\*\*P < 0.0001; \*\*\*P < 0.001; \*\*P < 0.01; \*P < 0.05). In all panels, error bars represent mean  $\pm$  s.d. (n=3).

### Cell uptake efficiency of dimers

After examining coiled-coil formation at the cell membrane between the K4-dimers and CPE4, cell uptake of CPE4-liposomes was investigated using the same approach. Again, cells were preincubated sequentially with CPE4 and the K4-dimers before fluorescent CPE4-liposomes were added and cell

uptake was quantified (**Fig. 2a**). As expected, CPE4-liposomes were homogeneously distributed on the cell membrane (**Fig. 2d**). However, marked differences were observed for the different K4-dimers. PK4 induced strong and enhanced cell-liposome uptake efficiency, while the linear dimers NK4, and CK4 were less efficient. When the CPE4 preincubation step of cells was omitted, PK4 also induced some binding, but the fluorescence was randomly dispersed on the cell membrane (**SI Fig. 1b**). As mentioned earlier, attractive interactions between PK4 and the cell membrane might be the cause for this observation. As expected, the linear dimers NK4 and CK4 were unable to bind to cells without CPE4 preincubation. The cell uptake efficiency differences between groups was again quantified with flow cytometry (**Fig. 2e-f**). Consistent with confocal imaging, the PK4 coiled-coil pair showed the highest cell uptake efficiency, which was superior to monomeric K4 and the linear dimers NK4 and CK4. Not surprisingly, in cells without CPE4 preincubation, the dimers resulted in weaker cell uptake efficiency (**SI Fig. 1c**). Combined, these studies revealed that PK4 interacts very efficiently with CPE4-preincubated cells.

### **Liposome-cell membrane fusion --NBD/propidium iodide (PI) delivery of dimers**

Next, membrane fusion between liposomes and cells was studied using propidium iodide (PI) as a model drug. This dye binds to DNA and is membrane impermeable requiring a drug delivery carrier to enter cells. Cells were sequentially pretreated with CPE4 and the K4-dimers before PI encapsulated in CPE4-liposomes was added to induce liposome-cell membrane fusion and concomitant PI delivery (**Fig. 3a**). Confocal imaging showed the green fluorescent dye NBD incorporated in CPE4-liposomes, evenly distributed on cell membranes, while PI was observed in the cytosol and nucleus of cells (**Fig. 3b**). As expected, CPK4-liposomes are able to deliver PI into cells, consistent with our previous study.<sup>31</sup> Importantly, PK4 induced the highest PI delivery inside cells and the dye was present in the cytosol and nucleus. In contrast, the linear K4-dimers induced only a low PI delivery efficiency. NK4 induced weak fluorescence both on the cell membrane and in the cytoplasm, and almost no membrane and cytoplasm fluorescence was observed when CK4 was used. When the cells were not pretreated with CPE4, PK4 was still able to induce liposome-cell fusion resulting in some PI uptake (**SI Fig. 2a**). Furthermore, liposomes lacking CPE4 showed neither PI delivery nor NBD-labeling of the cell plasma membrane irrespective of the K-dimer used (**SI Fig. 2b**). Next, the same experiment was performed using Chinese hamster ovary (CHO) cells to confirm that PI delivery is cell-type independent. Consistent with the previous studies in HeLa cells, PI was observed in CHO cells when PK4 was used, while CPK and the linear K-dimers were less efficient (**SI Fig. 3a**). Again, omitting the CPE4 preincubation step resulted in inefficient PI delivery (**SI Fig. 3b**).

In summary, these results revealed that all K4-dimers mediate cell-liposome membrane fusion resulting in cytosolic and nuclear PI delivery. The PK4-dimer outperformed all other designs due to the enhanced coiled-coil interaction between PK4 and E4, combined with the membrane affinity of PK4 facilitating efficient PI delivery efficiency.

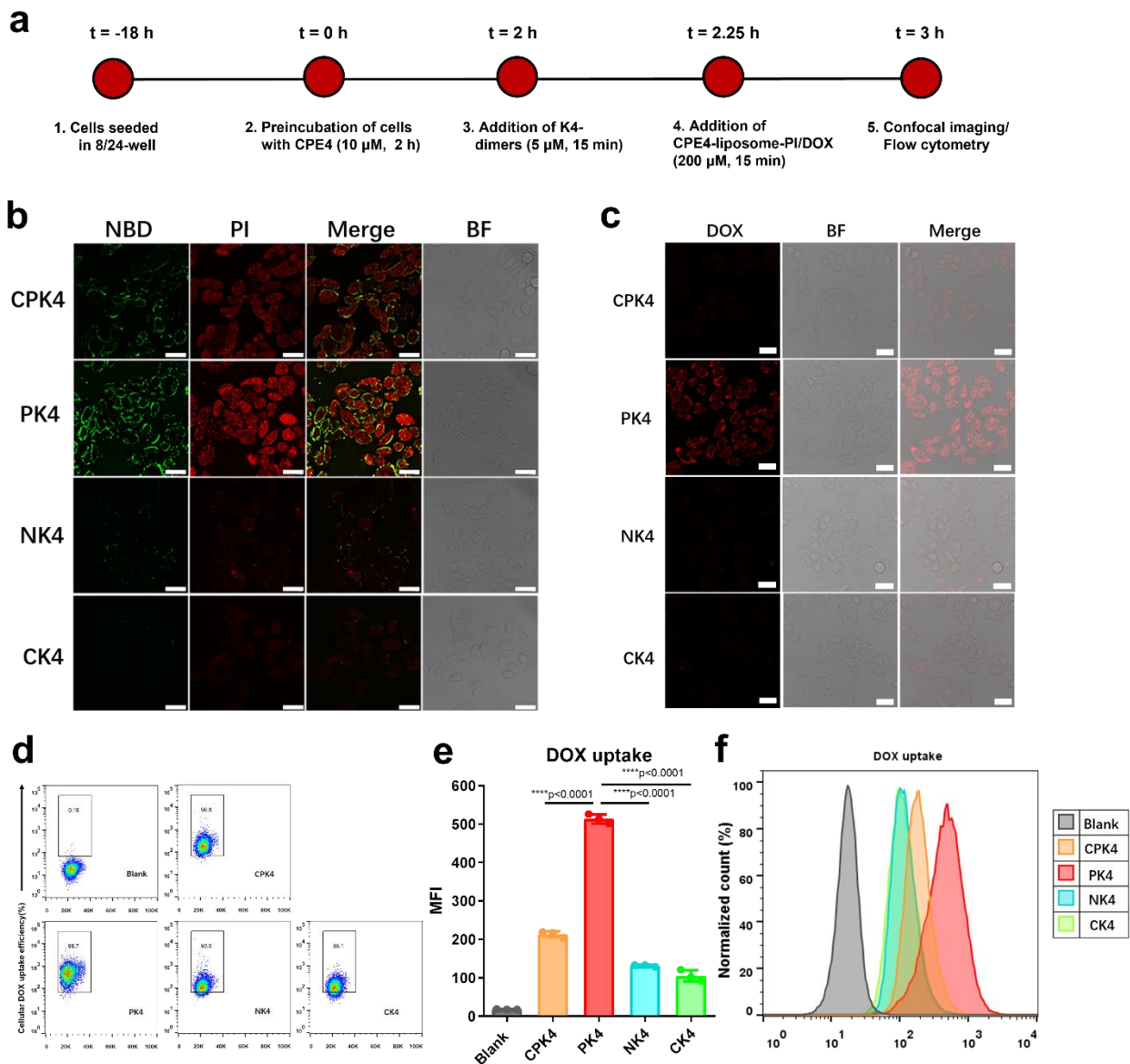


**Figure 3. Liposomal delivery (PI and DOX) to cells.** (a) Schematic representation of the liposomal delivery of PI and DOX to cells. (b) Confocal images of liposomal PI delivery by K4 monomer and dimers. Green: NBD-PE; red: PI; BF: bright field; scale bar is 30  $\mu$ m. (c) Confocal images of DOX uptake facilitated by K4 monomer and dimers in HeLa cells. Red: DOX; BF: bright field; scale bar is 30  $\mu$ m. (d) Quantification of DOX uptake percentages facilitated by K4 monomer and dimers in HeLa cells. (e-f) Quantification of internalized DOX intensity facilitated by K4 monomer and dimers. Unpaired student t-test was used to determine the significance of data comparisons (\*\*\*\*P < 0.0001; \*\*\*P < 0.001; \*\*P < 0.01; \*P < 0.05). In all panels, error bars represent mean  $\pm$  s.d. (n=3).

### Delivery of doxorubicin.

After proving that K4-dimers efficiently mediate liposomal PI delivery into cells via membrane fusion, drug delivery efficiency and subsequent pharmacological effects were further evaluated using doxorubicin (DOX) (Fig. 3a). This drug is an effective and frequently used chemotherapeutic agent for various malignancies, but cardiomyopathy is a life-threatening side effect.<sup>36, 37</sup> Therefore targeted DOX delivery is highly desired because it would increase the therapeutic dose while limiting the side effects. Furthermore, DOX becomes more fluorescent upon binding to DNA and tRNA, making it

suitable for cellular imaging and quantification.

CPE4-preincubated cells were treated with the K4-dimers before CPE4-liposomes containing DOX were added. Confocal imaging confirmed successful DOX delivery as its fluorescence was observed in both the nucleus and cytosol of cells (**Fig. 3c**). Again, PK4 induced the most effective DOX cellular delivery, as compared to the linear K4-dimers or CPK4. Untreated cells showed negligible DOX delivery confirming that CPE4 and K4-dimers are required for efficient drug delivery (**SI Fig. 4a**).

DOX delivery was quantified by flow cytometry. All coiled-coil pairs facilitated liposome-cell fusion resulting in a high percentage of DOX positive cells, >85% in all cases (**Fig. 3d**), indicative of successful DOX delivery. Importantly, the internalized DOX intensities varied significantly between the groups. In line with all previous results, PK4 achieved the highest DOX intensities in cells as compared to CPK4 and the linear K4-dimers (**Fig. 3e-f**). DOX was delivered by PK4 to cells that were not pretreated with CPE4, albeit with a lower intensity than CPE4-preincubated cells. All control groups did not show significant DOX delivery (**SI Fig. 4b**). These results demonstrate that the CPE4/PK4 pair achieved the highest DOX delivery in all experimental groups.

### **DOX uptake efficiency after endocytosis inhibitors**

CPE4/CPK4-mediated fusion of liposomes with cells was confirmed in a previous study using well-known endocytosis inhibitors.<sup>31</sup> In this study, PK4 was the most efficient at delivering content to cells and therefore we studied the uptake mechanism in the presence of common endocytosis inhibitors. After incubation of cells with the endocytosis inhibitors, uptake of liposomes and concomitant delivery of content was quantified. Flow cytometry was employed to quantify the intensity differences of internalized DOX with each endocytosis inhibitor treatment and compared to delivery in the absence of the inhibitors. Since the PK4-dimer is positively charged, we included cationic liposomes (DOTAP: DOPC, 1:1) in this study for comparison.

Nocodazole is an inhibitor of micropinocytosis, a microtubule-disrupting agent that prevents tubule formation and leads to the distribution of IgA-containing vesicles throughout the cytoplasm.<sup>38</sup> Wortmannin blocks PI3-kinase activity and acts as a micropinocytosis inhibitor.<sup>39, 40</sup> Dynasore is reported to inhibit GTPase and dynamin activities reversibly,<sup>41</sup> which is indispensable for clathrin-mediated and caveolae-mediated endocytosis in eukaryotic cells.<sup>42, 43</sup> Pitstop 2 is an inhibitor of clathrin-mediated endocytosis as it blocks the endocytotic ligand association with the clathrin terminal domain.<sup>44, 45</sup> Genistein blocks the tyrosin-phosphorylation process in Cav 1 and caveola-dependent endocytosis.<sup>46, 47</sup> Methyl- $\beta$ -cyclodextrin (M $\beta$ CD) is usually used to determine whether the endocytosis is dependent on the integrity of lipid rafts.<sup>47, 48</sup> Sodium azide (NaN<sub>3</sub>) is an ATP energy depletion agent that inhibits cytochrome C oxidase in the mitochondria of cells.<sup>49</sup>

The cellular uptake of cationic liposomes was greatly inhibited in the presence of NaN<sub>3</sub>, M $\beta$ CD, wortmannin and incubation at 4 °C. This experiment revealed that cationic liposome uptake is energy-dependent, mainly driven by micropinocytosis and depends on lipid raft integrity (**SI Fig. 5a**).<sup>50</sup>

Next, the effect of endocytosis inhibitors on cellular uptake of liposomes encapsulating DOX using the PK4 coiled-coil dimer was investigated (**Fig. 4a**). Most of the endocytosis inhibitors seemed to have a minimal effect on DOX uptake efficiency except for M $\beta$ CD, which disrupts the cholesterol-

rich caveolae-containing membrane microdomains by removing cholesterol from the plasma membrane.<sup>51</sup> Unlike the cationic DOTAP liposomes, the ATP energy depletion agent NaN<sub>3</sub> exerted no effect on the uptake efficiency for PK4-dimer, only the 4 °C incubation reduced the uptake efficiency slightly. This demonstrated that the cellular uptake of the PK4-dimer was mainly driven by membrane fusion independent of energy consumption, and also demands lipid integrity. We also tested the endocytosis inhibitors' effect on the PK4-dimer when the cells were not pretreated with CPE4 (SI Fig. 5b). Similar to the PK4 coiled-coil pair, MβCD and 4 °C incubation resulted in major cellular uptake reduction. Meanwhile, nocodazole and dynasore reduced the cellular uptake by about 25% and 15% respectively, indicating micropinocytosis and clathrin-mediated endocytosis were also involved. Taken together, these results prove that cellular DOX uptake of the PK4-dimer was mainly induced by membrane fusion requiring the presence of cholesterol. Due to the positive charges of the PK4 particles, it could also partially facilitate the lipopeptide CPE4-modified liposomes entering the cell through endocytosis, and this could further facilitate cellular delivery.

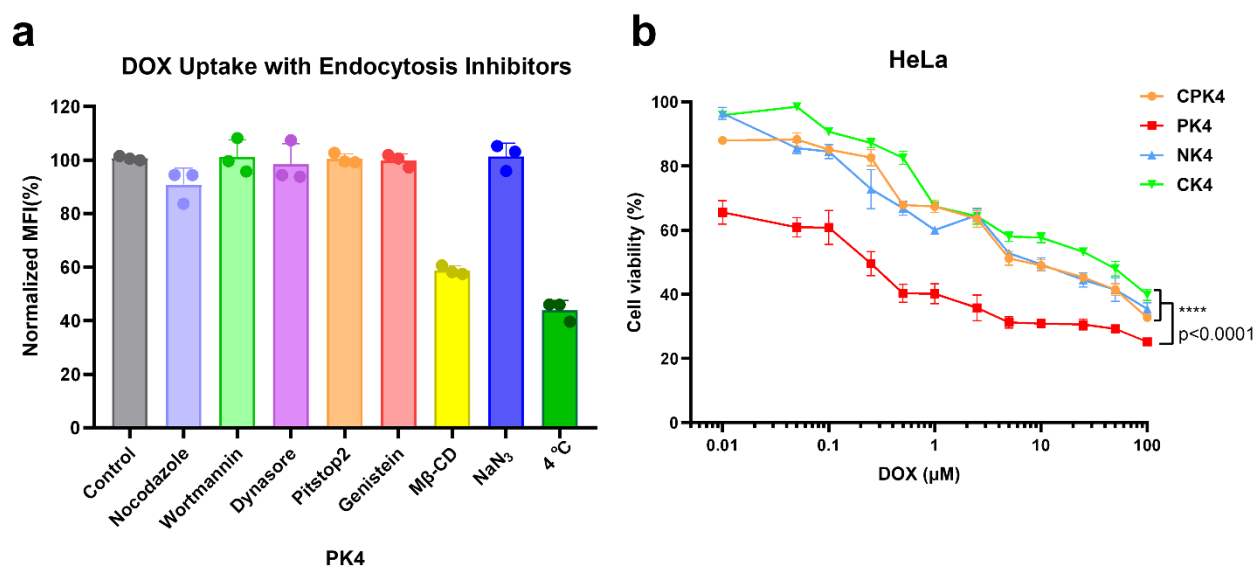


**Figure 4.** (a) Quantification of DOX uptake efficiency of HeLa cells with endocytosis inhibitors in the presence of the PK4-dimer pair. (b) Cytotoxicity evaluation of K4 monomer and dimers after delivery of DOX. Two-way ANOVA analysis was used to determine the significance of data comparisons (\*\*\*\* $P < 0.0001$ ; \*\*\* $P < 0.001$ ; \*\* $P < 0.01$ ; \* $P < 0.05$ ). In all panels, error bars represent mean  $\pm$  s.d. (n=3).

### ***In vitro* antitumor effect evaluation after delivery of DOX**

After confirming that CPE4/PK4 delivers liposomal DOX efficiently into cells, the antitumor effect induced by DOX delivery was evaluated. HeLa cells were decorated with CPE4, treated with the K4-dimers and then incubated for 2 h with CPE4-modified liposomes encapsulating DOX. Next, the cell viability was determined after 36 h. Efficient DOX cellular uptake requires both peptides to be present, thus we mainly focused on the comparison of the HeLa cytotoxicity differences between K4 monomer and dimers in which both peptides were included after the delivery of DOX. The K4 monomer and dimers induced an *in vitro* antitumor effect in a concentration-dependent manner (Fig. 4b). The parallel PK4-dimer induced potent cytotoxicity, and the viability of HeLa cells was

significantly lower than with the monomer and linear dimers for all the concentrations, demonstrating an improved antitumor effect by PK4-mediated delivery of DOX.

An MTT assay was used to proof that the peptides and lipomes in the absence of DOX were non-toxic. For this, cells were decorated with CPE4 and the K4-dimers were added, followed by the addition of CPE4 modified liposomes (without encapsulated DOX). The cell viability remained above 90% for all liposome concentrations, demonstrating the drug delivery system itself was biocompatible and presented no obvious cytotoxicity (**SI Fig. 5c**). Taken together, we showed that coiled-coil peptide dimers can be safely applied to facilitate cellular drug delivery, and the CPE4/PK4 pair can induce highly efficient cellular liposomal delivery with an enhanced therapeutic effect after loading antitumor drugs into the liposomes.

## Conclusion

We designed three coiled-coil peptide-K dimers by varying the conjugation position and investigated their structural differences, cellular uptake efficiency, and pharmacological effects after encapsulating an antitumor drug. CD spectroscopy revealed distinctive differences in helical structures between dimers, where PK4 exhibited the strongest coiled-coil interactions with the complementary peptide E4. The cell membrane labeling assay showed that PK4 triggered the highest cell membrane affinity while linear K4-dimers hardly interacted with the cell membrane. Cellular uptake studies showed liposome delivery into cells was depending on the dimer used. Among the three dimers, PK4 elicited the strongest cellular liposomal delivery and DOX cellular uptake. The uptake mechanism study proved that the efficient liposomal DOX delivery achieved using PK4, was mainly mediated by membrane fusion, although endocytosis was partially involved due to the non-specific interactions between positively charged PK4 and cell membranes. Consistent with the DOX cellular uptake result, a cytotoxicity evaluation confirmed PK4 induced an enhanced antitumor effect *in vitro*, which was superior to CPK4 and the linear dimers NK4 and CK4. These results indicate that PK4 possesses the strongest coiled-coil interaction with peptide E, leading to significant membrane fusion and concomitant efficient cellular liposomal delivery. Moreover, the high affinity of PK4 to lipid membranes aids fusion. In comparison, coiled-coil formation of linear dimers is notably weak and their lipid membrane affinity is also low, therefore they are unable to induce efficient membrane fusion. These results confirm our hypothesis that dimerization of peptide K could increase membrane fusion and lipid affinity, which is pivotal for achieving enhanced liposomal drug delivery. In summary, this study of peptide dimerization design and their cellular delivery evaluation not only contributes to the design and development of coiled-coil peptide-based membrane fusion systems but also provides a more efficient system for future drug delivery applications.

## Methods

### Chemicals and reagents

All Fmoc-protected amino acids were purchased from Novabiochem. Piperidine, trifluoroacetic acid, acetonitrile, dimethylformamide (DMF), dichloromethane (DCM), and ethanol were purchased from Sigma-Aldrich. 1,2-dioleoyl-*sn*-glycero-3-phosphocholine (DOPC), 1,2-dioleoyl-*sn*-glycero-3-phosphoethanolamine (DOPE), 1,2-dioleoyl-*sn*-glycero-3-phosphoethanolamine-N-(7-nitro-2-1,3-benzoxadiazol-4-yl) (PE-NBD), N-[1-(2,3-dioleoyloxy)propyl]-N,N,N-trimethylammonium methylsulfate (DOTAP) were purchased from Avanti Polar Lipids, propidium iodide, 5(6)-carboxyfluorescein, dynasore, wortmannin, nocodazole, pitstop2, genistein, methyl- $\beta$ -cyclodextrin (M $\beta$ CD), sodium azide (NaN<sub>3</sub>), doxorubicin hydrochloride (DOX), cholesterol was purchased from Sigma-Aldrich. DMEM growth medium, and fetal bovine serum were purchased from Sigma-Aldrich. L-glutamine, penicillin, and streptomycin were purchased from Thermo Fisher Scientific. Sephadex G25 size-exclusion PD-10 Columns were purchased from GE-Healthcare.

### Lipopeptide, peptide dimers synthesis, and purification

All peptides were synthesized using Fmoc chemistry on a CEM Liberty Blue microwave-assisted peptide synthesizer. The synthesis of peptides E4-GW, K4-GW, and lipopeptides CPE4, and CPK4 was described in Chapter 2.

For the synthesis of Fluo-K4 and Fluo-E4, two additional glycine residues were coupled to the N-terminus of the peptides on resin, before fluorescein was manually coupled by the addition of 0.2 mmol 5(6)-carboxyfluorescein, 0.4 mmol HCTU and 0.6 mmol DIPEA in 3 mL DMF. The reaction was shaken at room temperature overnight, the peptide was cleaved from the resin using 3 mL of a cleavage mixture (TFA:triisopropylsilane:H<sub>2</sub>O=95:2.5:2.5%) and shaken for 1.5 hours. The peptides were precipitated by pouring the reaction mixture into 45 mL cold diethyl ether (-20 °C) and isolated by centrifugation. The crude peptides were redissolved in H<sub>2</sub>O (20 mL) and lyophilized.

K4-dimer synthesis routes are shown in **SI Scheme 1**, and all the peptide sequences are listed in **Table S1**. A Tentagel HL RAM resin (0.22 mmol/g) was used for peptide synthesis. The Fmoc group was removed with 20% piperidine in DMF by heating to 90 °C for 1 min. In the reaction, 5 eqv. of DIC and 5 eqv. Oxyma and 5 eqv. of amino acid were added to the reaction vessel and heated to 90 °C and kept for 4 minutes. DMF was used as the solvent. Except for the lipidated and fluorescent peptides, all peptides were acetylated at the N-terminus.

Synthesis of PK4: K4GW-Cys14 (66 mg, 20  $\mu$ mol) was dissolved in water (15 mL) and added dropwise to 2,2'-Dithiobis(5-nitropyridine) (62 mg, 200  $\mu$ mol) dissolved in 5 mL of acetone and stirred overnight. The yellow reaction mixture was filtered and dried under a N<sub>2</sub> flow. The crude peptide was dissolved in water (20 mL) and purified by HPLC (see below), after lyophilization K4GW-Cys14-S-nitropyridine was obtained as a solid powder (50 mg, 14.5  $\mu$ mol, yield: 72.5%). K4GW-Cys14-S-nitropyridine (20 mg, 5.8  $\mu$ mol) was mixed with peptide K4-Cys14 (20 mg, 6.6  $\mu$ mol) in 10 mL HEPES buffer (pH 8.1). The solution turned yellow gradually and after 30 minutes the peptide was purified by injecting the reaction mixture into the HPLC (see below). After lyophilization, a white powder was obtained of PK4 (22mg, 3.5  $\mu$ mol, yield: 59.8%).

Synthesis of NK4: CG-K4GW (70 mg, 20  $\mu\text{mol}$ ) was dissolved in 15 mL of water in a flask and 5 mL 2,2'-Dithiobis(5-nitropyridine) (62mg, 200  $\mu\text{mol}$ ) solution in acetone was added dropwise while stirring. After filtration, the reaction mixture was dried under  $\text{N}_2$  flow. The crude peptide was dissolved in 20 mL water and purified by HPLC (see below) and lyophilized yielding a white CG-K4GW-S-nitropyridine solid powder (60 mg, 16.5  $\mu\text{mol}$ , yield: 82%). Peptide CG-K4GW-S-nitropyridine (20 mg, 5.5  $\mu\text{mol}$ ) was mixed with peptide CG-K4 (20 mg, 6.2  $\mu\text{mol}$ ) and dissolved in 10 mL HEPES buffer (pH 8.1). The solution turned yellow gradually and after 30 minutes, the peptide was purified by directly injecting the reaction mixture into the HPLC (see below) and lyophilization to yield a white powder (20 mg, 3  $\mu\text{mol}$ , yield: 54.2%).

Synthesis of CK4: WG-K4GC (70 mg, 20  $\mu\text{mol}$ ) was dissolved in 15 mL of water in a flask and 5 mL 2,2'-Dithiobis(5-nitropyridine) (62 mg, 200  $\mu\text{mol}$ ) solution in acetone was added dropwise while stirring. After filtration, the reaction mixture was dried under  $\text{N}_2$  flow. The crude peptide was dissolved in 20 mL water and purified by HPLC (see below) and lyophilized yielding a white WG-K4GC-S-nitropyridine solid powder (55 mg, 15.7  $\mu\text{mol}$ , yield: 78%). Peptide WG-K4GC-S-nitropyridine (20 mg, 5.5  $\mu\text{mol}$ ) was mixed with peptide K4-GC (20 mg, 6.2  $\mu\text{mol}$ ) and dissolved in 10 mL HEPES buffer (pH 8.1). The solution turned yellow gradually and after 30 minutes, the peptide was purified by directly injecting the reaction mixture into the HPLC (see below) and lyophilized to yield a white powder (18 mg, 2.7  $\mu\text{mol}$ , yield: 48.8%).

Peptides were purified by HPLC on a Shimadzu system consisting of two KC-20AR pumps and an SPD-20A or SPD-M20A detector equipped with a Kinetix Evo C18 column. Eluents consisted of 0.1% TFA in water (A) and 0.1% TFA in MeCN (B), with all peptides eluted using a gradient of 20-90% B over 35 minutes, with a flow rate of 12 mL/min. Collected fractions were checked for purity via LC-MS, with the pure fractions being pooled and lyophilized. LC-MS spectra were recorded using a Thermo Scientific TSQ quantum access MAX mass detector connected to an Ultimate 3000 liquid chromatography system fitted with a 50x4.6 mm Phenomenex Gemini 3  $\mu\text{m}$  C18 column. All peptides were characterized by LC-MS, see **Table S2**.

### **Circular dichroism comparison of coiled-coil peptide dimers interaction**

CD spectra were recorded on a JASCO J-815 CD spectrometer fitted with a Peltier temperature controller. Ac-K4GW, and Ac-E4GW were dissolved in  $\text{H}_2\text{O}$  and diluted in PBS to a concentration of 10  $\mu\text{M}$  separately, the same procedure was used for Ac-PK4GW, Ac-NK4GW, Ac-CK4GW groups with a concentration of 5  $\mu\text{M}$ . The CD spectrum was baseline corrected with PBS. Unless otherwise specified, samples were measured at 20  $^\circ\text{C}$  in a quartz cuvette with a 2 mm path length. Spectra were recorded from 200 to 250 nm at 1 nm intervals, with a bandwidth of 1 nm, with the final spectrum consisting of the average of 5 sequentially recorded spectra. The mean residue molar ellipticity ( $\theta$ ,  $\text{deg}\cdot\text{cm}^2\cdot\text{dmol}^{-1}$ ) was calculated according to equation ( $[\theta] = (100 * [\theta]_{\text{obs}})/(c * n * l)$ ),  $[\theta]_{\text{obs}}$  representing the observed ellipticity in mdeg,  $c$  is the peptide concentration in mM,  $n$  is the number of peptide bonds and  $l$  is the path length of the cuvette in cm. The percentage of helicity of the peptides ( $F_{\text{helix}}$ ) can be calculated by equation:  $F_{\text{helix}} = 100\% * ([\theta]_{222} - [\theta]_0) / ([\theta]_{\text{max}} - [\theta]_0)$ ,  $[\theta]_{222}$  represents the mean residue molar ellipticity of peptide at 222 nm,  $[\theta]_0$  is the mean residue ellipticity of the peptide when the peptide is in an entirely random coil conformation,  $[\theta]_{\text{max}}$  is the maximum theoretical mean residue ellipticity (**Table S3**).

### **Fluorescent peptide labeling experiments**

Cell culture: HeLa, and CHO cells purchased from ATCC were cultured according to ATCC guidelines. The DMEM growth medium containing sodium bicarbonate, without sodium pyruvate and HEPES, was supplemented with 10% fetal bovine serum, 1% of L-glutamine, and 1% penicillin/streptomycin, at 37 °C in the presence of 5% CO<sub>2</sub>.

HeLa cells were seeded on 8-well confocal plates at the density of 5\*10<sup>4</sup> cells/well on the day before experiments were performed. After 18 h incubation, CPK4 and CPE4 lipopeptides (10 μM, 200 μL) were added to the cells and incubated for 1-2 h. After the removal of the medium and washing 3 times with PBS, the medium containing PK4, NK4, and CK4 dimers were added and incubated for 15 min, then washed 3 times, fluorescein-E4 peptide (10 μM, 200 μL) was added and incubated for 15 min, washed 3 times and supplemented with phenol-red-free medium before confocal imaging (Leica TCS SP8). Quantification of interaction differences was conducted by flow cytometry (Guava easyCyte) with cells seeded on 24-well plates at 2.5\*10<sup>5</sup> cells/well, then the same procedure was followed before measuring.

### **Liposome preparation and characterization**

NBD-PE labeled liposomes: lipids were dissolved in CHCl<sub>3</sub> in the molar ratio DOPC, DOPE, and cholesterol 2:1:1 (total lipid concentration, 1 mM, with 1 mol% of NBD-PE) was dissolved in CHCl<sub>3</sub>. The solvent was evaporated, and then lipids were hydrated with 1X PBS, and sonicated at 55°C for 3 min. CPE4-modified liposomes were made by adding 1 mol% of CPE4 into the lipid film.

PI encapsulated liposomes: lipids were dissolved in CHCl<sub>3</sub> in the molar ratio DOPC, DOPE, and cholesterol of 2:1:1 (total lipid concentration, 1 mM, 1 mol% of NBD-PE). Then lipids were hydrated with propidium iodide (10 mg/mL dissolved in PBS, 1 mL), then sonicated at 55°C for 3 min. Free PI was removed by size exclusion chromatography using a Sephadex G25 size-exclusion PD-10 Columns.

DOX encapsulated liposomes: lipids were dissolved in CHCl<sub>3</sub> in the molar ratio DOPC, DOPE, cholesterol 2:1:1 [total lipid concentration] = 4 mM. Liposomes were prepared by mixing the appropriate amount of lipids in a glass vial and evaporating the solvents under air to form lipid films. These films were hydrated with 20 mM citrate buffer (pH 2.5) and extruded 11 times with 200 nm pores. The citrate buffer was replaced by PBS (pH 7.4) through Sephadex G25 size-exclusion PD-10 Columns. Doxorubicin (DOX) was added to the liposomes at a drug-to-lipid molar ratio of 1:3 and subsequently rotated overnight. Free DOX was removed by size exclusion chromatography using a Sephadex G25 size-exclusion PD-10 Columns. The DOX concentration was determined using UV-vis spectrophotometry with a standard curve of different DOX concentrations. The liposomes were post-modified with CPE4. For this, lipopeptides in 1X PBS were added to the DOX-loaded liposomes [final CPE4] = 1 mol%, vortexed for 1 minute, and incubated for another 2 h at RT before use.

All liposomes were characterized by dynamic light scattering (DLS) at 25 °C to determine the average diameter (see **Table S4**).

### **Cellular uptake efficiency experiments**

Flow cytometry analysis of cellular uptake efficiency was carried out using peptide-modified

liposomes to compare the uptake efficiency differences. CPK4 and CPE4 lipid films were made, hydrated with complete DMEM, and sonicated for 10 min at room temperature (final concentration is 10  $\mu$ M). For cellular uptake efficiency study, HeLa cells were seeded on 24-well plates at the density of  $2.5 \times 10^5$  cells/well 18 h in advance, then pretreated with a medium containing CPK4 or CPE4 for 1-2 h (10  $\mu$ M, 500  $\mu$ L), after the removal of medium, PK4, NK4, CK4 dimers (5  $\mu$ M, 500  $\mu$ L) were added and incubated for 15 min, and the cells were washed 3 times with PBS, NBD labeled liposomes modified with CPE4 (CPE4-Liposome-NBD) were added to the cells (200  $\mu$ M, 500  $\mu$ L) and after 15 min incubation, the medium was removed and cells were washed with PBS 3 times, then digested with trypsin, washed, and resuspended in 1X PBS, followed by flow cytometry measurements.

### **Propidium iodide (PI) cellular delivery**

HeLa cells were seeded on 8-well confocal plates at a density of  $5 \times 10^4$  cells/well. After 18 h, the cells were preincubated with a micellar solution of CPK4 and CPE4 (10  $\mu$ M, 200  $\mu$ L) for 1-2 h. After the removal of the medium and washing 3 times with PBS, the medium containing dimers PK4, NK4, and CK4 was added (5  $\mu$ M, 200  $\mu$ L) and incubated for 15 minutes, and the cells were washed 3 times with PBS before NBD-PE labeled CPE4-liposomes containing PI were added and incubated for 15 min. Next, the cells were washed 3 times with PBS, supplemented with the phenol-red-free medium, and cultured another 30 min before confocal imaging.

### **Doxorubicin uptake experiment**

To test the delivery of liposomal doxorubicin (DOX) with different dimers, HeLa cells were seeded on 8-well confocal plates at a density of  $5 \times 10^4$  cells/well the day before the experiment. After 18 h, HeLa cells were preincubated with a medium containing CPK4, and CPE4 for 1-2 h (10  $\mu$ M, 200  $\mu$ L), and subsequently exposed to the medium containing PK4, NK4, or CK4 dimer (5  $\mu$ M, 200  $\mu$ L) and incubated for 15 min. After removal of the medium and 3 times washing with PBS, CPE4 decorated liposomes encapsulating DOX were added and incubated for another 15 min. Cells were washed 3 times and supplemented with phenol-red-free medium and cultured another 30 min before confocal imaging. Quantification of DOX uptake followed a similar procedure in which cells were seeded in 96-well plates at the density of  $2 \times 10^4$  cells/well, then followed the same treatment of peptides and CPE4-liposomes encapsulated DOX (CPE4-Liposome-DOX) before flow cytometry measurements.

### **DOX uptake efficiency after endocytosis inhibitors incubation**

To test the cellular uptake pathway of liposomal doxorubicin (DOX) delivery of PK4, HeLa cells were seeded on a 96-well plate at the density of  $2 \times 10^4$  cells/well the day before the experiment. After 18 h, HeLa cells were preincubated with CPE4 (10  $\mu$ M, 100  $\mu$ L) for 2 h, and subsequently exposed to different endocytosis inhibitors: nocodazole (40  $\mu$ M), wortmannin (0.25  $\mu$ M), dynasore (80  $\mu$ M), pitstop2 (20  $\mu$ M), genistein (200  $\mu$ M), methyl- $\beta$ -cyclodextrin (M $\beta$ CD, 10 mM) sodium azide (0.1% w/v) in DMEM medium (100  $\mu$ L) together with fresh CPE4 for 2 h. The medium was removed and replaced by a medium containing PK4 dimer (5  $\mu$ M, 100  $\mu$ L) and incubated for 15 min. After the removal of the medium and 3 times washing with PBS, CPE4 decorated liposomes containing DOX were added and incubated for another 15 min (200  $\mu$ M, 100  $\mu$ L). Cells were washed 3 times and incubated for 30 min and analyzed by flow cytometry. The 4  $^{\circ}$ C treatment was carried out by putting the cells into the fridge and then following the same procedure as above. The uptake mechanism of cells without CPE4 pretreatment was carried out the same way by using CPE4 modified liposomes

without DOX encapsulation.

For comparison, NBD-labeled cationic DOTAP liposomes (DOTAP: DOPC, 1:1, 1 mol% PE-NBD) were used to study the cellular uptake efficiency in the presence of endocytosis inhibitors. Cells were pretreated with different endocytosis inhibitors for 2 h, after removal of the medium DOTAP liposomes (200  $\mu$ M, 100  $\mu$ L) were added and cultured for 2 h, then analyzed by flow cytometry.

### Cell viability measurements

The cytotoxicity of the peptides and liposomes in the absence of DOX was determined by a MTT assay. HeLa cells were seeded on a 96-well plate at a density of  $1.0 \times 10^4$  cells/well, HeLa cells were incubated with a medium containing CPK4, CPE4 (10  $\mu$ M, 100  $\mu$ L) for 2 h. After the removal of the medium and 3 times washing with PBS, different dimers PK4, NK4, and CK4 (5  $\mu$ M, 100  $\mu$ L) were added to the cells and incubated for 15 min, then cells were washed 3 times (PBS), and treated with a series of diluted CPE4 decorated liposomes without DOX encapsulation for 2h, the concentration of liposomes ranged from 500  $\mu$ M to 0.01  $\mu$ M (500  $\mu$ M, 300  $\mu$ M, 150  $\mu$ M, 75  $\mu$ M, 30  $\mu$ M, 15  $\mu$ M, 7.5  $\mu$ M, 3  $\mu$ M, 1.5  $\mu$ M, 0.75  $\mu$ M, 0.3  $\mu$ M, 0.15  $\mu$ M, 0.05  $\mu$ M, 0.01  $\mu$ M). Next, the medium was removed from the wells, and cells were incubated in a fresh medium for another 36 h. After that, the MTT reagent was added to cells (final concentration is 0.5 mg/mL) and incubated for 4 h. Next, 50  $\mu$ L medium was removed and 100  $\mu$ L of DMSO was added to solubilize the purple formazan crystals and the spectrophotometric absorbance of the samples was measured using a microplate reader (Tecan Infinite M1000). The absorbance at 570 nm was measured with a reference wavelength at 650 nm. HeLa cells without any treatment were set at 100% cell survival.

For the cell viability assay after DOX delivery, HeLa cells were seeded on a 96-well plate at a density of  $1.0 \times 10^4$  cells/well, then incubated with a medium containing CPK4, CPE4 (10  $\mu$ M, 100  $\mu$ L) for 2 h. After the removal of the medium and 3 times washing with PBS, different dimers PK4, NK4, and CK4 (5  $\mu$ M, 100  $\mu$ L) were added to the cells and incubated for 15 min. Then cells were treated with a series of diluted CPE4 decorated liposomes loaded with DOX; the final concentration of DOX in the liposomes ranged from 100  $\mu$ M to 0.01  $\mu$ M (100  $\mu$ M, 50  $\mu$ M, 25  $\mu$ M, 10  $\mu$ M, 5  $\mu$ M, 2.5  $\mu$ M, 1  $\mu$ M, 0.5  $\mu$ M, 0.25  $\mu$ M, 0.1  $\mu$ M, 0.05  $\mu$ M, 0.01  $\mu$ M). After 2 h, all the medium was removed from the wells, and cells were incubated in a fresh medium for 36 h before the MTT assay.

### Statistical analysis

All experiments were performed at least in triplicate (n=3) unless specified otherwise, and the significance was determined using an unpaired student t-test or two-way ANOVA analysis (Graphpad Prism). (\*\*\*\*P < 0.0001; \*\*\*P < 0.001; \*\*P < 0.01; \*P < 0.05)

## References

1. Farokhzad, O. C.; Langer, R., Nanomedicine: Developing smarter therapeutic and diagnostic modalities. *Advanced Drug Delivery Reviews* **2006**, 58 (14), 1456-1459.
2. Jain, R. K.; Stylianopoulos, T., Delivering nanomedicine to solid tumors. *Nature Reviews Clinical Oncology* **2010**, 7 (11), 653-664.
3. Scheinberg, D. A.; Villa, C. H.; Escorcía, F. E.; McDevitt, M. R., Conscripts of the infinite armada:

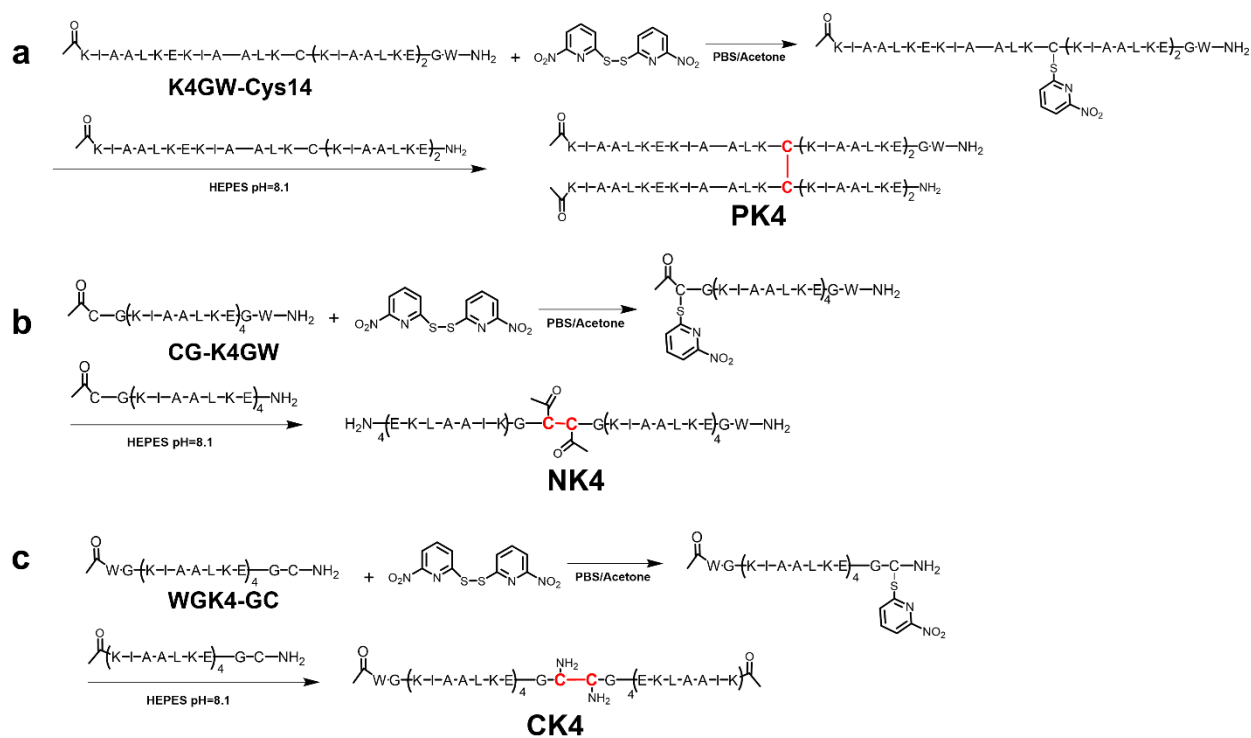
- systemic cancer therapy using nanomaterials. *Nature Reviews Clinical Oncology* **2010**, *7* (5), 266-276.
4. Shi, J.; Kantoff, P. W.; Wooster, R.; Farokhzad, O. C., Cancer nanomedicine: progress, challenges and opportunities. *Nature Reviews Cancer* **2017**, *17* (1), 20-37.
  5. Zhang, C.; Yan, L.; Wang, X.; Zhu, S.; Chen, C.; Gu, Z.; Zhao, Y., Progress, challenges, and future of nanomedicine. *Nano Today* **2020**, *35*, 101008.
  6. Wolfram, J.; Ferrari, M., Clinical Cancer Nanomedicine. *Nano Today* **2019**, *25*, 85-98.
  7. Canton, I.; Battaglia, G., Endocytosis at the nanoscale. *Chemical Society Reviews* **2012**, *41* (7), 2718-2739.
  8. Sahay, G.; Alakhova, D. Y.; Kabanov, A. V., Endocytosis of nanomedicines. *Journal of Controlled Release* **2010**, *145* (3), 182-195.
  9. Ruoslahti, E., Tumor penetrating peptides for improved drug delivery. *Advanced Drug Delivery Reviews* **2017**, *110-111*, 3-12.
  10. Zhang, C.; Wu, W.; Li, R.-Q.; Qiu, W.-X.; Zhuang, Z.-N.; Cheng, S.-X.; Zhang, X.-Z., Peptide-Based Multifunctional Nanomaterials for Tumor Imaging and Therapy. *Advanced Functional Materials* **2018**, *28* (50), 1804492.
  11. Jang, S.; Hyun, S.; Kim, S.; Lee, S.; Lee, I.-S.; Baba, M.; Lee, Y.; Yu, J., Cell-Penetrating, Dimeric  $\alpha$ -Helical Peptides: Nanomolar Inhibitors of HIV-1 Transcription. *Angewandte Chemie International Edition* **2014**, *53* (38), 10086-10089.
  12. Copolovici, D. M.; Langel, K.; Eriste, E.; Langel, Ü., Cell-Penetrating Peptides: Design, Synthesis, and Applications. *ACS Nano* **2014**, *8* (3), 1972-1994.
  13. Meade, B. R.; Dowdy, S. F., Exogenous siRNA delivery using peptide transduction domains/cell penetrating peptides. *Advanced Drug Delivery Reviews* **2007**, *59* (2), 134-140.
  14. Cheng, H.; Zhu, J.-Y.; Xu, X.-D.; Qiu, W.-X.; Lei, Q.; Han, K.; Cheng, Y.-J.; Zhang, X.-Z., Activable Cell-Penetrating Peptide Conjugated Prodrug for Tumor Targeted Drug Delivery. *ACS Applied Materials & Interfaces* **2015**, *7* (29), 16061-16069.
  15. Kauffman, W. B.; Fuselier, T.; He, J.; Wimley, W. C., Mechanism Matters: A Taxonomy of Cell Penetrating Peptides. *Trends in Biochemical Sciences* **2015**, *40* (12), 749-764.
  16. Richard, J. P.; Melikov, K.; Vives, E.; Ramos, C.; Verbeure, B.; Gait, M. J.; Chernomordik, L. V.; Lebleu, B., Cell-penetrating peptides: a reevaluation of the mechanism of cellular uptake. *Journal of Biological Chemistry* **2003**, *278* (1), 585-590.
  17. Schneider, A. F. L.; Kithil, M.; Cardoso, M. C.; Lehmann, M.; Hackenberger, C. P. R., Cellular uptake of large biomolecules enabled by cell-surface-reactive cell-penetrating peptide additives. *Nature Chemistry* **2021**, *13* (6), 530-539.
  18. Nam, S. H.; Jang, J.; Cheon, D. H.; Chong, S.-E.; Ahn, J. H.; Hyun, S.; Yu, J.; Lee, Y., pH-Activatable cell penetrating peptide dimers for potent delivery of anticancer drug to triple-negative breast cancer. *Journal of Controlled Release* **2021**, *330*, 898-906.
  19. Guo, X.; Wang, L.; Duval, K.; Fan, J.; Zhou, S.; Chen, Z., Dimeric Drug Polymeric Micelles with Acid-Active Tumor Targeting and FRET-Traceable Drug Release. *Advanced Materials* **2018**, *30* (3), 1705436.
  20. Pescina, S.; Ostacolo, C.; Gomez-Monterrey, I. M.; Sala, M.; Bertamino, A.; Sonvico, F.; Padula, C.; Santi, P.; Bianchera, A.; Nicoli, S., Cell penetrating peptides in ocular drug delivery: State of the art. *Journal of Controlled Release* **2018**, *284*, 84-102.
  21. Guidotti, G.; Brambilla, L.; Rossi, D., Cell-Penetrating Peptides: From Basic Research to Clinics. *Trends in Pharmacological Sciences* **2017**, *38* (4), 406-424.
  22. Vale, N.; Duarte, D.; Silva, S.; Correia, A. S.; Costa, B.; Gouveia, M. J.; Ferreira, A., Cell-penetrating peptides in oncologic pharmacotherapy: A review. *Pharmacological Research* **2020**, *162*, 105231.
  23. Desale, K.; Kuche, K.; Jain, S., Cell-penetrating peptides (CPPs): an overview of applications for improving

the potential of nanotherapeutics. *Biomaterials Science* **2021**, *9* (4), 1153-1188.

24. Zhang, F.; Angelova, A.; Garamus, V. M.; Angelov, B.; Tu, S.; Kong, L.; Zhang, X.; Li, N.; Zou, A., Mitochondrial Voltage-Dependent Anion Channel 1–Hexokinase-II Complex-Targeted Strategy for Melanoma Inhibition Using Designed Multiblock Peptide Amphiphiles. *ACS Applied Materials & Interfaces* **2021**, *13* (30), 35281-35293.
25. Kang, Z.; Ding, G.; Meng, Z.; Meng, Q., The rational design of cell-penetrating peptides for application in delivery systems. *Peptides* **2019**, *121*, 170149.
26. Südhof Thomas, C.; Rothman James, E., Membrane Fusion: Grappling with SNARE and SM Proteins. *Science* **2009**, *323* (5913), 474-477.
27. Jahn, R.; Scheller, R. H., SNAREs — engines for membrane fusion. *Nature Reviews Molecular Cell Biology* **2006**, *7* (9), 631-643.
28. Chen, Y. A.; Scheller, R. H., SNARE-mediated membrane fusion. *Nature Reviews Molecular Cell Biology* **2001**, *2* (2), 98-106.
29. Kong, L.; Askes, S. H. C.; Bonnet, S.; Kros, A.; Campbell, F., Temporal Control of Membrane Fusion through Photolabile PEGylation of Liposome Membranes. *Angewandte Chemie International Edition* **2016**, *55* (4), 1396-1400.
30. Yang, J.; Shimada, Y.; Olsthoorn, R. C. L.; Snaar-Jagalska, B. E.; Spaink, H. P.; Kros, A., Application of Coiled Coil Peptides in Liposomal Anticancer Drug Delivery Using a Zebrafish Xenograft Model. *ACS Nano* **2016**, *10* (8), 7428-7435.
31. Yang, J.; Bahreman, A.; Daudey, G.; Bussmann, J.; Olsthoorn, R. C. L.; Kros, A., Drug Delivery via Cell Membrane Fusion Using Lipopeptide Modified Liposomes. *ACS Central Science* **2016**, *2* (9), 621-630.
32. Daudey, G. A.; Shen, M.; Singhal, A.; van der Est, P.; Sevink, G. J. A.; Boyle, A. L.; Kros, A., Liposome fusion with orthogonal coiled coil peptides as fusogens: the efficacy of roleplaying peptides. *Chemical Science* **2021**, *12* (41), 13782-13792.
33. Rabe, M.; Aisenbrey, C.; Pluhackova, K.; de Wert, V.; Boyle, Aimee L.; Bruggeman, Didjay F.; Kirsch, Sonja A.; Böckmann, Rainer A.; Kros, A.; Raap, J.; Bechinger, B., A Coiled-Coil Peptide Shaping Lipid Bilayers upon Fusion. *Biophysical Journal* **2016**, *111* (10), 2162-2175.
34. Rabe, M.; Zope, H. R.; Kros, A., Interplay between Lipid Interaction and Homo-coiling of Membrane-Tethered Coiled-Coil Peptides. *Langmuir* **2015**, *31* (36), 9953-9964.
35. Rabe, M.; Schwieger, C.; Zope, H. R.; Versluis, F.; Kros, A., Membrane Interactions of Fusogenic Coiled-Coil Peptides: Implications for Lipopeptide Mediated Vesicle Fusion. *Langmuir* **2014**, *30* (26), 7724-7735.
36. Chatterjee, K.; Zhang, J.; Honbo, N.; Karliner, J. S., Doxorubicin Cardiomyopathy. *Cardiology* **2010**, *115* (2), 155-162.
37. Takemura, G.; Fujiwara, H., Doxorubicin-Induced Cardiomyopathy: From the Cardiotoxic Mechanisms to Management. *Progress in Cardiovascular Diseases* **2007**, *49* (5), 330-352.
38. Vercauteren, D.; Piest, M.; van der Aa, L. J.; Al Soraj, M.; Jones, A. T.; Engbersen, J. F. J.; De Smedt, S. C.; Braeckmans, K., Flotillin-dependent endocytosis and a phagocytosis-like mechanism for cellular internalization of disulfide-based poly(amido amine)/DNA polyplexes. *Biomaterials* **2011**, *32* (11), 3072-3084.
39. Tao, W.; Mao, X.; Davide, J. P.; Ng, B.; Cai, M.; Burke, P. A.; Sachs, A. B.; Sepp-Lorenzino, L., Mechanistically Probing Lipid-siRNA Nanoparticle-associated Toxicities Identifies Jak Inhibitors Effective in Mitigating Multifaceted Toxic Responses. *Molecular Therapy* **2011**, *19* (3), 567-575.
40. Arcaro, A.; Wymann, M. P., Wortmannin is a potent phosphatidylinositol 3-kinase inhibitor: the role of phosphatidylinositol 3,4,5-trisphosphate in neutrophil responses. *Biochemical Journal* **1993**, *296* (2), 297-301.
41. Macia, E.; Ehrlich, M.; Massol, R.; Boucrot, E.; Brunner, C.; Kirchhausen, T., Dynasore, a Cell-Permeable Inhibitor of Dynamin. *Developmental Cell* **2006**, *10* (6), 839-850.

42. Doherty, G. J.; McMahon, H. T., Mechanisms of Endocytosis. *Annual Review of Biochemistry* **2009**, *78* (1), 857-902.
43. Preta, G.; Cronin, J. G.; Sheldon, I. M., Dynasore - not just a dynamin inhibitor. *Cell Communication and Signaling* **2015**, *13* (1), 24.
44. Delvendahl, I.; Vyleta, Nicholas P.; von Gersdorff, H.; Hallermann, S., Fast, Temperature-Sensitive and Clathrin-Independent Endocytosis at Central Synapses. *Neuron* **2016**, *90* (3), 492-498.
45. von Kleist, L.; Stahlschmidt, W.; Bulut, H.; Gromova, K.; Puchkov, D.; Robertson, Mark J.; MacGregor, Kylie A.; Tomilin, N.; Pechstein, A.; Chau, N.; Chircop, M.; Sakoff, J.; von Kries, Jens P.; Saenger, W.; Kräusslich, H.-G.; Shupliakov, O.; Robinson, Phillip J.; McCluskey, A.; Haucke, V., Role of the Clathrin Terminal Domain in Regulating Coated Pit Dynamics Revealed by Small Molecule Inhibition. *Cell* **2011**, *146* (3), 471-484.
46. Rejman, J.; Bragonzi, A.; Conese, M., Role of clathrin- and caveolae-mediated endocytosis in gene transfer mediated by lipo- and polyplexes. *Molecular Therapy* **2005**, *12* (3), 468-474.
47. Vercauteren, D.; Vandenbroucke, R. E.; Jones, A. T.; Rejman, J.; Demeester, J.; De Smedt, S. C.; Sanders, N. N.; Braeckmans, K., The Use of Inhibitors to Study Endocytic Pathways of Gene Carriers: Optimization and Pitfalls. *Molecular Therapy* **2010**, *18* (3), 561-569.
48. Rodal, S. K.; Skretting, G.; Garred, Ø.; Vilhardt, F.; van Deurs, B.; Sandvig, K., Extraction of Cholesterol with Methyl- $\beta$ -Cyclodextrin Perturbs Formation of Clathrin-coated Endocytic Vesicles. *Molecular Biology of the Cell* **1999**, *10* (4), 961-974.
49. Novakowski, S.; Jiang, K.; Prakash, G.; Kastrup, C., Delivery of mRNA to platelets using lipid nanoparticles. *Scientific Reports* **2019**, *9* (1), 552.
50. Yao, C.; Wang, P.; Li, X.; Hu, X.; Hou, J.; Wang, L.; Zhang, F., Near-Infrared-Triggered Azobenzene-Liposome/Upconversion Nanoparticle Hybrid Vesicles for Remotely Controlled Drug Delivery to Overcome Cancer Multidrug Resistance. *Advanced Materials* **2016**, *28* (42), 9341-9348.
51. Marsh, M.; Helenius, A., Virus Entry: Open Sesame. *Cell* **2006**, *124* (4), 729-740.

## Supporting Information



SI scheme 1. (a) Synthetic route of K4-dimers, (a) PK4, (b) NK4, and (c) CK4.

Table S1. Sequences of peptides used in this work

Peptides	Sequences					
	<i>ef</i>	<i>gabcdef</i>	<i>gabcdef</i>	<i>gabcdef</i>	<i>gabcdef</i>	<i>ga</i>
<b>K4</b>		KIAALKE	KIAALKE	KIAALKE	KIAALKE	GW-NH <sub>2</sub>
<b>E4</b>		EIAALEK	EIAALEK	EIAALEK	EIAALEK	GW-NH <sub>2</sub>
<b>Fluo-K4</b>	Fluo-GG	KIAALKE	KIAALKE	KIAALKE	KIAALKE	GW-NH <sub>2</sub>
<b>Fluo-E4</b>	Fluo-GG	EIAALEK	EIAALEK	EIAALEK	EIAALEK	GW-NH <sub>2</sub>
<b>K4-Cys14</b>		KIAALKE	KIAALK <b>C</b>	KIAALKE	KIAALKE	-NH <sub>2</sub>
<b>K4GW-Cys14</b>		KIAALKE	KIAALK <b>C</b>	KIAALKE	KIAALKE	GW-NH <sub>2</sub>
<b>CG-K4</b>	<b>CG</b>	KIAALKE	KIAALKE	KIAALKE	KIAALKE	-NH <sub>2</sub>
<b>CG-K4GW</b>	<b>CG</b>	KIAALKE	KIAALKE	KIAALKE	KIAALKE	GW-NH <sub>2</sub>
<b>K4-GC</b>		KIAALKE	KIAALKE	KIAALKE	KIAALKE	<b>GC</b> -NH <sub>2</sub>
<b>WG-K4GC</b>	WG	KIAALKE	KIAALKE	KIAALKE	KIAALKE	<b>GC</b> -NH <sub>2</sub>

**Table S2. Theoretical and observed mass of peptides using LC-MS**

<b>Peptide</b>	<b>Mass(calculated)/Da</b>	<b>Mass(Found)/Da</b>
<b>PK4</b>	[M+5H] <sup>5+</sup> 1268.2	1267.5
	[M+4H] <sup>4+</sup> 1585.0	1584.3
	[M+3H] <sup>3+</sup> 2113.0	2113.0
	[M+5H] <sup>5+</sup> 1342.4	1341.8
<b>NK4</b>	[M+4H] <sup>4+</sup> 1677.8	1677.2
	[M+3H] <sup>3+</sup> 2236.7	2237.5
	[M+5H] <sup>5+</sup> 1342.4	1341.8
<b>CK4</b>	[M+4H] <sup>4+</sup> 1677.8	1677.9
	[M+3H] <sup>3+</sup> 2236.7	2237.5
<b>Fluo-E4</b>	[M+3H] <sup>3+</sup> 1252.7	1250.6
	[M+2H] <sup>2+</sup> 1878.5	1876.0
<b>Fluo-K4</b>	[M+3H] <sup>3+</sup> 1251.2	1249.3
	[M+2H] <sup>2+</sup> 1876.5	1874.0
<b>CPK4</b>	[M+3H] <sup>3+</sup> 1246.2	1244.3
	[M+2H] <sup>2+</sup> 1869.4	1866.4
<b>CPE4</b>	[M+3H] <sup>3+</sup> 1247.8	1245.4
	[M+2H] <sup>2+</sup> 1871.2	1868.8

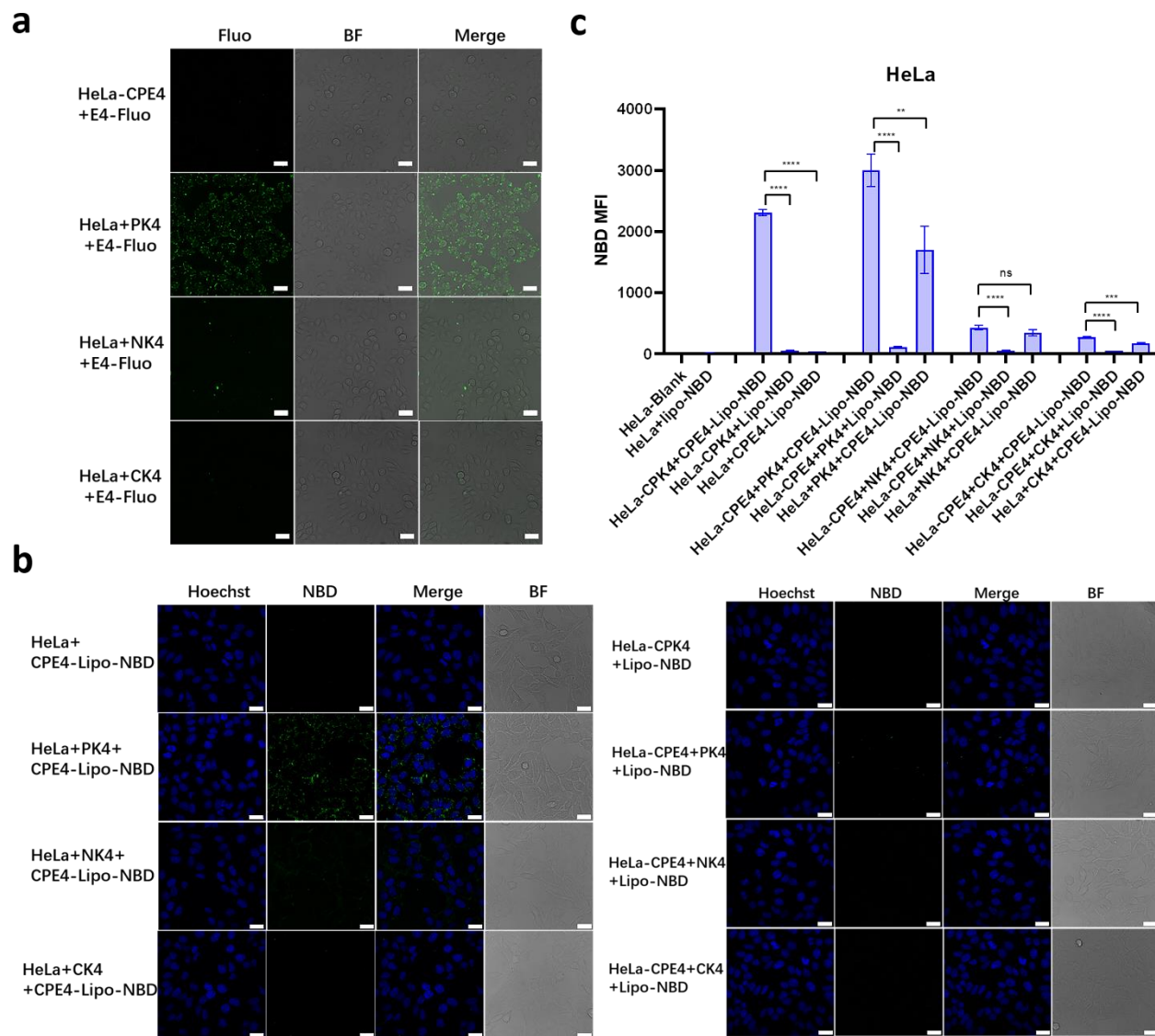
**Table S3. Normalized mean residue molar ellipticity and percentage helicity of peptides**

<b>Peptide</b>	<b>[<math>\theta</math>] / deg cm<sup>2</sup> dmol<sup>-1</sup></b>	<b>Helicity (%)<sup>a</sup></b>
<b>K4</b>	-29894.2	89
<b>E4</b>	-25063.8	80
<b>PK4</b>	-8550.3	25
<b>NK4</b>	-34322.4	92
<b>CK4</b>	-39613.2	105
<b>PK4+E4</b>	-34330.3	90
<b>NK4+E4</b>	-31438.4	83
<b>CK4+E4</b>	-35300.8	92

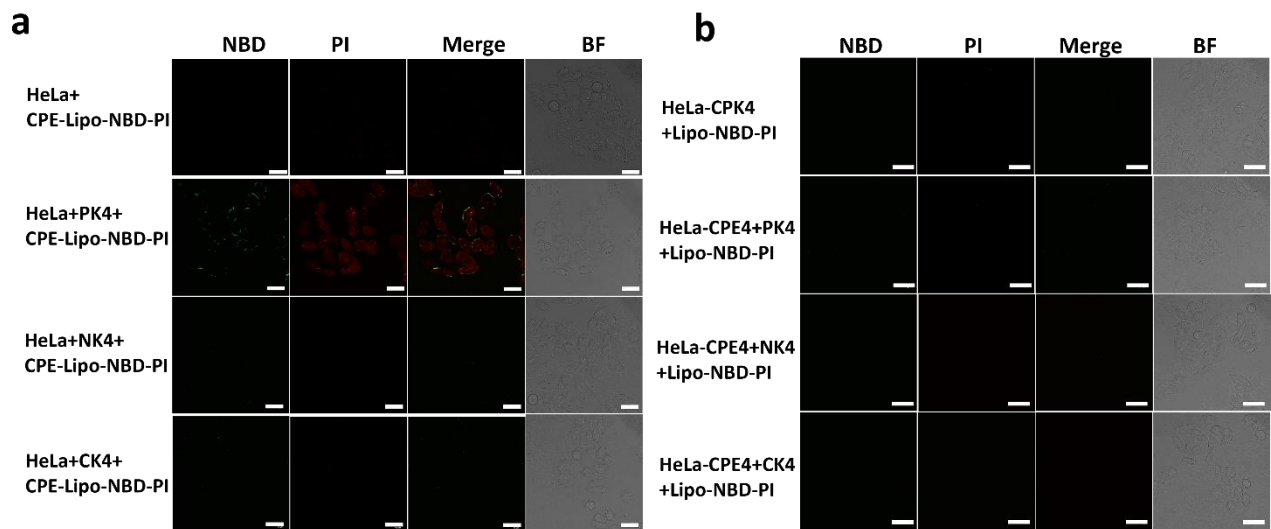
<sup>a</sup> The percentage of  $\alpha$ -helicity was calculated using the equation in section of experimental 3. The percentage of helicity of the peptides ( $F_{\text{helix}}$ ) can be calculated by equation:  $F_{\text{helix}} = 100\% \cdot ([\theta]_{222} - [\theta]_0) / ([\theta]_{\text{max}} - [\theta]_0)$ ,  $[\theta]_{222}$  represents the mean residue molar ellipticity of peptide at 222 nm,  $[\theta]_0$  is the mean residue ellipticity of the peptide when the peptide is in an entirely random coil conformation,  $[\theta]_{\text{max}}$  is the maximum theoretical mean residue ellipticity.

**Table S4. Characterization of liposomes used in this study**

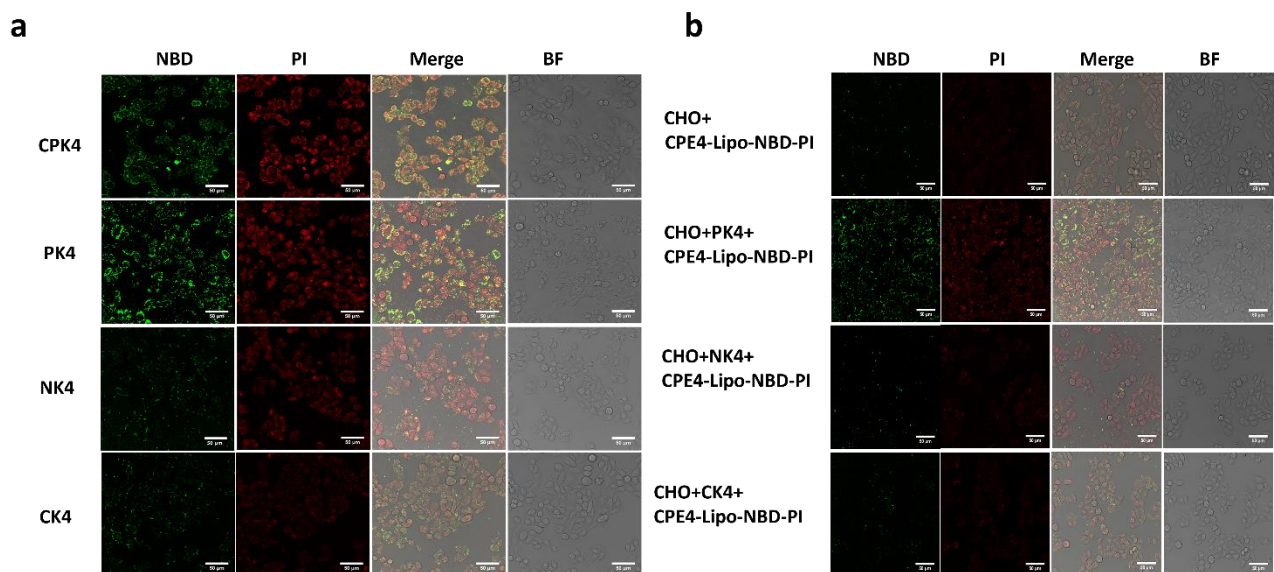
<b>Liposomes</b>	<b>Size(nm)</b>	<b>PDI</b>	<b>Zeta-potential(mV)</b>
<b>Liposome-NBD</b>	121.0 $\pm$ 3.9	0.168 $\pm$ 0.042	-3.23 $\pm$ 2.31
<b>CPE4-liposome-NBD</b>	96.7 $\pm$ 5.2	0.129 $\pm$ 0.023	-4.23 $\pm$ 2.56
<b>Liposome-NBD-PI</b>	151.1 $\pm$ 7.2	0.150 $\pm$ 0.035	-4.87 $\pm$ 1.23
<b>CPE4-liposome-NBD-PI</b>	157.2 $\pm$ 5.8	0.105 $\pm$ 0.021	-5.23 $\pm$ 2.06
<b>Liposome-NBD-Dox</b>	146.2 $\pm$ 4.8	0.116 $\pm$ 0.034	-5.35 $\pm$ 3.27
<b>CPE4-liposome-NBD-Dox</b>	171.6 $\pm$ 2.8	0.093 $\pm$ 0.043	-3.67 $\pm$ 2.23
<b>DOTAP-liposome-NBD</b>	154.2 $\pm$ 3.2	0.126 $\pm$ 0.027	54.23 $\pm$ 3.73



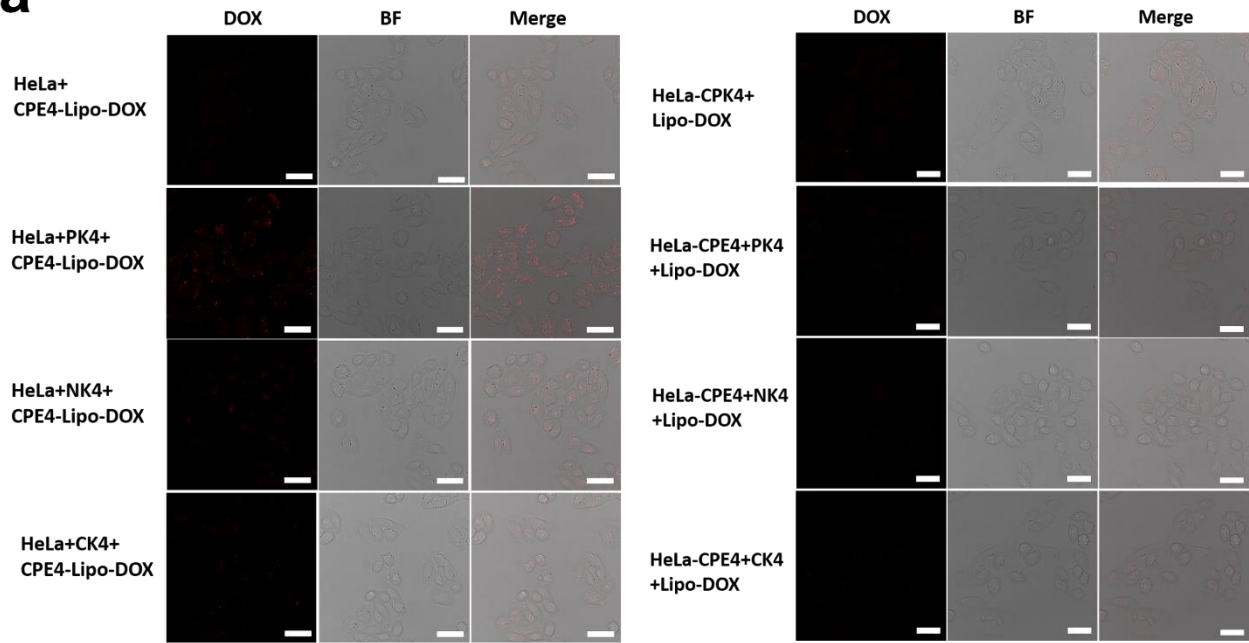
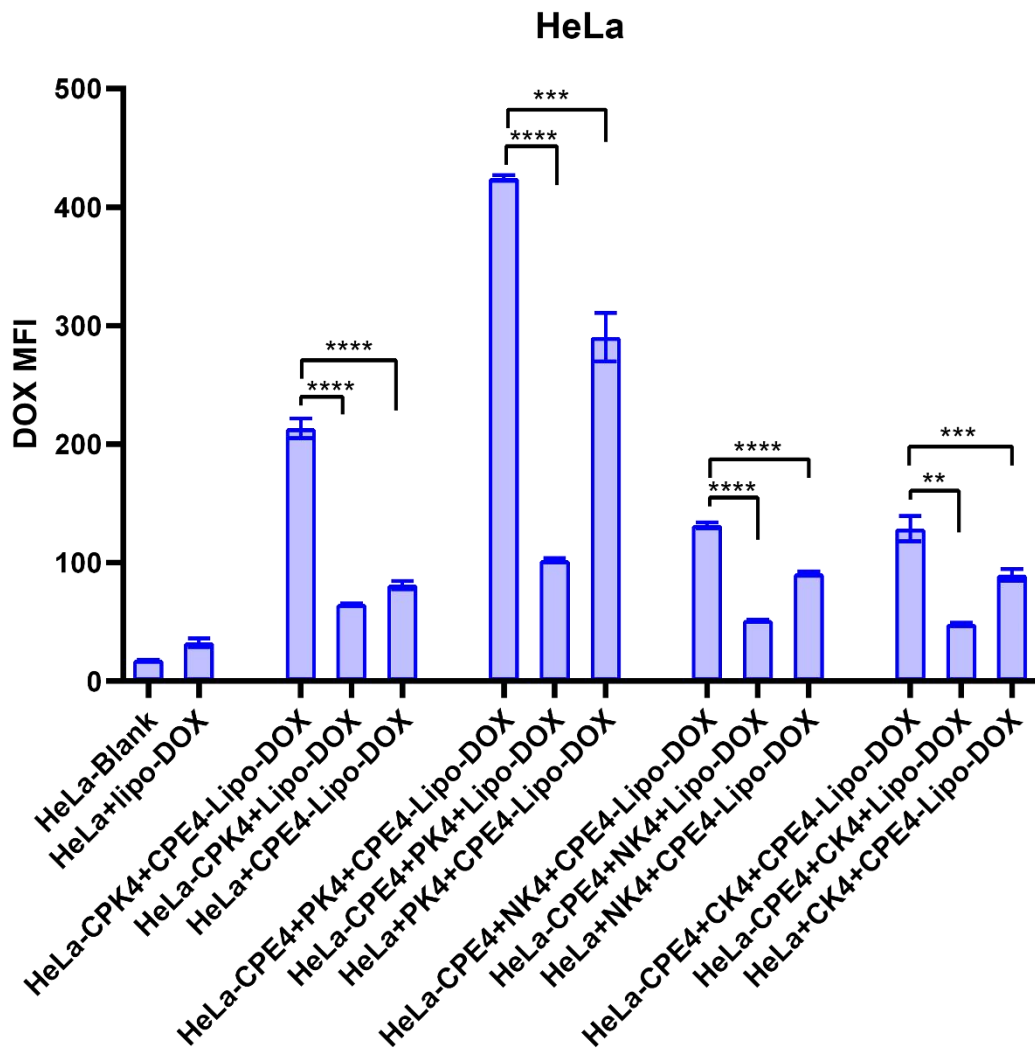
**SI Figure 1. (a)** Confocal images of cell membrane labeling between dimers and fluorescein-E4 of control groups. **(c)** Confocal images of K4 monomer and dimers with NBD-labeled liposomes modified with CPE4 of control groups. Green: NBD-PE; blue: Hoechst 33342; BF: bright field; scale bar is 30  $\mu$ m. **(b)** Quantification of NBD-liposome intensity by flow cytometry of all groups. Unpaired student t-test was used to determine the significance of data comparisons (\*\*\*\* $P < 0.0001$ ; \*\*\* $P < 0.001$ ; \*\* $P < 0.01$ ; \* $P < 0.05$ ). In all panels, error bars represent mean  $\pm$  s.d. (n=3).



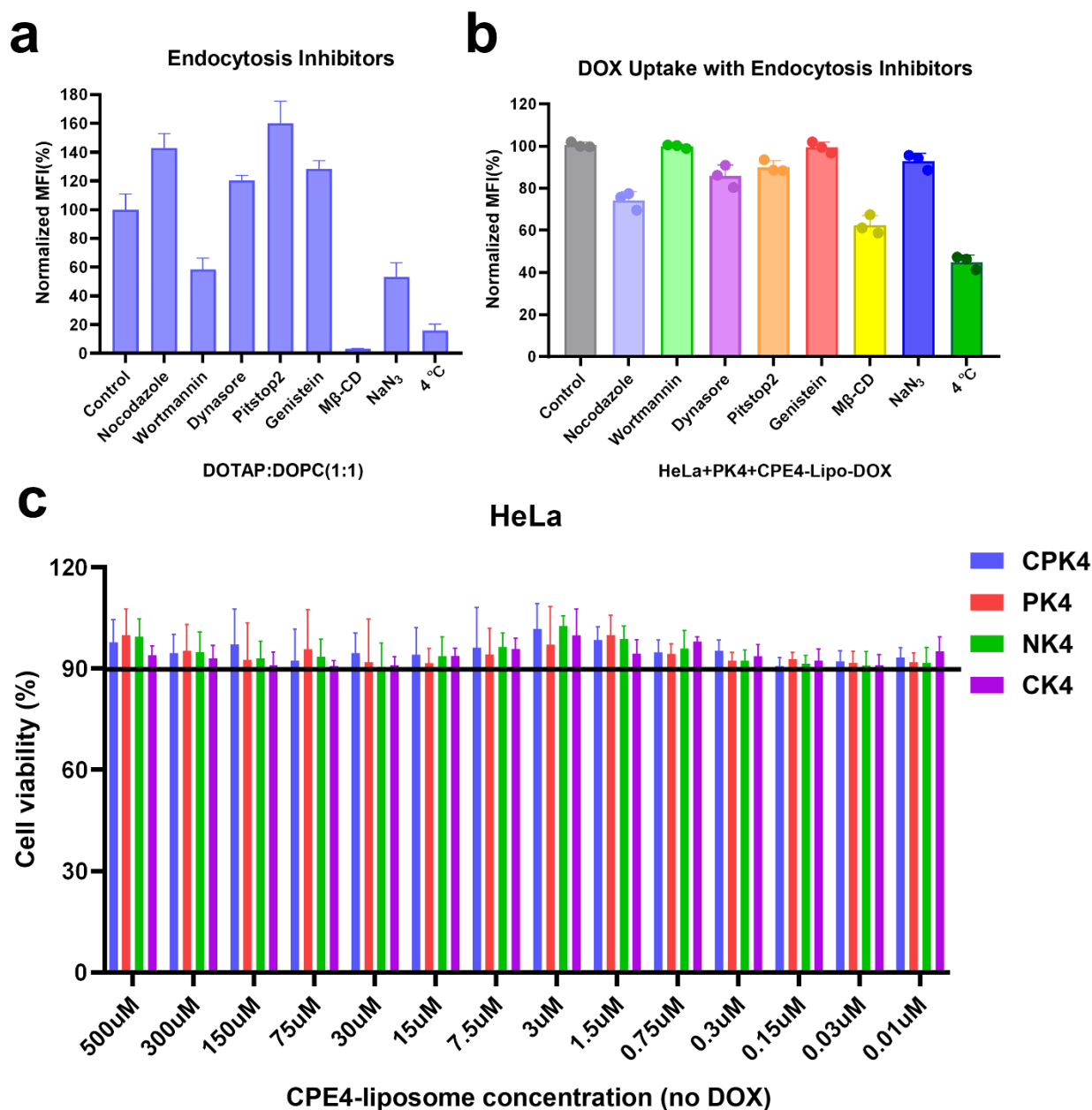
**SI Figure 2.** Confocal images of liposomal PI delivery by K4 monomer and dimers of control groups **(a)** cells without CPE4/CPK4 pretreatment **(b)** liposomes without CPE4 modification. Green: NBD-PE; red: PI; BF: bright field; scale bar is 30  $\mu\text{m}$ .



**SI Figure 3.** Confocal images of liposomal PI delivery by K4 monomer and dimers with the CHO cell line **(a)** cells with CPE4/CPK4 pretreatment **(b)** cells without CPE4/CPK4 pretreatment. Liposomes contain 1% NBD-PE and 1% CPE4 on the membrane and were loaded with 10 mg/mL PI. Green: NBD-PE; red: PI; BF: bright field; scale bar is 50  $\mu\text{m}$ . CPK4: CPK4-cell+CPE4-liposome-NBD-PI; PK4: CPE4-cell+PK4+CPE4-liposome-NBD-PI; NK4: CPE4-cell+NK4+CPE4-liposome-NBD-PI; CK4: CPE4-cell+CK4+CPE4-liposome-NBD-PI.

**a****b**

**SI Figure 4. (a)** Confocal images of DOX uptake of K4 monomer and dimers in HeLa cells of control groups. **(b)** Quantification of internalized DOX intensity of K4 monomer and dimers of all groups. Red: PI; BF: bright field; scale bar is 30  $\mu\text{m}$ . Unpaired student t-test was used to determine the significance of data comparisons (\*\*\*\* $P < 0.0001$ ; \*\*\* $P < 0.001$ ; \*\* $P < 0.01$ ; \* $P < 0.05$ ). In all panels, error bars represent mean  $\pm$  s.d. (n=3).



**SI Figure 5. (a)** Quantification of uptake efficiency of the cationic liposome DOTAP (DOTAP: DOPC=1:1, 1 mol% NBD-PE) with endocytosis inhibitors in HeLa cells. **(b)** Quantification of uptake efficiency of PK4 dimer with endocytosis inhibitors in HeLa calls without CPE4 pretreatment. **(c)** Cell viability of liposomes without DOX encapsulation. The solid line represents 90% cell viability. CPK4: CPK4-cell+CPE4-liposome; PK4: CPE4-cell+PK4+CPE4-liposome; NK4: CPE4-cell+NK4+CPE4-liposome; CK4: CPE4-cell+CK4+CPE4-liposome



## Chapter 4

### Efficient mRNA Delivery to Cardiomyocytes *in vitro* Using Fusogenic LNPs

## Abstract

Heart failure usually results from the loss of billions of specialized cardiac muscle cells known as cardiomyocytes (CMs), in a process induced by myocardial infarction (MI). To minimize health issues relating to the loss of cardiomyocytes, cardiac tissue repair is essential. However, optimizing cardiac tissue repair is difficult. This process could be improved by transient mRNA expression that regulates the behavior and fate of progenitor cells, thus a robust mRNA therapy could result in the regeneration of lost myocardium. Cardiomyocytes derived from induced pluripotent stem cells (iPSC-CMs) represent the best cell source for cardiac regeneration but require efficient mRNA delivery. To date, lipid nanoparticles (LNPs) represent the most efficient mRNA delivery platform. However, the transfection efficiency of LNPs is still hampered by endosomal entrapment after endocytosis by the cells. Enhanced mRNA transfection efficiency has been achieved by the introduction of fusogenic coiled-coil peptides into LNPs. Here, we modified LNPs with the coiled-coil peptide CPE4, while iPSC-CMs were pretreated with the complementary coiled-coil peptide CPK4, and we achieved improved mRNA transfection efficiency. Different incubation methods of coiled-coil peptide-modified LNPs were compared, and it was shown that the 1-step incubation protocol achieved a higher mRNA transfection efficiency. mRNA transfection enhancement of iPSC-CMs using this 1-step incubation protocol was independent of the LNP lipid composition. This study shows that the modification of LNPs with fusogenic coiled-coil peptides significantly improved mRNA expression in iPSC-CMs and holds great promise for future heart regenerative therapies.

## Introduction

Heart failure is a leading cause of morbidity and mortality worldwide.<sup>1</sup> In Europe alone, more than 3.5 million people are diagnosed with heart failure every year; 50% of these will die within 4 years.<sup>2</sup> <sup>3</sup> Moreover, due to aging and improved survival after myocardial infarction (MI), the incidence and prevalence of heart failure is increasing. To date, there is no cure, and treatment options are limited to drug therapies and a limited number of heart transplantations. One of the main causes leading to heart failure is the massive loss of cardiomyocytes (*i.e.* heart muscle cells) as a result of acute or chronic ischemia. Because the adult mammalian heart has limited capacity for regeneration after MI,<sup>4</sup> this loss of cardiomyocytes is considered to be irreversible, eventually leading to a loss of pump function and heart failure. Existing medical and device-based therapies can ameliorate the effects of heart failure but cannot regenerate the loss of functional myocardium.<sup>5</sup> Endogenous replenishment of cardiomyocytes is insufficient to repair the myocardial injury after MI, thus efficient delivery systems can deliver DNA, RNA, or proteins with specific functions to induce cardiac repair and ultimately facilitate regeneration of cardiomyocytes to rescue the ischemic myocardium are needed.<sup>6</sup>

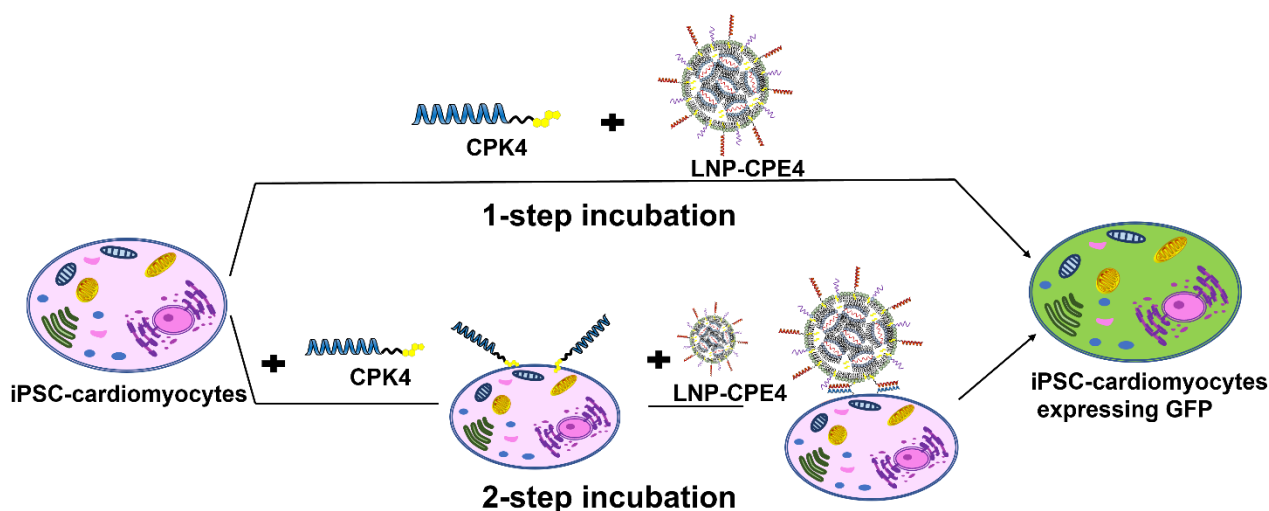
Primary cardiomyocytes are difficult to isolate and have a short lifespan, thus many techniques have been adopted to obtain reliable sources of human cardiomyocytes, including bone marrow-derived, embryonic stem cells (ESCs), and induced pluripotent stem cells (iPSCs).<sup>7, 8</sup> iPSC-derived cardiomyocytes (iPSC-CMs) are the most promising cell source for cardiac repair research, as they can proliferate indefinitely and differentiate into cardiac lineages, including cardiomyocytes, smooth muscle cells, endothelial cells, and cardiac progenitors.<sup>9-11</sup> iPSC-CMs mimic primary cardiac cell functional performance by expressing the correct electrical and physiological properties of the developing heart, which makes iPSCs an advantageous candidate for preclinical drug screening and cardiac research about signaling pathways that underpin myocardial development.<sup>8, 12, 13</sup>

Cardiac-specific protein expression, such as Yes-associated protein (YAP), VEGF, and angiopoietin-1 (Ang1), in adult mice could drive cardiomyocyte proliferation and improve cardiac function after MI.<sup>14-19</sup> The cardiac-specific protein expression needs to be tightly controlled, since continuous expression may lead to uncontrolled cardiac repair.<sup>17</sup> Fortunately, messenger RNA (mRNA) activity is temporary as a result of its natural degradation, allowing temporal control over protein expression to stimulate regeneration while avoiding uncontrolled long-term growth. mRNA therapeutics have shown the ability to induce vascular regeneration after myocardial infarction *in vitro* and *in vivo*.<sup>16, 20-22</sup> However, the major challenge remaining is the delivery of relevant therapeutic doses of mRNA to cardiomyocytes *in vivo*. For efficient functional cytosolic delivery to, and release within, target cells these highly charged, immunogenic, and membrane-impermeable mRNA molecules require the use of delivery systems.<sup>23, 24</sup> To this end, lipid nanoparticles (LNPs) serve as the state-of-the-art vector that can package, protect and release RNA molecules inside cells.<sup>25</sup> LNPs have realized the translation of RNA therapeutics to the clinic, highlighted by the successful use of the LNP-siRNA (Onpattro®) formulation for the treatment of polyneuropathies induced by hereditary transthyretin amyloidosis and the FDA approval of two Covid-19 LNP-mRNA vaccine formulations in 2020 that were optimized for mRNA delivery.<sup>25-29</sup> To achieve efficient transfection, disruption of the LNP structure and the endosomal membrane is crucial for sufficient RNA delivery into the cytoplasm.<sup>30</sup> However, in this process the majority ( $\geq 98\%$ ) of RNA molecules delivered with LNP systems remain trapped inside the endo/lysosome, leading to degradation or efflux out of the cell.<sup>31, 32</sup> Thus there is room to

improve the therapeutic efficacy of mRNA therapies if cytoplasm delivery could be enhanced.

Fusion of lipid membranes occurs in many biological processes, including organelle inheritance in cell growth and division, chemical synaptic transmission in the nervous system, and the modulation of synaptic strength in memory and learning evolution.<sup>33</sup> These fusion events are controlled by complementary specialized SNARE protein subunits, which form so-called coiled-coil complexes driving the docking of transport vesicles to the target plasma membrane resulting in membrane fusion and cargo delivery (*e.g.* in neuronal exocytosis).<sup>34</sup> Coiled-coil induced membrane fusion independent of endocytosis could be beneficial to facilitate endo/lysosome escape and boost the transfection efficiency of mRNA in cells.

In Chapter 2 we modified LNPs encapsulating mRNA with a heterodimeric coiled-coil peptide (denoted E4/K4) which induced prompt and highly efficient transfection and in this chapter mRNA delivery to iPSC-cardiomyocytes was studied. The Onpattro LNP formulation was modified with lipopeptide CPE4 (denoted as MC3-CPE4) and enhanced transfection of genetic cargo was observed following a 1-step incubation protocol of cells with a mixture of MC3-CPE4 and the complimentary lipopeptide CPK4. When this approach was used with the Covid-19 vaccine LNP-mRNA formulations, significantly enhanced mRNA expression was also obtained. In this study we apply coiled-coil peptide modified LNPs to transfect iPSC-CMs, resulting in a significant improvement of transfection (**Scheme 1**). These findings hold great promise for further *in vivo* research toward the development of efficient cardiomyocytes transfection and stimulation of cardiac repair and ultimately regeneration to rescue the ischemic myocardium.



**Scheme 1.** Schematic representation of fusogenic coiled-coil peptide modified lipid nanoparticles (LNPs) that induce efficient mRNA delivery within iPSC-cardiomyocytes using different delivery protocols.

## Results and discussion

### LNP design, formulation, and characterization

The clinically approved LNP formulation Onpattro (short name MC3) was designed for potent

silencing of protein expression in cells by delivering siRNA (**Fig. 1a-b**).<sup>35, 36</sup> Two other LNP formulations with ionizable lipids either ALC0315 or SM102 were also studied (**SI Fig. 1a**). In this study, lipopeptide CPE4 (1 mol%) was added to the LNP formulations, resulting in CPE4-modified LNPs (**Fig. 1b, SI Fig. 1b**). After encapsulating EGFP-mRNA, the hydrodynamic diameter, polydispersities (PDI), zeta potential, and mRNA encapsulation efficiency of these LNPs was not changed by the addition of lipopeptide CPE4 (**Fig. 1c, SI Fig. 1b**). This showed that various clinically approved LNP formulations can be modified with lipidated coiled-coil peptides without altering the physicochemical characteristics.

In chapter 2 we showed that coiled-coil peptide modification of LNPs significantly improved the transfection efficiency in many cell lines *in vitro*. Here we studied whether these fusogenic peptides could be used to transfect cardiomyocytes. For *in vivo* applications, the intramyocardial injection volume of mice is very small (10  $\mu$ L) requiring a high concentration of LNPs to obtain a sufficient mRNA dose. Dynamic light scattering measurements (DLS) revealed that the observed hydrodynamic diameter of the MC3-CPE4 was independent of concentration (**Fig. 1d**).

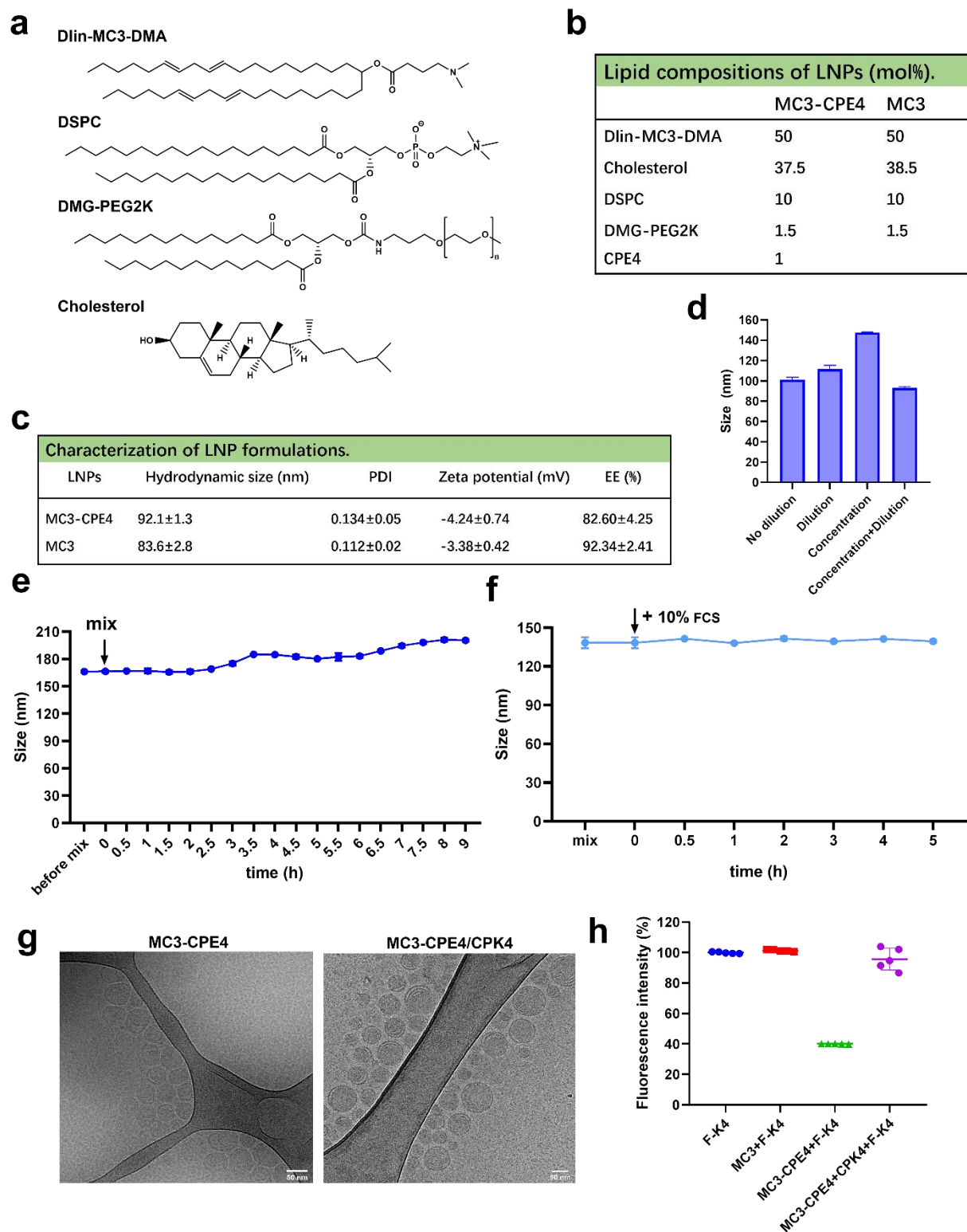


**Figure 1. Design and characterization of LNPs carrying EGFP-mRNA.** (a) Structures of lipids used for the preparation of MC3-LNPs. (b) Lipid composition of LNPs. (c) Characterization of LNPs. (d) Hydrodynamic diameter of MC3-CPE4 as an indication for concentration and dilution. (e) Hydrodynamic diameter changes over time after mixing MC3-CPE4 with CPK4. (f) Hydrodynamic diameter changes over time of the mixture of MC3-CPE4 and CPK4 after 10% FCS addition. The nanoparticle diameter and PDI were monitored by DLS (mean ± s.d.,

n = 3). **(g)** Representative cryo-EM images of coiled-coil peptide modified MC3-CPE4 before and after mixing with the complimentary peptide. Scale bar is 50 nm. **(h)** Fluorescence intensity changes of fluorescein-labeled K4 peptide after addition to LNPs.

### Nanoparticle characterizations of the 1-step incubation approach

Initially, we used a 2-step incubation protocol to deliver mRNA to cells, which requires the pretreatment of target cells before complementary LNPs are added. Cardiac mRNA delivery is usually achieved by direct intramyocardial injection of mRNA formulations in an open-chest surgery, and a shorter time of surgery will be beneficial for mouse survival.<sup>20</sup> Therefore a 1-step incubation protocol would be favorable. For this, we evaluated whether a 1-step incubation protocol was able to successfully transfect cells by premixing MC3-CPE4 and the complementary peptide CPK4 before mixing with cells. The hydrodynamic diameter change of this mixture was monitored by DLS as a function of time. After 2.5 h a slight increase in size was observed (**Fig. 1e**). Still, the overall diameter remained rather stable for a prolonged period of time and no massive aggregation was observed, which suggests that premixing does not negatively impact the colloidal stability of LNPs enabling a 1-step incubation protocol in future *in vivo* studies.

Next, the stability of the mixture MC3-CPE4 and CPK4 in the presence of 10% fetal calf serum (FCS) was studied. Again, no obvious size increase was observed (**Fig. 1f**). Cryogenic electron microscopy (cryo-EM) was applied to observe the morphology of MC3-CPE4 before and after mixing with the complimentary peptide CPK4 (**Fig. 1g**). No apparent changes in structure or aggregation was observed. Both amorphous and lamellar core structures of MC3-CPE4 were still present, whereas the core structure contained a mixture of amorphous, unilamellar, and polymorphic structures, as has been previously reported for mRNA containing LNPs.<sup>37, 38</sup>

LNP formulations consist of PEG chains (PEG2K), and mRNA delivery induced by coiled-coil peptide modified LNPs requires both coiled-coil peptides to be accessible, therefore to study whether CPE4 located on the surface of LNPs is still accessible to CPK4 even though the PEG chains are longer than the peptides, a fluorescence assay was used. Fluorescence intensity changes were monitored as an indication of binding affinity between peptides E and K after adding fluorescein-labeled K4 peptide (F-K4) to LNPs (**Fig. 1h**). Free F-K4 peptide served as a control, exhibiting 100% fluorescence intensity. As expected, when F-K4 was added to MC3, the fluorescence intensity was similar to free F-K4, demonstrating that free F-K4 failed to interact with the unmodified LNPs in the absence of CPE4. In contrast, when F-K4 was added to MC3-CPE4, the fluorescence intensity showed a significant reduction to 40%, indicating that F-K4 successfully binds to CPE4 at the LNP surface. When F-K4 was added to the mixture of MC3-CPE4 and CPK4, the fluorescence intensity was 96%, close to free F-K4, revealing that all CPE4 were already occupied by CPK4 via coiled-coil formation. This assay thus confirmed that the peptides are able to form coiled coils, even though the peptides are most likely buried in a PEG brush at the surface of LNPs.

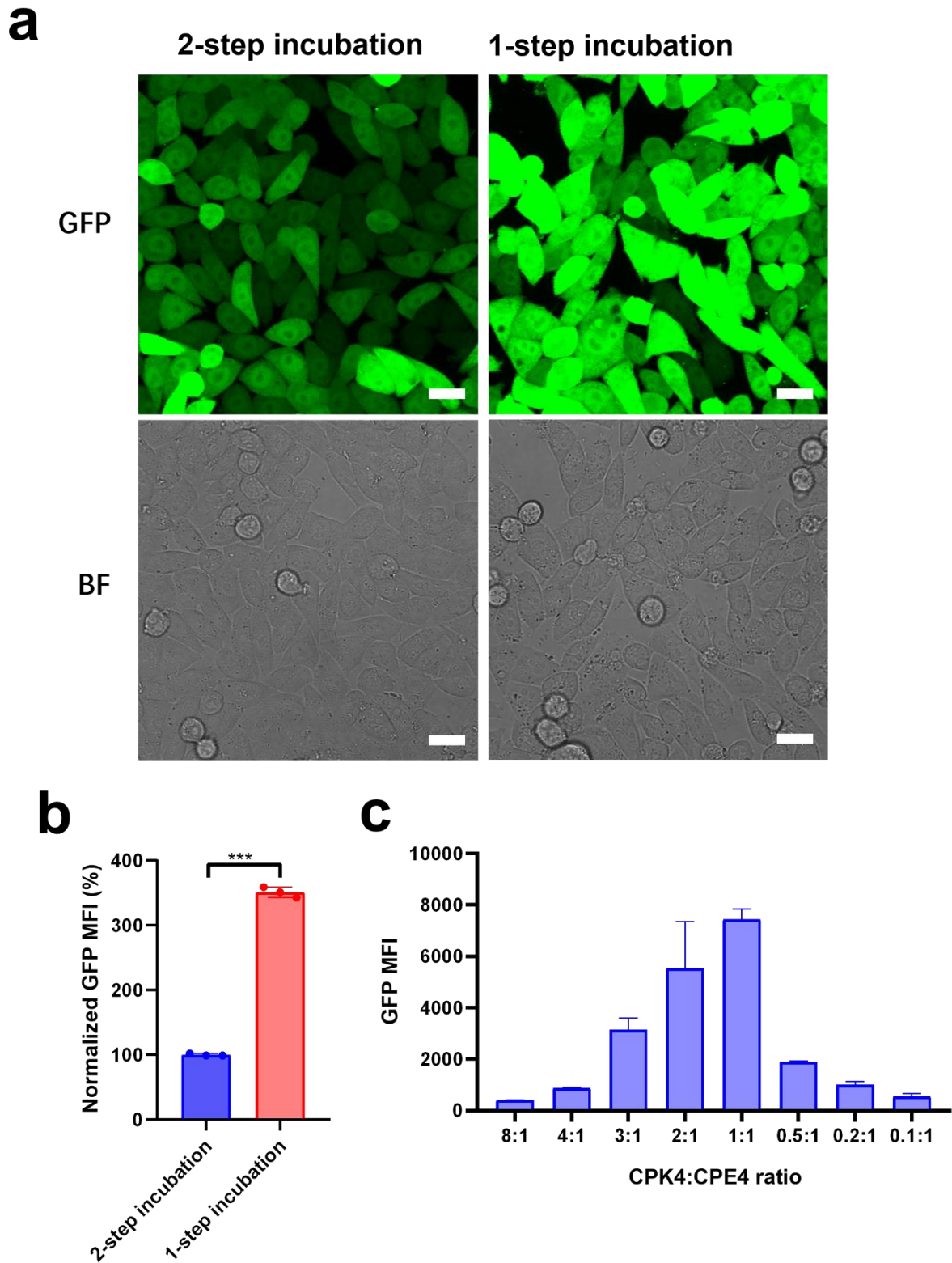


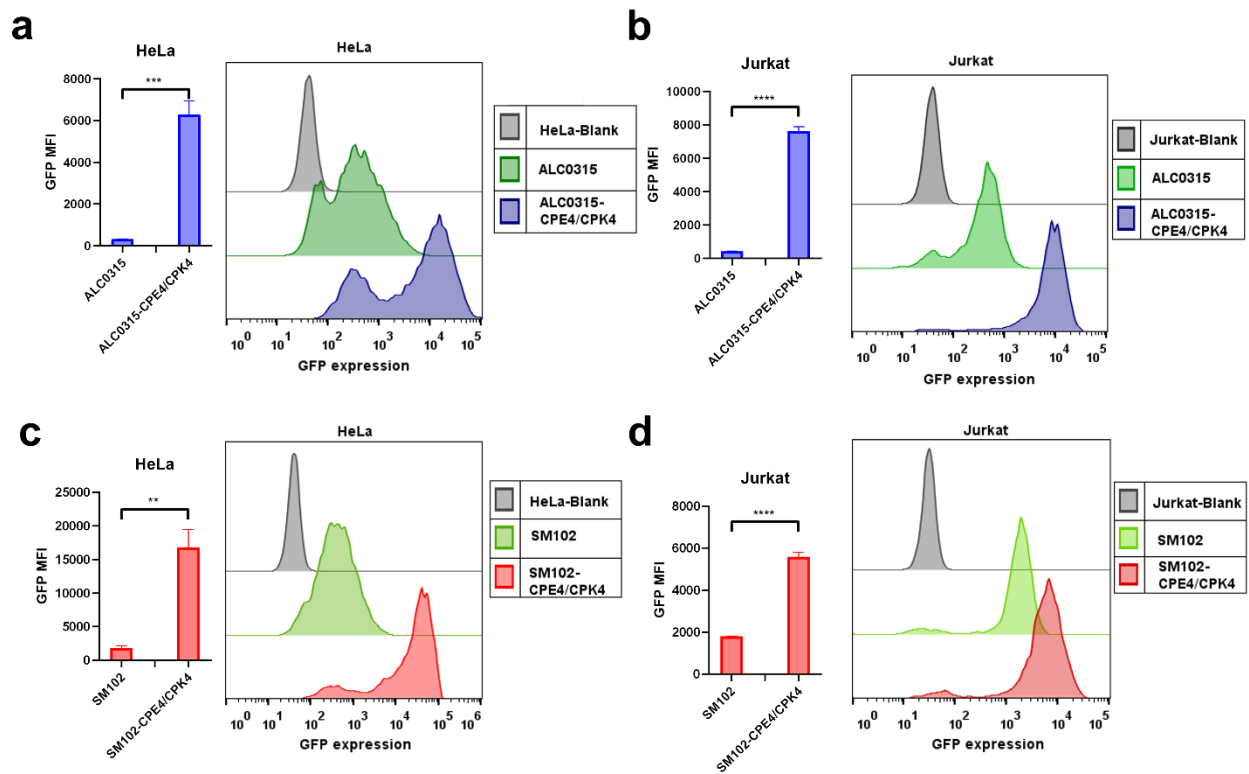
**Figure 2. Transfection efficiency evaluation of different incubation protocols with HeLa cells. (a)** Confocal microscopy images of mRNA transfection following different incubation protocols. 2-step incubation: cells were pretreated with CPK4 (10  $\mu$ M, 200  $\mu$ L) for 2 h, then the medium was removed and MC3-CPE4 was added (1  $\mu$ g/mL,

200  $\mu$ L) and incubated for 24 h before imaging. 1-step incubation: medium containing CPK4 and MC3-CPE4 (1  $\mu$ g/mL, 200  $\mu$ L, final concentration of CPK4:CPE4=1:1) was added to the cells and incubated for 24 h before imaging. GFP: green fluorescent protein; BF: bright field; scale bar is 20  $\mu$ m. **(b)** Flow cytometry measurements of GFP expression intensity (GFP MFI) of the two protocols. MFI of the 1-step incubation was normalized to the 2-step incubation. Unpaired student t-test was used to determine the significance of data comparisons (\*\*\*\*,  $P < 0.0001$ , \*\*\*,  $P < 0.001$ , \*\*,  $P < 0.01$ , \*,  $P < 0.05$ , ns, no significant difference). In all panels, error bars represent s.d. (n=3). **(c)** Transfection efficiency of CPK4:CPE4 ratio optimization following the 1-step incubation protocol. All LNPs were formulated using MC3 lipids and encapsulated with EGFP-mRNA. The EGFP-mRNA concentration encapsulated in MC3-CPE4 was 1  $\mu$ g/mL.

### **Transfection performance of different incubation protocols**

Next, we compared the transfection efficiencies between the 1-step and the 2-step incubation protocols as the former will be beneficial for future *in vivo* studies. Surprisingly, the 1-step incubation induced the strongest GFP expression (**Fig. 2a**). Flow cytometry analysis confirmed that the 1-step incubation indeed resulted in a higher mRNA transfection efficiency compared to the 2-step incubation, the former resulting in a 3-fold stronger GFP expression level (**Fig. 2b**). This experiment demonstrated that the 1-step incubation protocol is efficient and enables the future use in *in vivo* studies.

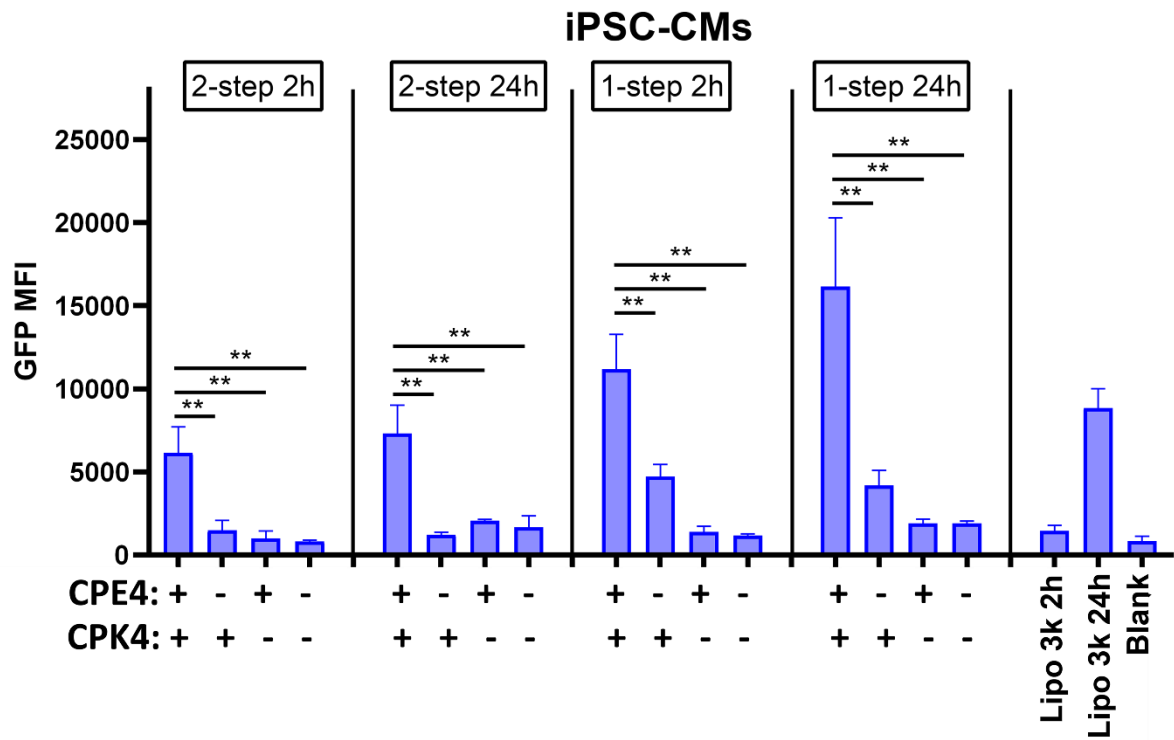
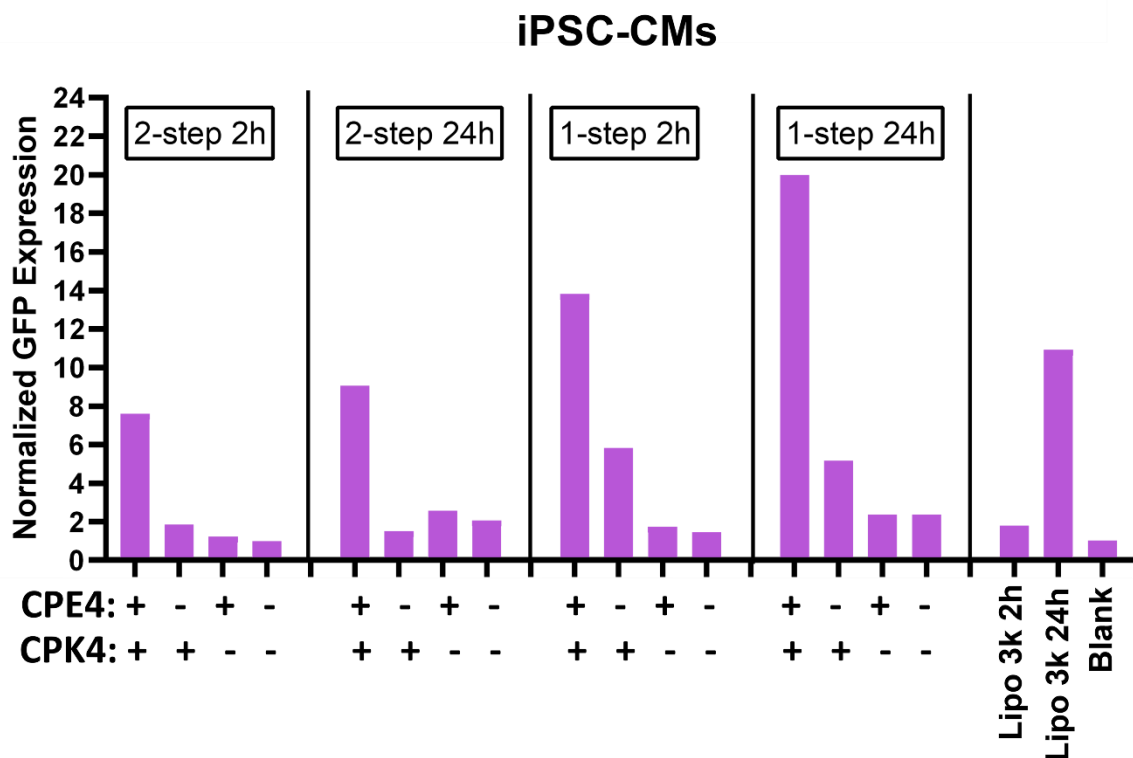
Next, we optimized the CPK4:CPE4 ratio for the 1-step incubation protocol. The mRNA concentration of MC3-CPE4 was kept constant while CPK4 and MC3-CPE4 were used at different final ratios. The highest GFP expression was obtained when an equimolar ratio of CPK4:CPE4 was used (**Fig. 2c**). In summary, the 1-step incubation protocol is a viable delivery approach, and the 1:1 ratio of CPK4:CPE4 is the most optimal ratio to achieve maximal transfection efficiency enhancement.



**Figure 3. Transfection efficiency using fusogenic coiled-coil modified LNPs is independent of lipid composition.** (a-b) The GFP expression fluorescence intensity (GFP MFI) of LNPs after encapsulating EGFP-mRNA (1  $\mu\text{g}/\text{mL}$ , 24 h) within HeLa and Jurkat cells using ALC0315 from Pfizer/BioNTech Covid-19 LNP-mRNA formulation following the 1-step incubation protocol and incubating for 24 h. (c-d) The GFP expression fluorescence intensity (GFP MFI) of LNPs after encapsulating EGFP-mRNA (1  $\mu\text{g}/\text{mL}$ , 24 h) within HeLa and Jurkat cells using SM102 from Moderna Covid-19 LNP-mRNA formulation following the 1-step incubation protocol and incubating for 24 h. Unpaired student t-test was used to determine the significance of data comparisons (\*\*\*\*,  $P < 0.0001$ , \*\*\*,  $P < 0.001$ , \*\*,  $P < 0.01$ , \*,  $P < 0.05$ , ns, no significant difference). In all panels, error bars represent mean  $\pm$  s.d. (n=3).

### Transfection performance with other ionizable lipids

LNP formulations contain ionizable lipids that condense the genetic cargo and once inside the cell will influence the endosomal escape affecting the transfection performance.<sup>39, 40</sup> Coiled-coil peptide modified LNPs using MC3 as the ionizable lipid showed enhanced mRNA transfection. Now we wondered whether this enhancement of transfection efficiency could be achieved using other ionizable lipids (*i.e.* ALC0315 and SM102 from two Covid-19 LNP-mRNA vaccine formulations).<sup>26, 28</sup> Improved GFP expression was again observed with the introduction of coiled-coil peptides to these LNP formulations when using the 1-step incubation protocol (**Fig. 3a-d**). Thus enhanced mRNA transfection was not only observed in the Onpattro LNP formulation but also in other clinically approved LNPs when using the fusogenic coiled-coil peptides.

**a****b**

**Figure 4. Transfection efficiency of the fusogenic coiled-coil modified LNPs using MC3 in iPSC-CMs *in vitro*.**

(a) The GFP expression fluorescence intensity (GFP MFI) of LNPs with iPSC-CMs was monitored by flow cytometry. (b) The GFP expression intensity normalized to MC3 (2-step incubation, 2 h). 2-step 2h: iPSC-CMs were pretreated with CPK4 (10  $\mu$ M, 100  $\mu$ L, 2 h), followed by incubation of MC3-CPE4 (2  $\mu$ g/mL, 100  $\mu$ L) for 2

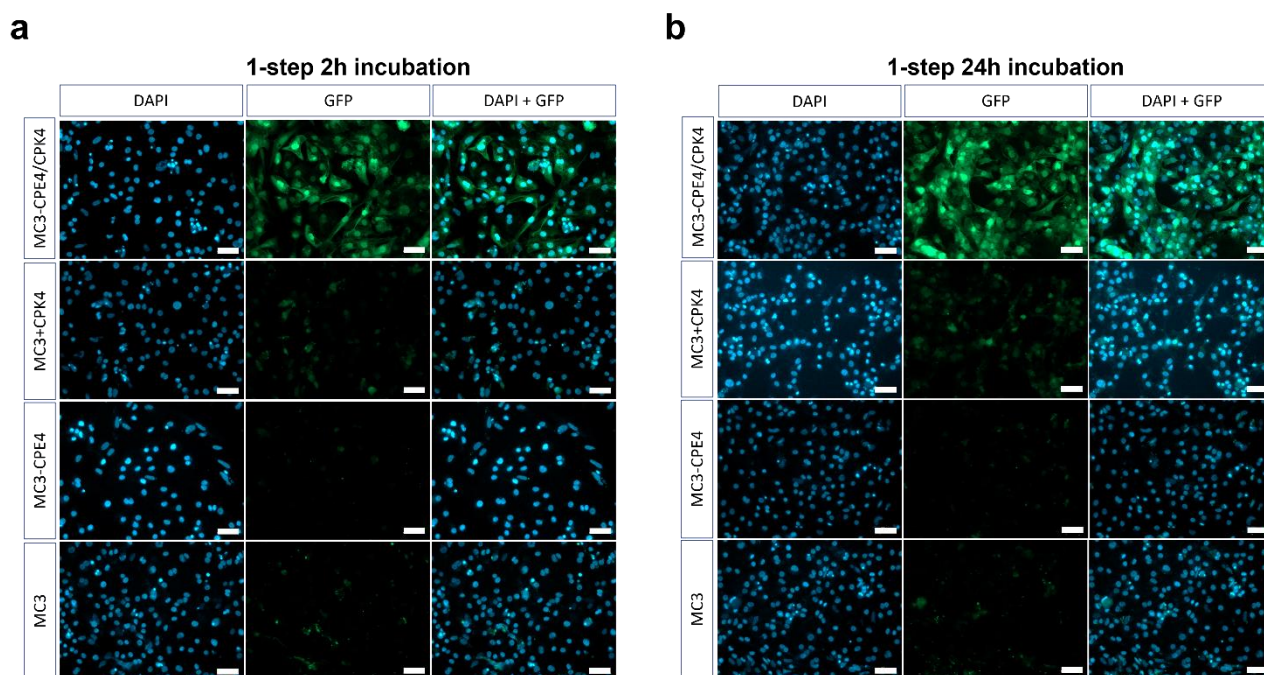
h, the supernatant was removed and cells were cultured for another 24 h before flow cytometry measurements. 1-step 2h incubation: a medium containing CPK4 and MC3-CPE4 (2  $\mu\text{g}/\text{mL}$ , 100  $\mu\text{L}$ , the final ratio of CPK4:CPE4=1:1) was added to the iPSC-CMs and incubated for 2 h, then the medium was removed and cells were cultured for another 24 h before flow cytometry measurements. For the 2-step 24h and 1-step 24h groups: iPSC-CMs were incubated with LNPs for 24 h before measuring, all other steps in the protocol remained the same. All LNPs were formulated using ionizable lipids MC3 and encapsulated with EGFP-mRNA. Unpaired student t-test was used to determine the significance of data comparisons (\*\*\*\*,  $P < 0.0001$ , \*\*\*,  $P < 0.001$ , \*\*,  $P < 0.01$ , \*,  $P < 0.05$ , ns, no significant difference). In all panels, error bars represent s.d. (n=3).

### Transfection efficiency in iPSC-CMs

Human-induced pluripotent stem cell-derived cardiomyocytes (iPSC-CMs) can produce relevant proteins found in adult human CMs, spontaneously contract, proliferate limitlessly, and differentiate into several cell types, therefore, they are often used for customized genome editing, cardiovascular disease modeling, and high-throughput drug screening.<sup>41, 42</sup> Here, we applied coiled-coil peptide modified MC3-LNPs to evaluate the *in vitro* transfection performance in iPSC-CMs and compared the transfection efficiency of different incubation protocols (2-step incubation vs 1-step incubation) and time (2 vs 24h). As expected, the introduction of fusogenic coiled-coil peptides to the LNPs induced highly efficient GFP transfection of iPSC-CMs for both incubation times. These transfection efficiencies were superior to unmodified LNPs and to the commercial transfection reagent Lipofectamine 3K (**Fig. 4a**). In line with previous experiments, the 1-step incubation protocol achieved better transfection performance than the 2-step incubation protocol, and increasing the incubation time from 2 to 24 h enhanced GFP expression.

Fusogenic coiled-coil peptides did significantly increase the transfection of iPSC-CMs; with up to a 19-fold increase when using the 1-step incubation protocol for 24 h (**Fig. 4b**), which is a significant transfection enhancement as compared to state-of-the-art LNPs.

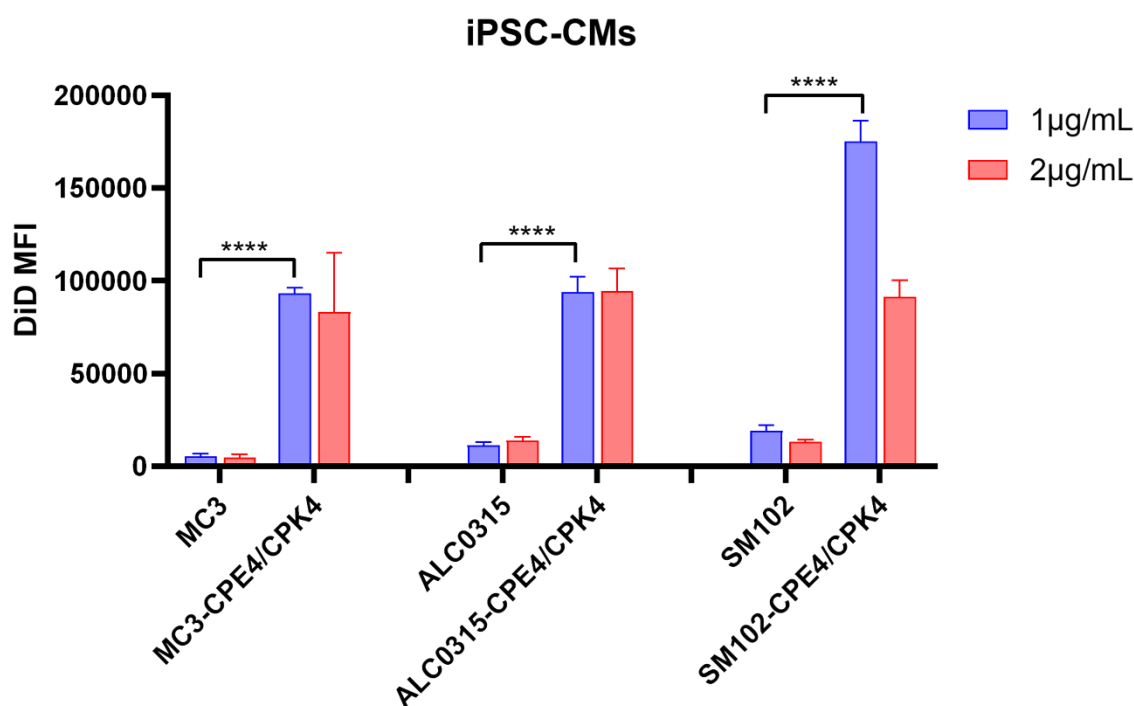
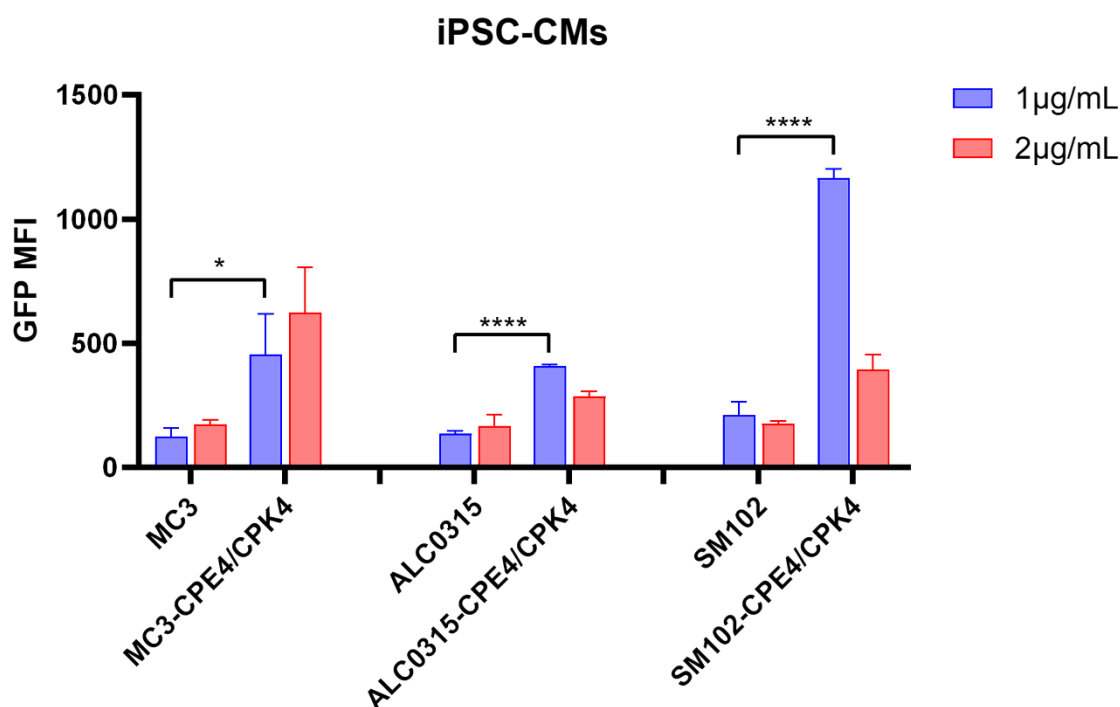
Confocal microscopy imaging was applied to visualize GFP expression in iPSC-CMs following the 1-step incubation protocol. Intense GFP fluorescence was uniform in the majority of iPSC-CMs when fusogenic coiled-coil peptide modified LNPs were used to deliver mRNA, independent of incubation time. In contrast, weak GFP fluorescence was observed when unmodified LNPs were used to transfect the cells with mRNA (**Fig. 5a-b**). In summary, the use of fusogenic coiled-coil peptides to modify LNPs greatly enhanced the transfection of iPSC-CMs *in vitro*, holding great promise for cardiomyocyte transfection *in vivo*.



**Figure 5. (a-b) Confocal images of the EGFP-mRNA transfection of LNPs following the 1-step incubation protocol.** 1-step 2h incubation: a medium containing CPK4 and MC3-CPE4 (2  $\mu\text{g}/\text{mL}$ , 500  $\mu\text{L}$ , the final ratio of CPK4:CPE4=1:1) was added to the iPSC-CMs and incubated for 2 h, then the medium was removed and cells were cultured for another 24 h before imaging. 1-step 24h incubation: a medium containing CPK4 and MC3-CPE4 (2  $\mu\text{g}/\text{mL}$ , 500  $\mu\text{L}$ , the final ratio of CPK4:CPE4=1:1) was added to the iPSC-CMs and incubated for 24 h before imaging. All LNPs were formulated using MC3 ionizable lipids and encapsulated with EGFP-mRNA. Blue: DAPI; green: GFP, green fluorescent protein; scale bar is 50  $\mu\text{m}$ .

### Transfection efficiency evaluation on iPSC-CMs of LNPs using other ionizable lipids

The transfection performance of coiled-coil peptide modified LNPs in iPSC-CMs using ALC0315 and SM102 lipids was also evaluated using the 1-step incubation protocol. Flow cytometry analysis showed that all coiled-coil peptide modified LNPs greatly facilitated the cellular uptake of LNPs composing the ionizable lipids MC3, ALC0315, and SM102 (**Fig. 6a**). Consistent with the cellular uptake efficiency, the introduction of fusogenic coiled-coil peptides to LNPs produced significantly improved GFP expression compared to three naked LNPs (**Fig. 6b**). This further proved that enhanced mRNA transfection performance in iPSC-CMs could be achieved by various LNP formulations after the introduction of fusogenic coiled-coil peptides.

**a****b**

**Figure 6. Transfection efficiency in iPSC-CMs of the coiled-coil modified LNPs using other ionizable lipids.** (a) The cellular uptake efficiency of LNPs in iPSC-CMs using the 1-step incubation protocol and incubating for 24 h was measured by quantifying DiD fluorescence. 0.5 mol% of DiD was added to the lipids as a. (b) The GFP expression fluorescence intensity (GFP MFI) of LNPs with iPSC-CMs was measured by flow cytometry using the 1-step incubation protocol and incubating for 24 h. MC3 was used in the Onpattro LNP-siRNA formulation;

ALC0315 was used in the Pfizer/BioNTech Covid-19 LNP-mRNA vaccine formulation; SM102 was used in the Moderna Covid-19 LNP-mRNA vaccine formulation. All LNPs were encapsulated with EGFP-mRNA. Statistical significance was calculated by an unpaired student t-test on the 1  $\mu$ g/mL data. (\*\*\*\*,  $P < 0.0001$ , \*\*\*,  $P < 0.001$ , \*\*,  $P < 0.01$ , \*,  $P < 0.05$ , ns, no significant difference) In all panels, error bars represent mean  $\pm$  s.d. (n=3).

## Conclusions

Enhanced mRNA delivery into hard to transfect iPSC-CMs can be obtained by the introduction of fusogenic coiled coil peptides into state-of-the-art LNP formulations. In this study MC3-LNPs were modified with 1 mol% CPE4 lipopeptide, and cells were pretreated with the complementary lipopeptide CPK4. mRNA delivery was optimized by premixing CPK4 and MC3-CPE4 before adding this mixture to cells and this 1-step incubation protocol is compatible with future *in vivo* applications. Modification of LNPs with these lipopeptides did not change the physicochemical properties of these mRNA-containing nanoparticles. We also evaluated two Covid-19 LNP-mRNA vaccine formulations, which also showed enhanced transfection using the 1-step incubation protocol. The *in vitro* mRNA delivery in iPSC-CMs proved that the introduction of coiled-coil peptides into different LNP formulations greatly boosted mRNA transfection efficiency compared to LNPs without modification, resulting in higher GFP expression when encapsulating EGFP-mRNA. In summary, the introduction of fusogenic coiled-coil peptides to LNPs could potentially lead to the enhanced mRNA delivery in future *in vivo* cardiomyocyte research, which holds great promise for the development of a myocardium regenerative therapy after injury to prevent or treat heart failure by carrying a functional mRNA.

## Methods

### Chemicals and materials

Lipopeptides CPE4 and CPK4 were synthesized as described in Chapter 2 (SI Fig. 1a). 1,2-distearoyl-*sn*-glycero-3-phosphocholine (DSPC), 1,2-dimyristoyl-*rac*-glycero-3-methoxypolyethylene glycol-2000 (DMG-PEG2K) were purchased from Avanti Polar Lipids, DLin-MC3-DMA was purchased from Biorbyt company (Cambridge, England), cholesterol was purchased from Sigma-Aldrich. Triton™ X-100 was purchased from Acros Organics. 100k MWCO centrifugal filters (Amicon® Ultra, Merck) were purchased from Sigma. 1,1-dioctadecyl-3,3,3,3-tetramethylindodicarbocyanine (DiD), QuantiT™ RiboGreen® RNA Assay Kit was purchased from Life Technologies. Clean cap EGFP-mRNA was purchased from Trilink biotechnology. The ionizable lipids ALC0315 and SM102 were synthesized according to the literature (SI Fig. 1a).<sup>39, 43</sup>

HeLa and Jurkat cell lines purchased from ATCC were cultured according to ATCC guidelines. The DMEM and RPMI-1640 growth medium (Sigma Aldrich) containing sodium bicarbonate, without sodium pyruvate and HEPES, was supplemented with 10% fetal bovine serum (Sigma), 1% L-glutamine (Thermo Fisher Scientific) and 1% penicillin/streptomycin (Thermo Fisher Scientific), at 37 °C in the presence of 5% CO<sub>2</sub>. HeLa was cultured with DMEM medium, Jurkat was cultured with RPMI-1640 medium. iPSC-CMs were cultured with RPMI/B27 medium (Thermo Fisher Scientific). Maturation media of iPSC-CMs was composed of DMEM without glucose (Thermo Fisher Scientific) supplemented with 3 mM glucose (Sigma Aldrich), 10 mM L-lactate (Sigma Aldrich), 5 mg/ml Vitamin B12 (Sigma Aldrich), 0.82 mM Biotin (Sigma Aldrich), 5 mM Creatine monohydrate (Sigma Aldrich), 2 mM Taurine (Sigma Aldrich), 2mM L-carnitine (Sigma Aldrich), 0.5 mM Ascorbic acid (Sigma Aldrich), 1x NEAA (Thermo Fisher Scientific), 0.5 % (w/v) Albumax (Thermo Fisher Scientific), 1x B27 and 1% KOSR (Thermo Fisher Scientific).

### Lipid nanoparticle formulation and characterization

Stock solutions of lipids and lipopeptides in chloroform:methanol (1:1, v/v) were mixed in a vial at the desired molar ratios, the solvents were evaporated under a nitrogen flow and residual solvent was removed *in vacuo* for at least 30 minutes. The lipid film was dissolved in absolute ethanol and used for the assembly ([total lipid] = 1 μmol, N/P=16). EGFP-mRNA was diluted in 50 mM RNase free citrate buffer (pH = 4). The solutions were loaded into two separate syringes and connected to a T-junction microfluidic mixer. The solutions were mixed in a 3:1 flow ratio of nucleic acid against lipids (1.5 mL/min for mRNA solution, 0.5 mL/min for lipids solution). After mixing, the solution was directly loaded into a 20 kDa MWCO dialysis cassette (Slide-A-Lyzer™, Thermo Scientific) and dialyzed against 1X PBS overnight. mRNA encapsulation efficiency and mRNA concentrations were determined by a Quanti-iT™ RiboGreen™ RNA Assay Kit.

All LNPs encapsulating EGFP-mRNA for transfection evaluation in HeLa, Jurkat, and iPSC-CMs cells were made in the same way. 0.5 mol% DiD was added to the lipids to prepare DiD-labeled LNPs for the quantification of LNP uptake on iPSC-CMs.

The hydrodynamic diameter, polydispersities, and zeta potentials of LNPs were measured using a Malvern zetasizer Nano ZS (DLS, Malvern).

MC3-CPE4 were concentrated using 100 kDa MWCO centrifugal filters, centrifuged at 4°C, 5000 RCF for 1-2 h. Adjustment and dilution of LNPs were done with 1X PBS. The hydrodynamic diameter changes over time after premixing CPK4 and MC3-CPE4 were monitored by the DLS measurements with the ratio of CPK4:CPE4=1:1. The serum stability was tested by measuring the hydrodynamic diameter changes of the mixture of CPK4 and MC3-CPE4 (CPK4:CPE4=1:1) after adding 10% FCS.

The morphology of LNPs was analyzed by cryogenic transmission electron microscopy (cryo-EM). Vitrification of concentrated (~10 mM) LNPs was performed using a Leica EM GP operating at 21 °C and 95% room humidity (RH). Sample suspensions were placed on glow discharged 100 µm lacey carbon films supported by 200 mesh copper grids (Electron Microscopy Sciences). Optimal results were achieved using a 60-second pre-blot and a 1-second blot time. After vitrification, sample grids were maintained below -170 °C, and imaging was performed on a Tecnai T12 (ThermoFisher) with a biotwin lens and LaB6 filament operating at 120 keV equipped with an Eagle 4K×4K CCD camera (ThermoFisher). Images were acquired at a nominal underfocus of -2 to -3 µm (49,000× magnification) with an electron dose of ~2000 e/nm<sup>2</sup>. For cryo-EM imaging, CPK4 was added to the MC3-CPE4 with the ratio of CPK4:CPE4=1:1, then incubated for 1 h before imaging.

For the coiled-coil peptide CPK4 binding assay, fluorescein-labeled K4 peptide was added to the MC3-CPE4 (final ratio of CPK4:CPE4=1:1) and incubated at RT for 1-2 h, followed by centrifugation (Amicon Ultra-0.5 Centrifugal Filter Unit, 5000 RCF, 30 min). The solution in the lower tube was collected and fluorescence intensity was quantified by Tecan plate reader (excitation wavelength: 480 nm; emission wavelength: 520 nm). The fluorescence intensity was normalized to free fluorescein-K4.

### **Transfection of HeLa cells**

HeLa cells were seeded in an 8-well confocal plate at a density of 5\*10<sup>4</sup> cells/well. 2-step incubation protocol: HeLa cells were pretreated with CPK4 (10 µM, 200 µL) for 2 h, then the medium was removed and MC3-CPE4 (1 µg/mL, 200 µL) was added and incubated for 24 h before imaging. 1-step incubation protocol: a medium containing CPK4 and MC3-CPE4 (EGFP-mRNA=1 µg/mL, CPE4=2.5 µM, CPK4=2.5 µM, 200µL, the final ratio of CPK4:CPE4=1:1) was added to the cells and incubated for 24 h before imaging. Flow cytometry measurements of the two incubation protocols were carried out with cells seeded in 96-well plates at a density of 1\*10<sup>4</sup> cells/well, then the same incubation protocols were followed. The mean fluorescence intensity of GFP expression for the 1-step incubation was normalized to the 2-step incubation.

To determine the optimal CPK4:CPE4 ratio for mRNA transfection, HeLa cells were seeded in a 96-well plate at a density of 1\*10<sup>4</sup> cells/well. The concentration of EGFP-mRNA added to cells was 1 µg/mL. CPK4 and MC3-CPE4 with different final ratios of CPK4:CPE4 (CPK4:CPE4=8:1, 4:1, 3:1, 2:1, 1:1, 0.5:1, 0.2:1, 0.1:1) were added together to cells and incubated for 24 h before analysis by flow cytometry.

For the transfection evaluation of LNP formulations composing other ionizable lipids ALC0315 and SM102 using the 1-step incubation protocol, HeLa and Jurkat cells were seeded in a 96-well plate with a density of 1\*10<sup>4</sup> cells/well, then ALC0315, SM102 (EGFP-mRNA=1 µg/mL, 100 µL),

ALC0315-CPE4/CPK4, and SM102-CPE4/CPK4 (EGFP-mRNA=1 µg/mL, 100 µL, CPK4:CPE4=1:1) were added to the cells and incubated for 24 h before flow cytometry measurements.

### Transfection evaluation of iPSC-CMs

iPSC-CMs were seeded at the density of  $1 \times 10^5$  cells/well in a 96-well plate for flow cytometry measurements. 2-step incubation 2h protocol: iPSC-CMs cells were pretreated with CPK4 (10 µM, 100 µL) for 2 h, then the medium was removed and MC3-CPE4 (2 µg/mL, 100 µL) was incubated for 2 h, the supernatant was removed and cells were cultured for another 24 h before flow cytometry measurements. 1-step incubation 2h protocol: a medium containing CPK4 and LNPs (2 µg/mL, 100 µL, the final ratio of CPK4:CPE4=1:1) was added to the iPSC-CMs and incubated for 2 h, then the medium was removed and cells were cultured for another 24 h before FACs measurements. 2-step incubation-24h and 1-step incubation-24h: The same incubation protocols were followed but iPSC-CMs were incubated with LNPs for 24 h before measuring. All LNPs were formulated using ionizable lipids MC3 and encapsulated with EGFP-mRNA.

For confocal imaging, iPSC-CMs were seeded at the density of  $5 \times 10^5$  cells/well in a 24-well confocal plate. 1-step 2h incubation group: a medium containing CPK4 and MC3-CPE4 (2 µg/mL, 500 µL, the final ratio of CPK4:CPE4=1:1) was added to the iPSC-CMs cells, incubated for 2 h, then the supernatant was removed and refreshed with new medium and cells were cultured for another 24 h before imaging. LNPs were incubated with iPSC-CMs for 24 h in the group of 1-step 24h incubation.

The transfection of iPSC-CMs of LNP formulations composing other ionizable lipids ALC0315 and SM102 was carried out by following the 1-step incubation protocol. Cellular uptake efficiency was measured by quantifying the DiD fluorescence of LNPs (0.5 mol% DiD was added to the lipids) by flow cytometry measurements. The fluorescence intensity of GFP expression was measured to compare the transfection efficiency.

### Statistical analysis

All experiments were performed at least in triplicate (n=3) unless specified otherwise, and the significance was determined using an unpaired student t-test (Graphpad Prism) for all comparisons. \*\*\*\*,  $P < 0.0001$ , \*\*\*,  $P < 0.001$ , \*\*,  $P < 0.01$ , \*,  $P < 0.05$ , ns, no significant difference.

### References

1. Bui, A. L.; Horwich, T. B.; Fonarow, G. C., Epidemiology and risk profile of heart failure. *Nature Reviews Cardiology* **2011**, *8* (1), 30-41.
2. Zoni-Berisso, M.; Lercari, F.; Carazza, T.; Domenicucci, S., Epidemiology of atrial fibrillation: European perspective. *Clinical epidemiology* **2014**, *6*, 213.
3. Groenewegen, A.; Rutten, F. H.; Mosterd, A.; Hoes, A. W., Epidemiology of heart failure. *European Journal of Heart Failure* **2020**, *22* (8), 1342-1356.
4. Senyo, S. E.; Steinhauser, M. L.; Pizzimenti, C. L.; Yang, V. K.; Cai, L.; Wang, M.; Wu, T.-D.; Guerin-Kern, J.-L.; Lechene, C. P.; Lee, R. T., Mammalian heart renewal by pre-existing cardiomyocytes. *Nature* **2013**, *493* (7432), 433-436.
5. Whelan, R. S.; Kaplinskiy, V.; Kitsis, R. N., Cell Death in the Pathogenesis of Heart Disease: Mechanisms

and Significance. *Annual Review of Physiology* **2010**, 72 (1), 19-44.

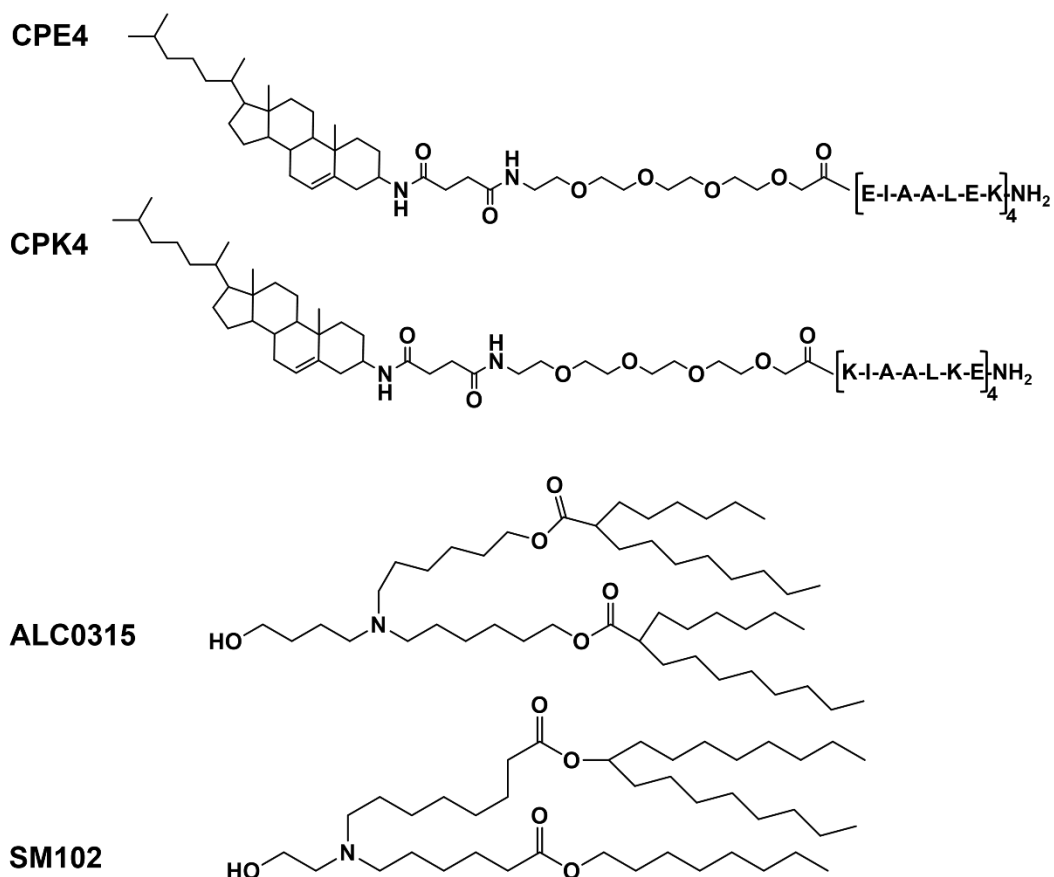
6. Yang, Q.; Fang, J.; Lei, Z.; Sluijter, J. P. G.; Schiffelers, R., Repairing the heart: State-of the art delivery strategies for biological therapeutics. *Advanced Drug Delivery Reviews* **2020**, 160, 1-18.
7. Laflamme, M. A.; Murry, C. E., Heart regeneration. *Nature* **2011**, 473 (7347), 326-335.
8. Smith, A. S. T.; Macadangdang, J.; Leung, W.; Laflamme, M. A.; Kim, D.-H., Human iPSC-derived cardiomyocytes and tissue engineering strategies for disease modeling and drug screening. *Biotechnology Advances* **2017**, 35 (1), 77-94.
9. Shiba, Y.; Gomibuchi, T.; Seto, T.; Wada, Y.; Ichimura, H.; Tanaka, Y.; Ogasawara, T.; Okada, K.; Shiba, N.; Sakamoto, K.; Ido, D.; Shiina, T.; Ohkura, M.; Nakai, J.; Uno, N.; Kazuki, Y.; Oshimura, M.; Minami, I.; Ikeda, U., Allogeneic transplantation of iPSC cell-derived cardiomyocytes regenerates primate hearts. *Nature* **2016**, 538 (7625), 388-391.
10. Lalit, P. A.; Hei, D. J.; Raval, A. N.; Kamp, T. J., Induced Pluripotent Stem Cells for Post-Myocardial Infarction Repair. *Circulation Research* **2014**, 114 (8), 1328-1345.
11. Lian, X.; Hsiao, C.; Wilson, G.; Zhu, K.; Hazeltine, L. B.; Azarin, S. M.; Raval, K. K.; Zhang, J.; Kamp, T. J.; Palecek, S. P., Robust cardiomyocyte differentiation from human pluripotent stem cells via temporal modulation of canonical Wnt signaling. *Proceedings of the National Academy of Sciences* **2012**, 109 (27), E1848-E1857.
12. Paige, Sharon L.; Thomas, S.; Stoick-Cooper, Cristi L.; Wang, H.; Maves, L.; Sandstrom, R.; Pabon, L.; Reinecke, H.; Pratt, G.; Keller, G.; Moon, Randall T.; Stamatoyannopoulos, J.; Murry, Charles E., A Temporal Chromatin Signature in Human Embryonic Stem Cells Identifies Regulators of Cardiac Development. *Cell* **2012**, 151 (1), 221-232.
13. Park, H.; Larson, B. L.; Kolewe, M. E.; Vunjak-Novakovic, G.; Freed, L. E., Biomimetic scaffold combined with electrical stimulation and growth factor promotes tissue engineered cardiac development. *Experimental Cell Research* **2014**, 321 (2), 297-306.
14. Lin, Z.; von Gise, A.; Zhou, P.; Gu, F.; Ma, Q.; Jiang, J.; Yau, A. L.; Buck, J. N.; Gouin, K. A.; van Gorp, P. R. R.; Zhou, B.; Chen, J.; Seidman, J. G.; Wang, D.-Z.; Pu, W. T., Cardiac-Specific YAP Activation Improves Cardiac Function and Survival in an Experimental Murine MI Model. *Circulation Research* **2014**, 115 (3), 354-363.
15. Tao, Z.; Chen, B.; Tan, X.; Zhao, Y.; Wang, L.; Zhu, T.; Cao, K.; Yang, Z.; Kan, Y. W.; Su, H., Coexpression of VEGF and angiopoietin-1 promotes angiogenesis and cardiomyocyte proliferation reduces apoptosis in porcine myocardial infarction (MI) heart. *Proceedings of the National Academy of Sciences* **2011**, 108 (5), 2064-2069.
16. Zangi, L.; Lui, K. O.; von Gise, A.; Ma, Q.; Ebina, W.; Ptaszek, L. M.; Später, D.; Xu, H.; Tabebordbar, M.; Gorbатов, R.; Sena, B.; Nahrendorf, M.; Briscoe, D. M.; Li, R. A.; Wagers, A. J.; Rossi, D. J.; Pu, W. T.; Chien, K. R., Modified mRNA directs the fate of heart progenitor cells and induces vascular regeneration after myocardial infarction. *Nature Biotechnology* **2013**, 31 (10), 898-907.
17. Gabisonia, K.; Prosdocimo, G.; Aquaro, G. D.; Carlucci, L.; Zentilin, L.; Secco, I.; Ali, H.; Braga, L.; Gorgodze, N.; Bernini, F.; Burchielli, S.; Collesi, C.; Zandona, L.; Sinagra, G.; Piacenti, M.; Zacchigna, S.; Bussani, R.; Recchia, F. A.; Giacca, M., MicroRNA therapy stimulates uncontrolled cardiac repair after myocardial infarction in pigs. *Nature* **2019**, 569 (7756), 418-422.
18. Su, H.; Joho, S.; Huang, Y.; Barcena, A.; Arakawa-Hoyt, J.; Grossman, W.; Kan, Y. W., Adeno-associated viral vector delivers cardiac-specific and hypoxia-inducible VEGF expression in ischemic mouse hearts. *Proceedings of the National Academy of Sciences* **2004**, 101 (46), 16280-16285.
19. Engel, F. B.; Hsieh, P. C.; Lee, R. T.; Keating, M. T., FGF1/p38 MAP kinase inhibitor therapy induces cardiomyocyte mitosis, reduces scarring, and rescues function after myocardial infarction. *Proceedings of the*

*National Academy of Sciences* **2006**, *103* (42), 15546-15551.

20. Sultana, N.; Magadum, A.; Hadas, Y.; Kondrat, J.; Singh, N.; Youssef, E.; Calderon, D.; Chepurko, E.; Dubois, N.; Hajjar, R. J.; Zangi, L., Optimizing Cardiac Delivery of Modified mRNA. *Molecular Therapy* **2017**, *25* (6), 1306-1315.
21. Kaur, K.; Zangi, L., Modified mRNA as a Therapeutic Tool for the Heart. *Cardiovascular Drugs and Therapy* **2020**, *34* (6), 871-880.
22. Hadas, Y.; Katz, M. G.; Bridges, C. R.; Zangi, L., Modified mRNA as a therapeutic tool to induce cardiac regeneration in ischemic heart disease. *WIREs Systems Biology and Medicine* **2017**, *9* (1), e1367.
23. Delivering the promise of RNA therapeutics. *Nature Medicine* **2019**, *25* (9), 1321-1321.
24. Yin, H.; Kanasty, R. L.; Eltoukhy, A. A.; Vegas, A. J.; Dorkin, J. R.; Anderson, D. G., Non-viral vectors for gene-based therapy. *Nature Reviews Genetics* **2014**, *15* (8), 541-555.
25. Kulkarni, J. A.; Witzigmann, D.; Thomson, S. B.; Chen, S.; Leavitt, B. R.; Cullis, P. R.; van der Meel, R., The current landscape of nucleic acid therapeutics. *Nature Nanotechnology* **2021**, *16* (6), 630-643.
26. Verbeke, R.; Lentacker, I.; De Smedt, S. C.; Dewitte, H., The dawn of mRNA vaccines: The COVID-19 case. *Journal of Controlled Release* **2021**, *333*, 511-520.
27. Polack, F. P.; Thomas, S. J.; Kitchin, N.; Absalon, J.; Gurtman, A.; Lockhart, S.; Perez, J. L.; Pérez Marc, G.; Moreira, E. D.; Zerbini, C.; Bailey, R.; Swanson, K. A.; Roychoudhury, S.; Koury, K.; Li, P.; Kalina, W. V.; Cooper, D.; Frenck, R. W.; Hammitt, L. L.; Türeci, Ö.; Nell, H.; Schaefer, A.; Ünal, S.; Tresnan, D. B.; Mather, S.; Dormitzer, P. R.; Şahin, U.; Jansen, K. U.; Gruber, W. C., Safety and Efficacy of the BNT162b2 mRNA Covid-19 Vaccine. *New England Journal of Medicine* **2020**, *383* (27), 2603-2615.
28. Shin, M. D.; Shukla, S.; Chung, Y. H.; Beiss, V.; Chan, S. K.; Ortega-Rivera, O. A.; Wirth, D. M.; Chen, A.; Sack, M.; Pokorski, J. K.; Steinmetz, N. F., COVID-19 vaccine development and a potential nanomaterial path forward. *Nature Nanotechnology* **2020**, *15* (8), 646-655.
29. Pilkington, E. H.; Suys, E. J. A.; Trevaskis, N. L.; Wheatley, A. K.; Zukancic, D.; Algarni, A.; Al-Wassiti, H.; Davis, T. P.; Pouton, C. W.; Kent, S. J.; Truong, N. P., From influenza to COVID-19: Lipid nanoparticle mRNA vaccines at the frontiers of infectious diseases. *Acta Biomaterialia* **2021**, *131*, 16-40.
30. Liu, S.; Cheng, Q.; Wei, T.; Yu, X.; Johnson, L. T.; Farbiak, L.; Siegwart, D. J., Membrane-destabilizing ionizable phospholipids for organ-selective mRNA delivery and CRISPR–Cas gene editing. *Nature Materials* **2021**, *20* (5), 701-710.
31. Gilleron, J.; Querbes, W.; Zeigerer, A.; Borodovsky, A.; Marsico, G.; Schubert, U.; Manygoats, K.; Seifert, S.; Andree, C.; Stöter, M.; Epstein-Barash, H.; Zhang, L.; Kotliansky, V.; Fitzgerald, K.; Fava, E.; Bickle, M.; Kalaidzidis, Y.; Akinc, A.; Maier, M.; Zerial, M., Image-based analysis of lipid nanoparticle-mediated siRNA delivery, intracellular trafficking and endosomal escape. *Nature Biotechnology* **2013**, *31* (7), 638-646.
32. Sahay, G.; Querbes, W.; Alabi, C.; Eltoukhy, A.; Sarkar, S.; Zurenko, C.; Karagiannis, E.; Love, K.; Chen, D.; Zoncu, R.; Buganim, Y.; Schroeder, A.; Langer, R.; Anderson, D. G., Efficiency of siRNA delivery by lipid nanoparticles is limited by endocytic recycling. *Nature Biotechnology* **2013**, *31* (7), 653-658.
33. Jahn, R.; Scheller, R. H., SNAREs — engines for membrane fusion. *Nature Reviews Molecular Cell Biology* **2006**, *7* (9), 631-643.
34. Chen, Y. A.; Scheller, R. H., SNARE-mediated membrane fusion. *Nature Reviews Molecular Cell Biology* **2001**, *2* (2), 98-106.
35. Akinc, A.; Maier, M. A.; Manoharan, M.; Fitzgerald, K.; Jayaraman, M.; Barros, S.; Ansell, S.; Du, X.; Hope, M. J.; Madden, T. D.; Mui, B. L.; Semple, S. C.; Tam, Y. K.; Ciufolini, M.; Witzigmann, D.; Kulkarni, J. A.; van der Meel, R.; Cullis, P. R., The Onpattro story and the clinical translation of nanomedicines containing nucleic acid-based drugs. *Nature Nanotechnology* **2019**, *14* (12), 1084-1087.

36. Kulkarni, J. A.; Witzigmann, D.; Leung, J.; van der Meel, R.; Zaifman, J.; Darjuan, M. M.; Grisch-Chan, H. M.; Thöny, B.; Tam, Y. Y. C.; Cullis, P. R., Fusion-dependent formation of lipid nanoparticles containing macromolecular payloads. *Nanoscale* **2019**, *11* (18), 9023-9031.
37. Eygeris, Y.; Patel, S.; Jozic, A.; Sahay, G., Deconvoluting Lipid Nanoparticle Structure for Messenger RNA Delivery. *Nano Letters* **2020**, *20* (6), 4543-4549.
38. Patel, S.; Ashwanikumar, N.; Robinson, E.; Xia, Y.; Mihai, C.; Griffith, J. P.; Hou, S.; Esposito, A. A.; Ketova, T.; Welscher, K.; Joyal, J. L.; Almarsson, Ö.; Sahay, G., Naturally-occurring cholesterol analogues in lipid nanoparticles induce polymorphic shape and enhance intracellular delivery of mRNA. *Nature Communications* **2020**, *11* (1), 983.
39. Hou, X.; Zaks, T.; Langer, R.; Dong, Y., Lipid nanoparticles for mRNA delivery. *Nature Reviews Materials* **2021**, *6* (12), 1078-1094.
40. Kanasty, R.; Dorkin, J. R.; Vegas, A.; Anderson, D., Delivery materials for siRNA therapeutics. *Nature Materials* **2013**, *12* (11), 967-977.
41. Huang, Y.; Wang, T.; López, M. E. U.; Hirano, M.; Hasan, A.; Shin, S. R., Recent advancements of human iPSC derived cardiomyocytes in drug screening and tissue regeneration. *Microphysiol. Syst.* **2020**, *4*.
42. Wagner, J. U. G.; Pham, M. D.; Nicin, L.; Hammer, M.; Bottermann, K.; Yuan, T.; Sharma, R.; John, D.; Muhly-Reinholz, M.; Tombor, L.; Hardt, M.; Madl, J.; Dimmeler, S.; Krishnan, J., Dissection of heterocellular cross-talk in vascularized cardiac tissue mimetics. *Journal of Molecular and Cellular Cardiology* **2020**, *138*, 269-282.
43. Hassett, K. J.; Benenato, K. E.; Jacquinet, E.; Lee, A.; Woods, A.; Yuzhakov, O.; Himansu, S.; Deterling, J.; Geilich, B. M.; Ketova, T.; Mihai, C.; Lynn, A.; McFadyen, I.; Moore, M. J.; Senn, J. J.; Stanton, M. G.; Almarsson, Ö.; Ciaramella, G.; Brito, L. A., Optimization of Lipid Nanoparticles for Intramuscular Administration of mRNA Vaccines. *Molecular Therapy - Nucleic Acids* **2019**, *15*, 1-11.

## **Supporting information**

**a****b**

Lipid compositions of LNPs (mol%).				
	ALC0315-CPE4	ALC0315	SM102-CPE4	SM102
ALC0315	50	50	/	/
SM102	/	/	50	50
Cholesterol	37.5	38.5	37.5	38.5
DSPC	10	10	10	10
DMG-PEG2K	1.5	1.5	1.5	1.5
CPE4	1	/	1	/

**c**

Characterization of LNP formulations.				
LNPs	Hydrodynamic diameter (nm)	PDI	Zeta potential (mV)	EE (%)
ALC0315-CPE4	98.5±2.3	0.154±0.05	-7.29±0.88	81.15±5.35
ALC0315	86.6±3.8	0.132±0.024	-4.01±0.66	90.20±2.71
SM102-CPE4	116.2±1.4	0.134±0.05	-8.13±0.68	82.48±3.47
SM102	95.55±2.7	0.172±0.024	-5.36±0.61	89.54±2.35

**SI Figure 1 (a)** Structures of CPE4, CPK4, and lipids ACL0315 and SM107 used for the preparation of LNPs. **(b)** Lipids compositions of LNPs. **(c)** Characterization of LNPs.

## **Chapter 5**

### **Lipid nanoparticle-based mRNA candidates elicit potent T cell immune responses**

## Abstract

The induction of a potent T cell response is essential for successful tumor immunotherapy and protection against many infectious diseases. In the past few years, mRNA vaccines have emerged as potent immune activators and inducers of a robust T cell immune response. The recent approval of the Moderna and the Pfizer/BioNTech vaccines based on lipid nanoparticles (LNP) encapsulating antigen-encoding mRNA has revolutionized the field of vaccines. The advantages of LNPs are their ease of design and formulation resulting in potent, effective, and safe vaccines. However, there is still plenty of room for improvement with respect to LNP efficacy, for instance, by optimizing the lipid composition and tuning LNP for specific purposes. mRNA delivery is known to be strongly dependent on the lipid composition of LNPs and the efficiency is mainly determined by the ionizable lipids. Besides that, cholesterol and helper lipids also play important roles in mRNA transfection potency. Here, a panel of LNP formulations was studied by keeping the ionizable lipids constant, replacing cholesterol with  $\beta$ -sitosterol, and changing the fusogenic helper lipid DOPE content. We studied the ability of this LNP library to induce antigen presentation and T cell proliferation to identify superior LNP candidates eliciting potent T cell immune responses. We hypothesize that using  $\beta$ -sitosterol and increasing DOPE content would boost the mRNA transfection on immune cells and result in enhanced immune responses. Transfection of immortal immune cell lines and bone marrow dendritic cells (BMDCs) with LNPs was studied. Delivery of mRNA coding for the model antigen ovalbumin (OVA-mRNA) to BMDCs with a number of LNP formulations, resulted in a high level of activation, as evidenced by the upregulation of the co-stimulatory receptors (CD40 and CD86) and IL-12 in BMDCs. The enhancement of BMDC activation and T cell proliferation induced by the introduction of  $\beta$ -sitosterol and fusogenic DOPE lipids were cell dependent. Four LNP formulations (C12-200-cho-10%DOPE, C12-200-sito-10%DOPE, cKK-E12-cho-10%DOPE and cKK-E12-sito-30%DOPE) were identified that induced robust T cell proliferation and enhanced IFN- $\gamma$ , TNF- $\alpha$ , IL-2 expression. These results demonstrate that T cell proliferation is strongly dependent on LNP composition and promising LNP-mRNA vaccine formulations were identified.

## Introduction

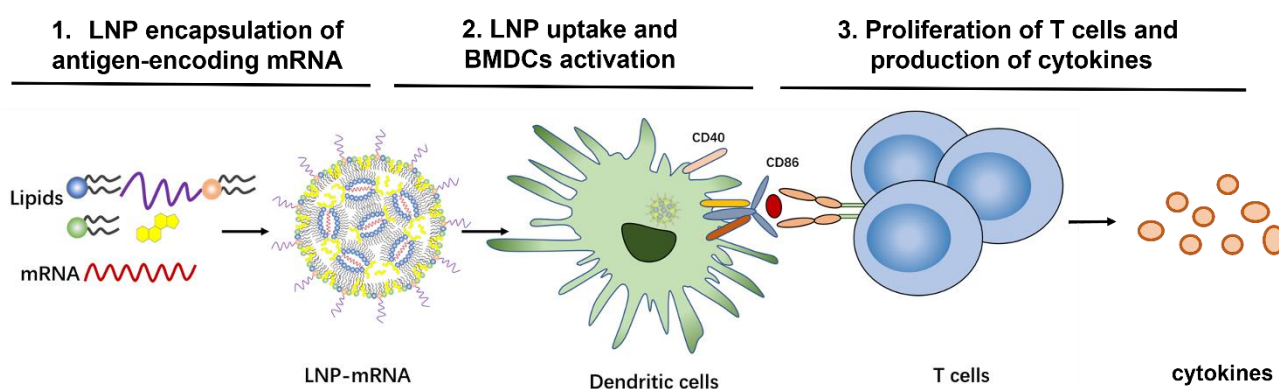
Messenger RNA (mRNA) is an intermediate genetic carrier that is used by organisms as a translational template; therefore, it can serve as a tool for protein expression by introducing exogenous mRNA into target cells.<sup>1</sup> The recent coronavirus pandemic dramatically accelerated the development of mRNA-based vaccines and also put a spotlight on other potential applications such as cancer immunotherapy, infectious disease vaccination, protein replacement, gene editing, and tissue engineering.<sup>2-5</sup> This surging interest and development of mRNA as a vaccine is driven by the following advantages: I) There is no potential infection or insertional mutagenesis risk as mRNA is a non-infectious, non-integrating genetic carrier;<sup>6</sup> II) mRNA is degraded by physiological metabolic pathways and the *in vivo* half-life can be tuned by the introduction of various chemical modifications and the delivery method;<sup>1, 7, 8</sup> III) *in vitro* transcription (IVT) enables rapid, inexpensive, and scalable industrial manufacturing of mRNA.<sup>2</sup> Combined these advantages contribute to the great promise of mRNA-based therapies for both infectious diseases and cancer.

Since mRNA is susceptible to degradation by nucleases *in vivo*, it needs to be protected from the environment upon administration. Furthermore, mRNA is unable to transfect cells and a drug delivery system is therefore required to overcome these problems. Thus, an ideal mRNA delivery system must protect against endonucleases, avoid rapid renal clearance, and promote cell entry of the tissue of interest.<sup>9, 10</sup> Lipid nanoparticles (LNPs) are the most advanced non-viral nucleic acid vector and the first RNA interference (RNAi) therapy, Onpattro, was approved in 2018 to treat hereditary amyloidogenic transthyretin amyloidosis (hATTRv).<sup>11</sup> LNPs are typically composed of 4 types of lipids: ionizable lipids, helper lipids, cholesterol, and PEGylated lipids. Each of these components is required to obtain stable LNPs with control over mRNA encapsulation efficiency, particle size, charge, and stability. Ionizable lipids are required to condense and protect the genetic cargo via electrostatic interactions and their chemical structure plays a crucial role in the resulting transfection efficiency. Helper lipids, cholesterol, and PEGylated lipids are required to control the LNP size as well as colloidal stability, and to minimize protein absorption.<sup>12, 13</sup> The two LNP-based vaccines against SARS-CoV-2 approved in 2020 are a milestone in mRNA-based therapeutics and accelerated the development of LNPs as a facile drug delivery tool for any nucleic acid-based therapy.<sup>14, 15</sup> LNPs have also been studied in cancer immunotherapy<sup>3, 16, 17</sup> and vaccination against infectious diseases, such as Zika virus,<sup>18, 19</sup> powassan virus,<sup>20</sup> HIV-1,<sup>21, 22</sup> and influenza virus.<sup>23-25</sup> In these studies, the immune response was interrogated mainly as a function of mRNA dose, but there is still room for improvement by optimizing the lipid composition of LNPs to achieve the desired cytotoxic T-cell production to mediate successful immunotherapy against many viral diseases and tumors.

For instance, replacing cholesterol with its analog  $\beta$ -sitosterol was reported to enhance the mRNA transfection efficiency.<sup>26</sup> Onpattro uses the lipid MC3 as the ionizable lipid, which was the first approved ionizable lipid for LNPs and showed effective gene silencing by delivering siRNA to hepatocytes.<sup>11, 27</sup> The two ionizable lipids, C12-200 and cKK-E12, were chosen for this study because they demonstrated to be more efficient in delivering siRNA as compared to MC3 and were also able to deliver mRNA, leading to potent immune responses in tumor immunotherapy.<sup>3, 28-30</sup> Helper lipids like 1,2-dioleoyl-*sn*-glycero-3-phosphoethanolamine (DOPE) can increase the fusogenicity of LNPs, aiding endosomal escape and cytosolic translation.<sup>31</sup> This is due to the fact that DOPE prefers to adopt an inverted hexagonal phase, which is assumed to be fusogenic, thereby promoting endosomal escape

resulting in enhanced transfection.<sup>32,33</sup>

To evaluate the effect of lipid composition on mRNA delivery, translation into proteins, antigen-presenting ability, and ultimately T-cell activation, we designed a library of LNPs by varying the lipid composition. In this study, the amount of the ionizable lipids (C12-200 and cKK-E12) and PEGylated lipid was kept constant, the replacement of cholesterol for  $\beta$ -sitosterol and different ratio of fusogenic lipid DOPE were studied to optimize the mRNA delivery efficiency. All studied LNPs induced in general high transfection of immortal cell lines regardless of the exact composition when encapsulating mRNA encoding a green fluorescent protein (EGFP-mRNA). Bone marrow dendritic cells (BMDCs) with a potent antigen-presenting capacity for stimulating naive, memory, and effector T cells were employed to evaluate the immune responses. In this study, mRNA which codes for the model immunology protein chicken ovalbumin (OVA-mRNA) was encapsulated in LNPs to activate BMDCs and stimulate T cell proliferation. BMDCs were highly activated and T cells were strongly proliferated after the internalization of OVA-mRNA-LNPs in a concentration-dependent manner (**Scheme 1**). Based on robust T cell proliferation and cytokine expression measurements, we obtained 4 efficient LNP candidates for future *in vivo* studies towards the development of superior LNP-mRNA formulation. This study provides evidence that the lipid composition optimization of LNPs is beneficial for maximizing T cell immune responses.



**Scheme 1.** Workflow to investigate the role of mRNA-LNP composition on T-cell activation and immune response.

## Results

### Design and characterization of LNPs

We previously showed that the silencing effect of siRNA using LNPs could be improved via tuning the internal LNP structure of the hydrophobic core from lamellar to inverse hexagonal by replacing DSPC with the fusogenic lipid DOPE in the LNP formulation, which is believed to be more fusogenic. In this study 1,2-dioleoyl-3-dimethylammonium-propane (DODAP) was used as the ionizable lipid. Inspired by this, we wondered whether mRNA transfection could also be enhanced by using other ionizable lipids. In the current study, two highly efficient ionizable lipids were used: C12-200 and cKK-E12. These ionizable lipids were efficient in siRNA delivery and the effective dose (ED<sub>50</sub>, C12-200~0.01 mg/kg, cKK-E12~0.002 mg/kg) was significantly lower than for MC3 (ED<sub>50</sub>~0.03 mg/kg). They also induced strong cytotoxic CD8<sup>+</sup> T cell responses against B16F10 melanoma tumors

after immunization with LNP containing OVA-mRNA, resulting in tumor shrinkage and extended overall survival of the treated mice.<sup>3, 28-30</sup> In a recent study, the cholesterol analog  $\beta$ -sitosterol was able to trigger enhanced mRNA transfection efficiency of LNPs in cancer cells compared to cholesterol due to the enhanced fragility, originating from an altered surface composition and shape,<sup>26</sup> and it was therefore included in our LNP library.

In this study, 10 LNP formulations were prepared, for which the ionizable lipids C12-200/cKK-E12 and the PEGylated lipid DMG-PEG2000 were kept constant at 50% and 1.5%, respectively. To study the effect of DOPE, its content varied from 10 to 49 mol% by replacing cholesterol (or its variant) (Fig. 1a-1b). All resulting LNPs had a comparable diameter ( $\sim 120$  nm) with a polydispersity index (PDI)  $< 0.20$  as determined by dynamic light scattering (DLS), as well as a near-neutral surface charge (Fig. 1c-1d). mRNA encapsulation efficiencies were also comparable for all LNPs and typically  $>80\%$  (Fig. 1e). Thus, replacing cholesterol with  $\beta$ -sitosterol or increasing DOPE did not change the physicochemical characteristics of the LNPs. The LNPs were stable for at least 1 month when stored at  $4^\circ\text{C}$  (SI Fig.1a-d).

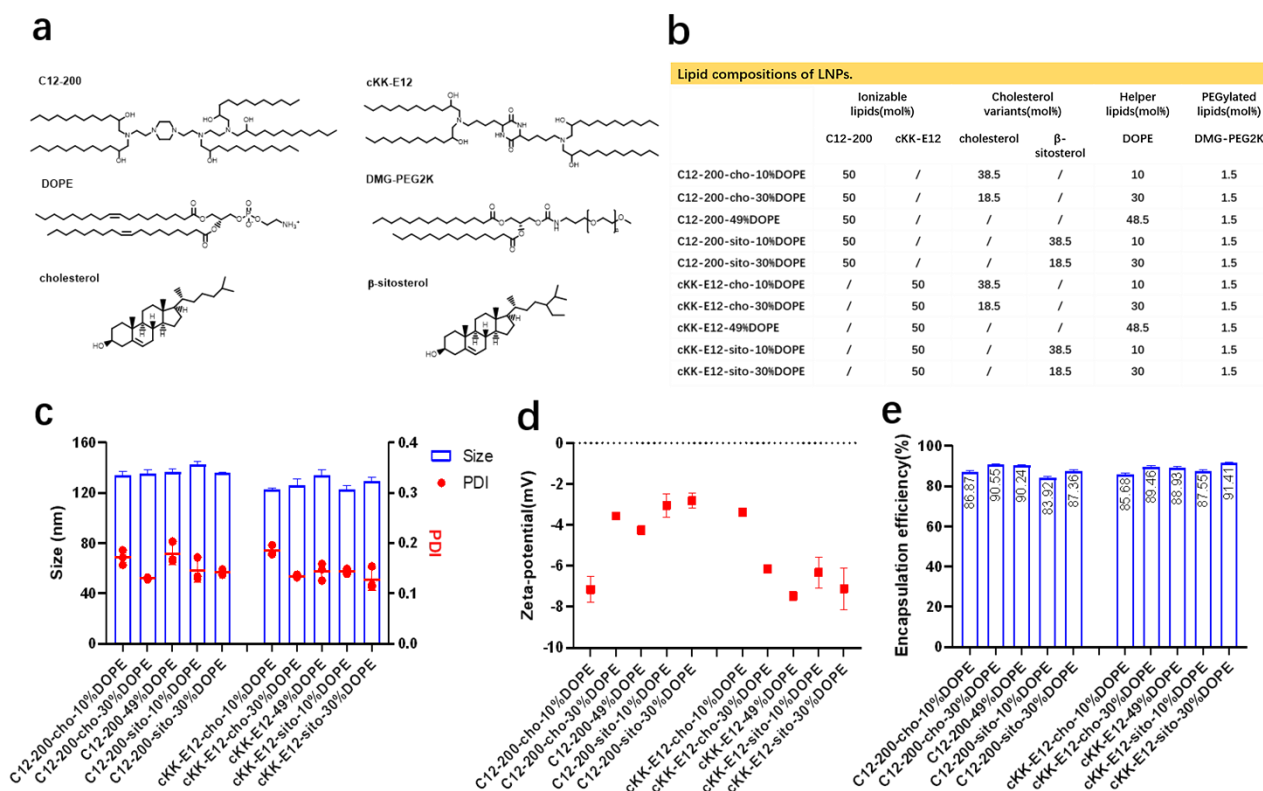


**Figure 1.** Design and characterization of different LNPs. (a) Lipids used in this study. (b) Lipid composition of LNPs. (c) Sizes and polydispersity index of LNPs as determined by DLS. (d) Zeta potential of LNPs determined by Laser Doppler Electrophoresis. (e) Encapsulation efficiency of OVA-mRNA in LNPs as determined by a Ribogreen RNA assay.

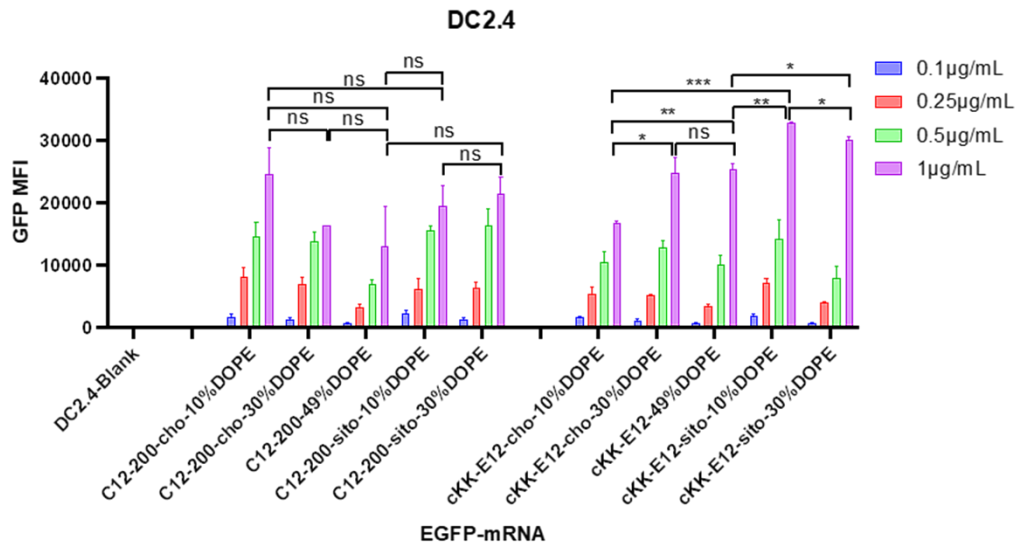
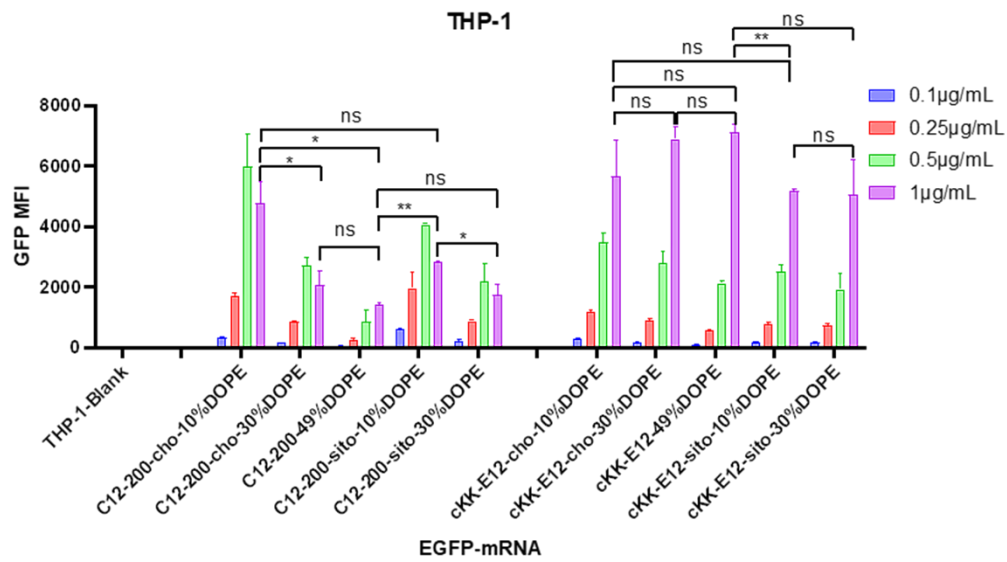
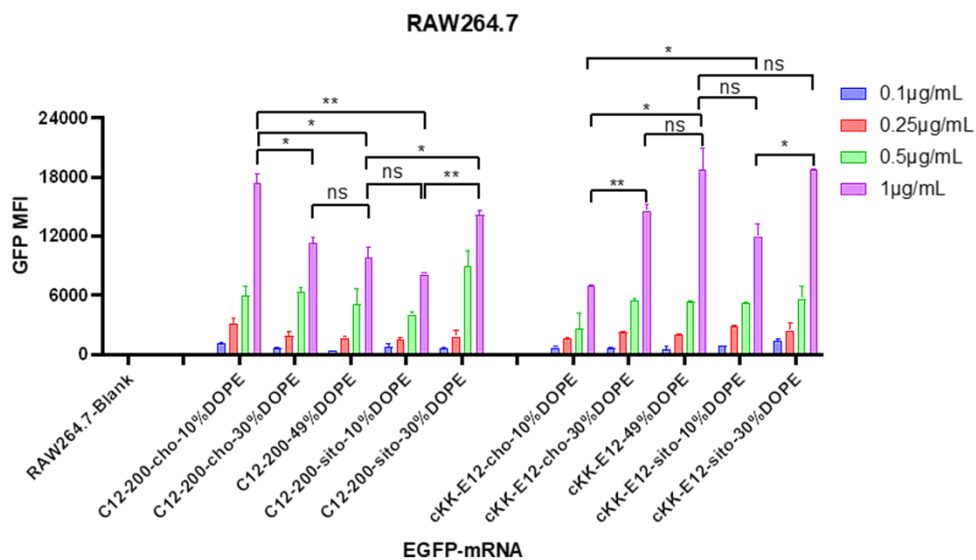
### Cell transfection efficiency

To study mRNA delivery and translation, EGFP-mRNA encoding for green fluorescent protein

(GFP) was encapsulated in the LNPs and the transfection efficiency was compared as a function of lipid composition in cervical carcinoma cells (HeLa) and Calu-3 cells.

Firstly, when comparing the transfection efficiency of different ionizable lipids, both C12-200 and cKK-E12 induced enhanced mRNA transfection efficiency on HeLa and Calu-3 as compared to MC3 (**SI Fig. 2a-b**). This is not unexpected as MC3 was designed for siRNA delivery while the mRNA delivery efficiency was less efficient.<sup>11, 27</sup> Maximum transfection of HeLa cells was obtained with an EGFP-mRNA concentration of 0.5  $\mu\text{g}/\text{mL}$  for all LNPs. In Calu-3 cells, the GFP expression of most LNPs increased with increasing EGFP-mRNA concentrations. Next, the effect of replacing cholesterol with  $\beta$ -sitosterol was studied. The introduction of the latter sterol significantly enhanced GFP expression for LNPs with MC3 as the ionizable lipid in both cell lines. When cKK-E12 was included in the LNPs, GFP expression was only enhanced in HeLa cells, while for C12-200-based LNP formulations no enhancement was observed at all. Finally, we studied whether increasing amounts of DOPE would enhance mRNA delivery and concomitant GFP expression. However, no general trend could be deduced from changing the DOPE ratio in LNP. Thus, we only observed a modest increase in transfection efficiency by replacing cholesterol with  $\beta$ -sitosterol.

Next, antigen-presenting cells (DC2.4) and macrophage cells (THP-1 and RAW264.7) were studied to evaluate the LNP-mRNA transfection performance on immortal cells mediating immune responses. Since LNPs with C12-200 and cKK-E12 as the ionizable lipids exhibited significantly higher transfection than MC3 containing LNPs, we continued this study with C12-200 and cKK-E12 only. In general, LNPs containing cKK-E12 induced a higher GFP expression than LNPs with C12-200 in three cell lines used (**Fig. 2a-2c**). On the other hand, introduction of  $\beta$ -sitosterol increased the transfection efficiency of the cKK-E12 LNPs in DC2.4 and RAW264.7, but not for C12-200 LNPs. When cholesterol was replaced by increasing amounts of DOPE, no transfection enhancement was observed for C12-200 LNPs. In contrast, enhanced transfection efficiency of cKK-E12 LNPs was observed in all tested cell lines. However, transfection enhancement was observed in DC2.4, and RAW264.7 cells when cKK-E12 LNPs contained  $\beta$ -sitosterol, but not in THP-1 cells (**Fig. 2a-2c**). Confocal microscopy imaging was used to visualize GFP expression and concomitant strong fluorescence intensity, and almost every cell produced strong and uniform GFP expression. In contrast, transfection with the commercial mRNA transfection reagent lipofectamine message MAX (lipofectamine) resulted in only a few fluorescent cells in the DC2.4 cell line (**Fig. S3**). In summary, all LNPs with either C12-200 or cKK-E12 as the ionizable lipid induced efficient transfection on immortal immune cell lines; however, the transfection efficiency enhancement by both the  $\beta$ -sitosterol replacement and the fusogenic helper lipid DOPE ratio increase was dependent on the cell line used.

**a****b****c**

**Figure 2.** Transfection efficiency of LNPs after encapsulating EGFP-mRNA on immortal immune cell lines. The GFP expression fluorescence intensity (GFP MFI) of LNPs within (a) DC2.4 cells, (b) THP-1 cells, and (c) RAW264.7. Data are presented as mean  $\pm$  sd. Statistical significance was calculated by unpaired student t-test on 1  $\mu$ g/mL. (\*\*\*\*,  $P < 0.0001$ , \*\*\*,  $P < 0.001$ , \*\*,  $P < 0.01$ , \*,  $P < 0.05$ , ns, no significant difference,  $n = 3$ )

### **BMDC transfection with EGFP-mRNA**

As APC cell lines provided mixed results, we next investigated primary APCs. As the next step towards both efficient intracellular antigen expression and subsequent immune cell activation to generate a robust immune response, the transfection efficiency of EGFP-mRNA loaded LNPs in BMDCs was investigated. Confocal microscopy imaging showed that all LNP formulations induced effective intracellular mRNA delivery to BMDCs, and performed better than the commercial transfection reagent Lipofectamine (**Fig. 3a**).  $\beta$ -Sitosterol boosted the transfection efficiency of the LNPs with cKK-E12 as the ionizable lipids but not for C12-200 (**Fig. 3b**). Finally, replacing cholesterol with DOPE did not enhance the GFP expression of either C12-200 and cKK-E12 LNPs (**Fig. 3b**).

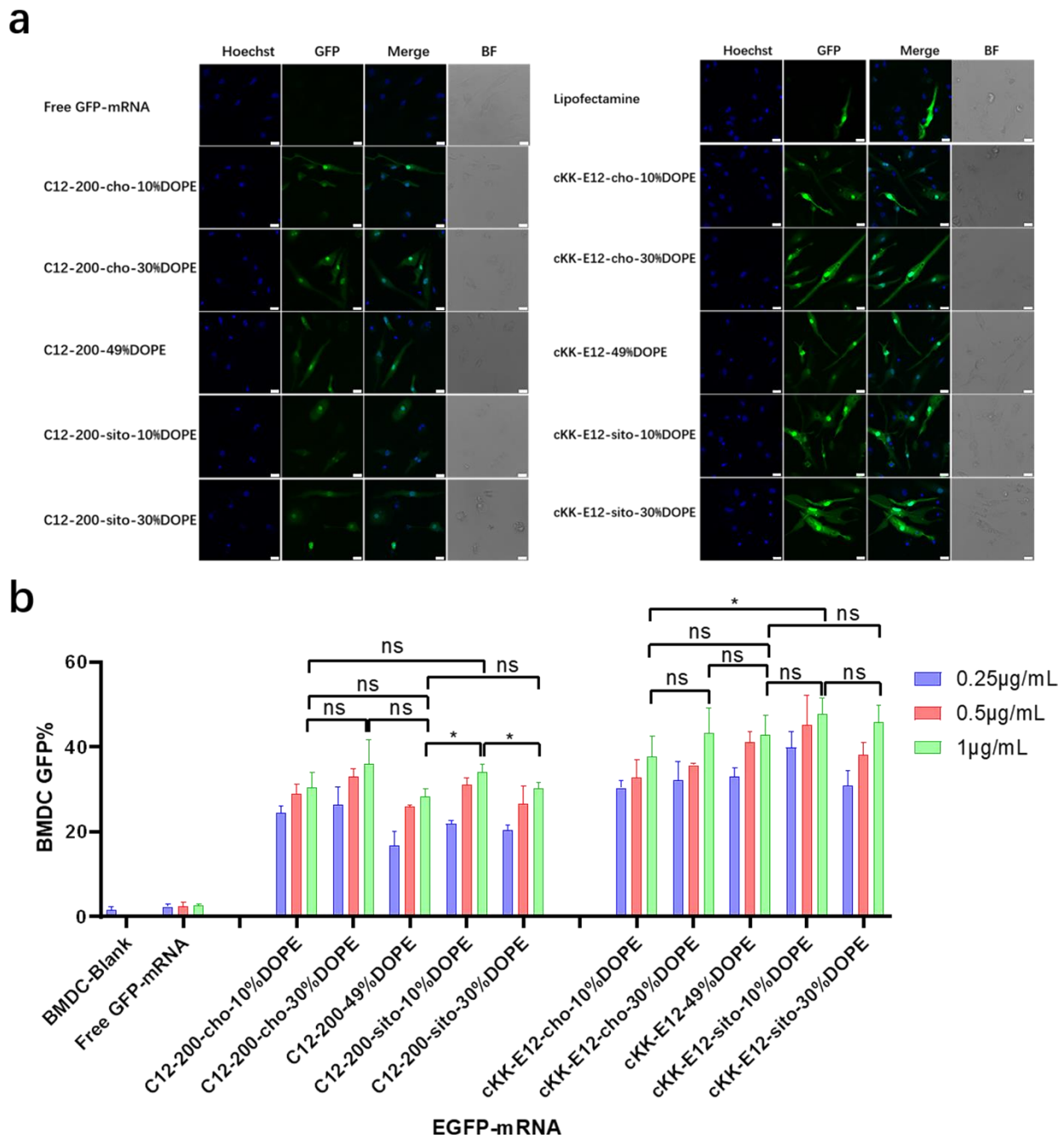


**Figure 3.** Transfection efficiency of LNPs after encapsulating EGFP-mRNA on BMDC cells. **(a)** Confocal images of the EGFP-mRNA transfection of LNPs on BMDC cells, EGFP-mRNA concentration was 0.5 µg/mL, incubated 24 h. Scale bar is 20 µm. **(b)** The GFP positive percentages of LNPs by flow cytometry analysis on BMDC cells of different EGFP-mRNA concentrations after 24 h incubation. Data are presented as mean ± sd. Statistical significance was calculated by unpaired student t-test on 1 µg/mL. (\*\*\*\*,  $P < 0.0001$ , \*\*\*,  $P < 0.001$ , \*\*,  $P < 0.01$ , \*,  $P < 0.05$ , ns, no significant difference,  $n = 3$ )

### Activation of BMDCs

Effective mRNA vaccination demands both efficient intracellular expression and subsequent APC activation to generate a robust immune response.<sup>16</sup> The model antigen chicken ovalbumin protein has been widely applied to evaluate the immune response, thus mRNA encoding ovalbumin (OVA-

mRNA) formulated in the LNPs was employed to activate BMDCs. The activation of BMDCs results in elevated expression of surface costimulatory molecules such as CD40, and CD86. To test APC activation induced by LNPs, we treated naïve BMDCs for 24 h with LNPs containing OVA-mRNA. All LNPs managed to produce increased expression of CD40 and CD86 compared to nontreated BMDCs or incubated with free OVA-mRNA, which indicates successful BMDC activation (**Fig. 4a-4b**). Both positive percentage and fluorescence intensity comparisons of CD40 and CD86 revealed no significant differences between C12-200 LNP formulations. Furthermore, neither the introduction of DOPE nor  $\beta$ -sitosterol at the expense of cholesterol boosted BMDC activation (**Fig. 4a-4b, SI Fig. 4a-4b**). For LNPs with cKK-E12, we observed that cKK-E12-cho-10%DOPE and cKK-E12-sito-30%DOPE induced a stronger upregulation of CD40 and CD86 expression (**SI Fig. 4a-4b**).

The activation of dendritic cells often promotes inflammatory cytokine gene expression. We, therefore, examined cytokine IL-12 (p70) expression in the supernatant of BMDCs. Interleukin-12 (IL-12) is a heterodimeric pro-inflammatory cytokine that regulates T helper 1 (Th1) and CD8<sup>+</sup> T-cell responses, and is mainly produced by dendritic cells and phagocytes in response to pathogens during infection.<sup>34</sup> Compared to blank BMDCs and free OVA-mRNA, all LNPs mediated superior IL-12 (p70) production (**Fig. 4c**); however, no significant differences among the tested LNPs were observed. The cell viability of BMDCs was determined to ensure that the LNPs were non-toxic at the concentrations used. All LNP formulations showed no detectable cytotoxicity (cell viability > 60%), even at a high concentration (1  $\mu$ g/mL), revealing that these LNPs are indeed non-toxic (**Fig. 4d**).

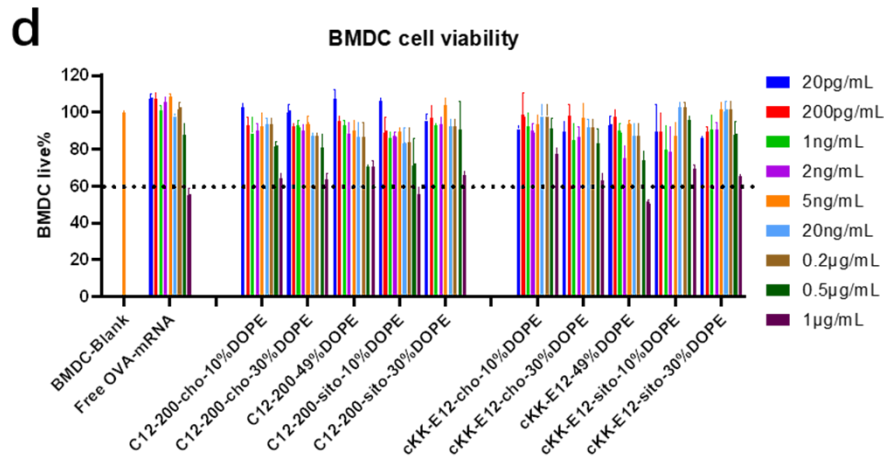
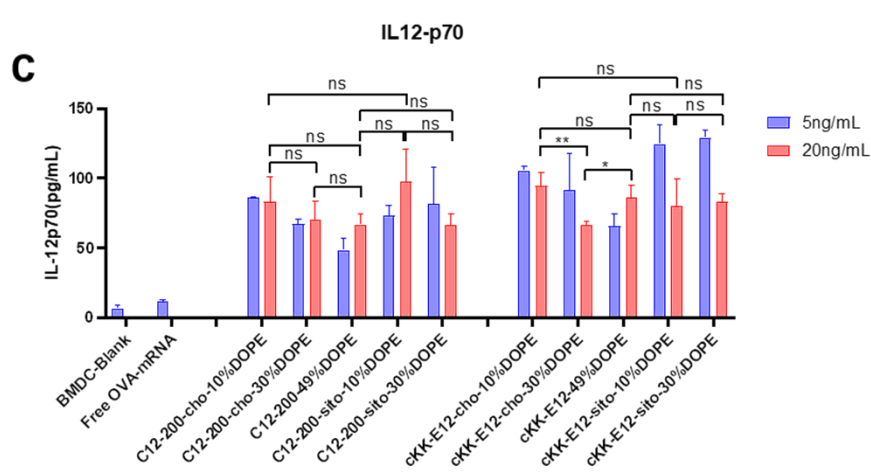
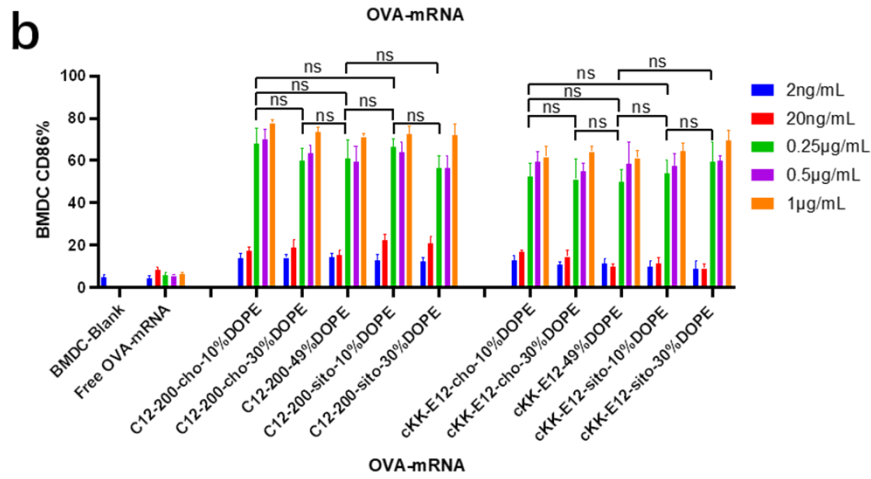
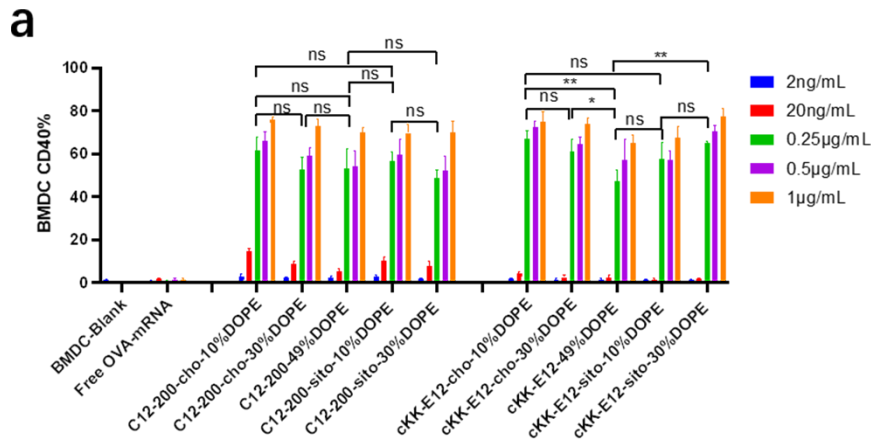
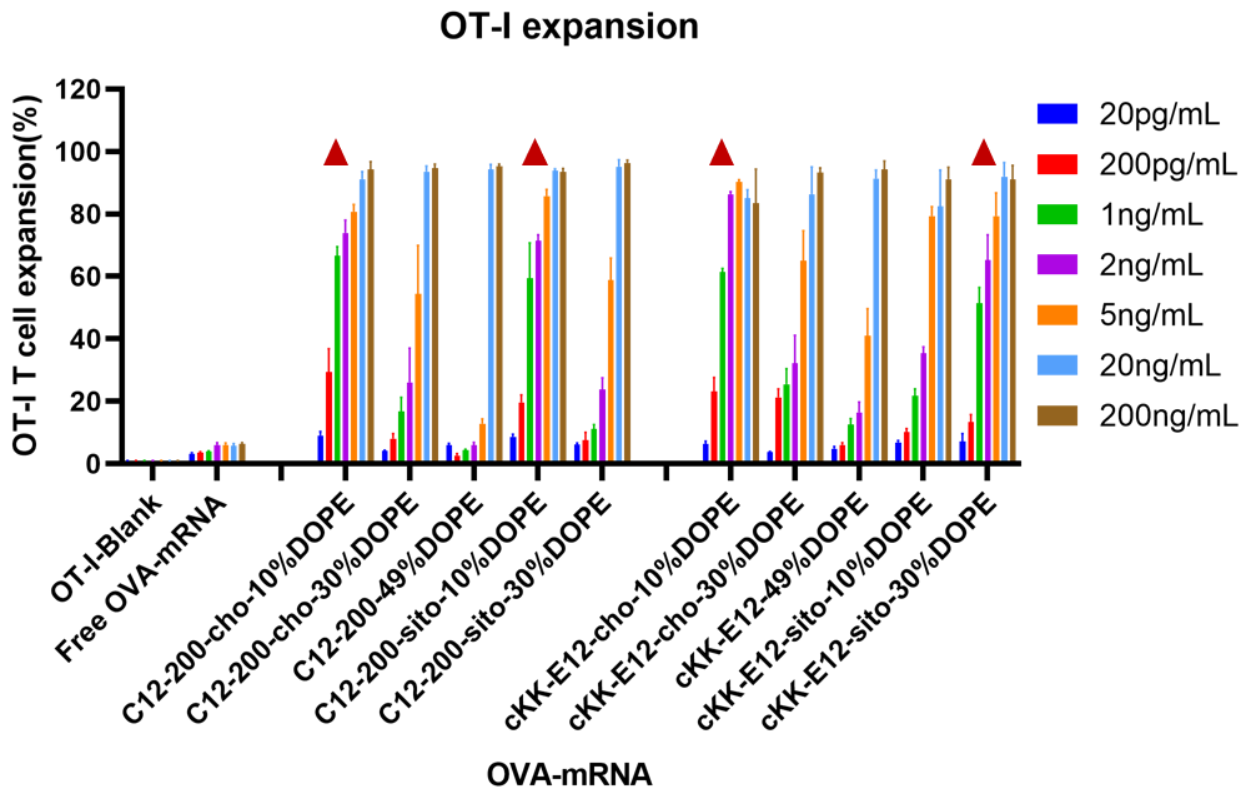


**Figure 4.** LNPs Transfection after encapsulating OVA-mRNA on BMDC cells. **(a)** BMDC activation was monitored through CD40 cellular marker on BMDCs by the different concentrations of LNPs. **(b)** BMDCs activation was monitored through CD86 cellular marker on BMDCs by the different concentrations of LNPs. **(c)** Cytokine IL-12 (p70) expression from BMDCs' supernatant. **(d)** Cell viability of BMDCs with different concentrations of LNPs, dotted line represents 60% cell viability. Data are presented as mean  $\pm$  sd. Statistical significance was calculated by unpaired student t-test on 0.25  $\mu$ g/mL **(a-b)**, 20 ng/mL **(c)**. (\*\*\*\*,  $P < 0.0001$ , \*\*\*,  $P < 0.001$ , \*\*,  $P < 0.01$ , \*,  $P < 0.05$ , ns, no significant difference,  $n = 3$ )

### **CD8<sup>+</sup> T-cell expansion by LNPs and cytokine production**

The goal of tumor and viral vaccination is to expand antigen-specific CD8<sup>+</sup> T cells through priming by APCs, creating a large pool of cytotoxic effector T cells that migrate through the body to clear tumors or infections.<sup>35-37</sup> Therefore, we evaluated OVA-specific T cell expansion induced by different LNPs. BMDCs were incubated with LNPs for 4 h, followed by the addition of CD8<sup>+</sup> (OT-I) T-cells, and the mixed cells were co-cultured for another 72 h.

All LNPs induced potent OT-I proliferation in a mRNA concentration-dependent manner, which was significantly stronger than the blank and free OVA-mRNA groups (**Fig. 5**). T cell proliferation was negligible in the lowest concentration (200 pg/mL), while it plateaued at ~90% with an OVA-mRNA concentration of 20 ng/mL. Next, we investigated the proliferation differences of LNPs in the middle mRNA concentration range. We observed that the C12-200-cho-10%DOPE, C12-200-sito-10%DOPE, cKK-E12-cho-10%DOPE and cKK-E12-sito-30%DOPE LNP formulations induced a potent OT-I T cell stimulation with 1 ng/mL of OVA-mRNA. This indicates these four LNP formulations are able to elicit a robust T cell proliferation even at low OVA-mRNA concentrations, which could serve as efficient LNP candidates eliciting potent T cell responses.

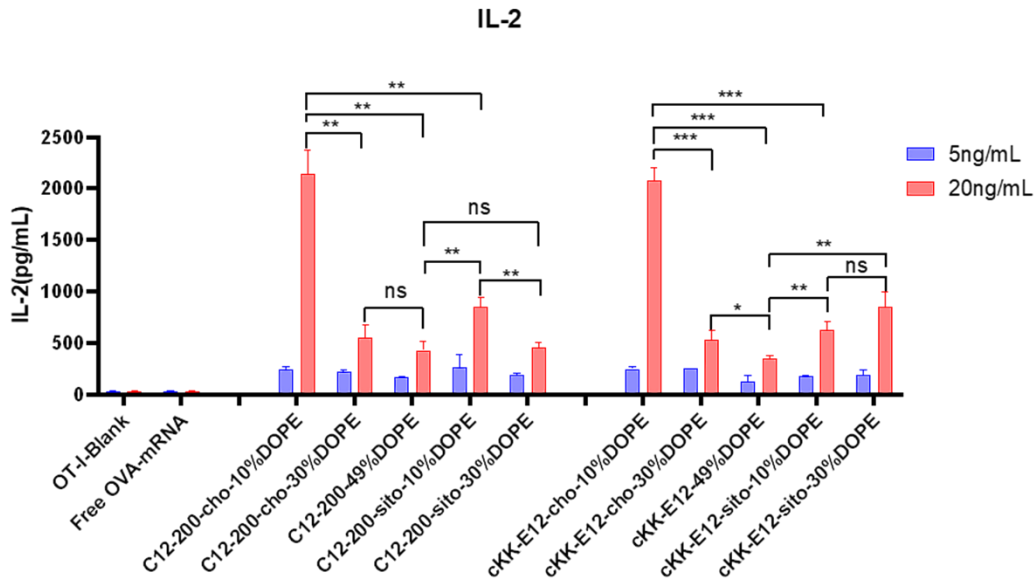
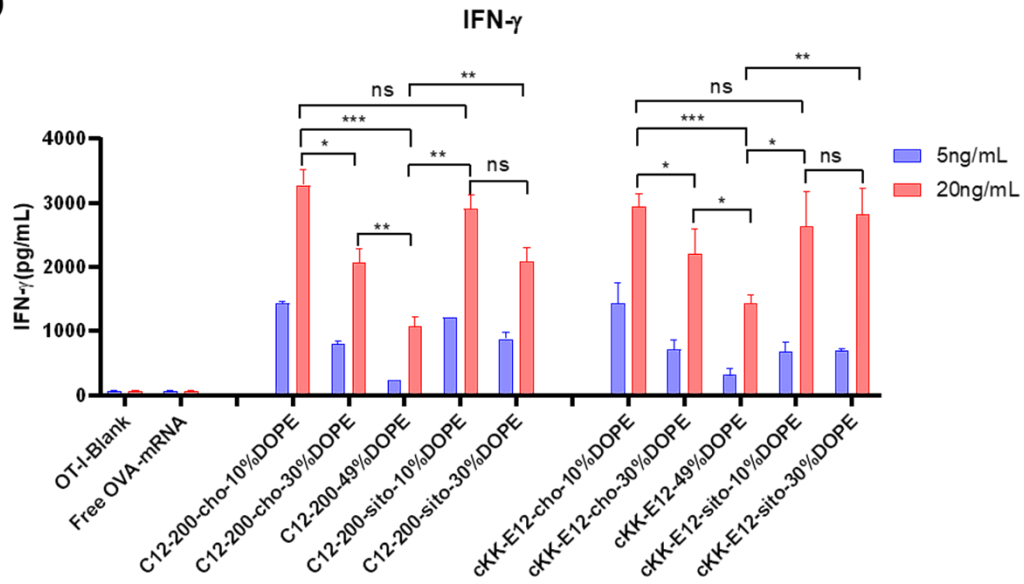
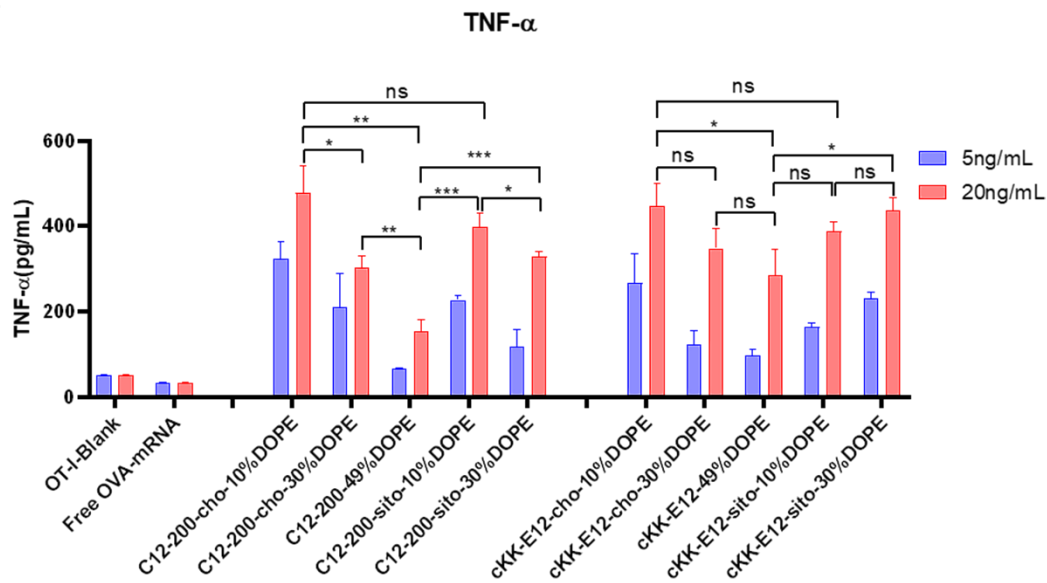


**Figure 5.** OT-I T cell expansion of LNPs with different OVA-mRNA concentrations. Triangle represents the four leading LNP candidates that induced superior OT-I responses when compared at 1 ng/mL.

### Cytokine production of T cell supernatant

When T cells divide and differentiate into effector T cells, cytokines like IFN- $\gamma$ , TNF- $\alpha$ , and cytotoxic proteins such as granzymes and perforin are simultaneously induced in response to acute infection.<sup>38</sup> Proinflammatory cytokines, such as interleukin-2 (IL-2), are pivotal for the proliferation of T cells and the generation of effector and memory cells.<sup>39,40</sup> Activated CD8<sup>+</sup> T cells possess superior effector functions when cultured in a high concentration of IL-2 compared to cells cultured in low concentrations of this cytokine.<sup>41</sup> Therefore, we quantified the expression of IL-2, IFN- $\gamma$ , and TNF- $\alpha$  in OT-I cells in the culture supernatant 72 h after LNP stimulation using an ELISA assay (**Fig. 6a-6c**). The cytokines were significantly upregulated after treating cells with LNPs as compared to non-treated or free OVA-mRNA treated cells. Differences in cytokine production among the evaluated LNPs were determined at two mRNA concentrations (5 and 20 ng/mL). Consistent with OT-I cell proliferation data, replacing cholesterol with  $\beta$ -sitosterol did not boost the T cell response and cytokine production for LNPs with C12-200. The increased molar ratio of fusogenic helper lipid DOPE in C12-200 LNPs neither enhanced the T cell response nor cytokine IL-2 production. The increased molar ratio of DOPE did not enhance the cytokine IL-2 production for cKK-E12 LNPs, and it only showed some enhancement in cytokine IL-2 production at 30% DOPE but decreased at 49% DOPE for cKK-E12 LNPs using  $\beta$ -sitosterol. On the other hand, for Th1 cytokine (IFN- $\gamma$ ) and proinflammatory cytokines (TNF- $\alpha$ ) production, we also observed that C12-200-cho-10%DOPE, C12-200-sito-10%DOPE, cKK-E12-cho-10%DOPE and cKK-E12-sito-30%DOPE LNP formulations triggered higher IFN- $\gamma$  and TNF- $\alpha$  levels in the OT-I T cell supernatant. Taken together, these results showed that four LNP formulations (*i.e.* C12-200-cho-10%DOPE, C12-200-sito-

10%DOPE, cKK-E12-cho-10%DOPE and cKK-E12-sito-30%DOPE) induced a potent T cell proliferation and concomitant inflammatory cytokine production.

**a****b****c**

**Figure 6.** Cytokine production levels of (a) IL-2, (b) IFN- $\gamma$ , (c) TNF- $\alpha$  in culture media of OT-I T cells by different LNPs, measured by ELISA. Data are presented as mean  $\pm$  sd. Statistical significance was calculated by unpaired student t-test on 20 ng/mL. (\*\*\*\*,  $P < 0.0001$ , \*\*\*,  $P < 0.001$ , \*\*,  $P < 0.01$ , \*,  $P < 0.05$ , ns, no significant difference,  $n = 3$ )

## Conclusion

We investigated a small library of LNP formulations to deliver mRNA into BMDCs and evaluate T cell activation towards the development of LNP-mRNA vaccine candidates. LNPs have been validated as effective and well-tolerated on mRNA delivery and recognized as an exceptional mRNA vaccine vector. Proper LNP vaccine candidate screening is essential to identify superior LNP formulations that could boost robust T cell proliferation. It has been reported that replacing cholesterol with  $\beta$ -sitosterol or fusogenic DOPE could enhance transfection efficiency. We discovered that the introduction of  $\beta$ -sitosterol only exerted enhanced transfection in LNPs using MC3 as the ionizable lipid, while exhibiting varied transfection efficiency effects on different cell lines when C12-200 and cKK-E12 were used. Replacing cholesterol with DOPE resulted in mixed mRNA transfection efficiencies in different cells. This may be due to the enhanced transfection efficiency requiring different helper lipids ratios when using different ionizable lipids of LNPs, and also the mechanism of mRNA release into cytoplasm seems to be cell type-dependent. We demonstrated that the LNP-mRNA vaccine candidates can generate significant activation of BMDCs, robust T cell proliferation, and enhanced cytokine production *ex vivo*. We identified four LNP formulations (C12-200-cho-10%DOPE, C12-200-sito-10%DOPE, cKK-E12-cho-10%DOPE, and cKK-E12-sito-30%DOPE) which exhibit efficient T cell expansion and cytokines production and these will be tested in a future *in vivo* study towards the development of a cancer vaccine.

## Methods

### Chemicals

All lipids, 1,2-dioleoyl-*sn*-glycero-3-phosphoethanolamine (DOPE), 1,2-distearoyl-*sn*-glycero-3-phosphocholine (DSPC), 1,2-dimyristoyl-*rac*-glycero-3-methoxypolyethylene glycol-2000 (DMG-PEG2K) were purchased from Avanti Polar Lipids, DLin-MC3-DMA was purchased from Biorbyt company (Cambridge, England), Hoechst 33342, cholesterol and  $\beta$ -sitosterol was purchased from Sigma-Aldrich. Triton™ X-100 was purchased from Acros Organics. QuantiT™ RiboGreen® RNA reagent and rRNA standards were purchased from Life Technologies. Clean cap EGFP-mRNA (5moU) and OVA-mRNA (5moU) were purchased from Trilink biotechnology. C12-200 and cKK-E12 lipids were synthesized according to the literatures.<sup>28, 29</sup> The following antibodies were used for flow cytometry: anti-Thy1.2 PeCy7, anti-CD8 efluor450, anti-CD25 APC, Live/Dead stain and purchased from BD Bioscience. CD4 and CD8 T-cell isolation kits were purchased from Miltenyi (Leiden, Netherlands).

### Cell culture

THP-1, RAW264.7, HeLa, Calu-3 cells were obtained from ATCC. DC2.4 is a murine dendritic cell line kindly provided by Kenneth Rock, University of Massachusetts Medical School, Worcester, MA. Cells were maintained either in DMEM or RPMI 1640 (Thermo Fisher Scientific) supplemented with 10% fetal bovine serum (FBS) (Gibco) and 1% penicillin-streptomycin antibiotic (Gibco). Cell culture and all biological experiments were performed at 37 °C in 5% CO<sub>2</sub> conditions in a cell culture incubator.

6 to 8-week-old female mice (C57BL/6 mice were used to isolate BMDCs. Briefly, the femur and tibia from mice hind legs were collected and bone marrow cells were flushed out with PBS using a syringe. Cells were resuspended into RPMI1640 medium with 10% FBS, antibiotics, and  $\beta$ -mercaptoethanol (55  $\mu$ M, Gibco). Cells were grown with a supplement of recombinant murine granulocyte-macrophage-colony-stimulating factor (GM-CSF) (20 ng/mL, Peprotech). The cell culture medium was refreshed every other day.

### Mouse experiments

C57BL/6, OT-I transgenic mice on a C57BL/6 background were purchased from Jackson Laboratory (CA, USA), bred in-house under standard laboratory conditions, and provided with food and water ad libitum. All animal experiments were performed in compliance with the Dutch government guidelines and the Directive 2010/63/EU of the European Parliament. Experiments were approved by the Ethics Committee for Animal Experiments of Leiden University.

### LNP-mRNA preparation and characterization

Lipids were combined at the desired molar ratios and concentrations from stock solutions dissolved in chloroform. Solvents were evaporated under a nitrogen flow and residual solvent was removed in vacuo for at least 30 minutes. The lipid film was dissolved in absolute ethanol (total lipids was 0.4  $\mu$ mol) and used for the assembly. A solution of mRNA was made by diluting mRNA (EGFP-mRNA, OVA-mRNA) in 50 mM citrate buffer (pH = 4, RNase free). The solutions were loaded into two separate syringes and connected to a T-junction microfluidic mixer. The solutions were mixed in a 3:1 flow ratio of mRNA against lipids (1.5 mL/min for mRNA solution, 0.5 mL/min for lipids solution,

lipids: mRNA (wt/wt) =40:1). After mixing, the solution was directly loaded in a 20 kDa MWCO dialysis cassette (Slide-A-Lyzer™, Thermo Scientific) and dialyzed against 1 x PBS overnight. The size and zeta potential of LNPs were measured using dynamic light scattering (DLS, Malvern) and Zetasizer (Malvern). Long term stability of LNPs was assessed by measuring the hydrodynamic radius using DLS for 1 month.

The encapsulation efficiency (EE) of mRNA was determined by Quant-iT™ RiboGreen™ RNA Assay Kit (Invitrogen). For the determination of non-encapsulated mRNA, LNPs after dialysis were diluted with 1 x TE buffer (RNase free) and treated with the RiboGreen™ reagent. For the determination of the total amount of mRNA, LNPs after dialysis were treated with 1% Triton X-100 in TE buffer (RNase free) and incubated for 5 minutes followed by dilution with TE buffer and treatment with the RiboGreen™ reagent. The supplied RNA standards were used to generate a standard curve and changes in fluorescence was measured in 96-well plates using a TECAN Infinite M1000 Pro microplate reader. The percentage of mRNA encapsulation (EE%) was determined using the fraction of  $(F_{\text{total RNA}} - F_{\text{free RNA}})/F_{\text{total RNA}} * 100\%$ .

### ***In vitro* GFP protein expression of LNPs**

Briefly, HeLa, and Calu-3, DC2.4, THP-1 and RAW264.7 cells were seeded in 96-well plates at a density of  $1 \times 10^4$  cells/well and cultured at 37 °C in 5% CO<sub>2</sub> overnight. Then cells were transfected with LNPs containing different concentrations of EGFP-mRNA overnight (0.1 µg/mL, 0.25 µg/mL, 0.5 µg/mL, 1 µg/mL). The expression of GFP protein was quantified by flow cytometry. Data analysis was performed using the FlowJo Software version 7.6. For confocal microscopy, DC2.4 cells were seeded on the 8-well confocal slide at a density of  $5 \times 10^4$  cells/well and cultured overnight, then LNPs were added and incubated overnight (1 µg/mL), after that Hoechst 33342 (5 µM) was added and incubated for 1 h before confocal microscopy imaging (Leica TCS SP8 confocal laser scanning microscope).

### **BMDC transfection**

Bone marrow-derived dendritic cells (BMDCs) were isolated from murine tibia and femurs of C57BL/6 mice. Bone marrow cells were stimulated for 10 days with 20 ng/mL GM-CSF in complete IMDM (supplemented with 100 U/mL PenStrep, 2 mM glutaMAX and 10% FCS). After 10 days of culture, 20,000 BMDCs were plated in 96-well plates (Greiner Bio-One B.V., Alphen aan den Rijn, Netherlands) and different LNPs encapsulating EGFP-mRNA were added at varying concentrations and incubated with BMDC overnight (0.25 µg/mL, 0.5 µg/mL, 1 µg/mL). Cells were analyzed by flow cytometry (CytoFLEX S, Beckman Coulter, CA, USA). Data were analyzed by using FlowJo software (Treestar, OR, USA). For confocal microscopy, BMDCs were seeded on the 8-well confocal slide at a density of  $5 \times 10^4$  cells/well and cultured overnight, then LNPs were added and incubated overnight (0.5 µg/mL), then followed with confocal microscopy measurement (Leica TCS SP8 confocal laser scanning microscope).

### **BMDC activation**

Bone marrow-derived dendritic cells (BMDCs) were isolated and cultured described as above. After 10 days, different LNPs containing OVA-mRNA were added to the BMDC cells and incubated overnight (2 ng/mL, 20 ng/mL, 0.25 µg/mL 0.5 µg/mL, 1 µg/mL). After 24 h of incubation, cells were collected and followed immunostaining of CD40 and CD86 to quantify the expression by flow

cytometry. Data analysis was performed using the FlowJo Software version 7.6. The supernatant was collected for measuring the expression level of cytokine (IL12-p70) by ELISA.

### ***Ex vivo* T-cell expansion**

Wild-type (WT) BMDCs were cultured as described above, after 10 days, the BMDCs (20,000 cells per well) were exposed to the different LNP formulations with various concentrations (20 pg/mL, 200 pg/mL, 1 ng/mL, 2 ng/mL, 5 ng/mL, 20 ng/mL, 200 ng/mL). Meanwhile, spleens were removed from OT-I mice and strained through a 70- $\mu$ m cell strainer to obtain a single-cell suspension. Erythrocytes were lysed with Ammonium-Chloride-Potassium (ACK) lysis buffer (0.15M NH<sub>4</sub>Cl, 1mM KHCO<sub>3</sub>, 0.1mM Na<sub>2</sub>EDTA; pH 7.3). CD8<sup>+</sup> T cells were isolated using a CD8<sup>+</sup> T cell isolation kit (Miltenyi Biotec B.V., Leiden, Netherlands) according to the manufacturer's protocol. After 4 h of LNP incubation, the BMDCs were centrifuged, the supernatant medium was removed, and replaced with 60,000 CD8<sup>+</sup> T-cells to obtain a number ratio of 3:1 CD8<sup>+</sup> T cells:BMDCs. Co-cultures were cultured for 72 h in complete RPMI 1640 medium supplemented with 2 mM glutamine, 10% FCS, 100 U/mL penicillin/streptomycin, and 50  $\mu$ M  $\beta$ -mercaptoethanol. After 72 h, the cell suspension was stained for anti-Thy1.2 PeCy7, anti-CD8 efluor450, anti-CD25 APC, Live/Dead stain indicating cell viability, and then analyzed by flow cytometry (CytoFLEX S, Beckman Coulter, CA, USA). The supernatant was collected for measuring the expression levels of cytokines by ELISA.

### **ELISA measurements of OT-I T cell supernatant**

Cytokines (IL-2, IFN- $\gamma$ , and TFN- $\alpha$ ) from OT-I T cell supernatants were detected by individual cytokine ELISA kits according to the manufacturer's instructions (BD Biosciences). In brief, the assay plate was coated with 50  $\mu$ l/well of capture antibody (IL-2, IFN- $\gamma$ , and TFN- $\alpha$ , respectively) in coating buffer, covered and incubated overnight at 4 °C. Next, the plate was washed (3x) with wash buffer (PBS with 0.05% Tween-20) and blocked with 100  $\mu$ l/well of assay diluent (PBS with 10%FCS) and incubated for 1 hour at RT. The plate was washed (3x) with wash buffer and 50  $\mu$ L/well (diluted) samples/standard/blank was added incubated for 2 hours at RT. Next, the plate was washed (3x) with wash buffer and 50  $\mu$ L/well of the working detector (Detection AB + Sav-HRP reagent) was added and incubated for another 1 hour at RT. After washing the plate (5X) with wash buffer, 50  $\mu$ L/well substrate solution was added and incubate for 15-30min at RT in the dark. Finally, 25  $\mu$ l/well stop solution was added and the absorbance at 450 nm was measured within 30 minutes.

### **Statistical analyses**

Statistical analyses were performed with Prism 8 (GraphPad). Data were compared using unpaired student t-test analysis. (\*\*\*\*, P < 0.0001, \*\*\*, P < 0.001, \*\*, P < 0.01, \*, P < 0.05, ns, no significant difference, n = 3)

## **References**

1. Thess, A.; Grund, S.; Mui, B. L.; Hope, M. J.; Baumhof, P.; Fotin-Mleczek, M.; Schlake, T., Sequence-engineered mRNA Without Chemical Nucleoside Modifications Enables an Effective Protein Therapy in Large Animals. *Molecular Therapy* **2015**, *23* (9), 1456-1464.
2. Sahin, U.; Karikó, K.; Türeci, Ö., mRNA-based therapeutics — developing a new class of drugs. *Nature Reviews Drug Discovery* **2014**, *13* (10), 759-780.

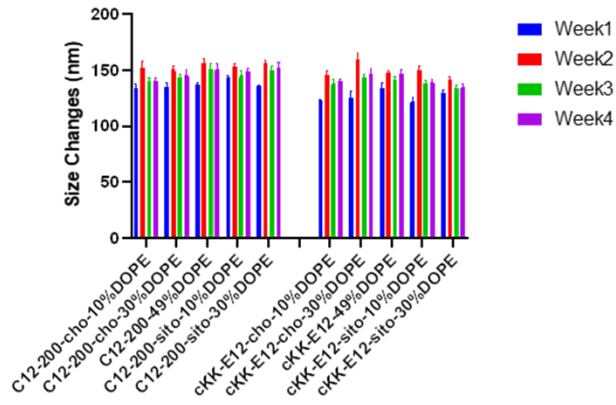
3. Oberli, M. A.; Reichmuth, A. M.; Dorkin, J. R.; Mitchell, M. J.; Fenton, O. S.; Jaklenec, A.; Anderson, D. G.; Langer, R.; Blankschtein, D., Lipid Nanoparticle Assisted mRNA Delivery for Potent Cancer Immunotherapy. *Nano Letters* **2017**, *17* (3), 1326-1335.
4. Cheng, Q.; Wei, T.; Farbiak, L.; Johnson, L. T.; Dilliard, S. A.; Siegwart, D. J., Selective organ targeting (SORT) nanoparticles for tissue-specific mRNA delivery and CRISPR–Cas gene editing. *Nature Nanotechnology* **2020**, *15* (4), 313-320.
5. Billingsley, M. M.; Singh, N.; Ravikumar, P.; Zhang, R.; June, C. H.; Mitchell, M. J., Ionizable Lipid Nanoparticle-Mediated mRNA Delivery for Human CAR T Cell Engineering. *Nano Letters* **2020**, *20* (3), 1578-1589.
6. Pardi, N.; Hogan, M. J.; Porter, F. W.; Weissman, D., mRNA vaccines — a new era in vaccinology. *Nature Reviews Drug Discovery* **2018**, *17* (4), 261-279.
7. Guan, S.; Rosenecker, J., Nanotechnologies in delivery of mRNA therapeutics using nonviral vector-based delivery systems. *Gene Therapy* **2017**, *24* (3), 133-143.
8. Karikó, K.; Muramatsu, H.; Welsh, F. A.; Ludwig, J.; Kato, H.; Akira, S.; Weissman, D., Incorporation of Pseudouridine Into mRNA Yields Superior Nonimmunogenic Vector With Increased Translational Capacity and Biological Stability. *Molecular Therapy* **2008**, *16* (11), 1833-1840.
9. Sabnis, S.; Kumarasinghe, E. S.; Salerno, T.; Mihai, C.; Ketova, T.; Senn, J. J.; Lynn, A.; Bulychev, A.; McFadyen, I.; Chan, J.; Almarsson, Ö.; Stanton, M. G.; Benenato, K. E., A Novel Amino Lipid Series for mRNA Delivery: Improved Endosomal Escape and Sustained Pharmacology and Safety in Non-human Primates. *Molecular Therapy* **2018**, *26* (6), 1509-1519.
10. Yin, H.; Kanasty, R. L.; Eltoukhy, A. A.; Vegas, A. J.; Dorkin, J. R.; Anderson, D. G., Non-viral vectors for gene-based therapy. *Nature Reviews Genetics* **2014**, *15* (8), 541-555.
11. Akinc, A.; Maier, M. A.; Manoharan, M.; Fitzgerald, K.; Jayaraman, M.; Barros, S.; Ansell, S.; Du, X.; Hope, M. J.; Madden, T. D.; Mui, B. L.; Semple, S. C.; Tam, Y. K.; Ciufolini, M.; Witzigmann, D.; Kulkarni, J. A.; van der Meel, R.; Cullis, P. R., The Onpattro story and the clinical translation of nanomedicines containing nucleic acid-based drugs. *Nature Nanotechnology* **2019**, *14* (12), 1084-1087.
12. Kowalski, P. S.; Rudra, A.; Miao, L.; Anderson, D. G., Delivering the Messenger: Advances in Technologies for Therapeutic mRNA Delivery. *Molecular Therapy* **2019**, *27* (4), 710-728.
13. Semple, S. C.; Akinc, A.; Chen, J.; Sandhu, A. P.; Mui, B. L.; Cho, C. K.; Sah, D. W. Y.; Stebbing, D.; Crosley, E. J.; Yaworski, E.; Hafez, I. M.; Dorkin, J. R.; Qin, J.; Lam, K.; Rajeev, K. G.; Wong, K. F.; Jeffs, L. B.; Nechev, L.; Eisenhardt, M. L.; Jayaraman, M.; Kazem, M.; Maier, M. A.; Srinivasulu, M.; Weinstein, M. J.; Chen, Q.; Alvarez, R.; Barros, S. A.; De, S.; Klimuk, S. K.; Borland, T.; Kosovrasti, V.; Cantley, W. L.; Tam, Y. K.; Manoharan, M.; Ciufolini, M. A.; Tracy, M. A.; de Fougères, A.; MacLachlan, I.; Cullis, P. R.; Madden, T. D.; Hope, M. J., Rational design of cationic lipids for siRNA delivery. *Nature Biotechnology* **2010**, *28* (2), 172-176.
14. Wang, C.; Zhang, Y.; Dong, Y., Lipid Nanoparticle–mRNA Formulations for Therapeutic Applications. *Accounts of Chemical Research* **2021**, *54* (23), 4283-4293.
15. Verbeke, R.; Lentacker, I.; De Smedt, S. C.; Dewitte, H., The dawn of mRNA vaccines: The COVID-19 case. *Journal of Controlled Release* **2021**, *333*, 511-520.
16. Miao, L.; Li, L.; Huang, Y.; Delcassian, D.; Chahal, J.; Han, J.; Shi, Y.; Sadtler, K.; Gao, W.; Lin, J.; Doloff, J. C.; Langer, R.; Anderson, D. G., Delivery of mRNA vaccines with heterocyclic lipids increases anti-tumor efficacy by STING-mediated immune cell activation. *Nature Biotechnology* **2019**, *37* (10), 1174-1185.
17. Klichinsky, M.; Ruella, M.; Shestova, O.; Lu, X. M.; Best, A.; Zeeman, M.; Schmierer, M.; Gabrusiewicz, K.; Anderson, N. R.; Petty, N. E.; Cummins, K. D.; Shen, F.; Shan, X.; Veliz, K.; Blouch, K.; Yashiro-Ohtani, Y.; Kenderian, S. S.; Kim, M. Y.; O'Connor, R. S.; Wallace, S. R.;

- Kozlowski, M. S.; Marchione, D. M.; Shestov, M.; Garcia, B. A.; June, C. H.; Gill, S., Human chimeric antigen receptor macrophages for cancer immunotherapy. *Nature Biotechnology* **2020**, *38* (8), 947-953.
18. Richner, J. M.; Himansu, S.; Dowd, K. A.; Butler, S. L.; Salazar, V.; Fox, J. M.; Julander, J. G.; Tang, W. W.; Shresta, S.; Pierson, T. C.; Ciaramella, G.; Diamond, M. S., Modified mRNA Vaccines Protect against Zika Virus Infection. *Cell* **2017**, *168* (6), 1114-1125.e10.
19. Pardi, N.; Hogan, M. J.; Pelc, R. S.; Muramatsu, H.; Andersen, H.; DeMaso, C. R.; Dowd, K. A.; Sutherland, L. L.; Scarce, R. M.; Parks, R.; Wagner, W.; Granados, A.; Greenhouse, J.; Walker, M.; Willis, E.; Yu, J.-S.; McGee, C. E.; Sempowski, G. D.; Mui, B. L.; Tam, Y. K.; Huang, Y.-J.; Vanlandingham, D.; Holmes, V. M.; Balachandran, H.; Sahu, S.; Lifton, M.; Higgs, S.; Hensley, S. E.; Madden, T. D.; Hope, M. J.; Karikó, K.; Santra, S.; Graham, B. S.; Lewis, M. G.; Pierson, T. C.; Haynes, B. F.; Weissman, D., Zika virus protection by a single low-dose nucleoside-modified mRNA vaccination. *Nature* **2017**, *543* (7644), 248-251.
20. VanBlargan, L. A.; Himansu, S.; Foreman, B. M.; Ebel, G. D.; Pierson, T. C.; Diamond, M. S., An mRNA Vaccine Protects Mice against Multiple Tick-Transmitted Flavivirus Infections. *Cell Reports* **2018**, *25* (12), 3382-3392.e3.
21. Pardi, N.; Secreto, A. J.; Shan, X.; Debonera, F.; Glover, J.; Yi, Y.; Muramatsu, H.; Ni, H.; Mui, B. L.; Tam, Y. K.; Shaheen, F.; Collman, R. G.; Karikó, K.; Danet-Desnoyers, G. A.; Madden, T. D.; Hope, M. J.; Weissman, D., Administration of nucleoside-modified mRNA encoding broadly neutralizing antibody protects humanized mice from HIV-1 challenge. *Nature Communications* **2017**, *8* (1), 14630.
22. Pardi, N.; LaBranche, C. C.; Ferrari, G.; Cain, D. W.; Tombácz, I.; Parks, R. J.; Muramatsu, H.; Mui, B. L.; Tam, Y. K.; Karikó, K.; Polacino, P.; Barbosa, C. J.; Madden, T. D.; Hope, M. J.; Haynes, B. F.; Montefiori, D. C.; Hu, S.-L.; Weissman, D., Characterization of HIV-1 Nucleoside-Modified mRNA Vaccines in Rabbits and Rhesus Macaques. *Molecular Therapy - Nucleic Acids* **2019**, *15*, 36-47.
23. Pardi, N.; Parkhouse, K.; Kirkpatrick, E.; McMahon, M.; Zost, S. J.; Mui, B. L.; Tam, Y. K.; Karikó, K.; Barbosa, C. J.; Madden, T. D.; Hope, M. J.; Krammer, F.; Hensley, S. E.; Weissman, D., Nucleoside-modified mRNA immunization elicits influenza virus hemagglutinin stalk-specific antibodies. *Nature Communications* **2018**, *9* (1), 3361.
24. Freyn, A. W.; Ramos da Silva, J.; Rosado, V. C.; Bliss, C. M.; Pine, M.; Mui, B. L.; Tam, Y. K.; Madden, T. D.; de Souza Ferreira, L. C.; Weissman, D.; Krammer, F.; Coughlan, L.; Palese, P.; Pardi, N.; Nachbagauer, R., A Multi-Targeting, Nucleoside-Modified mRNA Influenza Virus Vaccine Provides Broad Protection in Mice. *Molecular Therapy* **2020**, *28* (7), 1569-1584.
25. Bahl, K.; Senn, J. J.; Yuzhakov, O.; Bulychev, A.; Brito, L. A.; Hassett, K. J.; Laska, M. E.; Smith, M.; Almarsson, Ö.; Thompson, J.; Ribeiro, A.; Watson, M.; Zaks, T.; Ciaramella, G., Preclinical and Clinical Demonstration of Immunogenicity by mRNA Vaccines against H10N8 and H7N9 Influenza Viruses. *Molecular Therapy* **2017**, *25* (6), 1316-1327.
26. Patel, S.; Ashwanikumar, N.; Robinson, E.; Xia, Y.; Mihai, C.; Griffith, J. P.; Hou, S.; Esposito, A. A.; Ketova, T.; Welscher, K.; Joyal, J. L.; Almarsson, Ö.; Sahay, G., Naturally-occurring cholesterol analogues in lipid nanoparticles induce polymorphic shape and enhance intracellular delivery of mRNA. *Nature Communications* **2020**, *11* (1), 983.
27. Kulkarni, J. A.; Witzigmann, D.; Leung, J.; van der Meel, R.; Zaifman, J.; Darjuan, M. M.; Grisch-Chan, H. M.; Thöny, B.; Tam, Y. Y. C.; Cullis, P. R., Fusion-dependent formation of lipid nanoparticles containing macromolecular payloads. *Nanoscale* **2019**, *11* (18), 9023-9031.
28. Love, K. T.; Mahon, K. P.; Levins, C. G.; Whitehead, K. A.; Querbes, W.; Dorkin, J. R.; Qin, J.; Cantley, W.; Qin, L. L.; Racie, T.; Frank-Kamenetsky, M.; Yip, K. N.; Alvarez, R.; Sah, D. W. Y.; de Fogerolles, A.; Fitzgerald, K.; Koteliensky, V.; Akinc, A.; Langer, R.; Anderson, D. G., Lipid-like materials

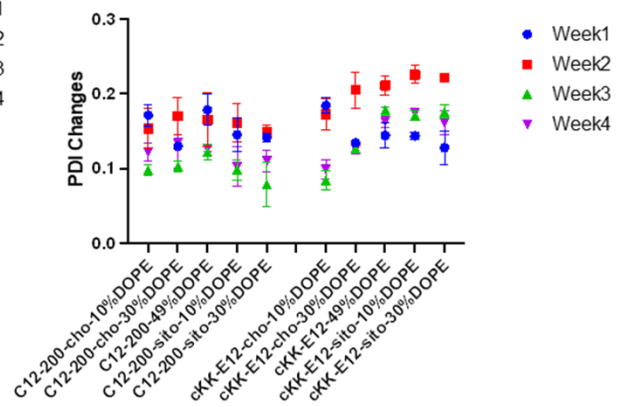
- for low-dose, in vivo gene silencing. *Proceedings of the National Academy of Sciences* **2010**, *107* (5), 1864-1869.
29. Dong, Y.; Love, K. T.; Dorkin, J. R.; Sirirungruang, S.; Zhang, Y.; Chen, D.; Bogorad, R. L.; Yin, H.; Chen, Y.; Vegas, A. J.; Alabi, C. A.; Sahay, G.; Olejnik, K. T.; Wang, W.; Schroeder, A.; Lytton-Jean, A. K. R.; Siegwart, D. J.; Akinc, A.; Barnes, C.; Barros, S. A.; Carioto, M.; Fitzgerald, K.; Hettinger, J.; Kumar, V.; Novobrantseva, T. I.; Qin, J.; Querbes, W.; Kotliansky, V.; Langer, R.; Anderson, D. G., Lipopeptide nanoparticles for potent and selective siRNA delivery in rodents and nonhuman primates. *Proceedings of the National Academy of Sciences* **2014**, *111* (11), 3955-3960.
30. Kauffman, K. J.; Dorkin, J. R.; Yang, J. H.; Heartlein, M. W.; DeRosa, F.; Mir, F. F.; Fenton, O. S.; Anderson, D. G., Optimization of Lipid Nanoparticle Formulations for mRNA Delivery in Vivo with Fractional Factorial and Definitive Screening Designs. *Nano Letters* **2015**, *15* (11), 7300-7306.
31. Pattipeiluhu, R.; Arias-Alpizar, G.; Basha, G.; Chan, K. Y. T.; Bussmann, J.; Sharp, T. H.; Moradi, M. A.; Sommerdijk, N.; Harris, E. N.; Cullis, P. R.; Kros, A.; Witzigmann, D.; Campbell, F., Anionic Lipid Nanoparticles Preferentially Deliver mRNA to the Hepatic Reticuloendothelial System. *Adv Mater* **2022**, *34* (16), e2201095.
32. Hafez, I. M.; Cullis, P. R., Roles of lipid polymorphism in intracellular delivery. *Advanced Drug Delivery Reviews* **2001**, *47* (2), 139-148.
33. Koltover, I.; Salditt, T.; Rädler, J. O.; Safinya, C. R., An Inverted Hexagonal Phase of Cationic Liposome-DNA Complexes Related to DNA Release and Delivery. *Science* **1998**, *281* (5373), 78-81.
34. Trinchieri, G., Interleukin-12 and the regulation of innate resistance and adaptive immunity. *Nature Reviews Immunology* **2003**, *3* (2), 133-146.
35. O'Sullivan, D.; Pearce, E. L., Expanding the role of metabolism in T cells. *Science* **2015**, *348* (6238), 976-977.
36. Appay, V.; Douek, D. C.; Price, D. A., CD8<sup>+</sup> T cell efficacy in vaccination and disease. *Nature Medicine* **2008**, *14* (6), 623-628.
37. Zhang, N.; Bevan, Michael J., CD8<sup>+</sup> T Cells: Foot Soldiers of the Immune System. *Immunity* **2011**, *35* (2), 161-168.
38. Laidlaw, B. J.; Craft, J. E.; Kaech, S. M., The multifaceted role of CD4(+) T cells in CD8(+) T cell memory. *Nat Rev Immunol* **2016**, *16* (2), 102-111.
39. Boyman, O.; Kovar, M.; Rubinstein, M. P.; Surh, C. D.; Sprent, J., Selective Stimulation of T Cell Subsets with Antibody-Cytokine Immune Complexes. *Science* **2006**, *311* (5769), 1924-1927.
40. Abbas, A. K.; Trotta, E.; R. Simeonov, D.; Marson, A.; Bluestone, J. A., Revisiting IL-2: Biology and therapeutic prospects. *Science Immunology* **2018**, *3* (25), eaat1482.
41. Pipkin, M. E.; Sacks, J. A.; Cruz-Guilloty, F.; Lichtenheld, M. G.; Bevan, M. J.; Rao, A., Interleukin-2 and Inflammation Induce Distinct Transcriptional Programs that Promote the Differentiation of Effector Cytolytic T Cells. *Immunity* **2010**, *32* (1), 79-90.

# Supporting Information

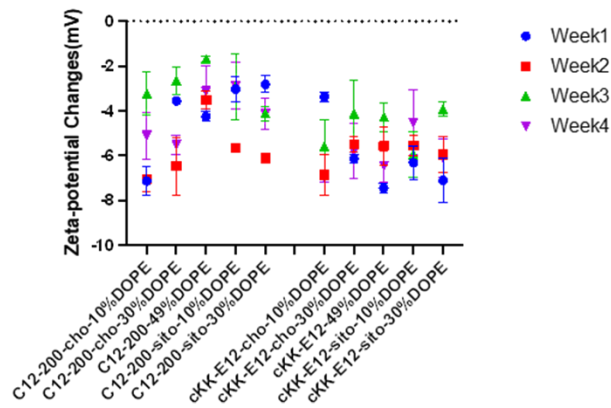
**a**



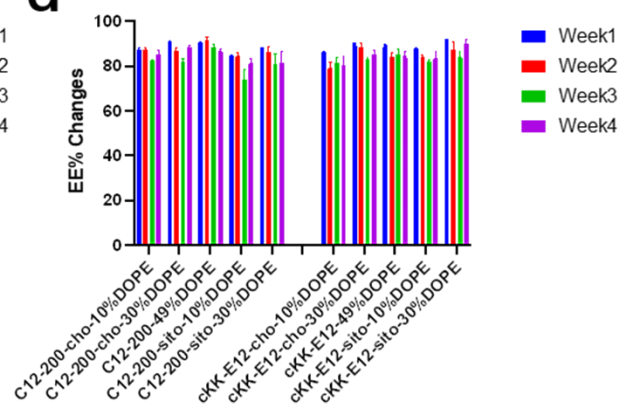
**b**



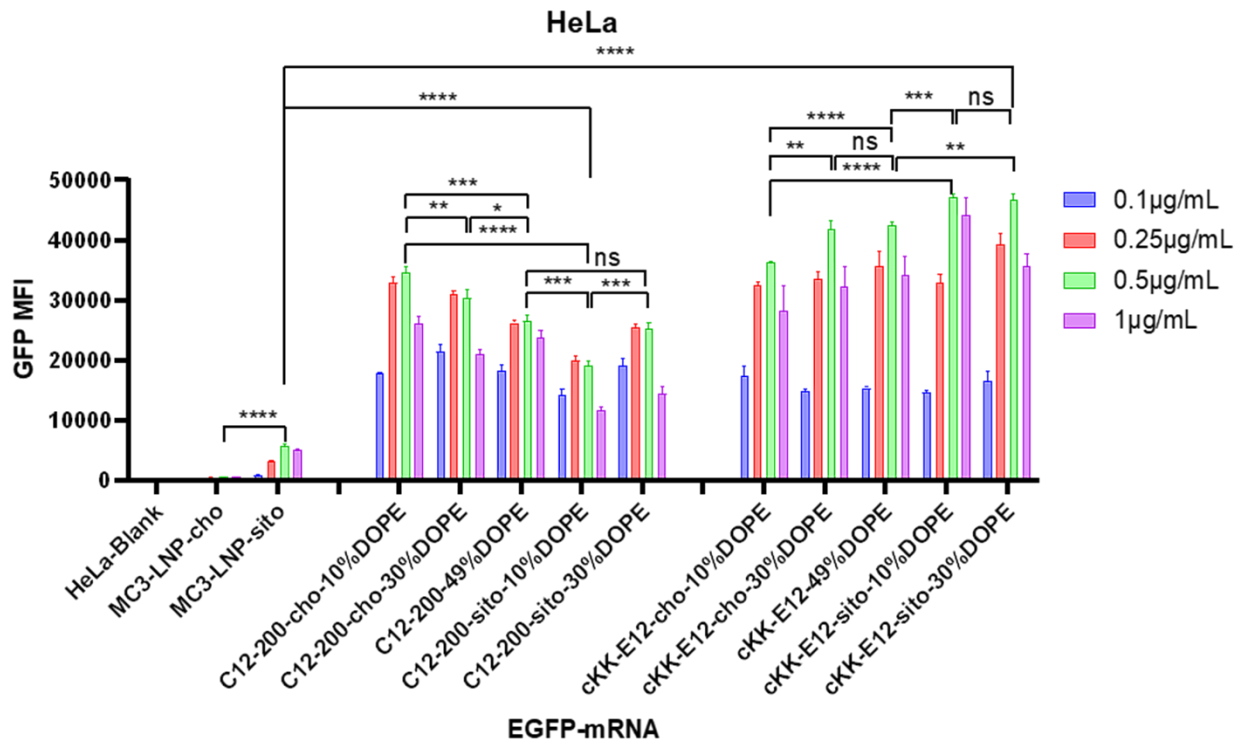
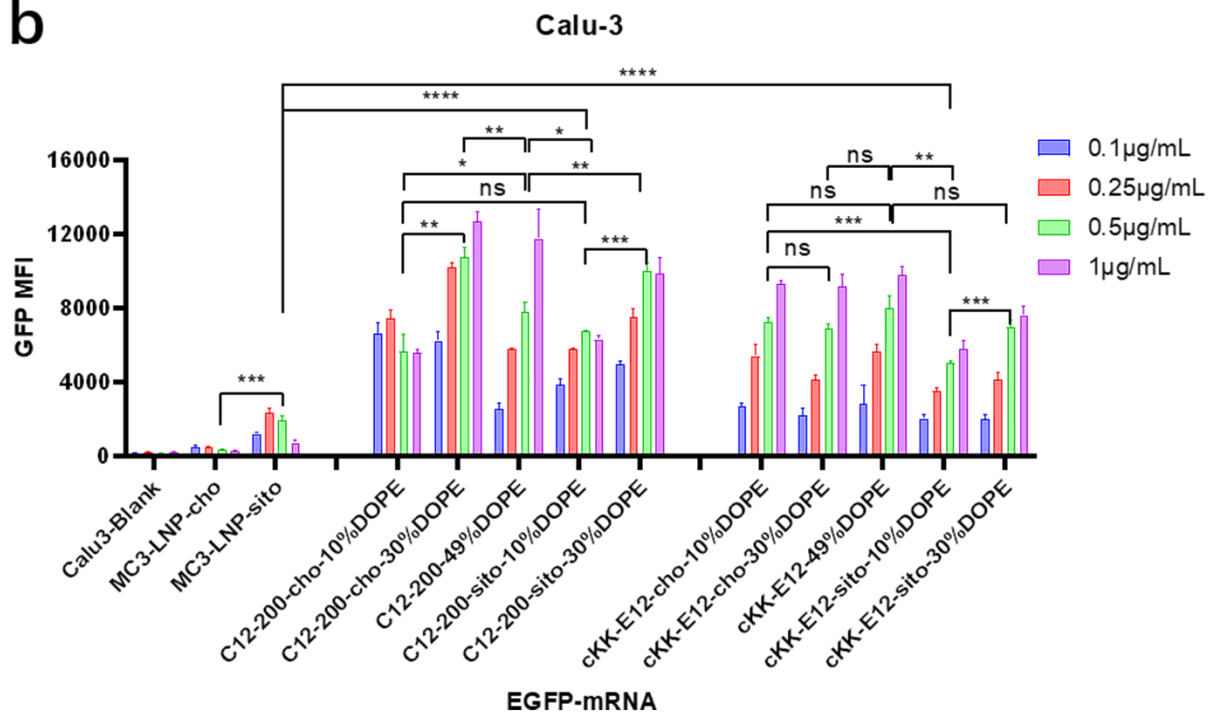
**c**



**d**

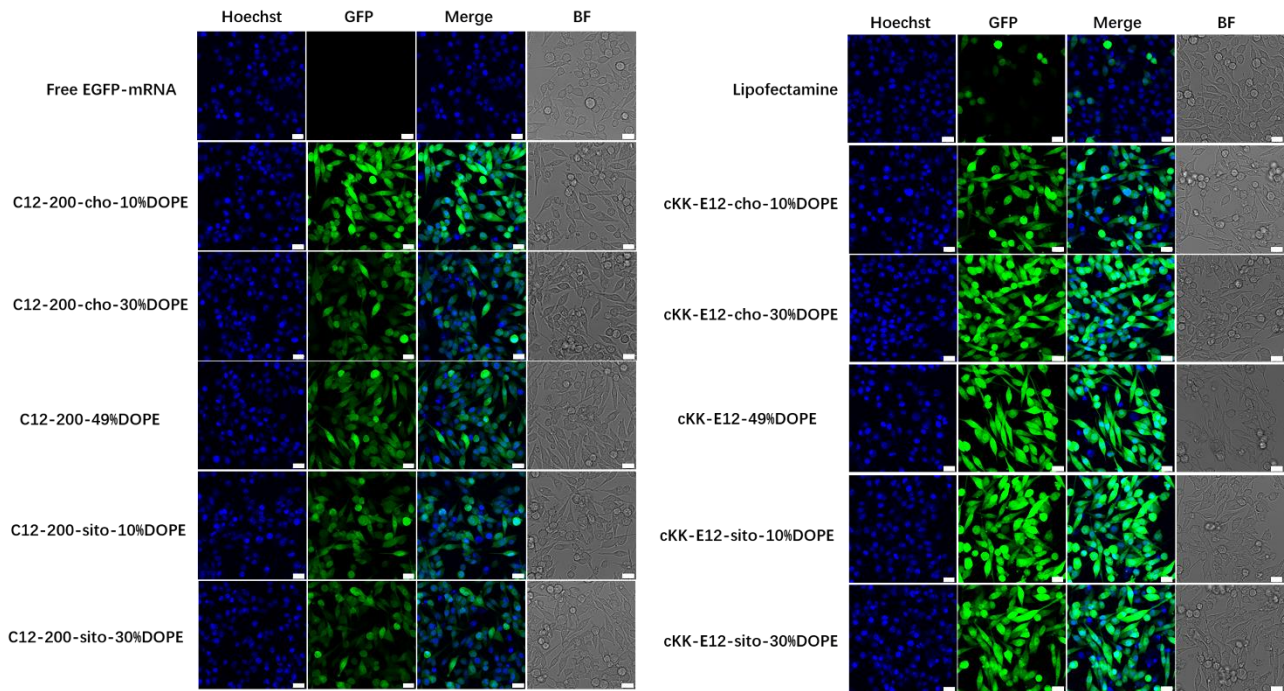


**SI Figure 1.** Stability of LNPs (stored at 4°C). **(a)** Sizes changes, **(b)** PDI changes, **(c)** Zeta potential changes, **(d)** Encapsulation efficiency changes of LNPs over 1 month.

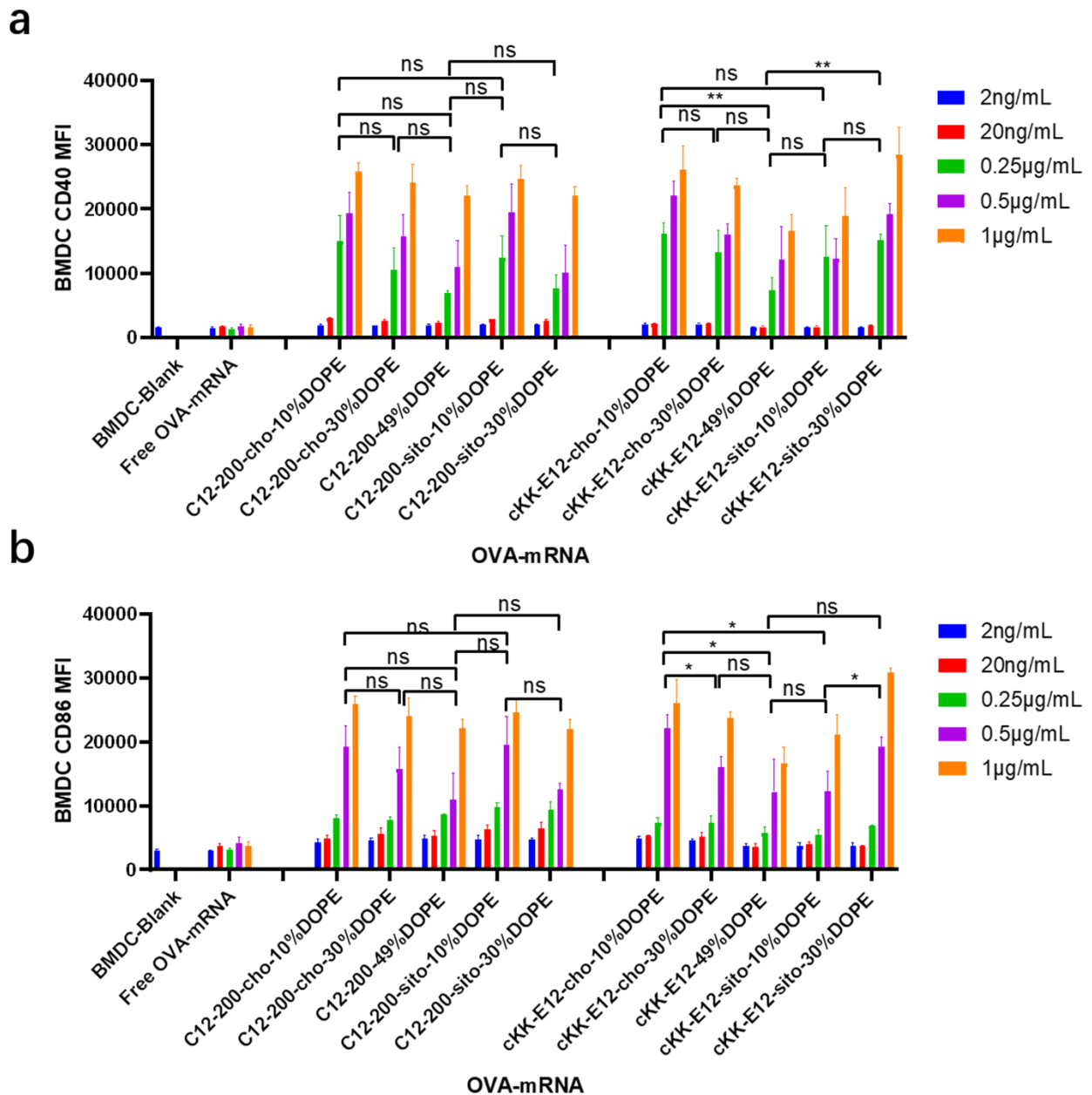
**a****b**

**SI Figure 2.** Transfection efficiency (mean fluorescence intensity, MFI) after encapsulating EGFP-mRNA within (a) HeLa cells and (b) Calu-3 cells. Data are presented as mean  $\pm$  sd. Statistical significance was calculated by unpaired student t-test on 0.5  $\mu$ g/mL. (\*\*\*\*,  $P < 0.0001$ , \*\*\*,  $P < 0.001$ , \*\*,  $P < 0.01$ , \*,  $P < 0.05$ , ns, no significant difference,  $n = 3$ )

DC2.4



**SI Figure 3.** Confocal images of the EGFP-mRNA transfection of LNPs on DC2.4 cells (EGFP-mRNA, 1  $\mu\text{g}/\text{mL}$ , 24 h). Scale bar is 20  $\mu\text{m}$ .



**SI Figure 4.** The mean fluorescence intensities (MFI) of cellular marker CD40 (a) and CD86 (b) after BMDCs activation by the different concentrations of LNPs. Data are presented as mean  $\pm$  sd. Statistical significance was calculated by unpaired student t-test on 0.25  $\mu$ g/mL (a) and 0.5  $\mu$ g/mL (b). (\*\*\*\*,  $P < 0.0001$ , \*\*\*,  $P < 0.001$ , \*\*,  $P < 0.01$ , \*,  $P < 0.05$ , ns, no significant difference,  $n = 3$ )

## Chapter 6

### Summary and Outlook

Nowadays, countless patients are struggling with genetic dysregulation-based diseases, such as cancer,<sup>1</sup> peripheral arterial disease,<sup>2</sup> hyperlipoproteinemia type I,<sup>3</sup> beta-thalassemia,<sup>4, 5</sup> adenosine deaminase-deficiency,<sup>6</sup> spinal muscular atrophy,<sup>7</sup> optic atrophy,<sup>8</sup> and polyneuropathy of hereditary transthyretin-mediated amyloidosis.<sup>9</sup> Furthermore, viruses are the cause of infectious diseases such as Zika,<sup>10, 11</sup> MERS,<sup>12</sup> Ebola,<sup>13</sup> influenzas,<sup>14, 15</sup> and SARS-CoV-2.<sup>16</sup> Multidisciplinary efforts between biologists, clinicians, engineers, and physical and chemical scientists are required to develop novel therapeutic strategies to treat these diseases at the transcriptional and translational level.<sup>17</sup>

To date, small molecule and recombinant protein-based drugs have been the focus of translational research with much successful medicine in clinical use. However, they also exhibit their own benefits and limitations. The inherent limitation of small molecule drugs is that they require a high systemic exposure to ensure sufficient therapeutic efficacy with the risk of potential off-target side effects.<sup>18, 19</sup> Recombinant protein-based drugs are investigated in protein replacement therapy (*e.g.* insulin to manage diabetes) and chemotherapeutic antibodies (*e.g.* checkpoint inhibitors to treat cancer). However, due to the high molecular weight and polarity of recombinant proteins, typically they cannot enter cells limiting their therapeutic effect.<sup>20</sup>

Nucleic acid-based therapeutics offer the opportunity to address a wide range of diseases at the transcriptional and translational level, and potentially to address the root cause of disease at the genetic level.<sup>21-23</sup> Nucleic acid-based therapeutics include short interfering RNA (siRNA), microRNA (miRNA), antisense oligonucleotides (ASO), and messenger RNA (mRNA). Depending on the type of RNA used, the therapeutic outcome ranges from gene knockdown to induced expression of a selected target protein with minimal adverse effects.<sup>23</sup> Among these RNA-based drugs, mRNA has become a promising therapeutic for many applications, including vaccine development for infectious disease,<sup>10, 11, 14, 16</sup> HIV,<sup>24</sup> and cancer,<sup>25</sup> and tissue regeneration to enhance wound healing or repair damaged organs and tissue.<sup>26-29</sup> Significant research has been devoted to the development of nanocarriers to overcome the delivery problem of mRNA. To date, lipid nanoparticles (LNPs) represent the most successful mRNA delivery vector, as evidenced by the clinical approvals of two LNP formulations, Pfizer's BNT162b2 and Moderna's mRNA-1273.<sup>30-32</sup> Their success is partly due to their unique properties, such as simple chemical synthesis of lipid components, scalable manufacturing processes of LNPs, and wide packaging capability.<sup>33</sup> However, their transfection performance is still hampered by endo/lysosomal escape efficiency, as only a small fraction of mRNA (<5%) was reported to reach the cytoplasm resulting in protein expression.<sup>34</sup>

In this thesis strategies to enhance the delivery efficiency of mRNA and drugs using LNPs and liposomes as the nanocarrier are described. Fusogenic coiled-coil peptides were introduced in LNPs and liposomes and the effect on mRNA/drug delivery in different cell lines was studied.

Inspired by SNARE proteins, we have previously shown that the coiled-coil peptide pair K4/E4 triggers efficient membrane fusion between liposomes and cells, facilitating efficient delivery of drugs into cells.<sup>35-37</sup> In **Chapter 2**, the fusogenic coiled-coil peptides were introduced into common LNP formulations to enhance mRNA transfection efficacy. The Onpattro LNP formulation was modified with lipopeptide CPE4, and the addition of CPE4 did not change the physicochemical characteristics of the nanoparticles nor the mRNA encapsulation efficiency. By employing confocal imaging and flow cytometry analysis, the cellular internalization efficiency was measured. It was shown that the coiled-coil peptides enhanced LNP uptake by 63-fold resulting in enhanced protein expression. Furthermore, mechanistic studies revealed that the major pathway for cell uptake was via membrane fusion thereby omitting the less efficient endocytosis pathways. This substantial transfection efficiency improvement after modification of the LNP with coiled-coil peptides can be applied to other cell types, including hard to transfect cell lines (*e.g.* T cells) required for T-cell therapy.

Our group has shown that efficient liposomal delivery could be achieved using coiled-coil peptides.<sup>35-37</sup> In **Chapter 3** the effect of peptide K dimerization on membrane fusion was investigated. Three different dimer designs were synthesized and their structural differences were characterized. Confocal microscopy and flow cytometry measurements showed that PK4 induced the highest binding affinity for cells pretreated with CPE4. Cellular uptake efficiency and the pharmacological effect of the antitumor drug doxorubicin was studied next. Liposome-cell fusion was efficient for this dimer as compared to the linear dimer designs and the benchmark peptide monomer. Thus the novel peptide dimer design is able to deliver drugs into cells more efficiently and will be tested in an *in vivo* setting in the future.

We have shown that fusogenic coiled-coil peptide modified LNPs deliver RNA more efficiently to cells as compared to LNPs. In **Chapter 4** the delivery of mRNA into cardiomyocytes was explored. Myocardial infarction (MI) has been the leading death cause in heart diseases since the human heart cardiomyocytes have a very limited regenerative capacity after MI, the injured cardiac cells only rely on scar tissue replacement to maintain organ integrity.<sup>38</sup> Cardiomyocytes derived from induced pluripotent stem cells (iPSC-CMs) represent the best cell source for human cardiac disorders and cardiac regeneration but require efficient transfection. A novel incubation protocol was developed to transfect these cells. mRNA transfection efficiency of different incubation protocols was compared, and the 1-step incubation protocol achieved improved mRNA transfection with an optimal CPK4:CPE4 ratio of 1:1. The mRNA transfection enhancement using 1-step incubation was compared for three clinically approved LNP formulations and observed that transfection was independent of LNP composition. In all cases the introduction of the fusogenic coiled-coil peptides significantly improved mRNA expression in iPSC-CMs. This optimized mRNA delivery platform could be very promising for further *in vivo* cardiomyocyte research towards the treatment of MI.

mRNA-LNPs are the current state-of-the-art in mRNA vaccination approach since the approval of the Covid-19 mRNA vaccines. In **Chapter 5**, we evaluated the influence of LNP lipid composition on the T cell immune response towards the development of cancer vaccines. In this study we varied the exact lipid composition by varying the ionizable lipid (IL), cholesterol (derivative) and the percentage of the fusogenic helper lipid DOPE. A small library of LNPs was evaluated on the ability to transfect bone marrow-derived dendritic cells, antigen presentation, and T cell stimulation responses. We studied whether replacing cholesterol by  $\beta$ -sitosterol and/or DOPE would boost mRNA

transfection resulting in an enhanced immune response. It was shown that the introduction of  $\beta$ -sitosterol only exerted enhanced transfection in LNPs when MC3 was used as the IL, while exhibiting varied transfection efficiency effects on different cell lines when C12-200 and cKK-E12 were used as the IL. Replacing cholesterol with DOPE resulted in mixed mRNA transfection efficiencies in different cell types. We demonstrated that the LNP-mRNA vaccine candidates can generate significant activation of BMDCs as evidenced by the upregulation of the co-stimulatory receptors (CD40 and CD86] and IL-12 expression, robust T cell proliferation, and enhanced cytokine production *ex vivo*.

We have shown fusogenic coiled-coil peptides enhance mRNA delivery using LNPs in multiple cell lines, including hard to transfect Jurkat cells and cardiomyocytes *in vitro*. However, sometimes the *in vitro* results do not translate to *in vivo* performance, further *in vivo* investigations are therefore required to validate the presented findings. Currently, *in vivo* studies using local injection of mice cardiomyocytes are in progress and will give insight in the ability to treat MI. The second open question is that after delivering mRNA, will it have a relevant therapeutic effect in a mice model? The presented mRNA delivery system based on coiled-coil peptides and LNPs is most likely suitable for local administration, while systemic (intravenous) administration might be more complex. Dimerization of peptide K4 resulted in an enhanced drug delivery efficiency, but the used incubation protocol needs to be also studied in a relevant *in vivo* model to truly validate its usefulness.

In this thesis, we successfully used fusogenic coiled-coil peptides to deliver low molecular weight drugs (*e.g.* doxorubicin) and macromolecular mRNA. This resulted in an enhanced antitumor effect and significantly increased the mRNA transfection efficiency compared to state of the art and clinically approved liposome/LNP formulations. This work further simplified the incubation protocol of our coiled-coil peptide modified LNP system resulting in the successful transfection of cardiomyocytes, which holds great promise for heart regeneration therapy after myocardial infarction. Finally, LNP-mRNA candidates that elicit potent BMDC activation and T cell proliferation were identified and can be used in the development of future candidate cancer vaccines. I hope this work will contribute to the mRNA delivery technology with enhanced *in vitro* and *in vivo* therapeutic performance and potent protective immunity against cancer.

## References

1. Saadatpour, Z.; Bjorklund, G.; Chirumbolo, S.; Alimohammadi, M.; Ehsani, H.; Ebrahiminejad, H.; Pourghadamyari, H.; Baghaei, B.; Mirzaei, H.; Sahebkar, A., Molecular imaging and cancer gene therapy. *Cancer gene therapy* **2016**, 1-5.
2. Ouriel, K., Peripheral arterial disease. *The Lancet* **2001**, 358 (9289), 1257-1264.
3. Vogt, A., Hyperlipoproteinaemia(a) – apheresis and emerging therapies. *Clinical Research in Cardiology Supplements* **2017**, 12 (1), 12-17.
4. Jessup, M.; Greenberg, B.; Mancini, D.; Cappola, T.; Pauly, D. F.; Jaski, B.; Yaroshinsky, A.; Zsebo, K. M.; Dittrich, H.; Hajjar, R. J., Calcium Upregulation by Percutaneous Administration of Gene Therapy in Cardiac Disease (CUPID). *Circulation* **2011**, 124 (3), 304-313.
5. Jaski, B. E.; Jessup, M. L.; Mancini, D. M.; Cappola, T. P.; Pauly, D. F.; Greenberg, B.; Borow, K.; Dittrich, H.; Zsebo, K. M.; Hajjar, R. J., Calcium Upregulation by Percutaneous Administration of Gene Therapy

- in Cardiac Disease (CUPID Trial), a First-in-Human Phase 1/2 Clinical Trial. *Journal of Cardiac Failure* **2009**, *15* (3), 171-181.
6. Kang, Z.; Ding, G.; Meng, Z.; Meng, Q., The rational design of cell-penetrating peptides for application in delivery systems. *Peptides* **2019**, *121*, 170149.
  7. d'Ydewalle, C.; Sumner, C. J., Spinal Muscular Atrophy Therapeutics: Where do we Stand? *Neurotherapeutics* **2015**, *12* (2), 303-316.
  8. Deverman, B. E.; Ravina, B. M.; Bankiewicz, K. S.; Paul, S. M.; Sah, D. W. Y., Gene therapy for neurological disorders: progress and prospects. *Nature Reviews Drug Discovery* **2018**, *17* (9), 641-659.
  9. Wang, F.; Qin, Z.; Lu, H.; He, S.; Luo, J.; Jin, C.; Song, X., Clinical translation of gene medicine. *The Journal of Gene Medicine* **2019**, *21* (7), e3108.
  10. Richner, J. M.; Himansu, S.; Dowd, K. A.; Butler, S. L.; Salazar, V.; Fox, J. M.; Julander, J. G.; Tang, W. W.; Shrestha, S.; Pierson, T. C.; Ciaramella, G.; Diamond, M. S., Modified mRNA Vaccines Protect against Zika Virus Infection. *Cell* **2017**, *168* (6), 1114-1125.e10.
  11. Pardi, N.; Hogan, M. J.; Pelc, R. S.; Muramatsu, H.; Andersen, H.; DeMaso, C. R.; Dowd, K. A.; Sutherland, L. L.; Scarce, R. M.; Parks, R.; Wagner, W.; Granados, A.; Greenhouse, J.; Walker, M.; Willis, E.; Yu, J.-S.; McGee, C. E.; Sempowski, G. D.; Mui, B. L.; Tam, Y. K.; Huang, Y.-J.; Vanlandingham, D.; Holmes, V. M.; Balachandran, H.; Sahu, S.; Lifton, M.; Higgs, S.; Hensley, S. E.; Madden, T. D.; Hope, M. J.; Karikó, K.; Santra, S.; Graham, B. S.; Lewis, M. G.; Pierson, T. C.; Haynes, B. F.; Weissman, D., Zika virus protection by a single low-dose nucleoside-modified mRNA vaccination. *Nature* **2017**, *543* (7644), 248-251.
  12. Wang, L.; Shi, W.; Joyce, M. G.; Modjarrad, K.; Zhang, Y.; Leung, K.; Lees, C. R.; Zhou, T.; Yassine, H. M.; Kanekiyo, M.; Yang, Z.-y.; Chen, X.; Becker, M. M.; Freeman, M.; Vogel, L.; Johnson, J. C.; Olinger, G.; Todd, J. P.; Bagci, U.; Solomon, J.; Mollura, D. J.; Hensley, L.; Jahrling, P.; Denison, M. R.; Rao, S. S.; Subbarao, K.; Kwong, P. D.; Mascola, J. R.; Kong, W.-P.; Graham, B. S., Evaluation of candidate vaccine approaches for MERS-CoV. *Nature Communications* **2015**, *6* (1), 7712.
  13. Donoff, B.; McDonough Je Fau - Riedy, C. A.; Riedy, C. A., Integrating oral and general health care. (1533-4406 (Electronic)).
  14. Petsch, B.; Schnee, M.; Vogel, A. B.; Lange, E.; Hoffmann, B.; Voss, D.; Schlake, T.; Thess, A.; Kallen, K.-J.; Stitz, L.; Kramps, T., Protective efficacy of in vitro synthesized, specific mRNA vaccines against influenza A virus infection. *Nature Biotechnology* **2012**, *30* (12), 1210-1216.
  15. Ping, J.; Lopes, T. J. S.; Nidom, C. A.; Ghedin, E.; Macken, C. A.; Fitch, A.; Imai, M.; Maher, E. A.; Neumann, G.; Kawaoka, Y., Development of high-yield influenza A virus vaccine viruses. *Nature Communications* **2015**, *6* (1), 8148.
  16. Zhang, N.-N.; Li, X.-F.; Deng, Y.-Q.; Zhao, H.; Huang, Y.-J.; Yang, G.; Huang, W.-J.; Gao, P.; Zhou, C.; Zhang, R.-R.; Guo, Y.; Sun, S.-H.; Fan, H.; Zu, S.-L.; Chen, Q.; He, Q.; Cao, T.-S.; Huang, X.-Y.; Qiu, H.-Y.; Nie, J.-H.; Jiang, Y.; Yan, H.-Y.; Ye, Q.; Zhong, X.; Xue, X.-L.; Zha, Z.-Y.; Zhou, D.; Yang, X.; Wang, Y.-C.; Ying, B.; Qin, C.-F., A Thermostable mRNA Vaccine against COVID-19. *Cell* **2020**, *182* (5), 1271-1283.e16.
  17. Fenton, O. S.; Olafson, K. N.; Pillai, P. S.; Mitchell, M. J.; Langer, R., Advances in Biomaterials for Drug Delivery. *Advanced Materials* **2018**, *30* (29), 1705328.
  18. Toure, M.; Crews, C. M., Small-Molecule PROTACS: New Approaches to Protein Degradation. *Angewandte Chemie International Edition* **2016**, *55* (6), 1966-1973.
  19. Lomenick, B.; Olsen, R. W.; Huang, J., Identification of Direct Protein Targets of Small Molecules. *ACS Chemical Biology* **2011**, *6* (1), 34-46.
  20. Stewart, M. P.; Langer, R.; Jensen, K. F., Intracellular Delivery by Membrane Disruption: Mechanisms,

Strategies, and Concepts. *Chemical Reviews* **2018**, *118* (16), 7409-7531.

21. Kaczmarek, J. C.; Kowalski, P. S.; Anderson, D. G., Advances in the delivery of RNA therapeutics: from concept to clinical reality. *Genome Medicine* **2017**, *9* (1), 60.
22. Kole, R.; Krainer, A. R.; Altman, S., RNA therapeutics: beyond RNA interference and antisense oligonucleotides. *Nature Reviews Drug Discovery* **2012**, *11* (2), 125-140.
23. Gupta, A.; Andresen, J. L.; Manan, R. S.; Langer, R., Nucleic acid delivery for therapeutic applications. *Advanced Drug Delivery Reviews* **2021**, *178*, 113834.
24. Pardi, N.; LaBranche, C. C.; Ferrari, G.; Cain, D. W.; Tombácz, I.; Parks, R. J.; Muramatsu, H.; Mui, B. L.; Tam, Y. K.; Karikó, K.; Polacino, P.; Barbosa, C. J.; Madden, T. D.; Hope, M. J.; Haynes, B. F.; Montefiori, D. C.; Hu, S.-L.; Weissman, D., Characterization of HIV-1 Nucleoside-Modified mRNA Vaccines in Rabbits and Rhesus Macaques. *Molecular Therapy - Nucleic Acids* **2019**, *15*, 36-47.
25. Irvine, D. J.; Dane, E. L., Enhancing cancer immunotherapy with nanomedicine. *Nature Reviews Immunology* **2020**, *20* (5), 321-334.
26. DeRosa, F.; Guild, B.; Karve, S.; Smith, L.; Love, K.; Dorkin, J. R.; Kauffman, K. J.; Zhang, J.; Yahalom, B.; Anderson, D. G.; Heartlein, M. W., Therapeutic efficacy in a hemophilia B model using a biosynthetic mRNA liver depot system. *Gene Therapy* **2016**, *23* (10), 699-707.
27. Ramaswamy, S.; Tonnu, N.; Tachikawa, K.; Limphong, P.; Vega, J. B.; Karmali, P. P.; Chivukula, P.; Verma, I. M., Systemic delivery of factor IX messenger RNA for protein replacement therapy. *Proceedings of the National Academy of Sciences* **2017**, *114* (10), E1941-E1950.
28. Zangi, L.; Lui, K. O.; von Gise, A.; Ma, Q.; Ebina, W.; Ptaszek, L. M.; Später, D.; Xu, H.; Tabebordbar, M.; Gorbатов, R.; Sena, B.; Nahrendorf, M.; Briscoe, D. M.; Li, R. A.; Wagers, A. J.; Rossi, D. J.; Pu, W. T.; Chien, K. R., Modified mRNA directs the fate of heart progenitor cells and induces vascular regeneration after myocardial infarction. *Nature Biotechnology* **2013**, *31* (10), 898-907.
29. Hou, X.; Zhang, X.; Zhao, W.; Zeng, C.; Deng, B.; McComb, D. W.; Du, S.; Zhang, C.; Li, W.; Dong, Y., Vitamin lipid nanoparticles enable adoptive macrophage transfer for the treatment of multidrug-resistant bacterial sepsis. *Nature Nanotechnology* **2020**, *15* (1), 41-46.
30. Hou, X.; Zaks, T.; Langer, R.; Dong, Y., Lipid nanoparticles for mRNA delivery. *Nature Reviews Materials* **2021**, *6* (12), 1078-1094.
31. Wang, C.; Zhang, Y.; Dong, Y., Lipid Nanoparticle–mRNA Formulations for Therapeutic Applications. *Accounts of Chemical Research* **2021**, *54* (23), 4283-4293.
32. Meyer, R. A.; Neshat, S. Y.; Green, J. J.; Santos, J. L.; Tuesca, A. D., Targeting strategies for mRNA delivery. *Materials Today Advances* **2022**, *14*, 100240.
33. Zhang, Y.; Sun, C.; Wang, C.; Jankovic, K. E.; Dong, Y., Lipids and Lipid Derivatives for RNA Delivery. *Chemical Reviews* **2021**, *121* (20), 12181-12277.
34. Paramasivam, P.; Franke, C.; Stöter, M.; Höijer, A.; Bartesaghi, S.; Sabirsh, A.; Lindfors, L.; Arteta, M. Y.; Dahlén, A.; Bak, A.; Andersson, S.; Kalaidzidis, Y.; Bickle, M.; Zerial, M., Endosomal escape of delivered mRNA from endosomal recycling tubules visualized at the nanoscale. *Journal of Cell Biology* **2021**, *221* (2), e202110137.
35. Yang, J.; Bahreman, A.; Daudey, G.; Bussmann, J.; Olsthoorn, R. C. L.; Kros, A., Drug Delivery via Cell Membrane Fusion Using Lipopeptide Modified Liposomes. *ACS Central Science* **2016**, *2* (9), 621-630.
36. Yang, J.; Shimada, Y.; Olsthoorn, R. C. L.; Snaar-Jagalska, B. E.; Spaank, H. P.; Kros, A., Application of Coiled Coil Peptides in Liposomal Anticancer Drug Delivery Using a Zebrafish Xenograft Model. *ACS Nano* **2016**, *10* (8), 7428-7435.
37. Kong, L.; Askes, S. H. C.; Bonnet, S.; Kros, A.; Campbell, F., Temporal Control of Membrane Fusion through Photolabile PEGylation of Liposome Membranes. *Angewandte Chemie International Edition* **2016**, *55* (4),

1396-1400.

38. Yang, Q.; Fang, J.; Lei, Z.; Sluiter, J. P. G.; Schiffelers, R., Repairing the heart: State-of the art delivery strategies for biological therapeutics. *Advanced Drug Delivery Reviews* **2020**, *160*, 1-18.

## Nederlandse samenvatting

Tallose patiënten hebben nog steeds te maken met ziekten veroorzaakt door genetische disregulatie, zoals kanker,<sup>1</sup> perifere arteriële ziekten,<sup>2</sup> hyperlipoproteïnemie type I,<sup>3</sup> bèta-thalassemie,<sup>4, 5</sup> adenosinedeaminase-deficiëntie,<sup>6</sup> spinale musculaire atrofie,<sup>7</sup> optische atrofie,<sup>8</sup> en polyneuropathie van erfelijke transthyretine-gemedieerde amyloïdose.<sup>9</sup> Bovendien veroorzaken virussen infectieziekten zoals Zika,<sup>10, 11</sup> MERS,<sup>12</sup> Ebola,<sup>13</sup> influenza's,<sup>14, 15</sup> en SARS-CoV-2.<sup>16</sup> Multidisciplinaire samenwerking tussen biologen, klinici, ingenieurs en fysische en chemische wetenschappers moet tot nieuwe therapeutische strategieën leiden om deze ziekten op transcriptioneel en translationeel niveau te behandelen.<sup>17</sup>

Tot op heden zijn geneesmiddelen op basis van kleine moleculen en recombinante eiwitten de focus geweest van translationeel onderzoek met succesvolle medicijnen in klinisch gebruik. Ze hebben echter ook beperkingen. De inherente beperking van geneesmiddelen met kleine moleculen is dat ze een hoge systemische blootstelling vereisen om voldoende therapeutische werkzaamheid te garanderen met het risico op mogelijke bijwerkingen die niet op het doel gericht zijn.<sup>18, 19</sup> Recombinante geneesmiddelen op basis van eiwitten worden onderzocht bij eiwitvervangings therapie (bijv. diabetes) en chemotherapeutische antilichamen (bijv. checkpointremmers voor de behandeling van kanker). Vanwege het hoge molecuulgewicht en de polariteit van recombinante eiwitten kunnen ze echter meestal cellen niet goed binnendringen, waardoor hun therapeutisch effect wordt beperkt.<sup>20</sup>

Op nucleïnezuur gebaseerde therapieën bieden de mogelijkheid om een breed scala aan ziekten op transcriptioneel en translationeel niveau aan te pakken en mogelijk om de hoofdoorzaak van ziekten op genetisch niveau te behandelen.<sup>21-23</sup> Voorbeelden zijn microRNA (miRNA), antisense-oligonucleotiden (ASO) en messenger RNA (mRNA). Afhankelijk van het type RNA dat wordt gebruikt, varieert het therapeutische resultaat van het uitschakelen van genen tot geïnduceerde expressie van een geselecteerd doeleiwit met minimale bijwerkingen.<sup>23</sup> Van deze op RNA gebaseerde geneesmiddelen is mRNA een veelbelovend therapeutisch middel geworden voor veel toepassingen, waaronder de ontwikkeling van vaccins voor infectieziekten,<sup>10, 11, 14, 16</sup> HIV,<sup>24</sup> kanker,<sup>25</sup> en weefselregeneratie om wondgenezing te verbeteren of beschadigde organen en weefsel te herstellen.<sup>26-29</sup> Er is veel onderzoek gedaan naar de ontwikkeling van nanodeeltjes om het afleveringsprobleem van mRNA op te lossen. Tot op heden zijn lipid nanoparticles (LNP's) de meest succesvolle mRNA-afgiftevector, zoals blijkt uit de klinische goedkeuringen van twee LNP-formuleringen, Pfizer's BNT162b2 en Moderna's mRNA-1273.<sup>30-32</sup> Het succes is deels te danken aan hun unieke eigenschappen, zoals eenvoudige chemische synthese van lipidecomponenten, schaalbare productieprocessen van LNP's en de encapsulatie van verschillende vormen van RNA.<sup>33</sup> Hun transfectieprestaties worden echter nog steeds belemmerd door suboptimale endo/lysosomale ontsnappingsefficiëntie, aangezien slechts een kleine fractie van mRNA (<5%) het cytoplasma bereikt en resulterend in eiwitexpressie.

In dit proefschrift worden strategieën beschreven om de afgifte-efficiëntie van mRNA en geneesmiddelen te verbeteren met behulp van LNP's en liposomen als nanodrager. Fusogene coiled-coil peptiden werden geïntroduceerd in LNP's en liposomen en het effect op mRNA/medicijnafgifte in verschillende cellijnen werd bestudeerd.<sup>1</sup>

Geïnspireerd door SNARE-eiwitten hebben we eerder aangetoond dat het coiled-coil-peptidepaar K4/E4 efficiënte membraanfusie tussen liposomen en cellen induceert, wat een efficiënte afgifte van medicijnen in cellen mogelijk maakt.<sup>35-37</sup> In Hoofdstuk 2 werden de fusogene coiled-coil-peptiden geïntroduceerd in algemene LNP-formuleringen om de werkzaamheid van mRNA-transfectie te verbeteren. De Onpattro LNP-formulering werd gemodificeerd met lipopeptide CPE4 en de toevoeging van CPE4 veranderde de fysisch-chemische kenmerken van de nanodeeltjes noch de mRNA-inkapselingsefficiëntie. Door confocale microscopie en flowcytometrie-analyse toe te passen, werd de cellulaire internalisatie-efficiëntie gemeten. Er werd aangetoond dat de coiled-coil-peptiden de LNP-opname met een factor 63 verhoogde, resulterend in een verhoogde eiwitexpressie. Bovendien onthulden mechanistische studies dat de belangrijkste route voor celopname membraanfusie was, waardoor de minder efficiënte endocytose-routes omzeild werden. Deze aanzienlijke verbetering van de transfectie-efficiëntie na modificatie van de LNP met coiled-coil-peptiden kan worden toegepast op andere celtypen, waaronder moeilijk te transfecteren cellijnen (bijv. T-cellen) die nodig zijn voor T-celtherapie.

Onze groep heeft laten zien dat een efficiënte liposomale afgifte kan worden bereikt met behulp van coiled-coil peptiden.<sup>35-37</sup> In Hoofdstuk 3 is het effect van peptide K-dimerisatie op membraanfusie onderzocht. Drie verschillende dimeerontwerpen werden gesynthetiseerd en hun structurele verschillen werden gekarakteriseerd. Confocale microscopie en flowcytometrie metingen toonden aan dat PK4 de hoogste bindingsaffiniteit induceerde voor cellen die waren voorbehandeld met CPE4. Vervolgens werd de efficiëntie van de cellulaire opname en het farmacologische effect van het antitumormiddel doxorubicine bestudeerd. Liposoom-celfusie was efficiënt voor dit dimeer in vergelijking met de lineaire dimeerontwerpen en het benchmark-peptidemonomeer. Het nieuwe peptide-dimeerontwerp is dus in staat om geneesmiddelen efficiënter in cellen af te leveren en zal in de toekomst in een in vivo setting worden getest.

We hebben aangetoond dat fusogene coiled-coil peptide-gemodificeerde LNP's RNA efficiënter aan cellen afleveren in vergelijking met LNP's zonder coiled-coil peptide. In Hoofdstuk 4 werd de afgifte van mRNA in cardiomyocyten onderzocht. Myocardinfarct (MI) is de belangrijkste doodsoorzaak bij hartaandoeningen, aangezien de hartspiercellen van het menselijk hart een zeer beperkte regeneratieve capaciteit hebben na een myocardinfarct, de gewonde hartcellen vertrouwen alleen op vervanging van littekenweefsel om de integriteit van de organen te behouden.<sup>38</sup> Geïnduceerde pluripotente stamcellen-cardiomyocyten (iPSC-CM's) vertegenwoordigen de beste celbron voor menselijke hartaandoeningen en hartregeneratie, maar vereisen een efficiënte transfectie. Er werd een nieuw incubatieprotocol ontwikkeld om deze cellen te transfecteren. De efficiëntie van mRNA-transfectie van verschillende incubatieprotocollen werd vergeleken en het 1-staps incubatieprotocol bereikte verbeterde mRNA-transfectie met een optimale CPK4:CPE4-verhouding van 1:1. De verbetering van de mRNA-transfectie met behulp van 1-staps incubatie werd vergeleken voor drie klinisch goedgekeurde LNP-formuleringen en waargenomen dat transfectie onafhankelijk was van de LNP-samenstelling. In alle gevallen verbeterde de introductie van de fusogene coiled-coil-peptiden de mRNA-expressie in iPSC-CM's aanzienlijk. Dit geoptimaliseerde mRNA-afgifteplatform zou veelbelovend kunnen zijn voor verder in vivo cardiomyocytenonderzoek naar de behandeling van MI.

mRNA-LNP's zijn de huidige state-of-the-art in mRNA-vaccinatietechnologie sinds de goedkeuring

van de COVID-19-mRNA-vaccins. In Hoofdstuk 5 evalueerden we de invloed van LNP-lipidensamenstelling op de T-cel immuunrespons in de ontwikkeling van kankervaccins. In deze studie hebben we de exacte lipidensamenstelling gevarieerd door het ioniseerbare lipide (IL), cholesterol (derivaat) en het percentage van de fusogene helper lipide DOPE te variëren. Een kleine collectie van LNP's werd geëvalueerd op het vermogen om van beenmerg afgeleide dendritische cellen te transfecteren, antigeenpresentatie en T-celstimulatiereponsen. We onderzochten of het vervangen van cholesterol door  $\beta$ -sitosterol en/of DOPE de mRNA-transfectie zou stimuleren, resulterend in een verhoogde immuunrespons. Er werd aangetoond dat de introductie van  $\beta$ -sitosterol alleen verbeterde transfectie in LNP's veroorzaakte wanneer MC3 werd gebruikt als de IL, terwijl het verschillende transfectie-efficiëntie-effecten vertoonde op verschillende cellijnen wanneer C12-200 en cKK-E12 werden gebruikt als de IL. Het vervangen van cholesterol door DOPE resulteerde in gemengde mRNA-transfectie-efficiënties in verschillende celtypen. We hebben aangetoond dat de LNP-mRNA-vaccinkandidaten significante activering van BMDC's kunnen genereren, zoals blijkt uit de verhoogde regulatie van de co-stimulerende receptoren (CD40 en CD86) en IL-12-expressie, robuuste T-celproliferatie en verhoogde cytokineproductie ex vivo.

We hebben aangetoond dat fusogene coiled-coil-peptiden de mRNA-afgifte verbeteren met behulp van LNP's in meerdere cellijnen, waaronder moeilijk te transfecteren Jurkatcellen en cardiomyocyten in vitro. Soms vertalen de in vitro resultaten zich echter niet naar in vivo prestaties, daarom is verder in vivo onderzoek nodig om de gepresenteerde bevindingen te valideren. Momenteel zijn in vivo studies met lokale injectie van cardiomyocyten van muizen gepland en zullen ze inzicht geven in het vermogen om MI te behandelen. De tweede open vraag is of het afleveren van mRNA een relevant therapeutisch effect zal hebben in een muizenmodel. Het gepresenteerde mRNA-afgiftesysteem op basis van coiled-coil-peptiden en LNP's is hoogstwaarschijnlijk geschikt voor lokale toediening, terwijl systemische (intraveneuze) toediening mogelijk complexer is. Dimerisatie van peptide K4 resulteerde in een verbeterde efficiëntie van medicijnafgifte, maar het gebruikte incubatieprotocol moet ook worden bestudeerd in een relevant in vivo model om het nut ervan te valideren.

In dit proefschrift hebben we met succes fusogene coiled-coil peptiden gebruikt om geneesmiddelen met een laag molecuulgewicht (bijv. doxorubicine) en macromoleculair mRNA af te leveren. Dit resulteerde in een versterkt antitumoreffect en verhoogde significant de mRNA-transfectie-efficiëntie in vergelijking met de meest geavanceerde en klinisch goedgekeurde liposoom/LNP-formuleringen. Dit werk vereenvoudigde het incubatieprotocol van ons met coiled-coil peptide gemodificeerde LNP-systeem verder, resulterend in de succesvolle transfectie van cardiomyocyten, wat een grote belofte is voor hartregeneratietherapie na een hartinfarct. Tenslotte werden LNP-mRNA-kandidaten die krachtige BMDC-activering en T-celproliferatie opwekken geïdentificeerd voor ontwikkeling van toekomstige kandidaat-kankervaccins. Ik hoop dat dit werk zal bijdragen aan de mRNA-afgiftetechnologie met verbeterde in vitro en in vivo therapeutische prestaties en krachtige beschermende immuniteit tegen kanker.

## Referenties

1. Saadatpour, Z.; Bjorklund, G.; Chirumbolo, S.; Alimohammadi, M.; Ehsani, H.; Ebrahiminejad, H.; Pourghadamyari, H.; Baghaei, B.; Mirzaei, H.; Sahebkar, A., Molecular imaging and cancer gene therapy.

*Cancer gene therapy* **2016**, 1-5.

2. Ouriel, K., Peripheral arterial disease. *The Lancet* **2001**, 358 (9289), 1257-1264.
3. Vogt, A., Hyperlipoproteinaemia(a) – apheresis and emerging therapies. *Clinical Research in Cardiology Supplements* **2017**, 12 (1), 12-17.
4. Jessup, M.; Greenberg, B.; Mancini, D.; Cappola, T.; Pauly, D. F.; Jaski, B.; Yaroshinsky, A.; Zsebo, K. M.; Dittrich, H.; Hajjar, R. J., Calcium Upregulation by Percutaneous Administration of Gene Therapy in Cardiac Disease (CUPID). *Circulation* **2011**, 124 (3), 304-313.
5. Jaski, B. E.; Jessup, M. L.; Mancini, D. M.; Cappola, T. P.; Pauly, D. F.; Greenberg, B.; Borow, K.; Dittrich, H.; Zsebo, K. M.; Hajjar, R. J., Calcium Upregulation by Percutaneous Administration of Gene Therapy in Cardiac Disease (CUPID Trial), a First-in-Human Phase 1/2 Clinical Trial. *Journal of Cardiac Failure* **2009**, 15 (3), 171-181.
6. Kang, Z.; Ding, G.; Meng, Z.; Meng, Q., The rational design of cell-penetrating peptides for application in delivery systems. *Peptides* **2019**, 121, 170149.
7. d'Ydewalle, C.; Sumner, C. J., Spinal Muscular Atrophy Therapeutics: Where do we Stand? *Neurotherapeutics* **2015**, 12 (2), 303-316.
8. Deverman, B. E.; Ravina, B. M.; Bankiewicz, K. S.; Paul, S. M.; Sah, D. W. Y., Gene therapy for neurological disorders: progress and prospects. *Nature Reviews Drug Discovery* **2018**, 17 (9), 641-659.
9. Wang, F.; Qin, Z.; Lu, H.; He, S.; Luo, J.; Jin, C.; Song, X., Clinical translation of gene medicine. *The Journal of Gene Medicine* **2019**, 21 (7), e3108.
10. Richner, J. M.; Himansu, S.; Dowd, K. A.; Butler, S. L.; Salazar, V.; Fox, J. M.; Julander, J. G.; Tang, W. W.; Shresta, S.; Pierson, T. C.; Ciaramella, G.; Diamond, M. S., Modified mRNA Vaccines Protect against Zika Virus Infection. *Cell* **2017**, 168 (6), 1114-1125.e10.
11. Pardi, N.; Hogan, M. J.; Pelc, R. S.; Muramatsu, H.; Andersen, H.; DeMaso, C. R.; Dowd, K. A.; Sutherland, L. L.; Searce, R. M.; Parks, R.; Wagner, W.; Granados, A.; Greenhouse, J.; Walker, M.; Willis, E.; Yu, J.-S.; McGee, C. E.; Sempowski, G. D.; Mui, B. L.; Tam, Y. K.; Huang, Y.-J.; Vanlandingham, D.; Holmes, V. M.; Balachandran, H.; Sahu, S.; Lifton, M.; Higgs, S.; Hensley, S. E.; Madden, T. D.; Hope, M. J.; Karikó, K.; Santra, S.; Graham, B. S.; Lewis, M. G.; Pierson, T. C.; Haynes, B. F.; Weissman, D., Zika virus protection by a single low-dose nucleoside-modified mRNA vaccination. *Nature* **2017**, 543 (7644), 248-251.
12. Wang, L.; Shi, W.; Joyce, M. G.; Modjarrad, K.; Zhang, Y.; Leung, K.; Lees, C. R.; Zhou, T.; Yassine, H. M.; Kanekiyo, M.; Yang, Z.-y.; Chen, X.; Becker, M. M.; Freeman, M.; Vogel, L.; Johnson, J. C.; Olinger, G.; Todd, J. P.; Bagci, U.; Solomon, J.; Mollura, D. J.; Hensley, L.; Jahrling, P.; Denison, M. R.; Rao, S. S.; Subbarao, K.; Kwong, P. D.; Mascola, J. R.; Kong, W.-P.; Graham, B. S., Evaluation of candidate vaccine approaches for MERS-CoV. *Nature Communications* **2015**, 6 (1), 7712.
13. Donoff, B.; McDonough Je Fau - Riedy, C. A.; Riedy, C. A., Integrating oral and general health care. (1533-4406 (Electronic)).
14. Petsch, B.; Schnee, M.; Vogel, A. B.; Lange, E.; Hoffmann, B.; Voss, D.; Schlake, T.; Thess, A.; Kallen, K.-J.; Stitz, L.; Kramps, T., Protective efficacy of in vitro synthesized, specific mRNA vaccines against influenza A virus infection. *Nature Biotechnology* **2012**, 30 (12), 1210-1216.
15. Ping, J.; Lopes, T. J. S.; Nidom, C. A.; Ghedin, E.; Macken, C. A.; Fitch, A.; Imai, M.; Maher, E. A.; Neumann, G.; Kawaoka, Y., Development of high-yield influenza A virus vaccine viruses. *Nature Communications* **2015**, 6 (1), 8148.
16. Zhang, N.-N.; Li, X.-F.; Deng, Y.-Q.; Zhao, H.; Huang, Y.-J.; Yang, G.; Huang, W.-J.; Gao, P.; Zhou, C.; Zhang, R.-R.; Guo, Y.; Sun, S.-H.; Fan, H.; Zu, S.-L.; Chen, Q.; He, Q.; Cao, T.-S.; Huang, X.-Y.; Qiu, H.-Y.; Nie, J.-H.; Jiang, Y.; Yan, H.-Y.; Ye, Q.; Zhong, X.; Xue, X.-L.; Zha, Z.-

- Y.; Zhou, D.; Yang, X.; Wang, Y.-C.; Ying, B.; Qin, C.-F., A Thermostable mRNA Vaccine against COVID-19. *Cell* **2020**, *182* (5), 1271-1283.e16.
17. Fenton, O. S.; Olafson, K. N.; Pillai, P. S.; Mitchell, M. J.; Langer, R., Advances in Biomaterials for Drug Delivery. *Advanced Materials* **2018**, *30* (29), 1705328.
18. Toure, M.; Crews, C. M., Small-Molecule PROTACS: New Approaches to Protein Degradation. *Angewandte Chemie International Edition* **2016**, *55* (6), 1966-1973.
19. Lomenick, B.; Olsen, R. W.; Huang, J., Identification of Direct Protein Targets of Small Molecules. *ACS Chemical Biology* **2011**, *6* (1), 34-46.
20. Stewart, M. P.; Langer, R.; Jensen, K. F., Intracellular Delivery by Membrane Disruption: Mechanisms, Strategies, and Concepts. *Chemical Reviews* **2018**, *118* (16), 7409-7531.
21. Kaczmarek, J. C.; Kowalski, P. S.; Anderson, D. G., Advances in the delivery of RNA therapeutics: from concept to clinical reality. *Genome Medicine* **2017**, *9* (1), 60.
22. Kole, R.; Krainer, A. R.; Altman, S., RNA therapeutics: beyond RNA interference and antisense oligonucleotides. *Nature Reviews Drug Discovery* **2012**, *11* (2), 125-140.
23. Gupta, A.; Andresen, J. L.; Manan, R. S.; Langer, R., Nucleic acid delivery for therapeutic applications. *Advanced Drug Delivery Reviews* **2021**, *178*, 113834.
24. Pardi, N.; LaBranche, C. C.; Ferrari, G.; Cain, D. W.; Tombácz, I.; Parks, R. J.; Muramatsu, H.; Mui, B. L.; Tam, Y. K.; Karikó, K.; Polacino, P.; Barbosa, C. J.; Madden, T. D.; Hope, M. J.; Haynes, B. F.; Montefiori, D. C.; Hu, S.-L.; Weissman, D., Characterization of HIV-1 Nucleoside-Modified mRNA Vaccines in Rabbits and Rhesus Macaques. *Molecular Therapy - Nucleic Acids* **2019**, *15*, 36-47.
25. Irvine, D. J.; Dane, E. L., Enhancing cancer immunotherapy with nanomedicine. *Nature Reviews Immunology* **2020**, *20* (5), 321-334.
26. DeRosa, F.; Guild, B.; Karve, S.; Smith, L.; Love, K.; Dorkin, J. R.; Kauffman, K. J.; Zhang, J.; Yahalom, B.; Anderson, D. G.; Heartlein, M. W., Therapeutic efficacy in a hemophilia B model using a biosynthetic mRNA liver depot system. *Gene Therapy* **2016**, *23* (10), 699-707.
27. Ramaswamy, S.; Tonnu, N.; Tachikawa, K.; Limphong, P.; Vega, J. B.; Karmali, P. P.; Chivukula, P.; Verma, I. M., Systemic delivery of factor IX messenger RNA for protein replacement therapy. *Proceedings of the National Academy of Sciences* **2017**, *114* (10), E1941-E1950.
28. Zangi, L.; Lui, K. O.; von Gise, A.; Ma, Q.; Ebina, W.; Ptaszek, L. M.; Später, D.; Xu, H.; Tabebordbar, M.; Gorbатов, R.; Sena, B.; Nahrendorf, M.; Briscoe, D. M.; Li, R. A.; Wagers, A. J.; Rossi, D. J.; Pu, W. T.; Chien, K. R., Modified mRNA directs the fate of heart progenitor cells and induces vascular regeneration after myocardial infarction. *Nature Biotechnology* **2013**, *31* (10), 898-907.
29. Hou, X.; Zhang, X.; Zhao, W.; Zeng, C.; Deng, B.; McComb, D. W.; Du, S.; Zhang, C.; Li, W.; Dong, Y., Vitamin lipid nanoparticles enable adoptive macrophage transfer for the treatment of multidrug-resistant bacterial sepsis. *Nature Nanotechnology* **2020**, *15* (1), 41-46.
30. Hou, X.; Zaks, T.; Langer, R.; Dong, Y., Lipid nanoparticles for mRNA delivery. *Nature Reviews Materials* **2021**, *6* (12), 1078-1094.
31. Wang, C.; Zhang, Y.; Dong, Y., Lipid Nanoparticle-mRNA Formulations for Therapeutic Applications. *Accounts of Chemical Research* **2021**, *54* (23), 4283-4293.
32. Meyer, R. A.; Neshat, S. Y.; Green, J. J.; Santos, J. L.; Tuesca, A. D., Targeting strategies for mRNA delivery. *Materials Today Advances* **2022**, *14*, 100240.
33. Zhang, Y.; Sun, C.; Wang, C.; Jankovic, K. E.; Dong, Y., Lipids and Lipid Derivatives for RNA Delivery. *Chemical Reviews* **2021**, *121* (20), 12181-12277.
34. Paramasivam, P.; Franke, C.; Stöter, M.; Höijer, A.; Bartesaghi, S.; Sabirsh, A.; Lindfors, L.; Arteta, M. Y.; Dahlén, A.; Bak, A.; Andersson, S.; Kalaidzidis, Y.; Bickle, M.; Zerial, M., Endosomal

escape of delivered mRNA from endosomal recycling tubules visualized at the nanoscale. *Journal of Cell Biology* **2021**, *221* (2), e202110137.

35. Yang, J.; Bahreman, A.; Daudey, G.; Bussmann, J.; Olsthoorn, R. C. L.; Kros, A., Drug Delivery via Cell Membrane Fusion Using Lipopeptide Modified Liposomes. *ACS Central Science* **2016**, *2* (9), 621-630.

36. Yang, J.; Shimada, Y.; Olsthoorn, R. C. L.; Snaar-Jagalska, B. E.; Spalink, H. P.; Kros, A., Application of Coiled Coil Peptides in Liposomal Anticancer Drug Delivery Using a Zebrafish Xenograft Model. *ACS Nano* **2016**, *10* (8), 7428-7435.

37. Kong, L.; Askes, S. H. C.; Bonnet, S.; Kros, A.; Campbell, F., Temporal Control of Membrane Fusion through Photolabile PEGylation of Liposome Membranes. *Angewandte Chemie International Edition* **2016**, *55* (4), 1396-1400.

38. Yang, Q.; Fang, J.; Lei, Z.; Sluiter, J. P. G.; Schiffelers, R., Repairing the heart: State-of the art delivery strategies for biological therapeutics. *Advanced Drug Delivery Reviews* **2020**, *160*, 1-18.

## Curriculum vitae

Ye Zeng was born October 29, 1990, in Yuanjiang, Yiyang city, Hunan province, P. R. China. In 2009, she graduated from Yuanjiang No.1 High School and commenced her Bachelor studies in Pharmacy at Hunan University of Chinese Medicine, Changsha, China, and obtained her bachelor degree in 2013. In 2013, she continued her study in Pharmaceuticals as a master student at Sichuan University under the supervision of Prof. Xun Sun. Her master thesis was entitled: “PEGylated Cationic Vectors Containing a Protease-Sensitive Peptide as a miRNA Delivery System for Treating Breast Cancer” and this work was published in *Molecular Pharmaceutics*. During her master’s education, she was awarded the “First Class Academic Scholarship” of Sichuan University. After obtaining her MSc degree in 2016, she worked as a researcher at the Gene Therapy Department of Salubris Biotherapeutics (Chengdu). In 2017, she decided to pursue a PhD degree, and was awarded a scholarship from Chinese Scholarship Council (CSC) to start her doctoral research in the group of Supramolecular & Biomaterials Chemistry under the supervision of Prof. dr. Alexander Kros and Dr. Aimee Boyle. Her PhD study focused on the development of coiled-coil-based biomaterials to enhance the delivery efficiency of mRNA and drugs, and evaluated different lipid nanoparticles for T cell immune responses. Currently, she is working as a postdoc at the Leiden Institute of Chemistry on RNA therapeutics delivery funded by a NWO-XS grant.

## Acknowledgements

First of all, I express my sincere appreciation to my supervisor Prof. Alexander Kros. Thank you for giving me the opportunity to join the big SBC group and for your trust, guidance, encouragement, freedom and support to pursue my research ideas and develop myself as an independent scientist over the years. I'm also thankful to Dr. Aimee Boyle for her kind help during my PhD and detailed revision of my thesis. Your broad knowledge of chemistry and drug delivery inspired my understanding of the field. I would like to express my gratitude to China Scholarship Council (CSC) and the Leiden Institute of Chemistry for funding support.

I sincerely thank all my collaborators. Dr. Peter Vader, and Mariona Estape Senti, thank you for the nice collaboration and the pleasant discussions. I am also very grateful for Dr. Bram Slütter, I gained a lot of immunity knowledge during our project. A big thanks to Kevin, who was an amazing student. Then, I would like to express my heartfelt gratitude to my colleagues. They are Mengjie, Lily, Ciqing, Tingxian, Renzo, Roy, Fred, Panagiota, Winant, Kevin, Oscar, Dinghao, Weizhe, Ying, April, Don, Xuecheng, Guangya, Xiaofang, Jianwei, Dennis, Niek, Elena, Jolinde, Gabriela, Viorica, Indigo, Michelle, Xue, Nol, Isabella, Jasper, Jorn, David, Sabine, Julia, Sofia Francesca, Merel, Sandeepa, Joyal, Max, Thomas, Grégory, Sander, Roxanne, and all other SBCers. All the group meetings helped me explore my perspectives in my research, really enjoyed the lunch discussions, group outings, and all the fun we had together.

I would like to thank all my friends in Leiden: Feng Jiang, Lin Jiang, Mengjie Shen, Chunmiao Ye, Yurong Chen, Chengyu Liu, Mingchuan Luo, Shengxiang Yang, Chen Tang, Diyu Zhang, Xuequan Zhou, Wanbing Hu, Xiaoting Chen, Zhen Wang, Juan Wu, Liyan Zhang, Lu Chen, Qi Yu, Yi Ding, Wensen Li, and all others. I remember all the wonderful times we spent together: celebrating Chinese traditional festivals, eating delicious foods, playing card games, and traveling in and out of the Netherlands. I also want to thank my tennis friends: Deyi Wang, Chenguang Gao, Yuchen Lian, Furong Ye, Jinyu Sheng, Yu Wei, Qiang Zhen, Qingwu Liu, and all others. I enjoyed the moments very much when we were playing tennis on the clay court regardless of rain and sunshine, and participated in tennis matches in Leiden and other cities in the Netherlands. All of you guys make my stay in Leiden more memorable. Special thanks to Feng and Yun Tian, and all the members of the Leiden Science China community. It is an unforgettable experience for me to organize symposiums, sports events, BBQs, and many other interesting activities together with you.

Finally, I would like to thank all my family members and close friends. Thank you for your unconditional love, support, and encouragement, which always help me go through difficult times. I will keep going with all of you beside me.

## List of publications

1. **Zeng, Y.**; Shen, M. J.; Pattipeiluhu, R.; Bakkum, T.; Sharp, T.H.; Boyle, A. L.; Kros, A. Efficient mRNA Delivery Using Fusogenic Coiled-coil Peptides. **Submitted.**
2. **Zeng, Y.**; Escalona-Rayó, O.; Knol, R.; Kros, A.; Slütter, B. Lipid Nanoparticle-based mRNA Candidates Elicit Potent T cell Immune Responses. **Submitted.**
3. **Zeng, Y.**; Zhou, Z.; Fan, M.; Gong, T.; Zhang, Z.; Sun, X. PEGylated Cationic Vectors Containing a Protease-Sensitive Peptide as a miRNA Delivery System for Treating Breast Cancer. *Molecular Pharmaceutics* **2017**, 14, 81.
4. Shen, M. J.; Olsthoorn, R. C. L.; **Zeng, Y.**, Bakkum, T.; Kros, A.; Boyle, A. L. Magnetic-Activated Cell Sorting Using Coiled-Coil Peptides: An Alternative Strategy for Isolating Cells with High Efficiency and Specificity. *ACS Applied Materials & Interfaces* **2021**, 13, 11621.
5. Zhou, X. Q.; Mytiliniou, M.; Hilgendorf, J.; **Zeng, Y.**; Papadopoulou, P.; Shao, Y.; Dominguez, M. P.; Zhang, L.; Hesselberth, M. B. S.; Bos, E.; Siegler, M. A.; Buda, F.; Brouwer, A. M.; Kros, A.; Koning, R. I.; Heinrich, D.; Bonnet, S. Intracellular Dynamic Assembly of Deep-Red Emitting Supramolecular Nanostructures Based on the Pt...Pt Metallophilic Interaction. *Advanced Materials* **2021**, 33, 2008613.
6. Pattipeiluhu, R.; **Zeng, Y.**; Hendrix, M.R.M.; Voets, I.K.; Kros, A.; Sharp, T.H. Paracrystalline Inverted Lipid Phases Encapsulating siRNA Enhance Lipid Nanoparticle Mediated Transfection. **Submitted.**
7. **Zeng, Y.\***; Shen, M. J.\*; Singhal, A.; Sevink, A.; Crone, N.; Boyle, A. L.; Kros, A. Enhanced Liposomal Drug Delivery via Membrane Fusion Triggered by Dimeric Coiled-coil Peptides. **Manuscript in preparation.**
8. **Zeng, Y.\***; Estape-Senti, M.\*; Kros A.; Vader, P. Fusogenic Coiled-coil Peptides Enhance LNP-mediated mRNA Delivery Locally upon Intramyocardial Injections. **Manuscript in preparation.**
9. Zhao, G.\*; **Zeng, Y.\***; Papadopoulou, P.; Snaar-Jagalska, E.; Kros, A. Therapeutic Gene Silencing Using CD44 Targeted Peptide Modified LNP-siRNA in Breast Cancer. **Manuscript in preparation.**
10. Bobilev, E. O.\*; **Zeng, Y.\***; Weijgertse, K.; Koelman, E.; Aarts, M.; Meijer, E. M.; Alarcón-Lladó, E.; Bruin, B.; Kros, A.; Reek, J. N.H. The Application of M12L24 nanocages as Cell-specific siRNA Delivery Agents. **Manuscript in preparation.**
11. Zeng, Y.\*; **Zhao, G.\***; Snaar-Jagalska, E.; Kros, A. Efficient Gene Editing of Tumor-targeted LNP-CRISPR/Cas9 Delivery. **Manuscript in preparation.**

\*These authors contributed equally.